ACTIVE SCREEN PLASMA SURFACE MODIFICATION OF POLYMERIC MATERIALS FOR BIOMEDICAL APPLICATIONS

By Xin Fu

School of Metallurgy and Materials
College of Engineering and Physical Sciences
The University of Birmingham

A thesis submitted to the
University of Birmingham
for the degree of

DOCTOR OF PHILOSOPHY

January 2012

Synopsis

Polymeric materials are important engineering materials and have been used in many industrial sectors. They are being used increasingly in biomedical applications because of their wide range of properties, relative ease of forming into a desired shape and relatively low cost. For example, polymeric biomaterials have been used for the direct replacement of hard and soft tissues and as biodegradable scaffolds for tissue engineering.

However, their surface properties such as surface hardness, wear resistance and biocompatibility need reinforcement for demanding engineering and biomedical applications. For instance, the hydrophobicity of a polymer surface, which results in poor cell attachment and proliferation rate, has limited its biocompatibility in biomedical applications. Therefore, polymeric materials must undergo surface modification to improve their hydrophilicity, cell adhesion, and biocompatibility via either introducing functional groups onto their surface or changing surface morphologies and surface energy.

Surface modification of polymers has long been known in polymer chemistry but has not yet been widely applied to biomaterials. Widely used surface modification techniques include coating, oxidation by low temperature plasma and surfactant addition, some of which are no longer used because of their high cost or environmental concerns. Among them, plasma treatment has received a great deal of attention for its numerous advantages, especially its ability to uniformly modify the surface without affecting the bulk properties.

As non-conductive materials, polymers are unable to be treated in DC plasma directly. However, a newly developed active screen plasma technology has great potential to treat non-conductive materials such as polymers to improve their surface properties since this is a low-temperature, low-cost and environmentally friendly process.

In this project, three kinds of polymeric materials: ultra high molecular weight polyethylene (UHMWPE), polyurethane and polycaprolactone, were surface-modified using newly developed active screen plasma nitriding technology. The change in surface topography was investigated by profilometry, atomic force microscopy (AFM) and scanning electron microscopy (SEM); the chemical composition and bonding structure of the plasma modified surface was characterized by X-ray photoelectron spectroscopy (XPS), Fourier transform infrared spectroscopy (FTIR) and Raman spectroscopy; the wettability of the modified surface was evaluated by contact angle and surface energy measurement; the biocompatibility of the surface treated UHMWPE samples was evaluated in vitro using MC3T3-E1 osteoblast-like cells.

The results demonstrated that it is feasible to conduct plasma surface modification of polymeric materials using the newly developed active-screen plasma technology without causing any arcing etching, significant sputtering or other surface damage.

Changes in chemical composition and structure have been found on all three polymeric surfaces following active screen plasma surface treatments. Crosslinking or/and new functional groups are formed on the topmost surface layer after the treatment.

Along with changes in surface morphologies and structural, the wettability of the surface of all three polymeric materials can also be effectively improved by the active screen plasma nitriding treatments.

Active-screen plasma nitriding technique is an effective and practical method to effectively improve osteoblast cell adhesion and spreading on the all surfaces of three polymeric materials.

Acknowledgement

Publications

(Related to PhD study)

Fu X, Jenkins MJ, Bertoti I, Dong H.

Active screen plasma surface modification of polyurethane.

Presentation at Euromat 2009 Conference, Glasgow, Sept 2009.

Xin Fu, Rachel L. Sammons, Imre Bertoti, Mike J. Jenkins, Hanshan Dong.

Active screen plasma surface modification of polycaprolactone to improve cell attachment.

Journal of Biomedical Materials Research, Part B-Applied Biomaterials. 2012; 100B(2): 314-320.

Xin Fu, Mike J. Jenkins1, Imre Bertoti, Hanshan Dong.

Characterization of Active Screen Plasma Modified Polyurethane Surfaces.

Surface & Coatings Technology (Submitted and on revision)

Xin Fu, Rachel L. Sammons, Mike J. Jenkins, Hanshan Dong

Effect of treatment temperature on surface characteristics and osteoblast cell attachment of plasma modified UHMWPE.

Journal of Biomedical Materials Research, Part B-Applied Biomaterials. (Submitted)

List of Tables

Figure Captions

Figure 2.1 Schematic of the chemical structure of ethylene and polyethylene

Figure 2.2 Generalized polyurethane reaction

Figure 2.3 Schematic of the chemical structure of polycaprolactone

Figure 2.4 Equilibrium contact angle θ

Figure 2.5 Active screen plasma system for surface modification of polymer a) Schematic diagram; b) Photo of plasma furnace

Figure 2.6 Schematic of structure of a vinyl polymer

Figure 2.7 A schematic representation of indentation load - displacement curves

Figure 2.8 A schematic representation of a section through an indentation

Figure 2.9 The arithmetic average roughness profile

Figure 2.10 Schematic illustration of the operation of AFM

Figure 2.11 Atomic force curves for interaction of two atoms

Figure 2.12 A schematic illustration of ATR-FTIR

Figure 3.1 Schematic of nano-indentation machine

Figure 3.2 Schematic of pin-on-disc machine and test configuration

Figure 4.1 DSC curve of UHMWPE

Figure 4.2 XRD pattern of untreated UHMWPE

Figure 4.3 XRD patterns of UHMWPE after ASPN treated at different temperatures

Figure 4.4 XRD patterns of UHMWPE after ASPN treated at different time

Figure 4.5 FTIR spectra of UHMWPE

Figure 4.6 FTIR spectra of UHMWPE from 1000 to 900 cm-1 wavenumbers

Figure 4.7 Crystal field splitting results in doublets at 730 and 720 cm−1

Figure 4.8 Crystal field splitting results in doublets at 1473 and 1460 cm−1

Figure 4.9 The AFM image of untreated UHMWPE

Table of Contents

1 Introduction

1.1 Background

Polymeric materials are important engineering materials and have been used in many industrial sectors and they are being used increasingly in biomedical applications because of their wide range of properties, relative ease of forming into a desired shape and relatively low cost. For example, polymeric biomaterials have been used for the direct replacement of hard and soft tissues and as biodegradable scaffolds for tissue engineering.

However, their surface properties such as surface hardness, wear resistance [1-3] and biocompatibility [4-8] need enhancement for demanding engineering and biomedical applications. For instance, the hydrophobicity of a polymer surface, which results in poor cell attachment and proliferation rate, has limited its biocompatibility in biomedical applications. Therefore, polymeric materials must undergo surface modification to improve their hydrophilicity, cell adhesion, and biocompatibility via either introduction of functional groups onto their surface [9, 10] or changing surface morphology and surface energy[11].

Surface engineering has been proved to be promising technology to improve the surface properties of many materials. For instance, an effective approach for developing a clinically applicable polymeric biomaterial is to modify the surface of the material which already has proved biofunctionality and desirable bulk properties.

Surface modification of polymers has long been known in polymer chemistry but has not yet widely applied to biomaterials. For longer than half a century, polymeric materials used in industry have been subjected to surface modification. Widely used surface modification techniques include coating, oxidation by low temperature plasma and surfactant

addition, some of which are no longer used because of their high cost or environmental concerns. For the medical purpose, addition and blending technologies are not recommended since the additives will leach out and cause potential cytotoxicity.

Surface modification of polymeric materials through covalent bonding without causing any bulk deterioration is most desirable for biomaterials. Consequently, there has been ever-growing interest in using surface engineering technology to change the surface composition and topography, thus improving the tribological and mechanical properties, wettability and biocompatibility [12-14] of polymeric materials.

A polymer surface can be modified by many surface modification techniques, such as wet chemical treatment, plasma treatment, ion beam, ion implantation, laser treatment, coating, alkaline hydrolysis [15-21]. Among them, plasma treatment has received a great deal of attention for its numerous advantages, especially its ability to uniformly modify the surface without affecting the bulk properties. The effects of using plasma techniques such as ion implantation [22-24], plasma ion implantation [25, 26] or plasma immersion ion implantation [3, 27] to modify the surface of polymeric materials have all been investigated.

In recent years, surface modification by cold plasma has become popular for wide industrial applications. Apart from increasing concern about environmental pollution problems, plasma treatment has received a great deal of attention for its numerous advantages, especially its ability to uniformly modify the surface without affecting the bulk properties. Typically, the depth of modification is 5-50 nm [28]. However, the direct current (DC) plasma requires electrically conductive electrodes because an insulator would charge up and terminate the discharge [29]. As non-conductive materials, polymers are unable to be treated in DC plasma directly.

To alleviate the problem, an alternating current (AC) power source with high frequencies has been used. However, these plasma treatments cannot avoid some shortcomings. Firstly, the process parameters are extremely complex and highly system-dependent. It is almost impossible to duplicate other research based on the descriptions published in the papers. Secondly, a significant limitation is the need to use high vacuum, which is often between 0.01-100 Pa, to achieve adequate plasma conditions [30]. This requirement increases the cost of operation. Thirdly, charging and arcing cannot be avoided during plasma treatment and may result in surface damage.

Therefore, the newly developed active screen plasma technology [31, 32], a low-temperature, low-cost and environmentally friendly plasma process, has - great potential to treat such non-conductive materials as polymers to improve their surface properties, which forms the theme of this PhD project. According to their structure and possible response to active species in plasma, polymeric materials can be divided into two groups [13] those which would form cross-linking (group I) and those which would cause chain scission (group II). So three typical polymers including UHMWPE (group I), PU (group II) and PCL (groupI or II) are used as substrate materials. Ultra high molecular weight polyethylene (UHMWPE) has been used in orthopedics as a bearing material in artificial joints because of its high impact strength, low friction coefficient, and good chemical resistance [33, 34]. Polyurethane is used for catheters and various orthopedic devices and instruments [35-37]. Polycaprolactone (PCL), a biodegradable polyester, has attracted growing interest for its biomedical applications in tissue engineering over the last few decades [38-44].

1.2 Aim of project

The proposed research seeks to realize the potential of active screen plasma technology for the surface modification of polymeric materials to improve the hardness and

wear resistance of polymer tribo-surfaces and to improve the biocompatibility of polymer bio-surface. The specific scientific and technologicial objectives of the research are:

- To improve the hardness, wear resistance of polymer tribo-surfaces for such articulating surfaces as joint prostheses, gear and bearings in functional devices.

- To explore the possibility of a generating functional polymer surface with desired surface texture and roughness, tailored surface wettability and improved cell biocompatibility.

- To characterise the structure, composition, nano-mechanical properties and wear resistance of active screen plasma modified polymers.

- To investigate the mechanisms involved in active screen plasma surface modification of polymeric materials, thus advancing scientific understanding

1.3   Structure of the thesis

To achieve the above four objectives, systematic research activities have been conducted including active-screen plasma modification of three polymers (UHMWPE, PU and PCL), characterisation of modified surfaces using a range of modern surface techniques and evaluation of surface mechanical and biological properties.

In this thesis, the fundamentals and surface properties of polymeric material,the state-of-the art of surface modification of polymers and surface characterisation methods are first reviewed in Chpater 2, followed by the experimental methods (Chapter 3). The experimental results and their interpretation for UHMWPE, PU and PCL are reported in Chapters 4, 5 and 6 respectively and a general discussion is given in Chapter 7 to compare the response of these three polymers to active-screen plasma modification. Finally, conclusions from this research and the suggestions for future work are presented in Chapters 8 and 9, respectively.

2 Literature Review

2.1 Polymeric materials

Polymer literally means many parts. Chemically, polymers are long-chain molecules of very high molecular weight, often measured in the hundreds of thousands. For this reason, the term ‒macromolecules" is frequently used when referring to polymeric materials. Polymeric materials have been widely used across most industrial sectors owing to their excellent physical, chemical and biological properties, coupled with relatively low cost, providing cost-effective solutions. During the past two decades significant advances have been made in the development of polymeric biomaterials for biomedical applications. Polymeric biomaterials, such as ultra high molecular weight polyethylene (UHMWPE), polyurethane(PU) and polycaprolactone(PCL), have been used also for the direct replacement of hard and soft tissues and as biodegradable scaffolds for tissue engineering [34, 45, 46].

2.1.1 Ultra high molecular weight polyethylene (UHMWPE)

2.1.1.1 Structure and properties

UHMWPE comes from a family of polymers with a deceptive simple chemical composition, consisting of only hydrogen and carbon. A schematic of the chemical structures for ethylene UHMWPE is shown in Figure 2.1. However, the simplicity inherent in its chemical composition belies a more complex hierarchy of organizational structures at the molecular and supermolecular length scales.

At a molecular level, the carbon backbone of polyethylene can twist, rotate, and fold into ordered crystalline regions. At a supermolecular lever, the UHMWPE consist of powder (also known as resin or flake) that must be consolidated at elevated temperature and pressure to form a bulk material. Further layers of complexity are introduced by chemical changes that arise in UHMWPE due to radiation sterilization and processing.

There are many kinds of polyethylene, such as low density polyethylene (LDPE), high density polyethylene (HDPE) and UHMWPE. LDPE and HDPE are linear polymers each with a molecular weight of less than 50,000 g/mol and up to 200,000 g/mol. In comparison, UHMWPE has a viscosity average molecular weight of up to 6 million g/mol.

In UHMWPE, the glass transition and the melting temperature occur at around -160℃ and 137 ℃ respectively. Most bulk UHMWPEs are approximately 50-55 % crystalline.

UHMWPE has a higher ultimate strength and impact strength than other polyehylenes. Therefore, UHMWPE is significantly more abrasion resistant and wear resistant from a clinical perspective. Table 2.1 summarizes the physical and mechanical properties of HDPE and UHMWPE [34].

2.1.1.2 Applications and problems

Since the 1950s, UHMWPE has been widely exploited for industrial applications, including textile machinery, coal chutes, dump trucks, as well as bumps and siding for ships and harbours. More than 90 % of the UHMWPE produced in the world is used by industry.

Since 1962, UHMWPE has been used in orthopedics as a bearing material in artificial joints. Each year, about 1.4 million joint replacement procedures are performed around the world [34]. However, the low surface hardness and poor wear resistance of polymers frequently limit their applications in both industrial and biomedical areas when contact and wear are involved. For example, both clinical and laboratory research has revealed that the wear and the resultant wear debris of UHMWPE is one of the major causes of premature failure of total joint replacement. It has been reported that ion implantation can improve the surface properties by tailoring the surface morphologies of polymers [3, 47-49]. However, conventional ion implantation is a line-of-sight process, so it is difficult in practice to uniformly treat three-dimensional objects (such as sockets in artificial hip joints).

2.1.2 Polyurethane (PU) rigid form

2.1.2.1 Structure and properties

Polyurethane polymers are formed by reaction of a monomer polyisocyanates (containing at least two isocyanate functional groups) with another monomer polyols (containing at least two alcohol groups) in the presence of a catalyst. The generalized polyurethane reaction is presented in the equation (Figure 2.2).

The first essential component of a polyurethane polymer is the isocyanate. Molecules that contain two isocyanate groups are called diisocyanates. These molecules are also referred to as monomers or monomer units, since they themselves are used to produce polymeric isocyanates that contain three or more isocyanate functional groups. The second essential component of a polyurethane polymer is the diols which contain two hydroxyl groups. The reaction of diisocyanates with diols according to Figure 2.2 leads to linear polyurethane. If there are polyisocyanates or polyols present in the reaction, branching and crosslinking of polymer chains occur.

Because a variety of polyisocyanates and a wide range of polyols can be used to produce polyurethane, a broad spectrum of materials can be produced to meet the needs of specific applications.

Rigid PU foam is a cross-linking closed cell thermo-setting plastic. Open celled foams are also available for special purposes. Depending on the blowing process used, the cells can be closed or open. Even intermediate stages are possible. Fine cells have a diameter of less than 0.25 mm and large cells have a diameter over 0.5 mm [50].

The cell structure has a very significant influence on the properties. One can describe the cell structure as having a skeleton and walls as the support construction of the foam. The properties of this model depend on the cell size and especially on the shape of the cell. Round

cells exhibit same properties in all directions; ellipsoid cells show anisotropic different properties.

The properties of PU foams can be modified within wide limits dependent on the raw materials used. This is also true for the area of PU rigid foams. The density, flowability, strength, thermal stability, combustibility and other properties can be adjusted to suit the requirements for a given application. Both polyols and isocyanates have major impacts on the properties of the foams. PU rigid form has low thermal conductivity. The mechanical properties are dependent on the density, the cell structure and manufacturing process.

2.1.2.2 Applications and problems

PU rigid form has been used industry as a insulation material, or a structural material or as a combination of both because of the low thermal conductivity and good mechanical properties.

Due to their good biocompatibility as well as mechanical properties, polyurethanes are commonly used in a number of medical applications including catheter and general purpose tubing, hospital bedding, surgical drapes, wound dressings, as well as in a variety of injection molded devices. While traditionally PUs have been widely used for their excellent mechanical properties and moderately good blood compatibility, they have also been singled out as being problematic in terms of their long-term in vivo biostability in tissues. Preliminary investigation by Li et al [51-53] has achieved some success in improving the wettability, anticoagulability and anticalcific behaviour of polyurethane through oxygen and silicon ion implantation.

2.1.3 Polycaprolactone (PCL)

2.1.3.1 Structure and properties

Polycaprolactone (PCL) (Figure 2.3) is a synthetic semicrystalline (about 50% of crystallinity) [54], linear resorbable aliphatic polyester and is of great interest as it can be obtained by the ring opened polymerization (ROP) of a monomeric unit "ε-caprolactone" which is relatively cheap. Polycaprolactone is thermoplastic polymer with hydrolytically labile aliphatic ester linkages in their backbone. Being aliphatic polyester with reasonably short aliphatic chains between ester bonds, PCL can hydrolytic or enzymatic degrade over the time frame required for most of the biomedical applications.

The PCL is very easy to process as it is soluble in a wide range of organic solvents, has a low melting point (55-60 ℃) and relative low glass transition temperature (-60 ℃) [45]. Therefore, it is always in a rubbery state at room temperature. PCL has high thermal stability because it has a higher decomposition temperature (T_d) of 350 ℃ than most other aliphatic polyesters (T_d between 235 to 255 ℃) [55]. The polymer undergoes hydrolytic degradation because of the presence of hydrolytically labile aliphatic ester linkages; however, the rate of degradation is rather slow (Degradation generally undergoes 2-3 years to complete). Due to its biodegradability, non-toxicity and biocompatibility, PCL has also been extensively investigated as drug delivery devices [56]and scaffolds for tissue engineering [9, 57].

2.1.3.2 Applications and problems

Polycaprolactone(PCL) are versatile low-melting point biodegradable polymers currently used in implanted devices for drug-delivery, e.g., for contraceptives and as antibiotic-impregnated beads for control of infection in orthopaedic surgery. Modified polycaprolactones have considerable future potential as biomaterials, e.g. as scaffods for bone and cartilage repair [38]. However, PCL has poor hydrophilicity, which results in poor cell attachment and proliferation rate. It has been shown that the initial surface properties of PCL

structures obtained by casting are not ideal for cellular culturing, with concurrent low cellular development *in vitro* [11]. It has been also found that the surface morphologies and surface energy of such polymers will greatly influence cellular adhesion, proliferation and phenotype [9, 11]. Therefore, plasma treatment could modify the rate of resorption of polycaprolactones in the body for a great variety of clinical applications.

2.2 Surface properties of polymeric materials

2.2.1 Friction and wear

Friction and wear are in fact very complicated phenomena, which depend on both bulk and surface properties. Friction and wear processes are inevitable when two surfaces undergo sliding or rolling under load. Friction is a serious cause of energy dissipation, and wear is a major cause of material wastage [58].

2.2.1.1 Friction

Friction is the resistance to relative motion of contacting bodies. The degree of friction is expressed as a coefficient of friction μ, which is the ratio of the force F_T required to initiate or sustain relative motion to the normal force F_N that presses the two surfaces together. Friction experienced during sliding conditions is known as sliding friction, and friction experienced during rolling conditions is known as rolling friction [59].

a. Sliding friction

The sliding between sliding surfaces is due to the various combined effects of adhesion between the flat surfaces, ploughing by wear particles and hard surface asperities, and asperity deformation. The relative contribution of these components depends on the specific material used, the surface topography, the conditions of sliding interface, and the environment [60].

The following factors mainly contribute to the friction in sliding contact: adhesion, ploughing, deformation and elastic hysteresis [60-62].

The adhesion component of friction is due to the formation and rupture of interfacial bonds. These bonds are the results of interfacial interatomic forces that depend on the degree of interpenetration of asperities and the surface composition. If sliding is to take place, the fiction force is needed to shear the weakest tangential plane at the areas of real (actual) contact.

If one of the sliding surfaces is harder than the other, the asperities of the harder surface may penetrate and plough into the softer surface. Ploughing into the softer surface also may occur as a result of impacted wear particles. In tangential motion, the ploughing resistance is an addition to the friction force. In addition to the material properties, the geometric properties of the asperities or the wear debris may significantly influence the ploughing component of friction [60-62].

When the asperities of two sliding surfaces come into contact with each other, they have to deform in such a way that the resulting displacement field is compatible with the sliding direction and that the sum of the vertical components of surface traction at the contacting asperities are equal to F_N, the normal load. Plastic deformation is always accompanied by a loss of energy, and it is this energy dissipation that accounts for the major part of friction. Most of the energy required in elastic deformation is recoverable, and elastic energy losses are therefore negligible compared with the energy losses associated with plastic deformation.

When viscoelastic surfaces with high hysteresis loss (i.e., high internal damping) slide against each other, external work must be done by tangential component of surface friction to overcome the cycle energy loss due to the hysteresis loss. This is known as friction due to

elastic hysteresis and is generally significant in the sliding of viscoelastic materials, e.g. polymers [59].

Friction force also can arise when the wear debris is viscoelastic or plastic substance that sticks to the sliding interface and undergoes repeated deformation resulting in consumption of energy.

b. Rolling friction

Rolling friction, although in general much smaller (coefficient of friction is typically 5×10^{-3} to 10^{-5}) than sliding friction (coefficient of friction is usually 10^{-1}) [60], is also a very complex phenomenon because of its dependence on so many factors, such as a varying amounts of sliding (or commonly referred to as slip) during rolling and energy losses during mixed elastic and plastic deformation.

2.2.1.2   Wear

Wear is a process of removal of material from one or both of two solid surfaces in solid-state contact. It occurs when solid surfaces are in sliding or rolling motion relative to each other. Similar to friction, the wear behaviour of a material is also a very complicated phenomenon in which various mechanisms and factors are involved.

The main types of wear are classified into several categories, based on quite distinct and independent phenomena, as follows: abrasive wear, adhesive wear, fatigue wear, and corrosive wear, etc [60].

a. Abrasive wear

Abrasive wear is caused by either hard asperities on counterface or hard particles (third body) between the articulating surfaces [63].

The surface roughness values of the counterfaces are the determining factors for the wear of a given polymer. Abrasive wear can be calculated by multiplying breaking strength and elongation resistance. Any measure enhancing the strength without diminishing the toughness is expected to improve abrasive wear resistance of polymeric materials.

b. Adhesive wear

Adhesive wear is associated with the intermolecular forces, including the attractive Van der Waals and the repulsive electrostatic force. When most polymers slide over clean, hard, smooth counterfaces, the interfacial shear strength of the adhesive junction is observed to be greater than that of a polymer. The contact ruptures within the polymer as sliding continues, owing to its soft or low strength nature. As a result, polymer is transferred to the harder counterface and subsequently removed as wear debris. Any measure that can effectively reduce polymer transfer (such as enhancing lubrication or cross-linking reaction) would be expected to improve the adhesive resistance of a polymer [59].

c. Fatigue wear

Fatigue wear results from the formation of cracks associated with predominantly elastic deformation over a number of contact cycles in the form of pitting, cracking, spalling and delamination.

Fatigue wear occurs only when the counterface is smooth and adhesive action is almost eliminated. If the counterface is relatively rough, the rate of removal of polymer by abrasive and adhesive actions may be so high that the surface does not have time to develop surface distress associated with fatigue [60].

Typical surface features of micro-fatigue (such as in UHMWPE acetabular cups) are regular and irregular arrays of surface ripples and bumps. The rate of fatigue wear is usually lower than that of either adhesive wear or abrasive wear [34].

d. Corrosive wear

The wear due to abrasive, adhesive and fatigue can be explained in terms of stress interactions and deformation properties of the mating surfaces, but in corrosive wear, the dynamic interaction between environment and mating material surfaces plays a significant role [64].

This interaction gives rise to a cycle stepwise process: in the first step, the contacting surfaces react with the environment, and reaction products are formed on the surface; in the second step, attrition of the reaction products occurs as a result of crack formation and/or abrasion in the contact interactions of the materials.

This process results in increased reactivity of the asperities because of increased temperature and changes in the mechanical properties of the asperities.

2.2.2 Wettability

Wettability can be defined as the ability of a fluid to cover a solid surface. It varies with both the completeness of the monolayer and its degree of order. Wettability also varies with the polarity of the monolayer surface functional groups. Besides, surface contamination and surface roughness can also modify the wettability [65].

2.2.3 Contact angle and the Young equation

An easily feasible and widely used method to determine the hydrophobicity degree is the measurement of the contact angles. The degree of hydrophobicity provides information

about the wettability of a material. A high degree of hydrophobicity is synonymous for a low wettability and vice versa.

As shown in Figure 2.4, a drop of liquid that is put on a solid surface will modify its shape under the pressure of the different surface/interfacial tensions until reaching equilibrium. Contact angle data can be obtain with low price instruments and with simple techniques.

Contact angle measurement is the most common method of solid surface tension measurement. In 1805, Thomas Young described the three-phase equilibrium shown in equation (2.2-1) and illustrated in Figure 2.4 [66].

$$\gamma_{sg} - \gamma_{sl} = \gamma_{lg} \cos\theta \qquad \text{(Equation 2.2-1)}$$

where γ_{ij} is the interface tension between phases i and j, subscripts s, l and g refer to solid, liquid and gas respectively and θ is the (Young) contact angle.

Wetting can be describe as the contact angle between a liquid and a solid is zero or so close to zero that the liquid spreads easily over the solid surface. On the other hand, non-wetting is that the contact angle is bigger than 90º, so that the liquid tends to ball-up and run off the surface easily.

2.2.4 Surface energy

Surface energy, γ (gamma), is used interchangeably with the terms "surface free energy" and "surface tension". The surface energies of liquids are readily determined by measuring the surface tension.

Surface tension can be thought of as the energy required creating a unit area of an interface. According Young equation, in order to promote wetting, both the liquid surface tension and the solid-liquid interface tension should be decreased [67, 68].

If the energy required to create the solid-liquid (sl) interface is greater than that required for creation of a solid-gas (sg) interface, then the critical angle will be greater than 90°. In other words, the liquid will ―bead up" on the surface to minimize the solid-liquid interfacial area.

2.2.5 Biocompatibility

2.2.5.1 Concept of biocompatibility

Williams proposed the definition of biocompatibility, which is the ability of a material to perform with an appropriate host response in a specific application [69].

The concept of biocompatibility is too general in theory rather than practical process. The biocompatibility of an artificial material in the body is extremely complicated, involving processes traditionally belonging to medical science, surface science, materials science, and molecular biotechnology. For example, if the material surface has a very sharp edge or is cationically charged, the cells and tissues in contact with it will be damaged physically or chemically. One can say in these cases that the biomaterial is lacking in biocompatibility.

The biocompatibility of polymeric material relies on various parameters. Some of the inherent properties of polymer can have an effect on their biocompatibility, which are characteristics of the bulk material and those of the surface, such as (1) shape, (2) size, (3) surface chemistry and roughness, (4) design, (5) morphology and porosity, (6) composition, (7) surface energy and water absorption (8) hydrophilicity/hydrophobicity, (9) contact duration and (10) degradation [4, 70-75].

Biocompatibility can be divided into two categories which are concerned with the characteristics of bulk property of the biomaterial and with those of surface property. Particularly, interfacial biocompatibility is closely related to the events occurring at the interface between the biomaterial and the living cell or tissue [14]. One purpose of surface

modification is to improve this kind of biocompatibility for the biomaterial which is not toxic and possesses good bulk and surface biocompatibility.

2.2.5.2   Biocompatibility assessment through cell culture

Cell culture is the process that cells removed from animal tissue will continue to grow if supplied with sufficient nutrients and growth factors[76]. Cytocompatibility may be evaluated in cell culture.

a.   Cell number measurement

The most straightforward way for cell number measurement such as cell adhesion and proliferation is to count the cell number after the cells are attached on substrate materials. Many colorimetric methods have been developed for cell number measurement. Among them, the MTT (Methylthiazoletetrazolium) method which is based on cell's metabolic viability test is widely employed. MTT can be reduced by the dehydrogenase enzymes in cell plasma to form a purple colored product. The total amount of the purple colored product can be quantified by optical absorption, giving the total reduction ability of the dehydrogenase enzymes in the cell population [77].

b.   Cell imaging

Cell morphology and distribution on biomaterials is an important issue in tissue engineering because it is often closely related to morphogenesis of the multicellular organisms. The changes in cell morphology during adhesion and flattening on to the substrate material surfaces in vitro can be studied with a scanning electron microscope (SEM) [78]or atomic force microscopy (AFM) [77, 79-81].

2.2.6 Degradation

The study of degradation of polymers is important in understanding their usability, recycling and reducing their impact on the environment [40, 45, 82-93]. The process of ‚degradation' describes the chain scission process during which polymer chains are cleaved to form oligomers and finally to form monomers. There are different types of polymer degradation such as photo-, thermal-, bio-, mechanical and oxidative and catalytic degradation [45, 91, 92, 94-97].

All biodegradable polymers contain hydrolysable bonds. Their most important degradation mechanism is, therefore, chemical degradation via hydrolysis or enzyme-catalysed hydrolysis. The latter effect is often referred to as biodegradation, meaning that the degradation is mediated at least partially by a biological system [45, 86]. Depending on the mode of degradation, polymeric biomaterials can be further classified into hydrolytically degradable polymers and enzymatically degradable polymers.

The main mechanism of *in vivo* degradation of polymers is hydrolytic degradation in which enzymes may also play a role. For both synthetic and natural biodegradable materials, particularly synthetic polymers, passive hydrolysis is the most important mode of degradation. The main factors that have effects on the rate and the extent of degradation reaction include: the type of chemical bond, molecular weight, crystallinity, glass transition temperature, geometrical factors, pH, copolymer composition and water uptake etc [88]. Chemical and physical changes go along with the degradation of biodegradable polymers so that *in vivo* degradation is a highly complex phenomenon.

2.2.7 Biomedical applications of polymeric materials

Both nondegradable and biodegradable polymers have been widely employed in biomedical applications. Although biomedical applications of natural polymers can be dated

back thousands of years, the synthetic biodegradable polymers with some of their medical uses started only in the latter half of 1960s [98]. The main fields of biomedical applications of polymeric materials include: orthopaedic implants (such as joint replacement, teeth), drug delivery vehicles, regenerative medicine and tissue engineering etc.

An important trend in biomaterials research and development has been the modification of synthetic polymers, which potentially exhibit improved biocompatibility, and could enhance healing and regeneration of tissues. Particularly, surface properties of biodegradable polymeric materials are important in biomedical applications, may be readily modified physically, chemically, or biochemically. In addition, the effects of polymer surface properties on the polymer-living system interface should be better understood. Many of the current polymers need to be improved by surface modification techniques in order to produce biomaterials with better performance in biomedical applications.

The better performances are determined by interactivity of the material with the host[99]. Specific biomaterials characteristics (such as identified in Section 2.2.5.1) control specific host responses (such as protein adsorption and desorption characteristics, endothelial proliferation, osteoblast/osteoclast responses, etc.) and that refinement of the former should lead to improvement of the latter and the production of better biocompatibility-based performance.

2.3   Surface modification of polymeric materials

2.3.1   Conventional surface modification techniques

2.3.1.1   Chemical modifications

Chemical modification is mainly based on direct chemical reaction with given chemical reagents. The main chemical modifications include wet treatment and surface grafting.

Wet treatments were the first surface modification techniques used to modify the chemical composition of polymer surface by direct chemical reaction with a given solution in order to improve surface properties of polymers. The chemical solutions employed in the treatment are usually acid solutions, organic solutions or other specific solutions, for example, some acid solutions were used to oxidize polymer surface [100].

Surface grafting was a technique of chemical modification of the surface by the covalent bonding of suitable macromolecular chains to the sample surface. The fundamental steps are creation of reactive groups on the substrate surface and diffusion of monomer onto the substrate [66].

2.3.1.2 Physical modifications

Physical modifications can be divided into two categories, one involved with high energy media applied on the surface layer, the other with depositing a layer on top of the surface. The main physical modifications include flame treatment, corona treatment, ultra violet (UV) treatments, X-ray and γ-ray treatments as well as plasma treatment [101-104].

Flame treatment can generate high energy by the high temperature include radicals, ions and molecules in excited state. This method is widely applied to introduce oxygen-containing functions at polyolefin surface.

Corona treatment exploit the corona effect to form excited species(ions, radicals, electrons, molecules in excited states) in surface modification at atmospheric pressure and relatively low temperature.

UV treatments involve active photons which are usually energetic species with low wavelength to activate many chemical reactions on surfaces.

Both X-ray and γ-ray treatments are high energy photon treatment which induces the formation of radical sites at surfaces and involves mainly crosslinking of polymeric coatings on surfaces.

2.3.1.3   Plasma treatment

Plasma-surface modification is an effective and economical surface treatment technique for many materials and has been widely investigated for polymer surface modification to obtain desired surface properties. Plasma and ion beam techniques are particularly attractive owing to their flexibility and environmentally friendly nature compared with conventional techniques. Consequently, there has been ever-growing interest in using surface engineering technology to change the surface composition and morphology, and thus to improve the wettability, surface mechanical properties and wear resistance of polymeric materials [13, 22]. The possibilities of using such plasma techniques as ion implantation [23, 25], plasma ion implantation [26] or plasma immersion ion implantation [3, 27] to modify the surface of polymeric materials have all been investigated. However, little work has been conducted to modify the surface properties of polymeric materials by active-screen plasma.

2.3.1.4   Definition of plasma

There are many definitions of the term plasma, according to the various disciplines generation of plasma being analogous to the transitions that occur when energy supplied to a material causes solids to melt liquids to become gases. Sufficient additional energy supplied to a gas creates plasma. Typically, a plasma is composed of a large concentration of highly excited atomic, molecular, ionic, and radical species [58, 105].

2.3.1.5   Plasma based technology

Plasma can be obtained when gases are excited to high energetic states. In laboratory conditions, the methods usually used are radio frequency (RF), microwave or electrons from a

hot filament discharge and direct current (DC) plasma. Plasma is a highly unusual and reactive chemical environmental in which ionized and excited species can change the surface properties of normally inert materials by introducing different functional groups into the polymer surface layer. It is possible to manipulate these groups and surface properties of polymer by carefully choosing the working gas or gases like argon, oxygen, nitrogen, hydrogen, fluorine, carbon dioxide and water vapour [28, 29, 106, 107].

Plasma-based techniques combining the advantages of conventional plasma and ion beam technologies are effective methods for surface modification of various materials.

a.   Ion beam surface modification

It has been reported that ion implantation can improve the surface properties by tailoring the surface morphologies of polymer [108-110]. However, conventional ion implantation is a line-of sight process, so it is difficult to uniformly treat three-dimensional objects (such as sockets in artificial hip joints).

A hybrid technology, plasma-enhanced ion implantation, has been developed recently, which can help to address the problems with conventional ion implantation of components with complex shapes [111]. This process does not utilize a light-of-sight ion gun, as in conventional ion implantation, but rather a plasma which is biased periodically to bombard the surface with ions from the plasma around the specimen. For instance, PI3 with nitrogen has been successfully used to improve the wear resistance of UHMWPE by a factor of three [112]. A recent comparison study has revealed that when implanted to the same dose, the PI3 treated UHMWPE showed a deeper and less brittle modified layer and thus a higher load bearing capacity than the ion implanted one [113].

There are, however, problems inherent to the application of PI3 to non-conductive polymeric materials such as the transfer of high-voltage bias to the polymer and surface

charging or arcing. Attempts to address these problems include using conductive substrate holders, covering the surface not to be treated with conductive metal foils or by applying a sacrificial conductive surface layer [114]. Although these approaches can, to some extent, address the non-conductive problem for laboratory research, such procedures impose difficulties (e.g., low efficiency, high cost and contamination) for the surface treatment of polymeric materials on a industrial scale.

b.   Low-pressure plasma surface modifacation

Low-pressure plasma surface modification can be used to modify the surface layer of polymers without altering their bulk properties. A DC glow discharge plasma requires the use of electrically conductive electrodes and therefore is not suitable for the surface modification of most non-conductive polymers. A RF plasma can address such problem since it can be initiated and sustained by external electrodes outside the reactor vessel. Although the mechanism involved in the plasma surface modification of polymers are still open to debate, the potential the interaction between plasma and polymer surface may include functional group introduction, cross-linking, etching and backbone session. While the generation of surface functional groups and cross-linking are desirable for most applications, excessive etching and backbone scission lead to surface damage and the formation of a weakened surface layer, which sometimes is referred to as surface degradation. Therefore, the efficacy of plasma surface modification depends on the combined contribution of all these reactions.

It has been found that surface degradation is unavoidable in direct plasma modification of polymers, in which samples are directly immersed in the plasma, and that the relative importance of desirable surface modification and degradation depends not only on the nature of polymers but also on the type of plasma. Therefore, how to minimize the degradation reaction is crucial for maximizing the efficacy of plasma surface modification of polymeric

materials. Inagaki et al. [115-117] have reported that the degradation effect can be reduced by 'remote plasma treatment', in which polymer samples to be treated are placed away from the plasma zone. They claimed that the bombardment of ions and electrons cause degradation and radicals in the plasma contribute to desirable surface modification. Therefore, in the remote plasma treatment there are the predominant species for surface modification since radicals have a much longer lifetime than electrons and ions.

Although their laboratory research demonstrated the important of remote plasma, it should be pointed out that it is not a simple process to scale up such a laboratory experimental set-up to a large production reactor. In addition, their work to date has been limited to fluoropolymers and the mechanisms involved in the remote plasma surface modification of polymers are far from being understood.

Limitations of low-pressure plasma surface modification

In recent years, surface modification by cold plasma is becoming popular in many industrial applications. Apart from increasing concern about environmental pollution problems, plasma treatment has received a great deal of attention for its numerous advantages, especially its ability to uniformly modify the surface without affecting the bulk properties. Typically, the depth of modification is 5-50 nm [28]. However, the direct current (DC) plasma requires electrically conductive electrodes because an insulator would charge up and terminate the discharge [29]. As non-conductive materials, polymers are unable to be treated in DC plasma directly. To alleviate the problem, an alternating current (AC) power source with high frequencies has been used. In general, the plasma power supply outputs a high frequency voltage with a peak value from 5 to 40 kV and the power between 5 and 600 W [107, 118-124]. This means that a more sophisticated, expensive oscillator and amplifier of the power supply and other facilities are required. Owing to achievements in electronic

technology, the frequencies may be changed from radio frequency (RF, 100 kHz to 100 MHz) to microwave (MW, above 1 GHz) [125]. Due to the complication of the plasma system, the plasma process is extremely complex and highly system-dependent. It is almost impossible to duplicate other research based on the descriptions published in the papers. Another significant limitation is the need to use high vacuum, which is often between 0.01-100 Pa, to achieve adequate plasma conditions [30]. This requirement increases the cost of operation. In addition, charging and arcing cannot be avoided during plasma treatment and may result in surface damage.

2.3.2 Active screen plasma technology

2.3.2.1 Fundamentals of active screen plasma technology

Recently, an innovate active screen plasma (ASP) technology（Figure 2.5）has been developed based on the DC glow discharge technology and the principle of post-discharge plasma [31, 32]. The entire workload is surrounded by a large screen, on which a high voltage cathodic potencial is applied and the plasma forms. The worktable and the samples to be treated are placed at floating potencial. The plasma formed on the screen contains a mixture of ions, eletrons and other active species, which are then encouraged to flow through the screen and over the workload by a specially designed gas flow.

Therefore, it may be possible to treat such non-conductive materials as polymers using this newly developed active screen plasma technology.

2.3.2.2 Advantages of active screen plasma technology

The new ASP technology has been gradually adopted by industrial sector due to its several distinct advantages [31, 126-128].

In a standard plasma furnace, the plasma surrounding the samples is used to heat them up directly. Therefore, it is impossible to ensure that the temperature is the same at the outside

of the load as in the centre, where it will tend to be higher. In active screen plasma equipment, the active screen is designed to surround the entire workload, and all parts are heated by radiation from plasma on the screen. The temperature can be controlled very closely by adjusting the current provided to the screen. Therefore, a uniform temperature distribution around the components during treatment is produced, assisted by the direction of gas flow. The parts bath continuously in a gentle flow of the active plasma species.

As the cathodic potential is applied to the metal screen, and not to the parts to be treated, many damage effects to components, such as arcing, edge effects and hollow-cathode damage, are completely avoided. Some arcing or hollow-cathode effects may well occur, but this would happen on the active grid, where it will do no harm to the parts being treated.

Active screen plasma technology is usually reliable, reproducible, non-line-of-sight, relatively inexpensive, and applicable to different sample geometries as well as different materials such as metals, polymers, ceramics, and composites.

As an economical and effective materials processing, active screen plasma processing can provide changes of a variety of surface characteristics, for example, chemical, tribological, electrical, optical, biological, and mechanical and can be applied to industrial production relatively easily.

2.3.2.3   Comparisons of low-pressure plasma and active screen plasma technology

The newly developed active screen plasma technology [31, 32] has great potential for treatment of non-conductive materials such as polymers. In active screen plasma equipment, an active screen is designed to surround the entire working table and all samples are heated by radiation from a plasma on the screen. As the cathodic potential is applied to the metal screen, and not to the samples to be treated, many damaging effects to work materials, such as arcing, edge effects and hollow-cathode damage, are completely avoided. This provides a flexible,

low-temperature, low-cost and environmentally friendly process that allows tailoring of the surface properties of the material to suit a specific need. From a technical point of view, the sample to be treated by active screen plasma is in contact with active species from all around the sample surface so that there is no restriction to the appearance of sample. The sample and the working table are placed in a floating potential so that electrical conductivity of the sample is not a necessary condition. From an economical point of view, active screen plasma treatment operates with much lower voltage (under 500V), lower vacuum (100-500 Pa) and similar low power (100-600 W) (Table 2.2) so that will effective reduce the cost of operating and equipment. From a practical point of view, active screen plasma system is much simple and effective than that of high frequency plasma so that will improve practical applicability and produce reliable and effective results in industry application.

2.3.2.4 Active screen plasma surface modification of polymers

a)   Plasma/ion interaction with polymer

  (1) Cross-linking

Cross-linking of a polymer is defined as the linking of two or more molecular chains by means of chemical (covalent) bonds. Cross-linking can be achieved by chemical or by radiochemical reactions. However, chemical cross-linking is not used to process polymers for medical applications because it usually generate hazardous chemical waste [129]. Essentially, radiation affects materials by the deposition of high-density energy. Energetic ions are slowed down in materials by momentum transfer to target atoms (nuclear stopping). The electronic excitation or removal of valence electrons (ionization) can result in the formation of free radicals that may readily cross-link the polymer chains, thereby, increasing the molecular weight, hardness and wear resistance. Continued cross-linking causes the surface region to become a three-dimensional network, which becomes an insoluble gel [130].

(2) Chain scission

Plasma/ion beam irradiation leads to irreversible changes in polymers. When energetic ions are slowed down in materials by exciting the electronic system of the target (electronic stopping), the displacement of the target atoms by energetic collisions can cause permanent damage in a polymer mainly in the form of chain scission by displacing atoms from polymer chains. If a bond that makes up part of the backbond of the molecule (such as C-C in UHMWPE) breaks, this main chain scission result in degradation, with products of a lower average molecular weight [131].

(3) Structure effect

A general empirical rule that irradiation deduce changes in polymer (cross-linking or chain scission) is concern with the structure of polymers [13]. It follows that when the structure of a vinyl polymer (Figure 2.6) is such that each carbon atom of the main chain carries at least one hydrogen atom (or either R_1 or R_2 is hydrogen), the polymer cross-linking and thus belongs to group I. Alternatively, if a tetrasubstituted carbon atom is present in the monomer unit (or neither R_1 or R_2 is hydrogen), the polymer degrades and belongs to group II. This may be due to the fact that the carbon bond in the main chain is weakened by the presence of the tetrasubstituted carbon atom since it causes a defect in the molecule by a steric repulsion effect.

b)   General principle of plasma modification of polymer

The plasma contains free electrons as well as other metastable particles that break covalent chemical bones upon collision with the surfaces of polymers placed in the plasma environment, thus creating free radicals on the polymer surface. The free radicals then undergo additional reactions, depending on the gases present in the plasma or subsequent

28

exposure to gases in the atmosphere. The result is that these gas radical reactions form a surface that is potentially very different from that of the starting bulk polymer. Because the process is conducted in a reactor under very controlled conditions, the end result is very reproducible.

Four mechanisms contribute to improvement in the adhesion of two components and the adhesion of coatings [28, 29, 132, 133]:

- Removal of surface contaminants and weakly bound polymer layers

- Enhancement of wettability through incorporation of polar groups that facilitate spontaneous spreading of adhesive or matrix resin

- Formation of functional groups on the surface that permit covalent bounding

- Aims of surface modification of polymers

2.3.2.5 Research status of ASP treatment of polymers

Supported by Advantage West Midlands (AWM), a Regional Authority Technology Program, an industrial scale active screen plasma unit has recently been introduced into Birmingham Surface Engineering Research Group, which is the first one installed in any higher education organization on world-wide. Initial experimental observations made by the Group have revealed that UHMWPE can be surface hardened by active screen plasma technology. However the mechanism in improving surface properties has not been investigated. Although a feasibility study of ASP treatment of PU has been conducted by an undergraduate student in his final year project, systematic work needs to be conducted. With regarding to PCL, no work has been conducted to modify its surface properties using the ASP technology.

Characterization methods

2.3.3 Differential scanning calorimetry (DSC)

Differential scanning calorimetry or DSC is a thermoanalytical technique. The basic principle underlying this technique is that, when the sample undergoes a physical transformation such as phase transitions, more or less heat will need to flow to it than the reference to maintain both at the same temperature. During a DSC analysis, the difference in the amount of heat to increase the temperature between a sample and reference is recorded as a function of temperature. The result of a DSC experiment is a curve of heat flow versus temperature or versus time.

DSC is used widely for examining polymers to check a number of characteristic properties, such as two major thermal transitions: the glass transition temperature (T_g), the melt temperature(T_m). The glass transition is the temperature below which the polymer chains behave like a brittle glass. Below T_g, the polymer chains cannot have enough thermal energy to slide past one another. As we raise the temperature above T_g, the amorphous regions within the polymer gain increase mobility. The transition appears as a step in the baseline of the recorded DSC signal. This is due to the sample undergoing a change in heat capacity; no formal phase change occurs. As the temperature increases, the smaller crystallites in the polymer begin to melt, the sample eventually reaches its melting temperature (T_m). The melting behavior of semicrystalline polymers is typically measured using DSC. The melting process results in an endothermic peak in the DSC curve. The ability to determine transition temperatures and enthalpies makes DSC an invaluable tool in producing phase diagrams for various chemical systems. As the temperature of a semicrystalline polymer is raised above the melt temperature, it may undergo a flow transition and become liquid.

2.3.4 Nano-indentation

Determining surface hardness and modulus of polymeric materials, from indentation tests requires ultra-low-load indentation. However, the contact area is very difficult to measure directly at such ultra-low-indentation.

Nanoindentation provides an effective technique to measure the local mechanical properties at the microscale and nanoscale [134]. The two mechanical properties, the modulus (E), and the hardness (H), are measured most frequently using load and depth sensing indentation techniques. In a commonly used method data are obtained from one complete cycle of loading and unloading. The method relies on the assumption that the contact area is a constant during the initial unloading stages.

Figure 2.7 shows a schematic representation of load versus indenter displacement data for an indentation experiment [135, 136]. In the Figure 2.7, P_{max} is the peak indentation load; h_{max} is the indenter displacement at peak load; h_f is the final depth of the contact impression after unloading.

Figure 2.8 shows a cross section of an indentation and identifies the parameters used in analysis [135]. The analysis begins by Equations (2.4-1) and (2.4-2).

$$E = \frac{\sqrt{\pi}}{2} \frac{S}{\sqrt{A}} \qquad \text{(Equation 2.4-1)}$$

$$H = \frac{P_{max}}{A} \qquad \text{(Equation 2.4-2)}$$

where A is the contact area and S is the measured stiffness. At peak load, the load is P_{max}. The contact area at peak load can be computed from the relation

$$A = F(h_c) \qquad \text{(Equation 2.4-3)}$$

where h_c is the vertical distance along which contact is made (hereafter called the contact depth).

The contact depth h_c can be determined by

$$h_c = h_{max} - h_s \qquad \text{(Equation 2.4-4)}$$

where h_s is the displacement of the surface at the perimeter of the contact. At peak load, the displacement is h_{max}.

$$h_s = \frac{(\pi-2)}{\pi} (h - h_f) \qquad \text{(Equation 2.4-5)}$$

2.3.5 Surface roughness measurement

Surface roughness, often shortened to roughness, is a measure of surface topography. Each of the roughness parameters is calculated using a formula for describing the surface. There are many different roughness parameters in use, but R_a is by far the most common. R_a is the arithmetic average of the roughness profile.

A section of standard length is sampled from the mean line on the roughness chart (Figure 2.9). The mean line is laid on a Cartesian coordinate system wherein the mean line runs in the direction of the x-axis and magnification is the y-axis. The value obtained with the formula on the right is expressed in micrometer (μm) when $y=f(x)$.

In the present research, a simply high performance stylus surface profilometer is used to determine the surface roughness and an AFM-style three dimensional topographic image of a surface.

2.3.6 Atomic force microscopy (AFM)

The atomic force microscope (AFM) was developed in 1986 by Binning, Quate, and Gerber as a collaboration between IBM and Stanford University. AFM is a powerful tool to

study the surface topography of insulators, conductors, and semiconductors [79, 137, 138]. AFM measures surfaces in three dimensions. The roughness over a scanned surface area (referring to the total distance the probe scanned) can be obtained.

In AFM, a cantilever is place parallel to the surface. The cantilever has a sharp, force-sensing tip at its end, and it is this that interacts with the surface. As the interaction force between the cantilever tip and the surface varies, deflections are produced in the cantilever. These deflections may be measured and used to compile a topographic image of the surface. The process is illustrated in Figure 2.10.

Atomic force microscopes have been designed which can monitor interactions due to a range of forces between a tip and the sample surface. There are two principal modes of interaction between tip and the surface: attractive and repulsive, which are in the range 10^{-9}-10^{-6} N. Figure 2.11 shows the relationship of atomic interaction and separation between the tip and the surface, where F is the atomic interaction force between the tip and the surface, r is the atomic separation between the tip and the surface.

There are three primary modes of AFM: contact mode AFM, non-contact mode AFM and tapping mode AFM. The comparisons among three modes are listed in Table 2.3.

In the present research, AFM was carried out in contact mode to compile a topographic image of the sample surface. Contact mode AFM operates by scanning a tip attached to the end of a cantilever across the sample surface while monitoring the change in cantilever deflection with a split photodiode detector. By maintaining a constant cantilever deflection, the force between the tip and the sample remains constant. The force is calculated from Hooke's Law: $F = -kx$, where F is force, k is spring constant and x is cantilever deflection. The distance the scanner moves vertically at each (x,y) data point is stored by the computer to form the topographic image of the sample surface.

2.3.7 Scan electronic microscopy (SEM)

A scanning electron microscope (SEM) is a type of electron microscope that images a sample by scanning it with a high-energy beam of electrons in a raster scan pattern.

When a sample is bombarded with electrons, it emits secondary electrons and X-rays. The intensity of the secondary electrons is detected to generate a high resolution surface image. Non-conducting polymers must be sputter-coated with gold or platinum prior to analysis. SEM is one of the more widely available tools in surface analysis and it is often used to measure surface topography [139-141].

SEM can produce very high-resolution images of a sample surface, revealing details about less than 1 to 5 nm in size. Due to the very narrow electron beam, SEM micrographs have a large depth of field yielding a characteristic three-dimensional appearance useful for understanding the surface structure of a sample. Therefore, resolution, magnification and depth of field are important elements of SEM.

a.   Resolution

The resolution of SEM is controlled by the electron beam diameter. It is clear that in order to resolve two features, the smaller the electron beam diameter, the better resolution effect can be achieved. But the increase of resolution has a limit because of defects of condenser and objective lenses (their function is to focus the beam to a spot), such as spherical aberration and chromatic aberration. In addition, if the electron beam diameter is too small, then the signal will be weaker, and may be noisy.

b.   Magnification

The magnification of SEM is concern with the resolution of screen display. The minimum size of beam spot which may be obtained on a high quality cathode tube is typically ～0.1mm (100 μm). The magnification is given by

M=100/d   (Equation 2.4-6)

where M is the magnification of SEM, d is beam spot diameter (μm).

c.   Depth of field

Apart from its good spatial resolution, one of the most important aspects of the scanning electron microscope is its large depth of field. The important consequence of the large depth of field of the SEM means providing a method of examining roughness or fracture surfaces at high resolution. The depth of field h is given by

$h = 0.2D_w/AM$ (mm)   (Equation 2.4-7)

where A is objective aperture diameter, D_w is working distance, M is magnification.

2.3.8 X-ray photoelectron spectroscopy (XPS)

XPS determines the atomic composition of a solid's top several nanometers.

A surface irradiated by a photon source (X-ray) of sufficiently high energy will emit electrons. The x-ray photon transfers its energy to a core-level electron imparting enough energy for the electron to leave the atom. The basic physics of this process can be described by the Einstein equation [66]:

$E_B = h\nu - E_K$ (Equation 2.4-8)

where E_B is the binding energy of the electron in the atom (a function of the type of atom and its environmental), $h\nu$ is the energy of X-ray source (a known value), and E_K is the kinetic energy of the emitted electron measured in the XPS spectrometer.

Binding energy will vary with the type of atom and the addition of other atoms bound to that atom. The variations in binding energy that provide us with chemical information are associated with covalent and ionic bonds between atoms. These changes in binding energy are called chemical shifts.

The E_B of an emitted photoelectron is simply the energy difference between the (n-1)-electron final state and the n-electron initial state:

$$E_B = E_f(n-1) － E_i(n) \qquad \text{(Equation 2.4-9)}$$

To covalent character polymers, it is usually assumed that initial state effects are responsible for the observed chemical shifts. So that, if the energy of the atom's initial state is changed, for example, by formation of chemical bonds with other atoms, then the E_B of electron in that atom will change.

In polymer surface modification, it is of interest to identify the presence of specific functional groups. Because XPS analysis is limited to the top few nanometers of the surface, samples must be handled carefully as even minor surface contamination is pronounced in the resulting spectrum.

Table 2.4 and Table 2.5 list typical C_{1s} and O_{1s} E_B values for functional groups present in polymers [66].

2.3.9 Fourier transform infrared spectroscopy (FTIR)

Infrared (IR) spectroscopy is a technique based on the vibrations of the atoms of a molecule. An infrared spectrum is commonly obtained by passing infrared radiation through a sample and determining what fraction of the incident radiation is absorbed at a particular energy because of vibration the atoms or molecules. The energy at which any peak in an absorption spectrum appears corresponds to the frequency of a vibration of a part of a sample molecule [66].

Fourier transform infrared spectroscopy (FTIR) is used to study the surface of the sample in terms of its separate chemical structures. The mathematical operation of transforming a signal which varies with path length to a spectrum in which intensity varies with wavelength is known as Fourier transformation. The advantage that FTIR method brings as compared to a dispersive instrument is that the signal level at the detector is always higher and this automatically improves the signal-to-noise ratio at any point in the spectrum.

Many samples are opaque to IR radiation and thus cannot be studied in transmission mode. Reflectance methods are particularly useful and have found wide application in surface analysis [142].

The method used in my study was attenuated total reflectance (ATR) FTIR (Figure 2.12), employing a crystal in contact with the sample surface to measure reflected infrared beams of different wavelengths. FTIR-ATR is a widely used technique in polymer research for investigation of the chemical composition and structure near surface. In practice, the IR radiation enters the prism and is incident on the surfaces of the prism at angles greater than the critical angle. If the geometry of the experiment is arranged correctly, then multiple internal reflection occurs. The detection region is within 10^3 nm beneath the surface depending on the refractive index different between the crystal and the polymer surface [142].

The information is obtained by passing the evanescent wave of the infrared radiation through a sample and determining which fraction of the incident radiation is absorbed at a particular frequency (or wavenumber) in the IR spectrum.

2.3.10 X-ray diffraction (XRD)

X-ray diffraction (XRD) provides important structural information for polymers. Useful XRD analysis data is obtained from crystalline, semi-crystalline, amorphous polymeric materials. For ordinary synthetic polymer, the non-uniformity of the molecules makes it impossible to form perfect single crystals. As a result, amorphous and crystalline phases are present in a real polymer, and these entities have complex organization [143, 144].

The structure of semi-crystalline polymer substance consisting of two phases, amorphous and crystalline as well as their fine texture, has a strong effect on physical and mechanical properties of polymer. A detailed knowledge of the characteristics and distribution of soft (amorphous) and hard (crystalline) domains and the interactions between these domains is necessary.

X-ray diffraction (XRD) has long been successfully used to study various aspects of these structures in semicrystalline polymers. The fraction of the material that is crystalline, the crystallinity or crystalline index, is an important parameter. X-ray diffraction (XRD) is a definitive technique for estimating the degree of crystallinity in polymers.

Relative crystallinity (crystalline index, CI) can be determined from a wide-angle X-ray diffraction (WAXD) scan by comparing the areas under the crystalline peaks to the total area under the scattering curve.

Polymer structural information obtained by XRD includes: polymer crystallinity, orientation of polymers (crystalline and amorphous), crystalline microstructure, non-

crystalline periodicity and size, phase identification and quantification, crystal structure variations (e.g. by lattice parameters), dynamic studies, in-situ studies at process temperatures, , nano-scale analysis and research using XRD, etc [143].

3   Experimental method

3.1   Materials and active screen plasma treatment

3.1.1   Materials and sample preparation

UHMWPE samples were manufactured by Ensinger Ltd Company, UK [145]. The commercial name of the product is TECAFINE PE10. It is a semi-crystalline, thermoplastic engineering material rod with a diameter of 30 mm and opaque colour. The main characteristics of the product are high toughness, good wear/abrasion resistance, and very good low temperature properties.

The typical physical properties of TECAFINE PE10 are listed in Table 3.1. The data sheet of TECAFINE PE10 is in appendix 1.

PU samples were purchased from TUFNOL Limited Company, UK [146]. The commercial name of the product is TUFSET rigid polyurethane. It is a thermosetting plastic material rod with a diameter of 30 mm and pale blue colour. It has good resistance to chemicals, weather and UV radiation; excellent electrical and mechanical properties as well as low water absorption.

The typical physical properties of TUFSET rigid polyurethane are listed in Table 3.2. The data sheet of TUFSET rigid polyurethane is in appendix 2.

Disc samples of UHMWPE and PU with a thickness of 6mm were cut from the as-received rods. The surface to be treated was wet ground with silicon carbide paper down to 2400.

Polycaprolactone row material was purchased from Sigma-Aldrich Company Ltd., UK. It is a biodegradable polymer with an appearance of white or off-white colour pellet.

The typical physical and chemical properties of polycaprolactone are listed in Table 3.3. The data sheet of polycaprolactone is in appendix 3.

Thin films of PCL are often used in biomaterials research to determine the effect of surface topography and chemical modifications on cell growth. The PCL film was manufactured from chloroform solvent system by a solvent casting technique [147]. PCL pellets (Aldrich, Mn = 80 K) were dissolved in chloroform and cast over glass sheets. The solvent was removed by a slow evaporation. Films were further dried in vacuum at room temperature for 48h.

3.1.2 Active screen plasma surface treatment

3.1.2.1 Equipments details

An active screen plasma treatment was performed in a conventional direct current (DC) plasma nitriding furnace (40kW Klöckner Ionon). The active screen was made of 0.7 mm thick perforated AISI 304 steel mesh with holes of 8 mm diameter throughout it, the overall dimension of the mesh was was 130 mm in height and 120 mm in diameter; and the sample-to-mesh distance was kept at around 15 mm. The AISI 304 mesh was subjected to the full cathodic potential, whilst the worktable was electrically insulated with ceramic spacers, thus leaving the specimens at floating potential (equipment details can be found elsewhere [148]). Figure 2.5 shows the schematic diagram of the active screen plasma system.

The active screen plasma nitriding procedures were similar to the normal DC plasma nitriding. It started with evacuating the chamber, back filled with treatment gases (nitrogen and hydrogen) to the demand treatment pressure. When an electrical potential (0.2-0.3 kV) was applied, plasma generated between the anodic furnace wall and the cathodic mesh, providing the active species for the possible nitriding treatment. The entire working table was surrounded by the large screen (cathodic mesh), on which a high voltage cathodic potencial

was applied and the plasma forms. The plasma formed on the screen contained a mixture of ions, electrons and other active species, which were then encouraged to flow through the screen and over the working table by a floating potential. Therefore, it is possible to treat such non-conductive materials as polymers on the working table using this newly developed active screen plasma technology.

3.1.2.2   Treatment conditions

A series of active screen plasma nitriding treatments were carried out with nitrogen (25%) and hydrogen (75%) at different temperatures below the melting temperature of the individual polymer. The chosen gases were selected based on the aim of incorporating new nitrogen functionalities which were suggested to be good promoters for cell attachment [149, 150]. The ratio of gases was selected based on previous work in this group [127]. The function of high concentration of hydrogen is the removal of surface oxides and cleaning of surface [151, 152]. Treatment temperatures were measured by a thermocouple inserted into a hole of 3mm diameter from the side wall to the centre of a dummy sample, which was also placed on the working table in a symmetrical position to the samples to be treated. The voltage applied on the screen during treatment was between 200 and 300 V. The treatment pressure was 2 mbar. The effects of treatment temperature and time variations were also investigated. The treatment conditions are listed in Table 3.4, Table 3.5and Table 3.6.

3.2   General materials characterisation

3.2.1 Structure and composition

3.2.1.1   Differential scanning calorimetry (DSC)

DSC tests were carried out using PERKIN-ELMER DSC7 differential scanning calorimeter. The normal operating temperature range was from room temperature to 170 °C with a heating rate of 10 ºC/min, 20 ºC/min and 40 ºC/min, respectively. The samples of 5 mg - 10 mg were heated in aluminium pans with nitrogen as a purge gas.

3.2.1.2   X-ray diffraction (XRD)

XRD is a non-destructive technique. Significance information of structure can be obtained from peaks in XRD pattern, including peak position, peak shape and peak width as well as peak intensity, to identify crystalline phases and orientation and determine structural properties: d-spacings and lattice parameters, residual strain, particle or grain size, phase composition, etc.

Diffraction occurs only when Bragg's Law is satisfied condition for constructive interference from planes with spacing d [143]:

$$2d\sin\theta = n\lambda \qquad\qquad \text{(Equation 3.2-1)}$$

where d is interplanar spacing, 2θ is diffraction angle, λ is the wavelength of the incident X-ray beam, n is integer.

The crystallite size (L) can be estimated from the breadth of the diffraction peak using the Scherrer equation [144]

$$L = \frac{0.94\lambda}{B(2\theta)\cos\theta} \qquad\qquad \text{(Equation 3.2-2)}$$

where λ, 2θ and B (2θ) represent the wavelength, the diffraction angle and the width (in radian) at the half maximum intensity.

The peak intensities were used to estimate the percent crystallinity. The change in the relative intensity and the shift of angular position can be explained by a change in lattice spacing [153].

The crystal structures of materials were characterized by X-ray diffraction (XRD) using a Philips X'pert MPD X-ray diffractometer with Cu-Kα radiation (wavelength is 0.154 nm) generated at 40 kV and 40 mA. The thin film samples of PCL were scanned from 0 to 70° and the plate samples of UHMWPE and PU were scanned from 5 to 100° with a step size of 0.02° and a scan step time of 1 s.

3.2.1.3 Fourier transform infrared spectroscopy (FTIR)

Fourier transform infrared spectroscopy (FTIR) is used to study the surface of the sample in terms of its separate chemical structures. The method used was attenuated total reflectance (ATR) FTIR, employing a crystal in contact with the sample surface to measure reflected infrared beams of different wavelengths. The wavelengths corresponding to different chemical bonds can be determined according to a baseline. Untreated and ASP treated samples were measured in order to determine if the chemical structure of the surface has been altered as a result of plasma surface modification. A Nicolet Magna-IR 860 spectrometer fitted with a golden gate diamond anvil optical unit (It is the most versatile infrared sampling system. And its outstanding sensitivity is achieved using high pressure contact against a solid.), DTGS KBr detector and KBr beamsplitter, was used for FTIR characterization. The golden gate setup provides reliability and accuracy of results because it ensures, with its ratchet torque action, constant load is applied to each sample. The analysis range was from wave numbers 4000 to 700 cm^{-1}. Analyses were done at 100 scans with a resolution of 4 cm^{-1}.

3.2.1.4 Raman spectroscopy

Raman technique has been applied to the study of a wide range of materials, including most solid surface. Raman spectroscopy is commonly used in chemistry, since vibrational information is specific to the chemical bonds and symmetry of molecules. It is complementary to infrared spectroscopy in that it is sensitive to those vibrational modes which are either not observed via IR or give rise to only weak IR absorption bands. Especially, Raman spectroscopy is suitable for the study of back bone structure of polymers.

Raman spectra were collected using a Renishaw InVia reflex Raman microscope. A 785 nm laser was focused using a long working distance 20× objective onto the sample with a spot diameter of approximately 50 μm and beam power of 20 mW. The analysis range was from wave numbers 4500 to 500 cm^{-1}.

3.2.1.5 X-ray photoelectron spectroscopy (XPS)

The change in chemical composition and structure on the surface after plasma treatment is characterized by X-ray photoelectron spectroscopy (XPS). XPS test was performed by a Kratos XSAM 800 spectrometer using Mg $K\alpha_{1,2}$(1253.6 eV) radiation and fixed analyzer transmission mode (80 and 40 eV pass energies for survey and detailed spectra, respectively). Data processing was performed by using the Kratos VISION 2000 program. The overview spectra were taken between 50 and 1300 eV with an energy step of 0.5 eV, while the detailed spectra of the peaks of interest (C ls，O ls and N 1s) were recorded with an energy step of 0.1 eV.

Peak-envelops of the detailed spectra were fitted with minimum number of component-peaks of Gauss-Lorentz (3:2) shape representing the chemical states of the given element. The half-widths of the components were restricted to 1.7-1.9 eV, corresponding to

the resolution of the applied instrument setting. The chemical shifts were determined with an accuracy of ±0.2 eV.

3.2.2 Surface morphology

3.2.2.1 Surface roughness test

Surface roughness R_a was measured by using surface roughness measuring instrument SE1700. The length used for measurement that the stylus traversed on the examined surface was 2.5 mm with a drive speed of 0.5 mm/s. All tests were repeated five times to improve the reproducibility of the results.

3.2.2.2 Optical microscopy

Optical microscopy is a convenient method for of observing the surface of polymer. It is very easy to use and the surface of polymer can be observed directly under an optical microscope without any special preparation.

An optical microscope (Leitz DMRX from Leica Microsystems, Germany) was used to observe and analyse the surface morphologies of the untreated and plasma surface treated surfaces to study the effect of ASPN surface modification on the surface morphologies.

However, no optical microscopy could be achieved which was better than that of scanning electron microscopy (SEM).

3.2.2.3 Scanning electron microscopy (SEM)

SEM is utilized to observe samples surface morphology. It is easy to prepare sample specimens. SEM provides us a important means of examining the surfaces at high resolution and large depth of field.

All polymer specimens were gold-metallized by sputter coating for 3 min and the thickness of sputtered Au was between 10 and 12 nm. Surface topography was observed at 5-

20 kV with a Philips XL-30 scanning electron microscope or Oxford JEOL 7000 scanning electron microscope.

3.2.2.4 Atomic force microscope (AFM)

AFM was used to study the effect of the ASPN surface modification on the surface morphologies and roughness. The cantilever of the AFM has a sharp, force-sensing tip at its end, and it is this that interacts with the surface. As the interaction force between the cantilever tip and the surface varies, deflections are produced in the cantilever. These deflections may be measured, and used to compile a topographic image of the surface.

AFM Dimension 3100 was used in contact mode to study the effect of ASPN surface treatment on surface morphology. Contact mode imaging was performed using a silicon nitride cantilever (nominal force constant 0.12 Nm^{-1}). Scans were acquired at room temperature in air at a tip velocity of 10.0 $\mu m.s^{-1}$. All tests were repeated over approximately three sample areas to assess the reproducibility of the results.

3.2.3 Mechanical property assessment
3.2.3.1 Nano-scale mechanical properties

Nano-scale mechanical properties in terms of nanohardness and modulus were carried out by an instrumented nano-indentation (Nano Test 600). A computer controlled Nano Test 600 machine (Micro Materials Ltd., UK), as shown in Figure 3.1, was used to evaluate the surface hardness (H) and modulus (E) of the untreated and ASPN treated UHMWPE and PU samples using a Berkovich indenter.

The indentation tests were carried out normal to the surface. Testing was performed with continuous loading at a rate of 0.025 mNs^{-1} until a maximum load of 0.5 mN, then the load was kept constant for 60 s and then fully unloaded. A totals of 49 points were tested on each sample for the determination of the H and E values.

47

3.2.3.2   Tribological properties

The tribological properties (wear resistance and coefficient of friction) of surface modified polymers were investigated employing a pin-on-disc tribometer for rotating movement wear testing and a TE79 Multi-Axis Tribometer for reciprocating movement wear testing in unlubricated conditions, respectively.

a.   Pin-on-disc wear tests

The pin-on-disc were tests were conducted sliding against a hardened 8mm stainless steel ball under a load of 6-10N at a rotational speed is 66 rpm for 4h. The wear loss was quantified by measuring the profile of wear track. Five areas were measured from one wear track and the average value was calculated.

In the test the sample is placed and secured inside a sample holder. The sample is rotated against a stationary stainless steel ball (8 mm in diameter) under non-lubricated conditions. The set up of the experiment can be seen in Figure 3.2. Once a wear profile had been established on the surface of the samples, it was then necessary to measure the profile in order to establish the wear rate experienced by each sample.

The following equation was used to calculate the wear factor.

The surface roughness measurement machine was used to obtain the wear volume. The wear factor, defined as

$$k = V/LS \qquad\qquad\qquad \text{(Equation 3.2-3)}$$

where, V is the wear volume which is measured in mm^3, L is the normal load which is measured in Newtons (N), and S is the total distance of sliding which is measured in meters (m), wear factor k, which is measured in $mm^3 m^{-1} N^{-1}$, was used to rank the wear performance of each material. Details of the calculation of the wear factor can be found in a previous

publication [3, 154]. The higher the wear resistance is the lower the wear factor. The wear volume loss was calculated by integrating the area across the wear profile measured by the stylus profilometer, and then multiplying the circumference length of the track.

The wear resistance R, defined as the reciprocal of the wear factor, was used to quantify the effect of the plasma on the wear performance.

R = LS/V   (Equation 3.2-4)

b.   Reciprocating movement wear tests

Reciprocating movement wear tests were conducted sliding against a hardened 8 mm stainless steel ball under different loads from 1.98 N to 19.8 N at a speed of 10 mms^{-1} for 1000-20000 cycles. Reciprocating movement was carried out along one track in the X direction. The sample was then rotated by 90º to carry out reciprocating movement in the Y direction.

3.2.4 Contact angle and surface energy measurement

Contact angles were measured using a KRÜSS GmbH EASYDROP Contact Angle Measuring System by the sessile drop method under distilled water, glycerol and ethylene glycol. The tests were performed at ambient humidity and temperature and five drop measurements were taken on each specimen to yield a statistical average.

The surface free energies were calculated according to Owens-Wendt method, which use two liquids and compute two components: decomposes solid σ_s into dispersive and polar components. Owens and Wends took the equation for the surface energy [155]:

$$\gamma_{sl} = \sigma_s + \sigma_l - 2(\sqrt{\sigma_s^D \cdot \sigma_l^D} + \sqrt{\sigma_s^P \cdot \sigma_l^P}) \qquad \text{(Equation 3.2-5)}$$

as their basis and combined it with the Young equation

$$\sigma_s = \gamma_{sl} + \sigma_l \cdot \cos\theta \qquad\qquad \text{(Equation 3.2-6)}$$

The combining rule equation is the geometric mean model calculating surface energy

$$\sigma_l(1 + \cos\theta) = 2(\sqrt{\sigma_s^D \cdot \sigma_l^D} + \sqrt{\sigma_s^P \cdot \sigma_l^P}) \qquad \text{(Equation 3.2-7)}$$

where s and l refers to the solid and liquid, respectively; σ^D is the dispersive component, and σ^P is the polar component of the surface energy; and θ is the contact angle. Measuring contact angles of drops of two liquids with known values of σ_l^D and σ_l^P, enables us to obtain a set of two equations. To solve the equation system, it is possible to calculate the polar (σ_s^P) and disperse (σ_s^D) fractions of the surface energy of the solid. The surface energy of the solid is calculated as:

$$\sigma_s = \sigma_s^D + \sigma_s^P \qquad\qquad \text{(Equation3.2-8)}$$

3.2.5 Biocompatibility assessment

Biocompatibility of the prepared UHMWPE samples was evaluated by *in vitro* cell culture testing with mouse MC3T3-E1 osteoblast-like cells as a test model.

3.2.5.1 Cell attachment

Cells were cultured in McCoy's 5A medium with 10 % foetal calf serum, 2.5 % Hepes and 1% Penicillin/Streptomycin. Polymer samples were sterilized with 70 % ethanol for 10 min and placed in the wells of 24-well tissue culture plates. Cell suspensions were obtained by culturing the cells in 75 ml flasks until confluent; the cells were then detached from the flask using trypsin-EDTA, centrifuged and resuspended in the same medium at a density of 5×10^4 cells ml^{-1}. 0.1 ml of this cell suspension was pipetted onto each sample and the cultures were incubated in a 5% CO_2 atmosphere incubator at 37 °C to allow cell attachment and proliferation [113].

After 1h, 3days and 7days respectively, the test materials were taken out. The attached cells on the test materials were washed three times in PBS and fixed in 0.1M sodium cacodylate buffer (pH=7.3) containing 2.5% glutaraldehyde. Samples were then dehydrated in ethanol and finally dried in hexamethyldisilisane. The numbers and morphology of the attached cells on the UHMWPE sample surfaces was examined by scanning electron microscopy (Philips XL-30) after gold sputter coating [78].

3.2.5.2 Cell proliferation and cell metabolic activity

As metabolically active cells reduce a tetrazolium salt (MTT), cellular activity, the ability of live cells, was measured by MTT assay [15, 156].

MTT is a yellow tetrazolium salt that is cleaved to water-insoluble purple formazan by viable cells via cell metabolism. After solution of the formazan, the amount of dye can be quantified with a spectrophoto meter.

MTT assay shows how well the cells are metabolising.

3.2.6 Self-degradation assessment

Self-degradation of PCL films (untreated and plasma treated) was carried out in phosphate buffered saline (PBS) solution [157]. Lipase from *Pseudomonas cepacia* was used as a catalyst in order to complete the experiments in a reasonable time, because PCL can take up to 1- 2 years to degrade appreciably [158, 159].

The degradation solution mixture was prepared as follows. Lipase from *Pseudomonas cepacia* (Grade 62309, ∼50 units/mg; Sigma, BioChemika, UK) was dissolved in 0.025 M PBS (Sigma, BioChemika, UK) at a concentration of 7 mg ml^{-1}.

PCL film samples with thickness about 0.7 mm were put into test tubes with a diameter of 25 mm to which 5.0ml solution mixture was added and then labelled, sealed and placed in a water bath at 37 ºC for certain time.

The samples were removed, washed with distilled water and touch-dried with a tissue towel to a constant mass and weighed. The degradation rate is expressed as percentage mass loss:

$$\text{Mass loss \%} = (W_0 - W_1)/W_0 \times 100 \% \qquad \text{(Equation 3.2-9)}$$

where, W_0 and W_1 are mass of PCL films before and after the degradation test, respectively.

4 Ultra high molecular weight polyethylene (UHMWPE) results

4.1 DSC

DSC was used to measure the melting temperature and enthalpy of fusion of untreated UHMWPE and Figure 4.1 shows the DSC curves obtained. It can be seen that as the temperature increased the heat flow increased first linearly before a peak appeared indicating that the UHMWPE sample eventually reached its melting temperature (T_m). The melting process resulted in the endothermic peak in the DSC curve. As shown in the curve, the melting point of UHMWPE is 130.3 ± 0.3 ºC with an onset temperature of 79.8 ±0.4ºC.

The degree of crystallinity was calculated to be 50 % ±2 % according to the equation below:

$$\text{Crystallinity \%} = (\Delta H_{sample}/\Delta H_{UHMWPE}) \times 100 \qquad \text{(Equation 4.1-1)}$$

where $\triangle H$ is an enthalpy of fusion value and the fusion enthalpy of the fully crystalline UHMWPE is taken as $\triangle H_{UHMWPE} = 290$ J g^{-1} [160].

4.2 XRD

In order to study the changes in crystal structures of UHMWPE induced by plasma treatment, XRD was carried out in the range of 2θ angles from 5° to 100° for active screen plasma treated samples and also for untreated samples for comparison. The XRD pattern of untreated UHMWPE is shown in Figure 4.2, and the effect of plasma treatment temperature and time is depicted Figures 4.3 and 4.4, respectively.

According to Figure 4.2, there are two main peaks at two-theta values of 21.66° and 23.98° corresponding to (110) and (200) peaks for the crystalline component of untreated

UHMWPE. There is also a wide halo at 19.8° corresponding to the amorphous component of the untreated material.

According to Figure 4.3, comparing to the ratio of peak intensity (I_{110}/I_{200}), the ratio increased as treatment temperature increased (I_{110}/I_{200} for untreated sample, PE80-05h and PE130-05h are 1.8324, 4.1177 and 4.2507, respectively), which indicated crystals along (200) plane transferred into those along the (110) plane. According to Figure 4.4, after ASPN treatment, the intensity of (110) peak increased while the (200) peak decreased, which indicates the increase of crystallinity at (110) and decrease of crystallinity at (200) compared to the untreated sample. In addition, it is noticed that the peaks of treated samples shifted to low angles following the increase of time (2-5 h) and temperature (100-130 ℃) of active screen plasma treatment. It is considered due to production of inner compressive stress after treatment. The width of peaks at (110) increased, while those at (200) decreased. Table 4.1 shows the calculated results of 2θ and d (d represents interplanar spacing) values from XRD patterns of UHMWPE.

Under identical experimental conditions, the angle of diffraction 2θ for X-rays diffracted by a set of crystal planes depends on the interplanar spacing d. To satisfy Bragg's Law, 2θ must change as d changes, e.g., 2θ decreases as d increases. It can be seen from Table 4.1 that plasma treatment can induce the changes in angle of diffraction 2θ and interplanar spacing d, which reflect the differences in the internal crystal structure. However, when plasma treatment performed at lower temperature (T≤ 80 ℃) or shorter time (t≤ 1 h), the changes both in 2θ and d are very limited. Only when plasma treatment performed at higher temperature (T≥ 100 ℃) and longer time (t≥ 2 h), the changes in 2θ and d are obvious

shown that 2θ moved to lower angle and d value increased. This implies that lattice strain occurs and effects on diffraction peak position shifting to lower angle after plasma treatment.

Wide-angle X-ray diffraction is another technique for the determination of degrees of crystallinity. The degrees of crystallinity can be calculated by quantitative decomposition of the diffraction pattern into its crystalline and noncrystalline components. In practice, the degree of crystallinity was calculated from the ratio of the area of crystalline peaks to the total area under the scattering curve:

$$\text{Crystallinity } \% = \frac{Ac}{Ac + Aa} \times 100 \qquad \text{(Equation 4.2-1)}$$

where A_c is the area of crystalline peak, A_a is the area of amorphous halo.

As evidenced in Figures 4.3 and 4.4, some changes in crystal crystallinity occurred during active screen plasma nitriding of UHMWPE. Table 4.2 shows the crystallinity of UHMWPE before and after plasma treatment (calculated from XRD pattern using Jade 6.0 XRD analysis software). It can be seen from Table 4.2 that crystallinity increased as treatment temperature or time increased.

4.3 FTIR

Fourier transform infrared spectroscopy (FTIR) was used to study the changes in chemical structures of plasma treated UHMWPE surfaces. FTIR spectra of UHMWPE are shown in Figures 4.5-4.8.

In Figure 4.5, for untreated UHMWPE, absorbance peaks at 2930 cm^{-1} and 2850 cm^{-1} are ascribed to the methylene ($-CH_2-CH_2-$) C-H asymmetric and symmetric stretching vibration, absorbance peak at 1460 cm^{-1} is ascribed to the methylene ($-CH_2-CH_2-$) C-H bending vibration, and absorbance peak at 720 cm^{-1} is ascribed to $(CH_2)_n$ rocking band[161]. After ASPN treatment, all the peaks above that show the main characteristic bands associated

with aliphatic hydrocarbons are still in the spectra with a little new peak appearing. The enlarged part from 1000 to 900 wavenumbers is shown in Figure 4.6. It can be seen that an absorbance peak at 965 cm^{-1} (ascribed to the transvinylene group, -CH=CH-) and a peak at 910 cm^{-1} (ascribed to the terminal vinyl group, -CH=CH$_2$) [34] were generated during the ASPN treatment of UHMWPE.

For UHPMWE, crystal field splitting results in doublets at 730 and 720 cm^{-1} (CH$_2$ rocking) and 1475 and 1460 cm^{-1} (CH$_2$ bending) in infrared spectra (Figures 4.7 and 4.8) [161].

There are three bands in the region between 735 and 715 cm^{-1}, two are associated with the crystalline fraction which appear near 730 and 720 cm^{-1} and are narrow than the third band which represents the amorphous fraction near 723 cm^{-1}.

The bands between 1480 and 1420 cm^{-1} due to methylene scissoring modes also include three bands. Two are narrow and belong to crystalline fraction which appear at 1473 and 1460 cm^{-1}. The boarder band near 1467 cm^{-1} is characteristic of the amorphous or conformationally disordered structure.

The amorphous band is highly asymmetric which makes band fitting more difficult and less accurate. For this reason, rocking bands in the 735-715 cm^{-1} region have been preferred to be used for determination of crystallinity.

4.4 Surface roughness

For each sample specimen, surface roughness was measured before and after plasma treatment to compared the effect on surface roughness induced by plasma treatment at different treatment conditions. Detailed surface roughness information can be found in Table 4.3.

Comparing the surface roughness data of the ASPN treated and untreated UHMWPE samples, it is clear that all the ASPN treatments increased the surface roughness of UHMWPE. It is noted that except for the 2 h treated sample, the surface roughness of all other ASPN treated samples increased with the treatment temperature especially when treated at 100 °C or above. When treated at 130 °C, the surface roughness increased rapidly with the treatment time.

4.5   AFM

An atomic force microscope (AFM) Dimension 3100 was used to study the effect of ASPN surface treatment on surface topography. The AFM images of UHMWPE were obtained in contact mode in air. Figures 4.9 –4.13 show the topographical measurements of the untreated and treated UHMWPE surface obtained by AFM.

Active screen plasma nitriding can modify the surface topography of UHMWPE. Comparison of the surface topography of the ASPN treated and untreated UHMWPE samples revealed evidence of changes in surface topography following the active screen plasma treatment. The surface of the untreated UHMWPE sample appears to be unorganised uneven topography (Figure 4.9). After ASPN treatment, highly ordered cylindrical topography on the surface is clearly visible running across the entire AFM images (Figures 4.10 and 4.11). With the increase of treatment temperature and time, especially when treated at higher temperature (100 °C and above) or for longer time (2 h and above), highly grooved surface topography is much clearer than those of treatment at lower temperature (80 °C and below) or shorter time (1h and below). According to surface roughness combining with AFM results, as treatment temperature and time increased, the changes in both surface topography and average surface roughness increased.

Such topographical changes could be attributed cross-linking, alignment of molecule chain and changes in crystal structure by interaction between the plasma species and the polymer surfaces and elevating temperature during plasma treatment.

4.6   SEM

Scanning electron microscopy (SEM) was utilized to observe and verify the changes in sample surface topography. SEM images of plasma treated and untreated UHMWPE are shown in Figures 4.14- 4.18.

Figure 4.14 shows that untreated UHMWPE presents bright strips with dark borders randomly embedded in a ridged structure. A series of SEM measurements (Figures 4.15-4.18) were performed after ASPN treatment. They demonstrated that the ribbons form as the increase of treatment temperature and time, especially when treatment temperature increase up to 100 °C and above or treatment time increase up to 2 h and above. SEM images give good agreement with the AFM results.

4.7   Nano-hardness and modulus

Hardness and modulus were determined directly by instrumented indentation techniques from indentation load and displacement measurements on the surface of UHMWPE materials.

Nano-hardness (H) and modulus (E) of the untreated and ASPN treated UHMWPE samples were measured and the results are shown in Table 4.4 and Figures 4.19-4.21.

It can be seen that both surface hardness and modulus of UHMWPE increased after plasma treatment. The effects of treatment temperature on H and E are the same. As the treatment performed at 130°C (no matter how long the treatment time is), both H and E increased to the highest compared with other samples. The effects of treatment time on H and

E are different. H of samples treated for 0.5 h showed more increase than other samples for the same treatment temperature. E increased following the increase of treatment time for all samples as the treatment performed at 60 and 130°C. As the treatment performed at 80 °C, E of samples treated for the 0.5 h showed the highest value; while the treatment performed at 100 °C, E of samples treated both for 0.5 h and 1 h showed the higher value.

4.8   Wear resistance

The important biomedical application of UHMWPE is the primary bearing material in total joint replacements. Modification of the surface of UHMWPE is essential for improving the wear resistance of the materials, such as, orthopedic implants. In order to predict the clinical wear performance of new materials researchers have designed various wear test apparatus of artificial hip for predicting the in vivo wear rate, mainly including four types: pin-on-plate, pin-on-disc, hip simulator, and ring-on-disc [162-166]. In this study, the unidirectional pin-on-disc wear and the reciprocating pin-on-plate wear were performed on both untreated and plasma treated UHMWPE surfaces.

a) Pin-on-disc wear test results

Wear behaviour of a series of UHMWPE samples (untreated and treated at 60-100°C) were studied by pin-on-disc wear tests. Consideration of the significant increase in surface roughness when treatment performed at 130 °C, there is no potential for application of these samples. Therefore, the samples treated at 130 °C were not selected for pin-on-disc wear test.

Optical microscopy was used to examine the specimen surfaces topography and the wear tracks before and after testing and Figures 4.22 show wear track topography for the untreated and ASPN treated UHMWPE (PE100-2h).

After wear test, it was found that a well-defined wear track was produced on the untreated UHMWPE sample surface, as shown in Figure 4.22a. The track was rough with many abrasive grooves, especially at the edge of wear track, and there were many trails of pulls and smears in the direction of sliding which signifies the occurrence of abrasive wear. In contrast, the wear track on the plasma nitrided sample (Figure 4.22b) was found to be very superficial. The edge between the wear track and the unworn surface was not clear, and the wear track was much narrow than that of untreated sample, suggesting less wear occurred on the nitrided surface.

The typical wear track profiles generated as shown in Figure 4.23 allow a visual representation of the cross section of the wear tracks. Quantitative wear factor was calculated based on the cross-sectional wear track profiles (see Chapter 3) and the results are summarised in Table 4.5.

As can be seen from the Figure 4.24 and Table 4.5, ASPN surface treatment at different conditions has different effects on the wear of UHMWPE. There is a marked improvement in the wear factor in certain treated samples and the most effective treatments are those carried out at 80 °C, 2 mbar for 2 h with an improvement by about 40 %.

From the wear results above, it seems that active screen plasma nitriding offers the possibility to improve the wear resistance of polymers although the effect is highly dependent on the treatment conditions. The results also indicate a strong correlation between wear behaviour and microstructure changes (e.g., cross-linking, crystallinity, nano-hardness and modulus, etc.) induced by plasma treatment.

b) Reciprocating pin-on-plate wear test results

According to nano-hardness and modulus results, the samples treated for 0.5 h can obtain high nano-hardness and modulus values which will be beneficial for wear resistance. For samples treated for 0.5 h, wear resistance all decreased. Therefore, a series of samples treated for 0.5 h at different temperature were chosen to perform reciprocating pin-on-plate wear test to investigate if any changes in wear resistance by different wear test apparatus. Wear properties of untreated and ASPN treated UHMWPE were studied with a computerized reciprocating pin-on-plate sliding wear apparatus at room temperature under unlubricated conditions in air.

Table 4.6 shows UHMWPE wear test (1000 cycles, 3.92 N) profile area and friction coefficient accordingly before and after plasma treatment. According to Table 4.6, the wear areas of the sample treated at 100 °C for 0.5h decreased comparing with untreated sample (PE) which indicated an increase of wear resistance in reciprocating wear test. While, the sample PE80-0.5h still showed the lower wear resistance which agrees with the pin-on-disc results. However, the friction coefficient of all treated samples greatly increased. This could be the reason for the decrease in wear resistance.

Furthermore, wear tests at longer distance and higher loads were performed to investigate the changes in the wear resistance. Table 4.7 and Figure 4.25 show wear area of UHMWPE at different loads (2000cycles). According to Table 4.7, with an increase of wear distance or loads, wear areas of treated samples are bigger than that of untreated sample. It is higher friction coefficient results in a greater wear area. When wear distance increased to 10000 cycles and loads increased to 9.81 N, wear area of all samples are almost same. It indicates the wear was conducted on bulk and the bulk wear performance is not influenced by plasma treatments.

4.9   Contact angle and surface energy

Static contact angle measurements of distilled water were performed to investigate the changes in hydrophilicity of UHMWPE surface after ASPN treatment and the results are listed in Table 4.8. According to Table 4.8, it can be seen that contact angles of all samples decrease or remain unchanged after ASPN treatment. This means that the hydrophilicity increased after ASPN treatment. As the treatment temperature increase, contact angles increase. Furthermore, a group of samples (treated at different temperature for 0.5 h) were chosen to investigate the surface properties in terms of surface free energy of the UHMWPE samples, as characterized by static contact angle measurements, and the results are reported in Table 4.9. This also shows the results of contact angle measurements of two liquids (distilled water and Ethylene glycol). From the results, it can seen that after plasma treatment at 80 °C/0.5 h, water tensile drop contact angle decreases from 79.9º to 68.3º, which indicates increased wettability of the plasma treated surface; while surface energy increases from 26.96 mN m^{-1} to 34.06 mN m^{-1}. When treatment temperature increased to 130 °C/0.5 h, surface energy (28.10 mN m^{-1}) further decreased as compared to those of treated at 80 °C/0.5 h, though it increased as compared to those of untreated samples.

4.10 Biocompatibility

The SEM micrographs (Figures 4.26-4.29) show both morphology and numbers of attached cells on different substrates.

The numbers of cells attached on untreated UHMWPE (Figure 4.26a) surface were much lower than on 80 °C/0.5 h and 100 °C/0.5 h ASPN treated UHMWPE (Figures 4.27a-4.28a). In addition, on the untreated surface, adhered cells were round or ovoid in shape (Figures 4.26b-4.26c), the cell edges did not appear attached and filopodial growth was minimal. According to the four stage classification of cell attachment [78], the cells were

mostly in Stage1 to Stage2. However, cells on the ASPN treated surface consisted of a small part of spherical appearance and a large part of flattened appearance with small peripheral filopodia and ruffled edges (Figures 4.27 b,c-4.28 b,c). The cells were more in Stage 2 to Stage 4 with large percentages at Stages 3 or 4. Figure 4.30 presents four stages of cells attaching on surface of UHMWPE ASPN treated at 80 °C and 100 °C.

However, for the UHMWPE sample treated at 130 ºC, the numbers of cells attached on the surface were lower than those on 80 °C/0.5 h and 100 °C/0.5 h ASPN treated UHMWPE but still increased comparing to those on untreated samples. The appearance of cells appeared progressively blebs and bigger size (Figures 4.29 b,c)

Three samples were used for cell attachment assessments for each condition (untreated and plasma treated). Cell density for all conditions (untreated and plasma treated) was compared by counting the average number of cells from 15 fields (i.e. 5 fields on each sample). The average and standard deviation are shown in Figure 4.31.

According to Figure 4.31, each mean of the two samples treated by plasma when compared with that of the untreated sample is significantly different (t test, two tailed, p = <0.01). Clearly, significantly more cells attached to the plasma treated UHMWPE surface than to the untreated UHMWPE surface.

Therefore, the comparative study indicates that osteoblast cell adhesion and spreading are better on the ASPN treated at 80-100 ºC UHMWPE surface than on the untreated surface.

5 Polyurethane (PU) results

5.1 DSC

DSC was carried out on untreated PU sample to study its glass transition temperature. In the test the temperature of PU sample increased from room temperature to 150-170 ºC with a heating rate of 10 ºC min^{-1}, 20 ºC min^{-1} and 40 ºC min^{-1}, respectively. Figure 5.1 shows DSC curves of polyurethane at three different heating rates. Glass transitions may occur as the temperature of an amorphous solid is increased. These transitions appear as a step in the baseline of the recorded DSC signal. This is due to the sample undergoing a change in heat capacity; no formal phase change occurs. As T_g depends on heating history and is subject to thermal lag, extrapolation to zero heating rate yields an accurate value for T_g, which is 112.5 ºC at 0 heating rate. Figure 5.2 shows the relation between glass transition temperature T_g and heating rate.

5.2 XRD

XRD was carried out on active screen plasma treated samples and also on untreated samples for comparison. The XRD results of PU before and after plasma treatment are shown in Figure 5.3.

As evidenced in Figure 5.3, the diffraction profiles show an amorphous broad shoulder, diffused diffraction maximum at $2\theta = 20°$. It is likely that some soft segment-hard segment phase mixing could occur in the system disturbing the soft segment crystallization [167]. This may account for the broader diffraction. The two patterns are very similar, which means no significant changes in crystal structure and degree of crystallinity during active screen plasma nitriding of PU.

5.3 FTIR

FTIR tests were carried out to study the change of surface functional groups during active screen plasma treatment, and the FTIR spectra of PU are shown in Figure 5.4.

On inspection of the higher wavenumber end of the spectrum, absorbance peak at 3300 cm^{-1} can be attributed to N-H stretching (hydrogen bonded) vibration, while the broad shoulder which appears at around 3450 cm^{-1} is due to non-hydrogen-bonded N–H bonds [161]. There are also absorbance peaks at 2930 cm^{-1} and 2850 cm^{-1}, due to C-H stretching vibration. Furthermore, there are important information given between 1800 cm^{-1} and 1000 cm^{-1}. The strong absorbance band at 1700 cm^{-1} is ascribed to C=O stretching in hydrogen-bonded urethane, while, the broad shoulder of the peak at 1730 cm^{-1} is indicative of C=O stretching in non-hydrogen-bonded urethane [161]. The absorbance peak at 1305 cm^{-1} is ascribed to C-O stretching, the absorbance peak at 1600 cm^{-1} is ascribe to N-H bending vibration, the absorbance peak at 1520 cm^{-1} is due to coupling of N–H bending and C–N stretching, and the absorbance peak at 1218 cm^{-1} is ascribe to C-N stretching band [161].

After ASPN treatment, all absorbance peaks decreased. Although variations in the peak intensity depend on operation of each test, the ratio of absorbance values of treated PUs compare with those of untreated PU at the same wavenumber ($A_{treated}/A_{untreated}$) provides a suitable approach to know the changes of each components. If the ratios ($A_{treated}/A_{untreated}$) at different wavenumber are all the same, it implies that there is no changes of each components after plasma treatment. If a ratio is smaller than others at specified wavenumber, the amounts of the component decrease after plasma treatment. If larger, the amounts of the component increase or a new component forms after plasma treatment.

The main description of FTIR data and the ratio of the absorbance value of treated sample compared with untreated sample at each wavenumber are listed in Table 5.1.

5.4 XPS

In order to know how the surface functional groups have changed during active screen plasma nitriding, XPS characterisation has been carried out in chemical research centre in Hungarian Academy of Science.

The chemical composition of the top surface of the pristine (untreated) and that of the ASPN treated sample is given in Table 5.2. In addition to the constituent elements, a minor amount of Si and, after treatment, also Fe contaminants were also detected. It is obvious that the most significant change is observed in the N-content. The alteration is expressed in the increase of its atomic concentration and it is even more pronounced in the N/C and in N/O atomic ratio.

These major compositional changes connected with major alterations in the chemical bonding states of the constituent elements. This is manifested in the changes of the shape and intensity of the C1s, O1s and N1s lines, as depicted in Figure 5.5a-5.5c. Fitting the lines with components the chemical states of the elements are presented for the untreated and treated states in Figure 5.6 a,b, Figure 5.7 a,b, and Figure 5.8 a,b for the C1s, O1s and N1s peaks, respectively. The chemical states were identified by the energy shift of the components [168].

The C 1s peak envelope, depicted in Figures 5.5a and 5.6a, is composed of three components. The major component at 285.0 eV (reference) corresponds to $-CH_2-$ type carbon of the polymer chain, while the one at 286.5 eV is assignable to $-C-O-$ and $-C-NH-$ and the one at 289.7 eV to carbon atoms in the ―$(C=O)-O$―bonding state [168].

After plasma treatment (Figures 5.5a and 5.6b), the peaks of $-CH_2-$, $-C-O-$ and $-(C=O)-O-$ groups decreased which means that in the urethane group ($-CO-O-R-$**O$-(C=O)-$**

66

NH–R'–NH–), the part of carboxyl groups (—(C=O)—O—) were broken and transformed to another, more probably, to HO—C groups.

In the O 1s spectra, shown in Figure 5.5b and 5.7a,b, the intensity of the peak at 533.2 eV, assigned to the C—O—C group [168] decreases significantly, while that at 532 eV increased. This increase could not be connected with the increase of the amount of –(C=O)–O–, because its decrease was clearly determined by the diminishing intensity of the 289.7 eV component of the C 1s line (Figure 5.5a). As a consequence, we attributed this increase (in accordance with the IR results) to the development of HO–C groups, because chemical shift of oxygen in the –OH groups may fall to this energy range. These self-consistent changes of the C 1s and O 1s lines indicate that the carboxyl groups are decomposed and hydroxyl groups are developed after plasma treatment.

The third component, appeared at 530.7 eV in the O 1s spectrum after treatment (Figure 5.7 b), corresponds to O atoms bonded to the oxidized FeOOH type contamination which came from the stainless steel mesh.

The most significant change was observed from the comparison of the N1s spectra (Figures 5.5 c and 5.8 a,b) recorded before and after plasma treatment. The large increase of the intensity of the N1s spectrum can be related partly to the relative stability of the C-NH-C bonds [169] at such treatment and partly to the preferential surface enhancement and aggregation of the N-containing groups due to the nitriding effect of the ASP treatment. In the light of the increased N-content the overall decrease of the carbon signal, even that of the –(CH$_2$)$_n$– polymer chain, can be easily understood.

As concerning the chemical state of nitrogen, the following observations could be made. In the untreated sample, as expected, the narrow N 1s line is at 400.4 eV, i.e. the nitrogen is in one single chemical state in the urethane (-OOC-NH-C-) group. As it was

expressed above, these groups are partly decomposed, and new species appeared: at 399.7 eV C-N-C and C≡N states developed and the low energy peak at 398.7 eV assignable to the – C=N– groups, multiply detected in and reported for the plasma deposited carbon-nitride (CN_x) coatings [170]. And another reason could probably be attributed to N_2 is being released from the polymer as bubbles to the surface.

5.5 Surface roughness

The surface roughness was measured before and after plasma treatments in order to study the plasma treatment effect. For each PU sample specimen, surface roughness was measured before and after plasma treatment to compare effects on surface roughness induced by plasma treatment at different treatment conditions. Detailed surface roughness information can be found in Table 5.3 and Figure 5.9.

All the results are also shown in these four bar charts (Figure 5.9). The blue bar is for untreated sample, while the red bar is for plasma treated sample.

From the results, it can be seen that for most samples after plasma treatment, their surface roughness changed little. When plasma treatments were performed under 80 °C, the increases of surface roughness are all under 15% no matter for how long the treatment was performed. When plasma treatment was performed at 100 °C, the increases of surface roughness are all under 18% after treatment for 0.5 or 1h; the surface roughness increased by 30% and 87% after treatment for 2 or 5h, respectively. When plasma treatment is performed at 130 °C for 0.5 and 1h, the increase of surface roughness are still under 30% (by 11% and 27%, respectively). Only at 130 °C, after treatment for 2 or 5 h, does surface roughness increase significantly (increased by 683% and 253%, respectively). It is because 130°C is beyond T_g (112°C) of PU, the polymer chains undergo a large change in mobility and produce

surface deformation at treatment performed at this temperature. The significant increase in surface roughness is probably due to surface deformation by thermal stress.

5.6   AFM

The AFM images of untreated and plasma treated PU were obtained in contact mode in air. Figures 5.10 –5.14 show the topographical measurements of the untreated and treated PU surface obtained by AFM.

According AFM images, the surface of untreated polyurethane presents a closed cell structure. After plasma treatments, cracks and pores can be formed on the surfaces. As the treatment temperature increases, the depth of cracks and pores also increase accordingly. See Section 7.2.1.1.

5.7   SEM

Surface morphology was characterised by SEM (Figures 5.15- 5.19).

From the SEM and AFM images, it can be seen that untreated polyurethane (Figure 5.10 and Figure 5.15) has a closed cell structure with only a small portion of open cells. The percentage of the pore area on the surface is only about 4.9% (calculated according Figure 5.10 by Image J 1.44 analysis software).

Treatment temperature and time play an important role in determining changes in surface topography. When plasma treatment is performed at relatively low temperatures (≤100°C) for not more than 1 hour, small cracks and pores can be formed on the surface; in contrast, higher proportion of larger, more rounded pores can also be found on the surface when plasma treatment performed at high temperature (130°C) for longer time (≥2 h).

For example, after plasma treatment at 80 °C for 0.5h, (Figure 5.17a and 5.12a), there are some small cracks and pores on the surface and no separate cells can be observed. The percentage of the pore area on the surface increased to about 9.2% (calculated according Figure 5.17a by Image J 1.44 analysis software). However, after plasma treatment 130 °C for 0.5h (Figure 5.19a and 5.14a), many cells are broken and there are some small pores at the bottom of the broken cells; in addition, more larger and round pores can also be found on the surface. The percentage of the pore area on the surface increased at about 24.2% (calculated according Figure 5.19a by Image J 1.44 analysis software).

5.8   Nano-hardness and modulus

Nano-hardness (H) and modulus (E) of the untreated and ASPN treated PU samples were measured and the results are shown in Table 5.4 and Figures 5.20-5.21.

According to Table 5.4 and Figures 5.20-5.21, the nano-hardness of PU surface increased after plasma treatment and modulus of plasma treated PU surface almost maintained the same values compared with untreated sample (except for PU80-0.5h). As a result, the value of H/E increased with the increase of treatment temperature and time.

5.9   Wear resistance

a) Pin-on-disc wear tests results

Pin-on-disc wear track topography for the untreated and ASPN treated polyurethane are shown in Figure 5.22.

According to Figure 5.22, the difference of wear tracks between untreated and treated samples is clear. After plasma treatment at 80°C for 1h, the wear track of the sample is more superficial and the track width is also found to be slightly smaller than that on untreated

sample. While, after plasma treatment at 130°C for 1h, the wear track of the sample is rougher and the track width is slightly wider than that on untreated sample.

The improvement of wear resistance is shown in Table 5.5 and Figure 5.23.

As can be seen from Figure 5.23, ASPN surface treatment has an interesting effect on polyurethane samples. Plasma treatment at 80-100 °C for half hour or 1h, wear resistance improved. As treatment temperature and time increased, the wear resistance decreased. It seems that active screen plasma nitriding offers the possibility to improve the wear resistance of polyurethane although the effect is highly dependent on the treatment conditions.

 b) Reciprocating movement wear tests results

According to the results of pin-on disc wear results, the samples treated by plasma for 0.5h at different temperature were chosen to perform reciprocating movement wear tests. For each sample, reciprocating movement wear tests were carried out with 10000 cycles under different loads (9.81N, 19.62N), respectively. Reciprocating movement wear areas of PU before and after plasma treatment are listed in Table 5.6.

According to Table 5.6, when reciprocating movement wear tests were carried out with 10000cycles and under 9.81N loads, the wear area of the samples plasma treated at 80°C for 0.5h decreased to a different extent.

For the sample PU80-0.5h and untreated sample (PU0), wear tests were carried out at 10000cycles under different loads (9.81N, 13.73N, 19.62N) to compare the effect of loads in wear tests. The wear areas of untreated (PU0) and plasma treated PU (PU80-0.5h) at different loads (10000cycles) are shown in Figure 5.24. According to Figure 5.24, the wear areas increase as loads increase. When load is 9.81N, wear areas of plasma treated samples are

smaller than those of untreated samples; when load increases to 13.73N, wear areas of plasma treated samples are bigger than those of untreated samples.

5.10 Contact angle and surface energy

The surface properties in terms of surface free energy of polyurethane samples, as characterization by static contact angle, are reported in Table 5.7 which also represents the results of contact angle of two liquids (distilled water and glycerol), with different polarity.

It is clear from the results that surface free energies of plasma treated samples for 0.5h and 1h are higher than that of untreated samples. When treatment time increased to 2h and 5h or decrease to 10min, surface free energies decreased. The increase in surface energy could be mainly attributed to the increase of polar part of the surface energy. In general, high energy surfaces are hydrophilic, it induce the increase of hydrophilicity of the surface.

On the other hand, it must be noted that contact angles of two liquids on plasma treated samples increased compared with untreated sample. However, the relation between θ_{Water} and $\theta_{Glycerol}$ changed from $\theta_{Water} > \theta_{Glycerol}$ for the untreated material to $\theta_{Water} < \theta_{Glycerol}$ for the plasma treated one. This is because plasma treatment induced the rearrangement of the whole polymer chain and formed a special layer on surface. This region exposed polymethylene chains (**R** and **R'** parts in –CO–O–**R**–O–CO–NH–**R'**–NH–) to the water droplet, thus yielding a moderate shielding effect and producing a higher than expected contact angle. Clearly, an important difference exists between hydrophilic surfaces and low contact angle surfaces: the former can adsorb some water or moisture from surroundings. Their surface and subsurface zone could be extensively hydrated, yet the water contact angle can be similar to that of hydrophobic polymers[66].

5.11 Biocompatibility

a) Cell Culture for 3Days on PU surface

The scanning electron micrographs (Figure 5.25-5.29) clearly show both morphology and proliferation of cells are different, depending on the substrate condition. All plasma treated PU samples show better cell proliferation.

b) Cell proliferation

Figure 5.30 shows the MTT assay result after cell culture for 7days. According to Figure 5.30, the MTT results increased for all plasma-treated PU samples. When the treatment temperature is 80°C, as treatment time increases from 0.5h to 5h, the MTT value decreases. When the treatment time is 0.5h, as treatment temperature increases from 80°C to 130°C, the MTT value increases first, then decreases. Among them, the MTT value of PU100-0.5h is the highest.

6 Polycaprolactone (PCL) results

6.1 DSC

DSC was carried out to identify the melting point of untreated polycaprolactone (PCL). During the test, the temperature of the PCL sample increased from room temperature to 80ºC at a heating rate of 10 ºC min^{-1}, and the measured DSC curve is shown in Figure 6.1.

It can be seen from Figure 6.1 that as the temperature increases from room temperature to around 60 ºC, a peak appears in the DSC curve. This indicates that the PCL sample eventually reached its melting temperature (T_m) and the melting process results in the endothermic peak in the DSC curve. The melting temperature of the PCL sample was determined to be 59.9 ºC ± 0.1 ºC from the original data of the DSC curve.

6.2 XRD

In order to study the effect of active screen plasma treatment on the structure of PCL, XRD was conducted on active screen plasma treated samples as well as on untreated samples for comparison. The XRD charts of PCL before and after plasma treatment are shown in Figure 6.2 and the quantitative results are summarised in Table 6.1.

According to Figure 6.2, PCL is a semi-crystalline material with an amorphous halo at around 20.5° and three crystal peaks at 21.4, 22.0 and 23.7°. After plasma treatment the crystal peaks increased their intensities and shifted to the right slightly. It is considered due to production of inner tensile stress after treatment.

As can be seen from XRD patterns, the crystal peaks increased and shifted to higher angle position (right) slightly by plasma treatment. Comparison of full width at half maxima

(FWHM) of the original crystalline peaks of the virgin sample with those of the plasma treated one (Table 6.1), decrease in FWHM value suggests that smaller lamellas (crystallites) are developing into bigger ones, and the increase in peak height and area suggests an increase of crystallinity.

The reasons are analysed below. When the semicrystalline polycaprolactone is treated by ASPN, the long molecular chains of the amorphous regions may be broken at different places, leaving a free smaller chain which immediately comes to a stable position by collecting its whole length to create new crystallites or lamellas; whereas the crystalline region lamellas may be rearranged by plasma treatment. This indicates that crystallites or lamellas are growing into bigger ones. The shifting in the diffraction peak position of the samples towards higher angle is because of developing the tensile microstrain of PCL crystallites due to presence of active screen plasma.

6.3 FTIR

In order to study the change of surface functional groups during plasma treatment, FTIR measurements were carried out on both plasma treated and untreated PCL films. The typical FTIR spectra of PCL films before and after plasma treatment are shown in Figures 6.3 and 6.4.

The infrared spectra of PCL (Figure 6.3) exhibit absorption bands from 4000 to 500 cm^{-1} associated with their characteristic groups. The bands at 2944 and 2865 cm^{-1} are characteristic of C-H stretching vibration. The strong absorbance band at 1721 cm^{-1} is ascribed to C=O stretching. The 1160 cm^{-1} band is due to the presence of a C–O–C group, while the 1238 cm^{-1} band is due to a C–C–O group in the structure. The spectra also show a band at 960 cm^{-1} due to C–CH$_3$ stretching [161].

After plasma treatment, the intensity of almost all peaks decreased marginally except for the band between 3500 cm^{-1} to 3100 cm^{-1}. According to Figure 6.4, a wide absorbance peak at about 3260 cm^{-1} (ascribed to the hydroxyl group, -OH) [161] was generated in PCL by the ASPN treatment.

It is known that during plasma treatment of polymers chain scission, crosslinking and the formation of hydroxyl groups are the most common reactions. Firstly, PCL is a crosslinkable polymer because it can produce insoluble gel when exposed to gamma rays [94, 171, 172]. The principle of the crosslinking process induced by plasma should be similar to that of an irradiation process. Secondly, new hydroxyl groups were formed by obtaining energy from plasma, followed by detachment of a hydrogen molecule in plasma.

6.4 XPS

XPS measurements were carried out to characterise changes in the composition and chemical structure of the surface during ASPN treatment. The chemical composition of the top surface of the untreated and that of the ASPN treated sample is given in Table 6.2. The composition of the as-prepared PCL film was as follows: C=75.7 at%, O=24.3 at%. After treatment it became C=77.5 at%, O=21.4 at% and N=1.1 at%, which indicate some oxygen loss and build-up of a small amount of nitrogen. The C 1s peak envelope, depicted in Figure 6.5, is composed of three components of approximate 1:1:4 atomic ratios, as expected. The major component at 285.0 eV (reference) correspond to –CH$_2$– type carbon, of the polymer chain, while the one at 286.5 eV assignable to –C–O– and the one at 288.9 eV to carbon atoms in the ―(C=O)―O― bonding state [168]. In the C 1s XPS spectra (Figure 6.5), it can be seen that after plasma treatment, the intensity of this latter component at 288.9 eV decrease which indicates that part of the ―(C=O)―O― groups were broken and transformed to another, more probably, to HO―C groups. In line with this, a new C 1s component appeared

at about 287.2 eV. In addition to this, some loss of C=O may also occur as indicated by the change of the overall composition.

In the O 1s spectra, shown in Figure 6.6, the intensity of the peak at 533.5 eV, assigned to the C—O—C group [168] decreases, in agreement with the decrease of the corresponding C 1s component at 288.9 eV.

The intensity of the O 1s peak-component for the C=O at 532.0 eV also decreased somewhat, and a new O 1s component appeared at 532.6 eV, assignable to oxygen atoms in C—OH bonding environment [168]. These self-consistent changes indicate that the carboxyl groups are decomposed and hydroxyl groups are developed. This result is in agreement with that obtained by FTIR (Section 6.3).

6.5 Raman spectra

Rama spectra of PCL films before and after plasma treatment are shown in Figure 6.7. The Raman spectra of PCL exhibit absorption bands from 4500 cm^{-1} to 500 cm^{-1} associated with their characteristic groups. The bands at 2918 and 2865 cm^{-1} are characteristic of C-H stretching vibration. The absorbance band at 1721 cm^{-1} is ascribed to C=O stretching. The 1440 cm^{-1} band is due to the presence of a C–H group, while the 1303 cm^{-1} band is due to a C–C group in the structure. The spectra also show a band at 1108 cm^{-1} due to C–O–C stretching [173, 174].

Before plasma treatment, the ratio of intensity at 1440cm^{-1} and 1303 cm^{-1} (I_{1440}/I_{1303}) is 1.3841>1, which means that the intensity of C-H group is higher than that of C-C group. After plasma treatment, the ratio of intensity at 1440cm^{-1} and 1303 cm^{-1} (I_{1440}/I_{1303}) is 0.9344 <1, which indicates that the intensity of C-H group is lower than that of C-C group. The change in the ratio of intensity at 1440cm^{-1} and 1303 cm^{-1} (I_{1440}/I_{1303}) demonstrates the

increase of C-C group after plasma treatment, which could be an indication of crosslinking of PCL chains on PCL surface after plasma treatment.

6.6 Surface topography

Surface roughness of PCL sample specimen was measured before and after plasma treatment to study the effect on surface roughness induced by plasma treatment. It can be seen from Table 6.3 that there is no significant change in surface roughness following active-screen plasma treatment.

Typical AFM images of PCL were obtained in contact mode in air. Figures 6.8 and 6.9 show respectively the topographical measurement results of the untreated and treated PCL surface obtained by AFM. It can be seen that no significant difference in surface topography could be observed for the plasma treated and untreated surfaces.

Figures 6.10 and 6.11 show the typical surface topography of the untreated and plasma treated PCL surfaces obtained by SEM. No appreciable difference in SEM surface topography could be found, which is in line with the results of AFM and profilometer measurements. Clearly, short-time active screen plasma treatment did not cause any appreciable change in the surface topography of PCL films.

6.7 Contact angle and surface energy

The surface free energy of plasma treated and untreated PCL samples were studied by measuring the static contact angle of two different liquids (distilled water and ethylene glycol). The measured contact angle of these two liquids with different polarities on both plasma treated and untreated are given in Table 6.4. Based on the method described in Chapter 3, the surface energy was calculated and the results are also shown in Table 6.4.

It is clear from the results that the surface free energy of the plasma treated samples is higher than that of the untreated samples. The contact angles of these two liquids on the surface of the plasma treated samples all decreased compared with the untreated samples. It can be seen from Table 6.4 that after plasma treatment, water tensile drop contact angle decreased from 75.1º to 71.0º, which indicates increased wettability of the plasma treated surface; correspondingly, the surface energy increased by 3.11 mN/m (from 28.76 to 31.87 mN/m). Among them, the polar part increased 2.8 mN/m (from 19.16 to 21.96 mN/m), which accounts for 90% of the increased surface energy.

6.8 Biocompatibility

a. Cell attachment for 1h

The SEM micrographs in Figures 6.12 and 6.13 clearly show that both topography and numbers of attached cells are different, depending on the substrates.

The number of cells attached to the untreated PCL film surface (Figure 6.12) is much lower than that attached to ASPN treated PCL (Figure 6.13). In addition, on the untreated surface, adherent cells were round or ovoid in shape, the cell edges did not appear attached and filopodial growth was minimal (Figure 6.12). According to Rajaraman's four stages of cell attachment [78], the cells on the untreated surfaces were more in Stage 1. On the other hand, however, cells on the ASPN treated surface had a spherical and flattened appearance with peripheral filopodia (Figure 6.13). The cells were in Stage1 to Stage 3 with large percentages at Stages 2 or 3.

Three samples were used for cell attachment assessments for each condition (untreated and plasma treated). Cell density for both conditions (untreated and plasma treated) was compared by counting the average number of cells from 15 fields (i.e. 5 fields on each sample). The average and standard deviation are shown in Figure 6.14. According to Figure

6.14, the mean of the two samples were significantly different (t test, two tailed, $p = 4.14 \times 10^{-7}$ <0.001). Clearly, significantly more cells attached to the plasma treated PCL surface than to the untreated PCL surface.

b. Cell proliferation

Figures 6.15 and 6.16 show typical SEM micrographs of cell culture for 3 days onto untreated and plasma treated PCL, respectively. As can be seen from Figures 6.15 and 6.16, MC3T3 cells on plasma treated PCL surface exhibit higher cell numbers and cover more surface area when compared with those on untreated PCL surface. It is clear that an increase in the cell proliferation was observed over the entire culture period (3 days).

c) Cell metabolic activity

One of the objectives of this study was to determine if plasma treatment affected cellular activity. To test this premise, the ability of live, metabolically active cells to reduce a tetrazolium salt, MTT, was measured.

MTT assay results after 7 days cell culture for untreated and plasma treated PCL surfaces are compared in Figure 6.17. It can be seen that after plasma treatment, the MTT value increased from 0.26 to 0.36 representing an increase of 38.5%. The results demonstrate that the activity of MC3T3 cells is higher when grown on plasma treated PCL surface than on untreated surfaces over a 7-day period.

6.9 Degradability

In order to study the effect of plasma surface treatment on the degradation of PCL, the mass lose of both untreated and plasma treated PCL in PBS solution containing lipase from *Pseudomonas cepacia* as a function time was recorded in Figure 6.18.

It can be seen that both the untreated and treated PCL films finally disappeared. The untreated PCL film was totally degraded within 24 h when it was in PBS solution containing lipase from *Pseudomonas cepacia*. In the first 17 h, the degradation rate was faster. With the plasma treated PCL film, degradation was completed within 36 h. In the first 29 h, the degradation rate was faster.

Figures 6.19 and 6.20 show respectively the SEM images of untreated and treated PCL films as a function of immersion time after enzymatic degradation. Before the degradation tests, the appearance of both untreated and treated PCL films was almost the same. During degradation of untreated PCL film, the roughness of the surface and the depth of holes increased with time. After degradation for 19 h, holes were produced in both the surface and the bulk body and the sample became highly porous.

From comparison of Figure 6.19 and Figure 6.20, it is clear that the topography of the plasma treated PCL film is quite different from that of the untreated PCL film. During degradation of plasma treated PCL film, as mass loss increases, the films become thinner without obvious large holes occurring on the surface. After degradation for 24 h, the plasma treated PCL film starts to be broken. This could be attributed to the crosslinking of the topmost surface layer of the PCL film after plasma treatment. It also shows that plasma treated PCL is degradable but needs a longer time to completely degrade.

7 General discussion

7.1 Effect on surface chemistry

The surface chemistry of a polymer is of importance in many of the applications. Therefore, detailed examination of the surface chemistry of plasma treated UHMWPE, PU and PCL has been conducted using FTIR, XPS and Raman.

7.1.1 UHMWPE

Infrared spectroscopic methods allow the surface chemical structure and composition in the order of microns to be characterized. FTIR spectra of UHMWPE are shown in Figure 4.5.

For untreated UHMWPE, absorbance peaks at 2930 cm^{-1} and 2850 cm^{-1} are ascribed to the methylene (CH_2-CH_2) C-H asymmetric and symmetric stretching vibration, absorbance peak at 1460 cm^{-1} is ascribed to the methylene (CH_2-CH_2) C-H bending vibration, absorbance peak at 720 cm^{-1} is ascribed to $(CH_2)_n$ rocking band. After ASPN treatment, all the peaks above that show the main characteristic bands associated with aliphatic hydrocarbons are still in spectra with a very small new peak appearing.

In Figure 4.5, it can be seen that an absorbance peak at 965 cm^{-1} (ascribed to the transvinylene group, -CH=CH-) and a peak at 910 cm^{-1} (ascribed to the terminal vinyl group, -CH=CH_2) are generated in UHMWPE after ASPN treatment. During plasma treatment of UHMWPE, chain scission, crosslinking, and the formation of transvinylene units are the most common reactions. The principle of the process should be similar to that of an irradiation process [175, 176]. Transvinylene unsaturations are formed by obtaining energy from plasma, followed by detachment of a hydrogen molecule and, to a lesser extent, by the recombination of two adjacent alkyl free radicals residing on the same chain. Transvinylene groups appear in
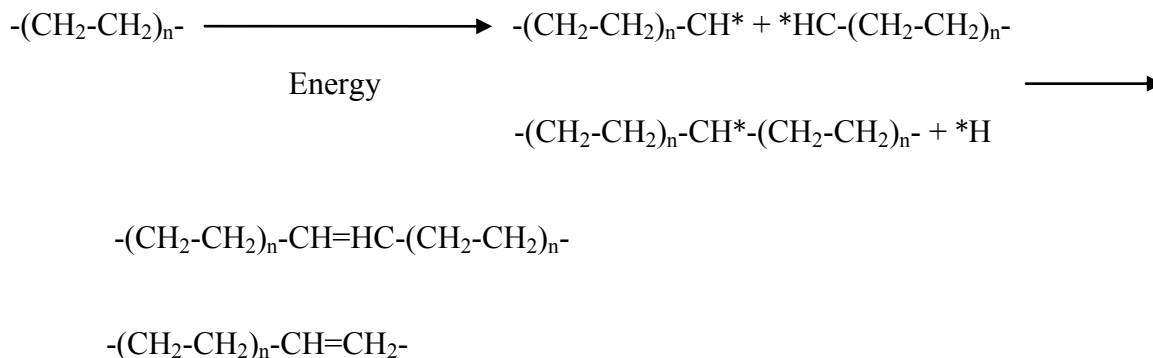
polyethylene as a plasma modification product during exposure to plasma environment with a yield related to the number of crosslinks formed [177]. The presence of a terminal vinyl group usually means that the polymer chain has broken, which will leave behind a vinyl group on each end [34].

Despite the fact that UHMWPE is the simplest polymer in terms of its structural repeat unit, it produces some complex infrared bands. The spectra of UHMWPEs are complicated because of the phenomenon of crystal field splitting. As PE has a small repeat unit which packs efficiently, an ethylene unit of one chain will be in close proximity to a unit in the adjacent part of the chain and there is an interaction between these units. Such an interaction results in the doubling of the normal modes, as one interacts with and perturbs the other unit. For UHPMWE, crystal field splitting results in doublets at 734 and 720 cm^{-1} (CH$_2$ rocking) and 1475 and 1460 cm^{-1} (CH$_2$ bending) in infrared spectra (Figure 7.1).

Considering of crosslinking reactions are governed by radical reactions and large amount of free radicals in plasma, as well as same new functional groups (transvinylene group and terminal vinyl group) produced, the mechanism of plasma induced cross-linking is very similar to that of irradiation method [34, 176-178]. The mechanism of cross-linking in UHMWPE under interaction of high-energy excited species can be visualized by following scheme:

1.   ASPN:

Excited species: electrons,
ions, atoms, molecules,
free radicals, metastables

$-(CH_2-CH_2)_n-$ $\longrightarrow$ $-(CH_2-CH_2)_n-CH^* + {}^*HC-(CH_2-CH_2)_n-$

Energy

$-(CH_2-CH_2)_n-CH^*-(CH_2-CH_2)_n- + {}^*H$ $\longrightarrow$

$-(CH_2-CH_2)_n-CH=HC-(CH_2-CH_2)_n-$

$-(CH_2-CH_2)_n-CH=CH_2-$

2. Cross-linking:

$2(CH_2-CH_2)_n-CH^*-(CH_2-CH_2)_n$ $\longrightarrow$ $(CH_2-CH_2)_n-CH-(CH_2-CH)_n$
$|$
$(CH_2-CH_2)_n-CH-(CH_2-CH)_n$

$-(CH_2-CH_2)_n-CH=CH_2 + -(CH_2-CH_2)_n-CH^*-(CH_2-CH_2)_n-$ $\longrightarrow$

$CH-CH_2-CH^*-(CH_2-CH_2)_n-$
$|$
$-(CH_2-CH_2)_n-CH-(CH_2-CH)_n-$
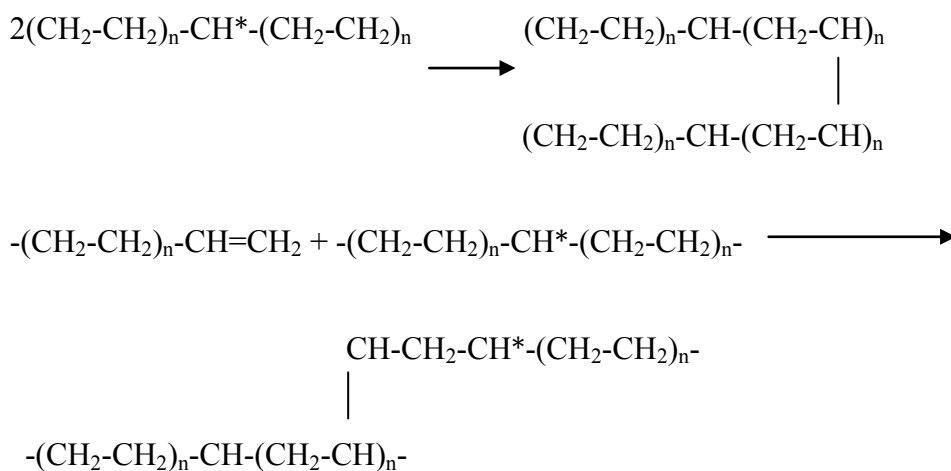
During ASPN treatment, samples are placed in plasma environment at elevated uniform temperature. The plasma is composed of a large concentration of highly excited atomic, molecular, ionic, and radical species. The free radicals as well as other metastable particles that break covalent chemical bones upon collision with the surfaces of polymers placed in the plasma environment, thus creating free radicals on the polymer surface. Their interaction with UHMWPE leads, through a complex energy transfer, to the scission of C-C and C-H bonds, giving H radicals and primary and secondary macroradicals. These

macroradicals are dispersed throughout both the crystalline and the amorphous phases of the polymer. The free radicals then undergo additional reactions, including chain scission, crosslinking, and the formation of transvinylene unites. The trans-vinylene groups appearing in UHMWPE are related to the number of crosslinks formed [177]. And the concentration of the trans-vinylene unites can be readily measured by infrared spectroscopy using the characteristic absorbance at wavenumber 965 cm^{-1} on the IR-spectrum of plasma treated UHMWPE. Figure 4.6 shows the IR-spectra of untreated and ASPN treated UHMWPE, demonstrating a characteristic absorbance of the trans-vinylene vibration after ASPN treatment. The amorphous phase in UHMWPE consists of randomly oriented and entangled polymer chains from neighboring molecules. Although radicals induced by plasma spread randomly throughout the polymer, the reactivity of alkyl radical is much higher in the amorphous region than in crystalline region due to chain mobility in the amorphous region [34, 178, 179]. Therefore, the crosslinks form preferentially in the amorphous region and the interfacial regions. The radicals in the crystalline regions migrate along the straight crystalline stems within the lattice without reacting. The reaction then occurs in the interfacial or amorphous regions [180].

7.1.2 PU

In order to know how the surface functional groups change on PU after ASPN treatment, FTIR and XPS tests have been carried out.

FTIR spectra of PU are shown in Figure 5.4.

For untreated PU, on inspection of the higher wavenumber end of the spectrum, absorbance peak at 3300 cm^{-1} can be attributed to N-H stretching (hydrogen bonded) vibration, while the broad shoulder which appears at around 3450 cm^{-1} is due to non-hydrogen-bonded N–H bonds. There are also absorbance peaks at 2930 cm^{-1} and 2850 cm^{-1}, due to C-H

stretching vibration [161]. Furthermore, there are important information given between 1800 cm^{-1} and 1000 cm^{-1}. The strong absorbance band at 1705 cm^{-1} is ascribe to C=O stretching in hydrogen-bonded urethane, while, the broad shoulder of the peak at 1730 cm^{-1} is indicative of C=O stretching in non-hydrogen-bonded urethane [161]. The absorbance peak at 1305 cm^{-1} is ascribed to C-O stretching, the absorbance peak at 1600 cm^{-1} is ascribed to N-H bending vibration, the absorbance peak at 1520 cm^{-1} is due to coupling of N–H bending and C–N stretching, the absorbance peak at 1218 cm^{-1} is ascribed to C-N stretching band [161].

After ASPN treatment, although all absorbance peaks decrease, the percentage of decreased absorbance values of plasma treated samples compare with those of untreated PU at same wavenumber is different. The main FTIR data before and after ASPN treatment are summarized in Table 7.1.

According to the information from infrared spectroscopy, there are two main changes in chemical structure on the PU surface after ASPN treatment. One is concerned with the changes of functional groups. The other is associated with the changes in hydrogen bonds. The two types of changes will be discussed below, respectively.

The physical properties of polymers are affected by the structures of the molecular chains. ASPN treatment gives an effective method to change functional groups on polymer surface. From Table 7.1, it can be easily observed that most absorbance peaks decrease about 20% with two exceptions. One peak is at 1705 cm^{-1} which is due to C=O stretching [161]. It decreased by 28%, more than most other peaks, which indicates that C=O groups were reduced after ASPN treatment. The other peak is at 3300 cm^{-1} which is due to N-H stretching [161]. It decreases only by 9.3%, less than most other peaks. As the N-H bending bands at 1596 cm^{-1} and 1521 cm^{-1} [161] all decrease at average lever (about 20%), there should be some new groups formed at 3300 cm-1 band. Because of O-H stretching appearing broad

band at 3300cm^{-1} [161], it can be identified that new O-H groups form after ASPN treatment. From the analysis above, a conclusion can be drawn that ASPN treatment results in broken C=OO groups and new O-H groups formed on the surface top layer.

Hydrogen bonding is defined as the attraction that occurs between a highly electronegative atom carrying a non-bonded electron pair (such as fluorine, oxygen or nitrogen) and a hydrogen atom, itself bonded to a small highly electronegative atom. Hydrogen bonding is also an issue for polyurethanes (PUs), which have the general structure, –CO–O–R–O–CO–NH–R'–NH–. PUs are extensively hydrogen bonded, with the proton donor being the N–H group of the urethane linkage. The hydrogen-bond acceptor may be in either the hard segment (the carbonyl of the urethane group) or in the soft segment (an ester carbonyl or ester oxygen). In the infrared spectra of PU, the ratio of the absorbances of C=O stretching (non-hydrogen bonded urethane) at 1730 cm^{-1} and C=O stretching (hydrogen bonded urethane) at 1705 cm^{-1} may be employed as a measure of changes in hydrogen bonding by plasma treatment. The main changes of FTIR data at 1730 cm^{-1} and 1705 cm^{-1} before and after ASPN treatment are listed in Table 7.2. Effects of treatment temperature and time on changes observed in the spectra are shown in Table 7.3

From Table 7.2, after ASPN treatment, the absorbance value of C=O stretching (hydrogen bonded urethane) at 1705 cm^{-1} decreased to 72.0%, while the absorbance value of C=O stretching (non-hydrogen bonded urethane) at 1730 cm^{-1} decreased to 75.6%. According to Table 7.3, before ASPN the ratio of A_{1730}/A_{1705} is 84.2%, while after ASPN the ratio of A_{1730}/A_{1705} (PU100-2h) increases to 88.4%. These data indicate hydrogen bonding decreases after ASPN treatment.

Hydrogen bonding plays a fundamental role in the structural and physical properties of PU and is the most significant type of intermolecular interaction that influences the infrared

spectrum of this polymer. The changes observed in the spectra with ASPN treatment are due to a breakdown of the hydrogen bonds which occur between adjacent chains. Two reasons can be considered for the decrease of hydrogen bonding.

The first is related to the energy from plasma. The hydrogen bond is stronger than a Van der Waals interaction, but weaker than covalent or ionic bonds. When sufficient energy is obtained from plasma, they can be broken. The second is related to the positions of functional groups. The relative positions of the N–H and C=O groups in the respective PU structures will affect the nature of the hydrogen bonding in each of these molecules. Some new functional groups (such as O-H, C-N, C=N and C≡N) formed by plasma treatment resulted in the changes of the relative positions of the N–H and C=O groups. This should lead to the broken hydrogen bonding not recovering when plasma treatment ends and the temperature drops.

From Table 7.3, effects of treatment temperature and time on hydrogen bonding can be observed. As temperature increases, the ratios of A_{1730}/A_{1705} increase, which indicates that hydrogen bonding decreases after ASPN treatment. Increasing temperature means that each molecule will have more energy on average and weak associative forces, such as hydrogen bonds, are likely to be broken. This should lead to a lesser degree of hydrogen bonding. As time increases, the ratios of A_{1730}/A_{1705} also increase, which indicate hydrogen bonding decreases too after ASPN treatment. It is because more energy will be gained from plasma as treatment time increases. This will cause hydrogen bonds to be broken.

In addition to FTIR, XPS was also used to study the changes in surface chemistry of PU during ASPN. XPS spectra of PU are shown in Figures 5.5-5.8.

In C 1s XPS spectra (Figure 5.5a, 5.6), the black line is for untreated sample and blue line is for the sample by plasma treated at 60°C for 2h. It shows that after plasma treatment the peaks of C-O (286.6eV) group and –(C=O)-O- (289.7eV) group all decrease which means

in urethane group (>HC)-**NH-C=OO-**(CH<), the carboxyl group is broken and changed to other group. While the peak of C-C (285eV) group also diminish which indicate C-C bonds are broken. In O 1s spectra (Figure 5.5b, 5.7), the intensity of the peak at 533.2 eV, assigned to the C—O—C group [168] decreases significantly, while that at 532 eV increased. This increase could not be connected with the increase of the amount of –(C=O)–O–, because its decrease was clearly determined by the diminishing intensity of the 289.7 eV component of the C 1s line (Figure 5.5a). As a consequence, we attributed this increase (in accordance with the IR results) to the development of HO–C groups, because chemical shift of oxygen in the –OH groups may fall to this energy range. These self-consistent changes of the C 1s and O 1s lines indicate that the carboxyl groups are decomposed and hydroxyl groups are developed after plasma treatment. N1s spectra (Figure 5.5c, 5.8) show the peaks of the C-NH (399.7eV) group and C=N (398.7eV) group all increase which indicates that new C-NH bonds , C=N and C≡N bonds are developed.

It is obvious that the main characteristic of the polyurethane chemical group, the (>HC)-**NH-C=OO-**(CH<) is destroyed or transformed to other types of bonds. The addition introduced by the treatment nitrogen will form new types of bonds preferably with the remaining carbon as indicated above. When new functional groups appeared: at 399.7 eV C-N-C and C≡N states developed and the low energy peak at 398.7 eV assignable to the –C=N– groups, multiply detected in and reported for the plasma deposited carbon-nitride (CN_x) coatings [170], the polymer chains are rearranged, cross-linking and three-dimensional (C-N, C=N and C≡N) networks possibly develop. In addition, the hydrophilicity of the surface has increased because hydroxyl group has increased on the surface.

7.1.3 PCL

In order to know how the surface functional groups change on PCL after ASPN treatment, FTIR, Raman and XPS tests have been carried out.

FTIR spectra of PCL films before and after plasma treatment are shown in Figures 6.3 and 6.4.

For untreated PCL, the structure of PCL is $-(-O-(CH_2)_5-CO-)_n-$. On inspection of the higher wavenumber of the spectrum, absorbance peaks are observed at 2944 cm^{-1} and 2860cm^{-1}, due to aliphatic symmetric and asymmetric C–H stretching, respectively. There is also a strong band at 1721 cm^{-1} is indicative of C=O stretching. There is a band due to CH$_2$ bending occur in the 1365 cm^{-1}. The absorbance at 1238 cm^{-1} and 1160 cm^{-1} are characteristic of C–C–O stretching and C–O–C bending, respectively, and the absorbance at 960 cm^{-1} is characteristic of C-CH$_3$ bending. The infrared assignments for this spectrum are listed in Table 7.4.

According to Figure 6.4, it can be seen that a wide absorbance peak at about 3260 cm^{-1} (ascribed to the hydroxyl group, -OH) was generated in PCL after ASPN treatment. The ratios of the peak intensity at 3260 cm^{-1} to 3440 cm^{-1} were 1.43 (treated) and 0.33(untreated), respectively. The ratio (A3260/A3440) of treated sample (1.43) is much higher than that of untreated sample (0.33), implying the increase of hydroxyl groups after plasma surface modification. During plasma treatment of PCL films, the formation of hydroxyl groups is the most common reactions. New hydroxyl groups are formed by obtaining energy from the plasma, followed by detachment of a hydrogen molecule from (or to) the plasma.

XPS measurements were carried out to characterise changes in the composition and chemical structure of the surface during ASPN treatment. The composition of the as-prepared PCL film was as follows: C=75.7 at%, O=24.3 at%. After treatment it became C=77.5 at%, O=21.4 at% and N=1.1 at%, which indicate some oxygen loss and build-up of a small amount of nitrogen. The C 1s peak envelope, depicted in Figure 6.5, is composed of three components of approx. 1:1:4 atomic ratios, as expected. The major component at 285.0eV (reference)

correspond to –CH2– type carbon, of the polymer chain, while the one at 286.5 eV assignable to –C–O– and the one at 288.9 eV to carbon atoms in the —(C=O)—O— bonding state [168]. In the C 1s XPS spectra (Figure 6.5), it can be seen that after plasma treatment, the intensity of this latter component at 288.9 eV decreases which indicates that part of the —(C=O)—O— groups were broken and transformed to another, more probably, to HO—C groups. In line with this, a new C 1s component appeared at about 287.2 eV. In addition to this, some loss of C=O may also occur as indicated by the change of the overall composition.

In the O 1s spectra, shown in Figure 6.6, it can be seen that the carboxyl groups are decomposed and hydroxyl groups are developed. This result is in agreement with that obtained by FTIR.

Raman spectra of PCL are shown in Figure 6.7. Raman spectrometer is also a powerful tool to characterize functionalized polymers. In Raman spectra, there is a band at 2921 cm^{-1} which is indicative of C-H stretching, bands at 1721 cm^{-1} and 1440 cm^{-1} due to C=O stretching and CH$_2$ bending. They are very similar to FTIR spectra of PCL. But specially, at about 1300 cm^{-1} a strong vibration can be observed which is indicative of C-C backbone vibration. The Raman assignments for PCL spectra are listed in Table 7.5.

From Table 7.5, it can be easily observe that the ratio of most absorbance peaks after ASPN treatment to those before treatment decrease to about 30%. Only the peak at 1303cm^{-1} is different. It decreases only to 47%, which means there are more C-C groups than most other groups after ASPN treatment. Therefore, crosslinking can be confirmed forming at the topmost surface layer of the PCL film after plasma treatment.

From the data and results of FTIR, XPS and Raman spectra aforementioned, we can conclude that during plasma treatment of PCL films, chain scission, crosslinking, and the formation of hydroxyl groups are the most common reactions. Firstly, PCL is a crosslinkable

polymer, as it can produce an insoluble gel when exposed to gamma rays [157]. The principle of the crosslinking process induced by plasma should be similar to that of an irradiation process. Secondly, new hydroxyl groups are formed by obtaining energy from the plasma, followed by detachment of a hydrogen molecule in the plasma. Summarising the observed chemical changes at ASPN treatment we demonstrated that the characteristic polycaprolactone chemical group, the carboxylic —(C=O)—O— group, is destroyed and transformed to other types of bonds. During this process the whole polymer chain is rearranged, thus cross-linking and a three-dimensional network would form [29, 171, 172, 181]. In addition, a significant amount of hydroxyl groups developed on the surface, the hydrophilicity of the surface is expected to increase, which will be discussed in the next section.

7.2 Effect on surface physics

7.2.1 Changes in surface topography

7.2.1.1 PU

Surface topography was characterized by SEM and AFM. From SEM images we can see that untreated polyurethane (Figure 5.15) has a closed cell structure with only a small proportion of open cells. The percentage of the pore area on the surface is only about 4.9%. After plasma treatment at 80 ℃ for 0.5 h (Figure 5.17/PU80-05h), there are some small cracks and pores on the surface and no separate cell can be found. The percentage of the pore area on the surface increased at about 9.2%. And after plasma treatment at 130 ℃ for 0.5 h (Figure 5.19/PU130-05h), many cells are broken in half and there are some larger and round pores on the surface. The percentage of the pore area on the surface increased at about 24.2%.

The changes of surface topography can be confirmed by AFM measurement. AFM results (Figures 5.10, 5.12/PU80-05h and 5.14/PU130-05h) are almost as the same as those of SEM. And after treatment at 130 ºC for 1 h, the AFM 3D image (Figure 5.14/PU130-1h) shows the broken cells very clearly.

Clearly, a porous surface system with pores and cracks formed on PU surface. The formation of these pores may be attributed to the interaction between the active species and the PU surface although the mechanism is still under investigation.

In order to identify the changes in surface topography produced by thermal treatment or by plasma treatment, an experiment was designed; two samples were put in plasma furnace and the surface of one sample was covered with foil. Therefore, during the experiment process, there will no plasma on to the surface of this sample, while the temperature and other conditions are the same with the other sample. After treatment at 130ºC for 2 h, the two samples were subjected to AFM measurement. From AFM images (Figure 7.2) it is noticed that after thermal treatment, there are many small and unregulated cracks formed on the surface. Only the plasma treated sample shows broken cells and bigger and round pores. Therefore, it can be confirmed that the changes in surface topography are produced by plasma treatment.

The shape, size and distribution of pores on the PU surfaces varied with the plasma treatments conditions. Two reasons can be considered on the changes observed in surface topography. The first is related to the energy from plasma. Formation of bigger and round pores needs higher energy which can only be offered by plasma treatment. The second is related to the mobility of PU molecular chain. It is known from the DSC results (Section 5.1) that the glass transition point T_g of the PU material is 112.5 °C. When treated at 130 °C (above the T_g), the molecular chains of PU become more mobile relative to each other and

hence pores could be easily formed under the action of the active species from plasma. Either insufficient energy or lower temperature will result in small and unregulated pores and cracks surface topography.

The different treatment conditions such as temperature and time all have effects on the changes in surface topography.

In ASPN treatment different temperature can adversely affect surface topography. If a lower temperature (such as 80 °C) is used for treatment, the result is the formation of surface small cracks and pores. If a higher temperature (such as 130 °C) is used for treatment, the result is the formation of large, spherical pores. In addition, large, spherical pores can only formed when temperature is at 130 °C. When temperature is below 100 °C, large, spherical cells cannot be formed even after a long duration of treatment. The reason of this is thought of concern with glass transfer point of PU material. As our test in DSC, the glass transfer point T_g of PU material is 112.5 °C. If treatment temperature rises up T_g, the molecular chains of PU become mobile relative to each other. This is the key factor of result in the difference of surface topography at 130 °C and below 100 °C.

The treatment time also affects the surface morphorlogy. When treatments carried out at same temperature (either at 80, 100 or 130 °C), the percentage of cracks and pores on surfaces are increasing clear as treatment time increase. i.e. After ASPN treatment for 5 h, cracks and pores are much clearer than those of treatment for 0.5 h.

Most probably, during plasma treatment, electrons, ions and other active species bombarded on the surface can effectively change the surface physical structure from a close cell structure into porous open structure. The changes in surface topography following plasma

surface modification are the combined effects of plasma energy and mobility of PU molecular chain at different temperatures.

7.2.1.2 PCL

PCL film samples were made by casting from chloroform. When PCL samples crystallised from solution, the most obvious of the observed structures are the sphere-shaped crystalline structures. The detailed topography of the spherulites is shown in the SEM image in Figure 6.10. The spherulites are really spherical only during the initial stages of crystallization. During the latter stages, the spherulites impinge upon their neighbours, causing the boundaries between them to be straight. When the spherulites have been nucleated at the different times, they are different in size when impinging on each other, and their boundaries form hyperbolas.

As in Figure 6.10, untreated PCL film shows a spherical shape characteristic of the surface topography.

After ASPN treatment little change has been found in surface topography (Figure 6.11), which is the almost same spherical shape characteristic surface topography with same smoothness and roughness. ASPN treatment has little affected on surface roughness and topography of PCL.

It is because of the conditions of plasma treatments of PCL. During plasma treatment, the treatment temperature (50 °C) was below its melting point (59.9 °C), which is known from the DSC results (Section 6.1). Treatment time was controlled at 10 min. The treatments performed at the low temperature for short time could not induce obvious changes in surface topography.

7.2.2 Changes in surface energy and wettability

From the previous discussion it is clear that ASPN treatment could effectively tailor surface morphologies and/or chemical nature of the polymeric materials studied. The main factors that normally affect surface free energy of polymeric materials include surface topography and/or surface chemistry. With regards to surface topography, two important physical features affecting surface energy are surface roughness and surface heterogeneity. From surface chemistry side, it is important to consider how the functional groups on the top surface of polymers are changed by ASPN treatment.

7.2.2.1 UHMWPE

a. Effect of surface topography on surface energy

According to surface roughness results (Table 4.3), surface roughness increase as temperature increase and the increase is apparently only when temperature is at 130 ℃. Treatment time has no obvious effects on surface roughness. In principle, an increase of surface roughness can result in the increase of surface energy. But according to surface energy results (Table 4.9), surface energy decrease as treated temperature increase, which means the increase of surface roughness does not enough to cause the increase of surface energy. Therefore, the change of surface energy after ASPN treatment does not result from the change of surface roughness.

b. Effect of functional groups on surface energy

As previous discussion, surface energy is also related to surface chemistry. In general, increase of surface free energy of polymer involves an increase of the surface amount of groups which are generally called polar. The introduction of surface hydrophilic groups leads necessarily to an increase of the surface free energy over that of the parent polymer. Before ASPN treatment, UHMWPE consists of its structural repeat unit of–($-CH_2-CH_2-$)$_n$–to form

backbone main chain. After ASPN treatment, the transvinylene groups (-CH=CH-) are introduced in the surface structure. Comparing with saturated hydrocarbon ($-CH_2-CH_2-$)$_n$, the transvinylene group (-CH=CH-) is hydrophilic group which results in the increase of surface free energy. Evidence can be found from FTIR data (Table 7.6). In addition, according to Table 4.9, surface energy increased more after ASPN treatment at 80 ºC than that of treatment at 130 ºC. This is because plasma treatment at high temperature (melting point) induced the rearrangement of whole polymer chain and formed a disordered layer on surface. This disordered region exposed polymethylene chains to the water droplet, thus yielding a moderate shielding effect and producing a higher than expected contact angle [66].

In this study, plasma treatment introduces trans-vinylene groups into the molecular chain and makes the normally saturated chain contain unsaturated bonds which cause the surface to be more hydrophilic. According to Table 4.8, the water tensile drop contact angle decreases for almost all plasma treated samples, such as, from 79.9º (untreated) to 68.3º (treated at 80 ℃ for 0.5 h) and 77.7º (treated at 130 °C for 0.5 h). The contact angle results indicate that the wettability of the plasma treated surface increases. The exception is the sample of PE130-5h which remains almost the same contact angle value as the untreated sample. The reason is as stated above, as yielding a moderate shielding effect.

7.2.2.2   PU

a.   Effect of surface topography on surface energy

According to surface roughness results (Table 5.3), it can be seen that after plasma treatment at lower temperature or for shorter time, surface roughness changed little (not more than 30%). Only at 100 ºC, after treatment for 5 h, surface roughness increased by 87%; at 130 ºC, after treatment for 2 or 5 h, surface roughness increased by 683% and 253%. This is because of surface deformation by thermal stress. But according to the surface energy results

(Table 5.7), when treated for shorter time (0.5-1 hour), surface energy increased, while treatment carried out for longer time (2-5 hours), surface energy decreased. It is indicative that the effect of surface roughness on the change of surface energy is very limited.

Surface topography changed from closed cell structure into open cell structure after plasma treatment. It is indicative that a porous system with pores and cracks formed on PU surface. The shape, size and distribution of pores on the surfaces are different when plasma treatments perform at different conditions. According to surface energy results (Table 5.7), samples for which surface energy increases the most are PU100-1h (increase by 137%) and PU80-1h (increase by 42%). The two samples have almost same surface topography character which is smaller pores or cracks formed on surface after plasma treatment. In these cases, water occupies the smaller pores and dead-end pores, and exists as a film covering the surfaces of the larger pores of the surface. Therefore, water exists as a continuous phase throughout the porous surface. While, samples for which surface energy decreases the most are PU80-5h (decrease by 35%) and PU130-5h (decrease by 31%). The two samples have almost same surface topography character which is larger pores or cracks formed on surface after plasma treatment. In these cases, instead of penetrating the pores and cracks on the surface, water is generally in center of the pores and loses continuity and becomes isolated in the large pores. Therefore, water will not adsorb on surface and form a nonwetting spherical drop resting on the surface.

b. Effect of functional groups on surface energy

As previous discussion, the changes of surface functional groups induced by plasma are very complicated, including rearrangement of whole polymer chain, development of cross-linking and three-dimensional (C-N) network and introduction of new functional groups, etc. Hydrophilic groups –OH are introduced into the PU chain after plasma treatment. It leads

to an increase of the surface free energy over the surface of PU. Meanwhile, decrease of carboxyl group results in decrease of surface free energy.

c. Effect of hydrogen bonding on surface energy

Polyurethanes which have the general structure -CO–O–R–O–CO–NH–R'–NH– are suitable to form hydrogen bonding between adjacent chains. Therefore, significant contributions to surface energy can arise from hydrogen bounding. According to Table 7.3, the decrease of hydrogen bonding after plasma treatment carried out at low temperature or for short time is limited. But the decrease is apparently when treatment carried out at high temperature or for a long time. In principle, the decrease of hydrogen bonding can result in the decrease of surface energy. Table 5.7 shows that surface energy decreases as plasma treatment temperature or time increase.

d. The Change in surface wettability

After plasma treatment for short time (0.5-1 hour), the surface energy of PU increased (Table 5.7), which indicated surface wettabillity increased.

Firstly, the introduction of surface hydrophilic groups leads necessarily to an increase of the surface free energy over that of the parent polymer. According to XPS and FTIR results, the hydroxyl group increased on the plasma treated surfaces, which increased the hydrophilicity of the plasma treated surface. Secondly, breakdown of the intermolecular hydrogen bonds which occur between adjacent chains increase the chance of the molecules forming hydrogen bonds with water.

On the other hand, it must be noted that contact angles of two liquids on plasma treated samples increased compared with untreated sample. However, the relation between θ_{Water} and $\theta_{Glycerol}$ changed from $\theta_{Water} > \theta_{Glycerol}$ for the untreated material to $\theta_{Water} < \theta_{Glycerol}$

for the plasma treated sample. This is because plasma treatment induced the rearrangement of the whole polymer chain and formed a special layer on surface. This region exposed polymethylene chains (**R** and **R'** parts in –CO–O–**R**–O–CO–NH–**R'**–NH–) to the water droplet, thus yielding a moderate shielding effect and producing a higher than expected contact angle. Clearly, an important difference exists between hydrophilic surfaces and low contact angle surfaces: the former can adsorb some water or moisture from surroundings. Their surface and subsurface zone could be extensively hydrated, yet the water contact angle can be similar to that of hydrophobic polymers [66].

In addition, in general terms, wetting can be divided into contact angle and capillary action phenomena. The former involves smooth or moderately rough surfaces. On the other hand, on porous surfaces, capillary action sums to contact angles in the mechanism of wetting.

In summary, plasma surface modified polyurethane for short time (0.5-1 hour) has high energy surface and thus is hydrophilic; moreover, its surface has a porous, open structure which makes it vulnerable to capillary penetration.

After plasma treatment for longer times (2-5 hours), the surface energy of PU decreased (Table 5.7), which indicated surface wettabillity decreased.

Although introduction of hydrophilic groups could increase the surface energy, the factors which can effect on surface energy are complicated, including the changes in surface topography, atomic bonds, hydrogen bonds, etc. Longer duration plasma treatments not only result in larger pores or cracks but also produce atomic bond breakages (degradations) and hydrogen bond breakages. The combination of multi factors finally lead to the decrease of surface energy as well as wettability.

7.2.2.3 PCL

According to surface roughness results (Table 6.3) and AFM (Figures 6.8 and 6.9), SEM (Figures 6.10 and 6.11) results, ASPN treatment has little affected on surface roughness and topography of PCL. Therefore, the effect of surface roughness and surface topography on the change of surface energy should be very limited.

During plasma treatment of PCL films, the formation of hydroxyl groups is the most common reactions, which have been identified by XPS (Figures 6.5 and 6.6) and FTIR (Figure 6.4) tests. The introduction of hydrophilic hydroxyl group leads to increase of surface energy.

According to contact angle and surface energy results (Table 6.4), it is clear that the surface free energies of the plasma treated samples are higher than those of the untreated samples. The contact angles of the two liquids of the plasma treated samples both decreased compared with the untreated samples after plasma treatment. In general, high energy surfaces are hydrophilic. From a chemical composition point of view, the introduction of surface hydrophilic groups on the material surface leads to an increase in the surface free energy over that of the parent polymer. According to the XPS and FTIR results, the amount of hydroxyl groups increases on the top-most surface layer after plasma treatment, accompanied by an increase of hydrophilicity of the surface. A high degree of hydrophilicity is synonymous with good wettability.

7.3 Effect on mechanical properties

7.3.1 Surface nano-hardness (H) and modulus (E)

7.3.1.1 UHMWPE

The mechanical properties of UHMWPE in terms of surface nano-hardness (H) and modulus (E) are highly dependent on its surface topography and microstructure, which are

characterized by degree of crystallinity, crystalline lamellae size and distribution, and degree of crosslinking etc [1, 2, 164, 184, 185].

a. Changes in nano-hardness (H) and modulus (E)

According to Table 4.4 and Figures 4.19-4.20, the nano-hardness and modulus of UHMWPE surface increase as treatment temperature increases. Especially, after plasma treatment at 130 ℃ , nano-hardness and modulus rise even more sharply than other samples including untreated and plasma treated at 60-100 ℃ .

b. Effect factors on nano-hardness (H) and modulus (E)

The modulus (E) of a sample is a measure of its rigidity, the higher the modulus, the stiffer the sample. For the most isotropic samples, the modulus (E) increases almost linearly with the degree of crystallinity and orientation [186]. The contact stiffness of surface (nano-hardness), which is related to modulus, is correctly larger for the samples with higher degree of crystallinity. Figures 7.3 and 7.4 show the relationship between nano-hardness, modulus and crystallinity before and after plasma treatment.

The mechanical properties of UHMWPE are also determined by the number and nature of connections within the amorphous regions, including the degree of mechanical entanglements and crosslinkings [185]. As discussed in 7.1.1, plasma treatment induces the crosslinkings to form preferentially in the amorphous region and the interfacial regions. With increasing degree of crosslinking of the UHMWPE, the nano-hardness and modulus of UHMWPE surface increase after plasma treatment.

7.3.1.2 PU

Polyurethane rigid forms used in this study are highly crosslinked hard thermosetting plastics. According XRD results, they are amorphous polymers.

a.   Changes in nano-hardness (H) and modulus (E)

According to Table 5.4 and Figures 5.20-5.21, the nano-hardness of PU surface increase after plasma treatment. Especially, as treatment temperature or time increase (treatment performed at high temperature or for long a long time), nano-hardness rise accordingly. While the modulus is almost the same or even a little bit decrease after plasma treatment.

b.   Factors affecting nano-hardness (H) and modulus (E)

As shown in SEM (Figures 5.15-5.19) and AFM (Figures 5.10-5.14) images, the surface physical microstructure changed from a close cell structure to porous open structure during active screen plasma treatment.   Clearly, the formation of these pores may be attributed to the interaction between the active species and the PU surface although the mechanism is still under investigation. The cell structure on surface has a significant influence on mechanical properties. The cell structure can be described as having a skeleton and walls as the support construction of the form. After plasma treatment, many weak walls of cells collapse so that the ratio of skeleton to walls increases. Because of the reasons above, nano-hardarness of PU surface increases after plasma treatment.

According to XPS (Figures 5.5-5.8) and FTIR (Figures 5.4) results, the chemical composition and functional groups have been changed by plasma treatment. Plasma treatment offers an effective method to change functional groups on polymer surface. whereby the whole polymer chain is rearranged, and cross-linking and three-dimensional (C-N, C=N and C≡N bonds) network possibly develops. The mechanical properties of polymers are affected by the structures of the molecular chains. The changes in chemical composition and functional groups also result in the increase of nano-hardness after ASPN treatment.

7.3.2 Changes in friction behaviour and wear resistance

7.3.2.1 UHMWPE

a.   Friction behaviour

The experimental results (Table 4.6) in Section 4.8 indicate that plasma treatment has significant influence on the wear and friction behavior of plasma treated UHMWPE against stainless steel balls. The friction coefficients of plasma treated UHMWPE are higher (0.14-0.19) than those of the untreated material (0.05).

The interfacial adhesion and ploughing constitute the friction force of UHMWPE polymer against stainless steel ball. The ploughing force is controlled by the shear strength of UHMWPE surfaces, which is a main fraction of the friction coefficients. The adhesion force is influenced by the effective modulus, in which they have inversely proportional relationship [187]. Therefore, friction coefficient mainly depends on the effective modulus and the shear strength of the polymer. When the stainless steel ball is rubbing on the UHMWPE surface, hardened surface of the plasma treated UHMWPE will lead to the increase of the ploughing force against the hard asperity on the stainless steel surface. Meanwhile, the surface modulus of UHMWPE increases along with the surface nano-hardness enhancement (Table 4.4). For this reason, the increment in effective modulus may reduce the adhesive force of stainless steel ball on treated UHMWPE surface. Consequently, the summation of the ploughing and adhesion forces will result in the high friction coefficients for treated UHMWPE.

b.   Pin-on-disc wear characteristics

As has been shown in Table 4.5 and Figure 4.24, it is interestingly found that the wear rates of plasma treated UHMWPE for short time (0.5 h) increase but decrease with the increase of treatment time (1-2 h). Then with the treatment time increases further to 5h, the wear rate increases again.

When treated for short time (0.5 h), the modified layer on the surface is very thin and hard. During wear, the surface layer was separated from the matrix when the shear force applied exceeded the fatigue limit of UHMWPE, thus produced a higher wear mass loss [188]. When adhered debris of sheared polymer is smeared across worn surface, it leads to increase of wear rate (Figure 7.5).

With the increase of treatment time (1-2 h), the modified layer on the surface becomes thicker and more stable. In plasma modified surface structure, stacked lamellae are interwoven together with crosslinking amorphous regions to form a grid.

In crystalline regions, stacked lamellae align in order. These lamellae are embedded within amorphous regions and may communicate with surrounding lamellae by tie molecules which lie partly in one crystallite and partly in another. This kind of structure can improve wear resisitance by preventing lamellae from interlamellar slip and lamellar separation. Additionally, the wear resistance of UHMWPE increases significantly as the degree of crosslinking increases [189, 190]. In amorphous regions and interfacial regions plasma induced crosslinking of molecular chains form a crosslinking network. Crosslinking of supermolecular structure have been suggested to reduce abrasive wear by improving the resistance of the polymer molecules to plastic deformation [1, 164]. The evidence of reduction of abrasive wear can also be found in this study (Figure 4.22). Moreover, hard lamellar crystals forming on plasma modified surface layer results in the increase of nanohardness and modulus which are beneficial to the improvement of wear resistance by producing high-strength and high-modulus.

With the increase of treatment time, the wear resistance decreases. It is considered to lead to surface degradation after long time treatment. Particularly, when treatment performed at 100 °C for 5h, the wear resistance dramatically decreased. The reasons can be consider of

increase of surface roughness (Table 4.3) and production of cracks on surface (Figure 4.17) as well as surface degradation. In the wear process, ruffles, ripples and cracks on the rough wear surfaces are likely to cause the wear debris (Figure 7.6) which result in wear rate increases.

c.   Reciprocating wear characteristics

As has been shown in Table 4.7 and Figure 4.25, at a lower load (3.92 N), the wear rate of plasma treated UHMWPE at lower temperature (80 ℃) increase but decrease with the increase of treatment temperature (100 ℃). However, when load increase to 9.81 N, the wear rates of both surfaces treated at different temperature all increase.

The schematic of reciprocating wear characteristics is shown in Figure 7.7. Under lower load (3.92 N), when treated at lower temperature (80 ℃), the modified layer on the surface is very thin. During wear, debris is easily produced to lead to wear rate increase. On the contrary, the modified layer is thicker when treated at higher temperature (100 ℃) and no debris produced during wear process. While, under higher loads (9.81 N), both thin and thick layers are destroyed during wear process so that wear rates all increase.

7.3.2.2   PU

Having a highly crosslinked structure, PU rigid form exhibits initial good wear resistance. After ASPN treatment, the changes in wear resistance depend on treatment temperature and time. In general, the influence factors on wear resistance mainly result from surface topography and surface roughness, as well as chemical composition and structure.

a)   Pin-on-disc wear characteristics

According to Table 5.5 and Figure 5.23, the wear resistance of plasma treated surface increase at lower temperatures (80-100 ℃) for shorter times (0.5-1 h) increase. With the

treatment temperature and time increase, wear resistance of the plasma treated surface decreases.

Firstly, from the view of surface topography, during plasma treatment, active species with high energy strike on the polyurethane sample surface, some thin walls of cells are removed to form open cells. In fact, these thin walls are easy to wear into particulate wear debris which can increase wear rate. In addition, collapse of some thin walls of cells results in increase of nanohardness on the surface. Therefore, wear resistance increase due to decrease of wear debris and increase of surface hardness. However, as treatment temperature and time increase, more and more walls are broken and these broken cells are very easy worn away which result in decreased wear resistance. Secondly, from the view of surface roughness, after plasma treatment at 130°C for long time, surface roughness increase dramatically, which result in a decrease in wear resistance.

Plasma treatment causes whole polymer chain rearrangement which results in the changes in chemical composition and structure on the surface. On the one hand, cross-linking and three dimension network (C-N, C=N and C≡N bonds) formed on the surface, which result in the improvement of wear resistance; on the other hand, some bonds broken making chain scission occur, which results in the decrease of wear resistance. In addition, the breakdown of hydrogen bonds results in the decrease of intermolecular interaction, which is another reason for the decrease of wear resistance.

b)   Reciprocating wear characteristics

According to Table 5.6 and Figure 5.24, under low load (9.81 N), wear rate of plasma treated surface decreases. With load increase (13.73 N, 19.62 N), wear rates of plasma treated surfaces decrease. It is because the plasma modified layer remained intact under lower load

which was helpful to reduce wear rate. While, under higher loads, the plasma modified layer was destroyed to make wear rate increase.

7.4   Improvement of cell biocompatibility

7.4.1 UHMWPE

From the results of the study（Section 4.10), it is obvious that active screen plasma nitriding offers the possibility to improve the osteoblast cell biocompatibility of UHMWPE. Particularly, on the surface of UHMWPE treated at 80-100 ℃ , large numbers of osteoblast cell adhesion and spreading in four stages (Figure 4.30) can be easily seen. While, on untreated surface only a few numbers of osteoblast cell in stage 1 can be observed (Figure 4.26a). Osteoblasts are anchorage-dependent cells, and their ability to attach to the surface is determined by physical and chemical properties of substrate surface. Therefore, the improvement results from changes of surface roughness, surface topography and chemical composition, as well as surface wettability and surface energy tailored by ASPN technology.

a.   Effect of surface roughness

The surface topography of a material affects cells through contact guidance, a phenomenon which has also been described with osteoblastic cells. In this study, although cell attachment and spreading all improved on plasma treated surface, the 80 °C treated surfaces showed the best cell attachment results (Figure 4.31).

Although the surface topography and roughness of all samples have been changed after ASPN treatment, the changes are within a very limited range on the 80 °C treated surfaces; while on the surface treated at 130 ℃ , the changes are much more significant. Stacked lamellae lead to grooves morphologies Cell alignment has been shown to be inversely influenced by the spacing of the grooves [70, 71, 191]. Besides, according to previous research [192-194], cell spreading and continuous cell layer formation on smooth

surfaces is better than on rough ones. Therefore, the changes in surface roughness by plasma surface modification may have influenced cell attachment onto surfaces of UHMWPE.

However, it should be indicated that all the plasma treatments increase, more or less, the surface roughness of UHMWPE (Table 4.3) but all the plasma treated surfaces show improved cell biocompatibility. This implies that surface roughness is not a strong factor affecting cell attachment onto plasma treated UHMWPE surfaces and other factors have played more important role in determining the cell biocompatibility.

b.   Effect of surface chemistry

It is very likely that cells are sensitive to changes in surface chemistry and it has been shown, for example, that differences in chemistry of the outermost functional groups of a surface clearly affect endothelial cell attachment and proliferation, although the exact mechanism is not very clear [4, 195].

As described in Chapter 3, during ASPN treatment, samples are subjected to a plasma environment at elevated temperature. The plasma is composed of a dense concentration of highly excited atomic, molecular, ionic, and radical species. Their interaction with UHMWPE leads, through a complex energy transfer, to the scission of C-C and C-H bonds, giving H radicals and primary and secondary macroradicals.

As discussed in Section 7.1, the free radicals then undergo additional reactions, including the formation of transvinylene units. Figure 4.6 demonstrates a characteristic absorbance of the trans-vinylene vibration after ASPN treatment. For thermodynamic reasons the trans-vinylene units contain unsaturated bonds which leads to the formation of surface reactive layers [196], which may account for the increase in cell attachment and spreading.

The concentration of the trans-vinylene units can be readily measured by infrared spectroscopy using the characteristic absorbance at wavenumber 965 cm^{-1} on the IR-spectrum of plasma treated UHMWPE. Figure 4.5 shows the IR-spectra of untreated, 80°C and 130°C ASPN treated UHMWPE. It seems that the intensity of the characteristic absorbance peak at wavenumber 965 cm^{-1} is very similar for the IR-spectrum of 80°C and 130°C plasma treated UHMWPE. Hence, the formation of the trans-vinylene units during the ASPN treatment may have contributed to enhanced cell attachment and spreading of the plasma treated UHMWPE. However, the difference in cell biocompatibility for 80 °C and 130 °C plasma treated UHMWPE surfaces cannot be explained by the generation of the trans-vinylene units during the ASPN treatment.

    c.   Effect of wettability and surface energy

    The hydrophilic and hydrophobic characteristics of a surface are also of great importance for cell adhesion. Cell adhesion is generally better on hydrophilic than on hydrophobic surfaces [197]. As discussed in Section 7.1.1, plasma treatment introduces trans-vinylene groups into the molecular chain and makes the normally saturated chain contain unsaturated bonds which make the surface more hydrophilic. According to Table 4.8, the water tensile drop contact angle decreases from 79.9º to 68.3º (treated at 80 °C for 0.5h) and 77.7º (treated at 130 °C for 0.5h) after plasma treatment indicating that the wettability of the plasma treated surface has increased. Reduced contact angle or enhanced wettability can promote cell adhesion and spreading during the in vitro cell attachment test.

    Surface energy may influence protein adsorption and the structural rearrangement of the proteins of a material [198]. The energy at the surface of a biomaterial is defined by its general charge density and the net polarity of the charge. Thus, a surface with a net positive or negative charge may be hydrophilic in character, whereas a surface with a neutral charge may

be more hydrophobic. The net effect of the surface charge is to create a local environment with a specific surface tension, surface free energy and energy of adhesion. As listed in Table 4.9, the ASPN treatment can effectively increase the surface energy from 26.96 to 34.06 (treated at 80 °C for 0.5h) and 28.10 mNm^{-1} (treated at 130 °C for 0.5h). More importantly, the percentage of the polar part has increased from 47.7 for the untreated UHMWPE to 51.9 and 68.2% following the ASPN treatment for 0.5h at 130 and 80°C, respectively.

Therefore, it is reasonable to conclude that the improved cell biocompatibility of UHMWPE by ASPN treatment can be mainly attributed to the improved wettability and increased surface energy although surface roughness and composition might also play a role to some extent. In particular, the formation of a high energy surface with a large net polarity charge conferred by the ASPN treatment could be a major contributing factor for the significantly enhanced cell biocompatibility of UHMWPE.

7.4.2 PU

It is obvious from the results of osteoblast cell culture (Figures 5.25-5.29) that active screen plasma nitriding can improve the osteoblast cell biocompatibility of PU. Particularly, adhesion, spreading and proliferation of osteoblast cell on the surface of PU treated at 80-100 °C have been greatly improved. As discussed above, osteoblasts are anchorage-dependent cells and their ability to attach to a surface is determined by its physical and chemical properties. Therefore, the improved cell biocompatibility could be related to the changes in surface roughness, surface topography and chemical composition, as well as surface wettability and surface energy tailored by ASPN technology.

Firstly, according to AFM and SEM results (Sections 5.6-5.7), the surface physical microstructure changed from a close cell structure to porous open structure during active screen plasma treatment. Accordingly, a porous surface system with pores and cracks was

formed on PU surface following the ASPN treatment. It seems that the porous surfaces would be beneficial to cell adhesion, spreading and proliferation. However, quantitative results (Figure 7.8) show that the percentage of pore area is much larger for the 130°/0.5h treated (24.2) than for the 80°/0.5h (9.2) treated samples; nevertheless, the MTT behaviour of the latter is superior to the former (Figure 5.30).

Secondly, it has been reported that differences in chemistry of the outermost functional groups of a surface clearly affect endothelial cell attachment and proliferation [199]. As has discussed in Section 7.1.2, plasma treatments can promote the conversion of C=OO groups into new O-H groups on the plasma treated top surface layer of PU. Therefore, the hydrophilicity of the surface has increased because of the increased hydroxyl group on the surface. Meanwhile, it is also important to note that new C-N, –C=N– and C≡N groups, which incorporate new nitrogen functionalities are suggested to be good promoters for cell attachment [149, 150].

Finally, the effect of surface energy on the cell biocompatibility of plasma treated PU is complicated. As shown in Figure 5.30, all these plasma treatments can effectively enhance the cell biocompatibility of PU. However, as evidenced in Table 5.7, while PU80-0.5h and PU130-0.5h show increased surface energy following the plasma treatments, the surface energy of PU80-5h was reduced by 35%. Clearly, the total surface energy (including both disperse and polar parts) is not a good indication for the cell biocompatibility of plasma treated PU. It is of great interest to find that the percentage of the polar part increased from 64.1 for the untreated PU to 85.1% for the plasma treated PU80-5h sample although the total surface energy of the latter is much lower than the former. It seems that the large polar part of surface energy may have played an important role in enhancing the cell biocompatibility of PU.

7.4.3 PCL

Cell attachment is the first phase of cell/material interaction and the quality of this phase will influence the cells ability to proliferate and to differentiate on contact with the material [200, 201]. Using an in vitro study, cell attachment can be determined by the cell topography and cell numbers. Figures 6.12-6.17 show that osteoblast cell adhesion and spreading are much better not only by cell topography but also by cell numbers on the ASPN treated PCL surface than on the untreated surface.

Osteoblasts are anchorage-dependent cells, and their ability to attach to the surface is related to the physical and chemical properties of substrate surface. As discussed in Section 7.2, no appreciable changes in surface roughness could be detected after ASPN treatment. Therefore, the improved cell attachment cannot be attributed to surface roughness but to other factors. As shown in Table 6.4, the contact angle of water and ethylene glycol on PCL is reduced by plasma treatment, thus leading to improved wettability. The calculated surface energy and the percentage of the polar part are increased accordingly. The plasma treated surface become more hydrophilic because of the decomposition of the carboxyl groups and the development of hydroxyl groups (Section 7.1.3). It is known that cell adhesion is generally better on hydrophilic surfaces [197]. Therefore, the improved cell compatibility of the plasma treated PCL can be mainly attributed to the changes in surface chemistry and improved surface wettability.

7.5   Effect on degradability

It is well known that PCL is a biodegradable polymer and the study of degradation of plasma treated PCL is an important issue for its application in the medical fields. In this study, enzymatic degradation rate of PCL confirmed to be reduced after active screen plasma treatment.

From comparison of Figure 6.19 and Figure 6.20, it is clear that the topography of the plasma treated PCL film is quite different from that of the untreated PCL film during the degradation tests. Before degradation, the appearance of both untreated and treated PCL films shows almost the same smooth surface in that there is evidence of spherulitic growth masked by an amorphous layer of material. During degradation of untreated PCL film, the amorphous layer is etched away, progressively revealing the spherulitic textures. As the degradation proceeds, the crystalline polymer also begins to degrade, the roughness on the film surface and deepness of holes increase, fragmenting the spherulites and increasing the porosity of the material. When degradation for 19h, holes are produced in both surface and bulk body and the sample become highly porous.

During degradation of plasma treated PCL film, as mass loss increases, the films become progressively thinner but without the appearance of clear crystalline textures. When degradation for 24h, the plasma treated PCL film starts to be broken. It is clear from Figures 6.19 and 6.20 that the fragmentation of the film is delayed in the samples that have been subjected to plasma treatment. This could be attributed to the crosslinking of the topmost surface layer of the PCL film after plasma treatment [94, 172, 181, 200]. The results indicate that plasma treated PCL is still degradable although it needs a slightly longer time to complete. This should not cause any undue complications for most applications.

8 Conclusions

Based on the experimental results and the discussion presented in the last chapter, the following conclusions can be drawn:

8.1 UHMWPE

1. An absorbance peak at 965 cm^{-1} (ascribed to the transvinylene group, -CH=CH-) and a peak at 910 cm^{-1} (ascribed to the terminal vinyl group, -CH=CH$_2$) are generated in the surface UHMWPE after active-screen nitrogen plasma treatment.

2. Active-screen plasma nitriding can change the crystallinity and structure of UHMWPE. In crystalline regions, the molecular chains rearrange along the (110) plane into the stacked lamellae by plasma induced chain scission. In amorphous and interfacial regions, the crosslinks form preferentially by free radical reactions induced by plasma treatment.

3. The morphological and structural changes as well as the improvement of wear properties under certain treatment conditions could be attributed to production of cross-linking, rearrangement of molecule chains and high degree of orientation induced by the active-screen plasma treatment.

4. Active-screen plasma nitriding technique is an effective and practical method to effectively improve osteoblast cell adhesion and spreading on the UHMWPE surface mainly due to the modified surface chemistry and improved wettability.

8.2 Polyurethane (PU)

5. Active-screen plasma surface modification can effectively alter the surface morphologies of polyurethane from a closed cell structure into porous because of the interaction between the active species and the PU surface.

6. It is clear from the FTIR results that the active screen nitrogen plasma treatment has resulted in partial transfer of C=OO groups into new O-H groups in the plasma treated surface top layer.

7. It can be concluded from XPS study that during the active screen nitrogen plasma treatment, the most characteristic polyurethane chemical group, the (>HC)-NH-C=OO-(CH<) group in the surface of PU is destroyed; the carboxyl group (C=OO) has transformed to hydroxyl group (-OH).

8. The wettability of the surface of polyurethane has been improved by the active screen nitrogen plasma treatment. The improvement in hydrophilicity of plasma treated PU surfaces could be attributed to the introduction of surface hydrophilic groups and a porous, open surface structure resulting from the active screen plasma treatment.

8.3 Polycaprolactone (PCL)

9. Changes in chemical composition and structure have been found on a polycaprolactone surface following active screen plasma surface treatment. Crosslinking and new hydroxyl groups are formed on the topmost surface layer after the treatment.

10. The hydrophilicity of polycaprolactone can also be improved by the active screen nitrogen plasma treatment mainly due to the plasma treatment induced change in surface chemistry (e.g. formation of new hydroxyl group) and increased surface free energy.

11. The osteoblast cell adhesion and spreading on PCL can be significantly improved by active-screen nitrogen plasma surface modification probably due to improved hydrophilicity of the treated surfaces.

12. After active-screen plasma treatment, the PCL film is still degradable but the enzymatic degradation rate is slower compared with untreated PCL film. This could be attributed to cross-linking of molecule chains on the top surface layer by plasma treatment.

8.4 General conclusions

13. It is feasible to conduct plasma surface modification of UHMWPE, PU and PCL using the newly developed active-screen plasma technology without causing any arcing etching, significant sputtering or any other surface damage.

14. Active-screen nitrogen plasma modification is a successful surface engineering technology to effectively change the surface chemistry by introducing new functional groups, to modify the surface morphologies and to significantly increase the wettability and surface energy of UHMWPE, PU and PCL.

15. Active-screen nitrogen plasma modification is a promising surface engineering technology for the enhancement of the cell biocompatibility of UHMWPE, PU and PCL in terms of increased cell adhesion and spreading mainly due to the formation of hydroxyl group and improved hydrophilicity.

9 Future work

Some significant observations have been made in the development of novel active screen plasma surface modification of polymers. However, this technology is still at its early stage and future research is needed. To this end, the following future work has been suggested.

Firstly, surface reactions induced by active screen plasma are very complicated. Evidences obtained on the mechanisms of reactions between plasma and polymer surface are limited by techniques currently available. It is important to investigate the mechanisms involved when new plasma diagnostic technologies are available in future. For example, laser diagnostic measurements provide three-dimensional *in situ* measurement of concentration gradients for reactive ions in the plasma, velocities and temperatures. It is possible to do experimental and theoretical research in three main areas: plasma generation and transport; calculation of particle energy in plasma; plasma-surface interaction.

Secondly, very promising results have been achieved in this study using active screen nitrogen plasma. Therefore, it is interesting to investigate the feasibility of using other gases (for example Ar, CH_4, etc.) to treat these biomedical polymers.

Thirdly, from the point of view of biomedical applications, it is very important to investigate the long-term effect of active screen plasma treatment on the biocompatibility of polymers.

It is well-known that cell lines are sensitive to the physical and chemical characteristics of the materials with which they interact and that different cell lines have different response to the same biomaterials surfaces. It is important to investigate different cell lines adhesion and proliferation characteristics of active screen plasma modified polymers

It should be possible to investigate long-term maintenance for *in vitro* testing of cultured polymers under different culture conditions (e.g., compare conventional static cultures with and without serum supplementation to a serum-free perfusion culture) over an extended period of time (e.g.,15, 30, 60,100 days).

Apart from cell biocompatibility, protein adsorption and desorption characteristics as well as blood adhesion, activation and aggregation could also be researched.

10 References

1. McKellop H, Shen FW, Lu B, Campbell P, Salovey R. Development of an extremely wear-resistant ultra high molecular weight polyethylene for total hip replacements. Journal of Orthopaedic Research, 1999; 17(2): 157-167.
2. Muratoglu OK, Bragdon CR, O'Connor DO, Jasty M, Harris WH. A novel method of cross-linking ultra-high-molecular-weight polyethylene to improve wear, reduce oxidation, and retain mechanical properties - Recipient of the 1999 HAP Paul Award. Journal of Arthroplasty, 2001; 16(2): 149-160.
3. Shi W, Li XY, Dong H. Improved wear resistance of ultra-high molecular weight polyethylene by plasma immersion ion implantation. Wear, 2001; 250: 544-552.
4. Kaklamani G, Mehrban N, Chen J, Bowen J, Dong H, Grover L, Stamboulis A. Effect of plasma surface modification on the biocompatibility of UHMWPE. Biomedical Materials, 2010; 5(5).
5. Oztarhan A, Urkac ES, Kaya N, Yenigul M, Tihminlioglu F, Ezdesir A, Zimmerman R, Budak S, Muntele C, Chhay B, Ila D, Oks E, Nikolaev A, Tek Z, Eltem R. Modification of surface morphology of UHMWPE for biomedical implants. in: Ila DBJKNCPK, Editor. Ion-Beam-Based Nanofabrication. 2007. 91-100.
6. Hutmacher DW, Schantz T, Zein I, Ng KW, Teoh SH, Tan KC. Mechanical properties and cell cultural response of polycaprolactone scaffolds designed and fabricated via fused deposition modeling. Journal of Biomedical Materials Research, 2001; 55(2): 203-216.
7. Xu FJ, Wang ZH, Yang WT. Surface functionalization of polycaprolactone films via surface-initiated atom transfer radical polymerization for covalently coupling cell-adhesive biomolecules. Biomaterials, 2010; 31(12): 3139-3147.
8. Hsu SH, Tseng HJ, Fang ZK. Polyurethane blended with polylactides for improved cell adhesion and reduced platelet activation. Artificial Organs, 1999; 23(10): 958-961.
9. Cheng ZY, Teoh SH. Surface modification of ultra thin poly (epsilon-caprolactone) films using acrylic acid and collagen. Biomaterials, 2004; 25(11): 1991-2001.
10. Lindberg T, Wirsen A, Albertsson AC. Graft polymerisation of acrylamide onto PCL film by electron beam pre-irradiation in air or argon. Morphology in the final grafted state. Polymer, 2000; 41(11): 4099-4111.
11. Yang F, Wolke JGC, Jansen JA. Biomimetic calcium phosphate coating on electrospun poly (epsilon-caprolactone) scaffolds for bone tissue engineering. Chemical Engineering Journal, 2008; 137(1): 154-161.
12. Bazaka K, Jacob MV, Crawford RJ, Ivanova EP. Plasma-assisted surface modification of organic biopolymers to prevent bacterial attachment. Acta Biomaterialia, 2011; 7(5): 2015-2028.
13. Dong H, Bell T. State-of-the-art overview: ion beam surface modification of polymers towards improving tribological properties. Surface & Coatings Technology, 1999; 111(1): 29-40.
14. Ikada Y. Surface modification of polymers for medical applications. Biomaterials, 1994; 15(10): 725-736.
15. Dubas ST, Kittitheeranun P, Rangkupan R, Sanchavanakit N, Potiyaraj P. Coating of Polyelectrolyte Multilayer Thin Films on Nanofibrous Scaffolds to Improve Cell Adhesion. Journal of Applied Polymer Science, 2009; 114(3): 1574-1579.
16. Ghasemi-Mobarakeh L, Prabhakaran MP, Morshed M, Nasr-Esfahani MH, Ramakrishna S. Bio-functionalized PCL nanofibrous scaffolds for nerve tissue

engineering. Materials Science & Engineering C-Materials for Biological Applications, 2010; 30(8): 1129-1136.

17. Lee H-U, Jeong Y-S, Jeong S-Y, Park S-Y, Bae J-S, Kim H-G, Cho C-R. Role of reactive gas in atmospheric plasma for cell attachment and proliferation on biocompatible poly epsilon-caprolactone film. Applied Surface Science, 2008; 254(18): 5700-5705.

18. Manso M, Valsesia A, Lejeune M, Gilliland D, Ceccone G, Rossi F. Tailoring surface properties of biomedical polymers by implantation of Ar and He ions. Acta Biomaterialia, 2005; 1(4): 431-440.

19. Raucci MG, D'Anto V, Guarino V, Sardella E, Zeppetelli S, Favia P, Ambrosio L. Biomineralized porous composite scaffolds prepared by chemical synthesis for bone tissue regeneration. Acta Biomaterialia, 2010; 6(10): 4090-4099.

20. Satriano C, Carnazza S, Guglielmino S, Marletta G. Surface free energy and cell attachment onto ion-beam irradiated polymer surfaces. Nuclear Instruments & Methods in Physics Research Section B-Beam Interactions with Materials and Atoms, 2003; 208: 287-293.

21. Tiaw KS, Goh SW, Hong M, Wang Z, Lan B, Teoh SH. Laser surface modification of poly(epsilon-caprolactone) (PCL) membrane for tissue engineering applications. Biomaterials, 2005; 26(7): 763-769.

22. Guzman L, Celva R, Miotello A, Voltolini E, Ferrari F, Adami M. Polymer surface modification by ion implantation and reactive deposition of transparent films. Surface & Coatings Technology, 1998; 104: 375-379.

23. Toth A, Bell T, Bertoti I, Mohai M, Zelei B. Surface modification of polyethylene by low keV ion beams. Nuclear Instruments & Methods in Physics Research Section B-Beam Interactions with Materials and Atoms, 1999; 148(1-4): 1131-1135.

24. Toth A, Bertoti I, Szilagyi E, Dong H, Bell T, Juhasz A, Nagy PM. Surface characterization of ultrahigh molecular weight polyethylene after nitrogen ion implantation. Surface and Interface Analysis, 2000; 30(1): 434-438.

25. Ikeda D, Ogawa M, Hara Y, Nishimura Y, Odusanya O, Azuma K, Matsuda S, Yatsuzuka M, Murakami A. Effect of nitrogen plasma-based ion implantation on joint prosthetic material. Surface & Coatings Technology, 2002; 156(1-3): 301-305.

26. Matossian JN, Wei RH. Challenges and progress toward a 250 kV, 100 kW plasma ion implantation facility. Surface & Coatings Technology, 1996; 85(1-2): 111-119.

27. Dong H, Bell T, Blawert C, Mordike BL. Plasma immersion ion implantation of UHMWPE. Journal of Materials Science Letters, 2000; 19(13): 1147-1149.

28. Arefi F, Andre V, Montazerrahmati P, Amouroux J. Plasma polymerization and surface-treatment of polymers. Pure and Applied Chemistry, 1992; 64(5): 715-723.

29. Chan CM, Ko TM, Hiraoka H. Polymer surface modification by plasmas and photons. Surface Science Reports, 1996; 24(1-2): 3-54.

30. Biederman H. RF sputtering of polymers and its potential application. Vacuum, 2000; 59(2-3): 594-599.

31. Georges J. TC plasma nitriding. Heat Treatment of Metals, 2001; 28(2): 33-37.

32. Georges J, Cleugh D. Active screen plasma nitriding. in: Bell T, Akamatsu K, Editors. Stainless Steel 2000—Thermochemical Surface Engineering of Stainless Steel. The Institute of Materials, UK. 2001. 377–387.

33. Khorasani MT, Zaghiyan M, Mirzadeh H. Ultra high molecular weight polyethylene and polydimethylsiloxane blend as acetabular cup material. Colloids and Surfaces B-Biointerfaces, 2005; 41(2-3): 169-174.

34. Kurtz SM. The UHMWPE Handbook: Ultra-High Molecular Weight Polyethylene in Total Joint Replacement. Elsevier Academic Press, San Diego, California. 2004.

35. Mackay TG, Bernacca GM, Fisher AC, Hindle CS, Wheatley DJ. In vitro function and durability assessment of a novel polyurethane heart valve prosthesis. Artificial Organs, 1996; 20(9): 1017-1025.

36. Phillips RE, Smith MC, Thoma RJ. Biomedical applications of polyurethanes: implications of failure mechanisms. Journal of Biomaterials Applications, 1988; 3(2): 207-27.

37. Stokes K, Cobian K. Polyether polyurethanes for implantable pacemaker leads. Biomaterials, 1982; 3(4): 225-231.

38. Choong C, Triffitt JT, Cui ZF. Polycaprolactone scaffolds for bone tissue engineering - Effects of a calcium phosphate coating layer on osteogenic cells. Food and Bioproducts Processing, 2004; 82(C2): 117-125.

39. Gabriel M, Amerongen GPV, Van Hinsbergh VWM, Amerongen AVV, Zentner A. Direct grafting of RGD-motif-containing peptide on the surface of polycaprolactone films. Journal of Biomaterials Science-Polymer Edition, 2006; 17(5): 567-577.

40. Jeong SI, Kim BS, Kang SW, Kwon JH, Lee YM, Kim SH, Kim YH. In vivo biocompatibilty and degradation behavior of elastic poly(L-lactide-co-epsilon-caprolactone) scaffolds. Biomaterials, 2004; 25(28): 5939-5946.

41. Leong DT, Khor WM, Chew FT, Lim TC, Hutmacher DW. Characterization of osteogenically induced adipose tissue-derived precursor cells in 2-dimensional and 3-dimensional environments. Cells Tissues Organs, 2006; 182(1): 1-11.

42. Lowry KJ, Hamson KR, Bear L, Peng YB, Calaluce R, Evans ML, Anglen JO, Allen WC. Polycaprolactone/glass bioabsorbable implant in a rabbit humerus fracture model. Journal of Biomedical Materials Research, 1997; 36(4): 536-541.

43. Marletta G, Ciapetti G, Satriano C, Perut F, Salerno M, Baldini N. Improved osteogenic differentiation of human marrow stromal cells cultured on ion-induced chemically structured poly-epsilon-caprolactone. Biomaterials, 2007; 28(6): 1132-1140.

44. Ng KW, Hutmacher DW, Schantz J-T, Ng CS, Too H-P, Lim TC, Phan TT, Teoh SH. Evaluation of ultra-thin poly(epsilon-caprolactone) films for tissue-engineered skin. Tissue Engineering, 2001; 7(4): 441-455.

45. Nair LS, Laurencin CT. Biodegradable polymers as biomaterials. Progress in Polymer Science, 2007; 32(8-9): 762-798.

46. Sidouni FZ, Nurdin N, Chabrecek P, Lohmann D, Vogt J, Xanthopoulos N, Mathieu HJ, Francois P, Vaudaux P, Descouts P. Surface properties of a specifically modified high-grade medical polyurethane. Surface Science, 2001; 491(3): 355-369.

47. Bertoti I, Mohai M, Toth A, Ujvari T. Nitrogen-PBII modification of ultra-high molecular weight polyethylene: Composition, structure and nanomechanical properties. Surface & Coatings Technology, 2007; 201(15): 6839-6842.

48. Kondyurin A, Karmanov V, Guenzel R. Plasma immersion ion implantation of polyethylene. Vacuum, 2001; 64(2): 105-111.

49. Shi W, Dong H. Surface modification of UHMWPE by nitrogen implantation. Contributions of Surface Engineering to Modern Manufacturing and Remanufacturing, ed. Zhang S, Zhou ZR, Liu JJ, Zhu MH. 2002. 379-383.

50. Oertel G, ed. Polyurethane Handbook. Carl Hanser Verlag: Munich. 1985.

51. Li DJ, Cui FZ, Feng QL, Zhao J. Oxygen ion beam and plasma induced blood compatibility of polyetherurethane. Chinese Physics Letters, 1997; 14(7): 531-534.

52. Li DJ, Zhao J. The structure of biomedical behavior of ion-bombarded and plasma-polymerized segmented polyurethane. Applied Surface Science, 1994; 78(2): 195-201.

53. Li DJ, Zhao J. Surface biomedical effects of plasma on polyetherurethane. Journal of Adhesion Science and Technology, 1995; 9(9): 1249-1261.

54. Chrissafis K, Antoniadis G, Paraskevopoulos KM, Vassiliou A, Bikiaris DN. Comparative study of the effect of different nanoparticles on the mechanical properties and thermal degradation mechanism of in situ prepared poly(e-caprolactone) nanocomposites. Composites Science and Technology, 2007; 67: 2165–2174.

55. Engelberg I, Kohn J. Physicomechanical properties of degradable polymers used in medical applications - a comparative-study. Biomaterials, 1991; 12(3): 292-304.

56. Pitt CG, Schinder A. Capronor-A biodegradable delivery system for levonorgestrel. in: Zatachini GL, Editor. Long-acting contraceptive systems. Harpen and Row, Philadelphia. 1984. 63-84.

57. Khor HL, Ng KW, Schantz JT, Phan TT, Lim TC, Teoh SH, Hutmacher DW. Poly(epsilon-caprolactone) films as a potential substrate for tissue engineering an epidermal equivalent. Materials Science & Engineering C-Biomimetic and Supramolecular Systems, 2002; 20(1-2): 71-75.

58. Clark DT, Feast WJ, eds. Polymer Surfaces. John Wiley & Sons: Chichester. 1978.

59. Brisoe BJ, Tabor D. Friction and wear of polymers. in: Clark DT, Feast WJ, Editors. Polymer surfaces. John Wiley & Sons, Chichester. 1978. 1-20.

60. Bhushan B, Gupta BK. Handbook of tribology: materials, coatings and surface treatment. Krieger Publishing Company, New York. 1991.

61. Bowden FP, Tabor D. Friction and lubrication of solids. Clarendon Press, Oxford. 1964.

62. Buckley DH. Surface effects in adhesion, friction, wear and lubrication. Elsevier, Amsterdam. 1981.

63. Khruschov MM. Principles of abrasive wear. Wear, 1974; 6: 353-365.

64. Fischer TE. Tribochemistry. Ann Rev Mater Sci, 1988; 18: 303-323.

65. Schrader ME, Loed D, eds. Modern approach to wettability: theory and application. Marcel Dekker: New York. 1982.

66. Garbassi F, Morra M, Occhiello E. Polymer Surfaces: from Physical to Technology. John Wiley and Sons, Chichester. 1998.

67. Awaja F, Gilbert M, Kelly G, Fox B, Pigram PJ. Adhesion of polymers. Progress in Polymer Science, 2009; 34(9): 948-968.

68. Tavana H, Neumann AW. Recent progress in the determination of solid surface tensions from contact angles. Advances in Colloid and Interface Science, 2007; 132(1): 1-32.

69. Williams DF. The Williams Dictionary of Biomaterials. Liverpool University Press, Liverpool. 1999.

70. Chesmel KD, Black J. Cellular-responses to chemical and morphologic aspects of biomaterial surfaces .1. a novel in-vitro model system. Journal of Biomedical Materials Research, 1995; 29(9): 1089-1099.

71. Chesmel KD, Clark CC, Brighton CT, Black J. Cellular-responses to chemical and morphologic aspects of biomaterial surfaces .2. the biosynthetic and migratory response of bone cell-populations. Journal of Biomedical Materials Research, 1995; 29(9): 1101-1110.

72. Dabagh M, Abdekhodaie MJ, Khorasani MT. Effects of polydimethylsiloxane grafting on the calcification, physical properties, and biocompatibility of polyurethane in a heart valve. Journal of Applied Polymer Science, 2005; 98(2): 758-766.

73. Ishihara K. New polymeric biomaterials: Phospholipid polymers with a biocompatible surface. Frontiers of Medical and Biological Engineering, 2000; 10(2): 83-95.

74. Vasita R, Shanmugam K, Katti DS. Improved biomaterials for tissue engineering applications: Surface modification of polymers. Current Topics in Medicinal Chemistry, 2008; 8(4): 341-353.

75. Zhang YZ, Venugopal J, Huang ZM, Lim CT, Ramakrishna S. Characterization of the surface biocompatibility of the electrospun PCL-collagen nanofibers using fibroblasts. Biomacromolecules, 2005; 6(5): 2583-2589.
76. Butler M. Animal cell culture and technology: the basics. Oxford University Press, Oxford. 1996.
77. Ma Z, Mao Z, Gao C. Surface modification and property analysis of biomedical polymers used for tissue engineering. Colloids and Surfaces B-Biointerfaces, 2007; 60(2): 137-157.
78. Rajaraman.R, Rounds DE, Yen SPS, Rembaum A. Scanning electron-microscope study of cell adhesion and spreading in vitro. Experimental Cell Research, 1974; 88(2): 327-339.
79. Dvorak JA. The application of atomic force microscopy to the study of living vertebrate cells in culture. Methods, 2003; 29(1): 86-96.
80. Dvorak JA, Nagao E. Kinetic analysis of the mitotic cycle of living vertebrate cells by atomic force microscopy. Experimental Cell Research, 1998; 242(1): 69-74.
81. Nagao E, Dvorak JA. An integrated approach to the study of living cells by atomic force microscopy. Journal of Microscopy-Oxford, 1998; 191: 8-19.
82. Armani DK, Liu C. Mircofabrication technology for polycaprolactone, a biodegradable polymer. Journal of Micromechanics and Microengineering, 2000; 10(1): 80-84.
83. Cannizzaro SM, Padera RF, Langer R, Rogers RA, Black FE, Davies MC, Tendler SJB, Shakesheff KM. A novel biotinylated degradable polymer for cell-interactive applications. Biotechnology and Bioengineering, 1998; 58(5): 529-535.
84. Chrissafis K, Paraskevopoulos KM, Tsiaoussis I, Bikiaris D. Comparative Study of the Effect of Different Nanoparticles on the Mechanical Properties, Permeability, and Thermal Degradation Mechanism of HDPE. Journal of Applied Polymer Science, 2009; 114(3): 1606-1618.
85. Gopferich A. Polymer degradation and erosion: Mechanisms and applications. European Journal of Pharmaceutics and Biopharmaceutics, 1996; 42(1): 1-11.
86. Gopferich A. Mechanisms of polymer degradation and erosion. Biomaterials, 1996; 17(2): 103-114.
87. Gopferich A, Tessmar J. Polyanhydride degradation and erosion. Advanced Drug Delivery Reviews, 2002; 54(7): 911-931.
88. Piskin E. Biodegradable polymers as biomaterials. Journal of Biomaterials Science-Polymer Edition, 1994; 6(9): 775-795.
89. Santerre JP, Woodhouse K, Laroche G, Labow RS. Understanding the biodegradation of polyurethanes: From classical implants to tissue engineering materials. Biomaterials, 2005; 26(35): 7457-7470.
90. Shimao M. Biodegradation of plastics. Current Opinion in Biotechnology, 2001; 12(3): 242-247.
91. Sivalingam G, Chattopadhyay S, Madras G. Enzymatic degradation of poly (epsilon-caprolactone), poly (vinyl acetate) and their blends by lipases. Chemical Engineering Science, 2003; 58(13): 2911-2919.
92. Sivalingam G, Madras G. Thermal degradation of poly (epsilon-caprolactone). Polymer Degradation and Stability, 2003; 80(1): 11-16.
93. Sun H, Mei L, Song C, Cui X, Wang P. The in vivo degradation, absorption and excretion of PCL-based implant. Biomaterials, 2006; 27(9): 1735-1740.
94. Darwis D, Mitomo H, Enjoji T, Yoshi F, Makuuchi K. Enzymatic degradation of radiation crosslinked poly(epsilon-caprolactone). Polymer Degradation and Stability, 1998; 62(2): 259-265.

95.   Sivalingam G, Madras G. Oxidative degradation of poly (vinyl acetate) and poly (epsilon-caprolactone) and their mixtures in solution. Chemical Engineering Science, 2004; 59(7): 1577-1587.

96.   Sivalingam G, Vijayalakshmi SP, Madras G. Enzymatic and thermal degradation of poly(epsilon-caprolactone), poly(D,L-lactide), and their blends. Industrial & Engineering Chemistry Research, 2004; 43(24): 7702-7709.

97.   Tsuji H, Ono T, Saeki T, Daimon H, Fujie K. Hydrolytic degradation of poly(epsilon-caprolactone) in the melt. Polymer Degradation and Stability, 2005; 89(2): 336-343.

98.   Barbucci R, ed. Integrated biomaterial science. Kluwer Academic/Plenum Publishers: New York. 2002.

99.   Williams D. Tissue Engineering. Academic Press, Amsterdam. 2008.

100.   Goddard JM, Hotchkiss JH. Polymer surface modification for the attachment of bioactive compounds. Progress in Polymer Science, 2007; 32(7): 698-725.

101.   Morent R, De Geyter N, Desmet T, Dubruel P, Leys C. Plasma Surface Modification of Biodegradable Polymers: A Review. Plasma Processes and Polymers, 2011; 8(3): 171-190.

102.   Farris S, Pozzoli S, Biagioni P, Duo L, Mancinelli S, Piergiovanni L. The fundamentals of flame treatment for the surface activation of polyolefin polymers - A review. Polymer, 2010; 51(16): 3591-3605.

103.   Tuominen M, Lahti J, Kuusipalo J. Effects of flame and corona treatment on extrusion coated paper properties. Tappi Journal, 2011; 10(10): 29-37.

104.   Lippert T. Interaction of photons with polymers: From surface modification to ablation. Plasma Processes and Polymers, 2005; 2(7): 525-546.

105.   Sturrock PA. Plasma Physics: An Introduction to the Theory of Astrophysical, Geophysical & Laboratory Plasmas. Cambridge University Press. 1994.

106.   Hegemann D, Brunner H, Oehr C. Plasma treatment of polymers for surface and adhesion improvement. Nuclear Instruments & Methods in Physics Research Section B-Beam Interactions with Materials and Atoms, 2003; 208: 281-286.

107.   Kuzuya M, Sawa T, Mouri M, Kondo SI, Takai O. Plasma technique for the fabrication of a durable functional surface on organic polymers. Surface & Coatings Technology, 2003; 169: 587-591.

108.   Dong H. Surface modification of ultra-high molecular weight polyethylene for joint prosthesis and sports applications. in Proc. of the 4th Inter. Conf. on surf. Eng. 2004. Beijing: Science Press.

109.   Sammons RL, Elhaj AJ, Marquis PM. Novel culture procedure permitting the synthesis of proteins by rat calvarial cells cultured on hydroxyapatite particles to be quantified. Biomaterials, 1994; 15(7): 536-542.

110.   Sharpe JR, Sammons RL, Marquis PM. Effect of pH on protein adsorption to hydroxyapatite and tricalcium phosphate ceramics. Biomaterials, 1997; 18(6): 471-476.

111.   Bland R, Sammons RL, Sheppard MC, Williams GR. Thyroid hormone, vitamin D and retinoid receptor expression and signalling in primary cultures of rat osteoblastic and immortalised osteosarcoma cells. Journal of Endocrinology, 1997; 154(1): 63-74.

112.   Lumbikananda N, Sammons R. Bone cell attachment to dental implants of different surface characteristics. International Journal of Oral and Maxillofacial Implants, 2001; 16(5): 627-636.

113.   Sammons RL, Lumbikanonda N, Gross M, Cantzler P. Comparison of osteoblast spreading on microstructured dental implant surfaces and cell behaviour in an explant model of osseointegration. Clinical Oral Implants Research, 2005; 16(6): 657-666.

114.   Murdoch FE, Sammons RL, Chapple ILC. Isolation and characterization of subgingival staphylococci from periodontitis patients and controls. Oral Diseases, 2004; 10(3): 155-162.

115. Inagaki N, Narushim K, Ejima S, Ikeda Y, Lim SK, Park YW, Miyazaki K. Hydrophobic recovery of plasma-modified film surfaces of ethylene-co-tetrafluoroethylene co-polymer. Journal of Adhesion Science and Technology, 2003; 17(11): 1457-1475.

116. Inagaki N, Narushima K, Tsutsui Y, Ohyama Y. Surface modification and degradation of poly(lactic acid) films by Ar-plasma. Journal of Adhesion Science and Technology, 2002; 16(8): 1041-1054.

117. Inagaki N, Tasaka S, Shimada S. Comparative studies on surface modification of poly(ethylene terephthalate) by remote and direct argon plasmas. Journal of Applied Polymer Science, 2001; 79(5): 808-815.

118. Brown NMD, Cui NY, McKinley A. A study of the topography of a glassy carbon surface following low-power radio-frequency oxygen plasma treatment. Applied Surface Science, 1998; 133(3): 157-165.

119. Caro JC, Lappan U, Simon F, Pleul D, Lunkwitz K. On the low-pressure plasma treatment of PTFE (polytetrafluoroethylene) with SO2 as process gas. European Polymer Journal, 1999; 35(6): 1149-1152.

120. Liu C, Brown NMD, Meenan BJ. Dielectric barrier discharge (DBD) processing of PMMA surface: Optimization of operational parameters. Surface & Coatings Technology, 2006; 201(6): 2341-2350.

121. Liu CZ, Cui NY, Brown NMD, Meenan BJ. Effects of DBD plasma operating parameters on the polymer surface modification. Surface & Coatings Technology, 2004; 185(2-3): 311-320.

122. Safinia L, Datan N, Hohse M, Mantalaris A, Bismarck A. Towards a methodology for the effective surface modification of porous polymer scaffolds. Biomaterials, 2005; 26(36): 7537-7547.

123. Setsuhara Y, Cho K, Takenaka K, Ebe A, Shiratani M, Sekine M, Hori M, Ikenaga E, Kondo H, Nakatsuka O, Zaima S. Plasma surface treatment of polymers with inductivity-coupled RF plasmas driven by low-inductance antenna units. Thin Solid Films, 2009; 518(3): 1006-1011.

124. Vesel A, Mozetic M, Strnad S. Improvement of adhesion of fucoidan on polyethylene terephthalate surface using gas plasma treatments. Vacuum, 2011; 85(12): 1083-1086.

125. Li RZ, Ye L, Mai YW. Application of plasma technologies in fibre-reinforced polymer composites: A review of recent developments. Composites Part a-Applied Science and Manufacturing, 1997; 28(1): 73-86.

126. Li CX, Bell T. Principles, mechanisms and applications of active screen plasma nitriding. Heat Treatment of Metals, 2003; 30(1): 1-7.

127. Li CX, Bell T. Potential of plasma nitriding of polymer for improved hardness and wear resistance. Journal of Materials Processing Technology, 2005; 168(2): 219-224.

128. Li CX, Bell T, Dong H. A study of active screen plasma nitriding. Surface Engineering, 2002; 18(3): 174-181.

129. Desai S, Singh RP. Surface modification of polyethylene. in: Albertsson A, Editor. Long-term properties of polyolefins. Springer, New York. 2004. 231-293.

130. Chapiro A. Radiation Chemistry of Polymeric Systems. Interscience Publishers, London. 1962.

131. Venkatesan T, Calcagno L, Elman BS, Foti G. Ion Beam Modification of Insulators, ed. Mazzoldi P, Arnold GW. Elsevier, Amsterdam. 1987. 301-379.

132. Chu PK, Chen JY, Wang LP, Huang N. Plasma-surface modification of biomaterials. Materials Science & Engineering R-Reports, 2002; 36(5-6): 143-206.

133. Oehr C. Plasma surface modification of polymers for biomedical use. Nuclear Instruments & Methods in Physics Research Section B-Beam Interactions with Materials and Atoms, 2003; 208: 40-47.

134. VanLandingham MR, Villarrubia JS, Guthrie WF, Meyers GF. Nanoindentation of polymers: An overview. Macromolecular Symposia, 2001; 167: 15-43.

135. Oliver WC, Pharr GM. An improved technique for determining hardness and elastic-modulus using load and displacement sensing indentation experiments. Journal of Materials Research, 1992; 7(6): 1564-1583.

136. Oliver WC, Pharr GM. Measurement of hardness and elastic modulus by instrumented indentation: Advances in understanding and refinements to methodology. Journal of Materials Research, 2004; 19(1): 3-20.

137. Poletti G, Orsini F, Riccardi C, Raffaele-Addamo A, Barni R. Atomic force microscopy investigation of cold-plasma-treated poly(ethyleneterephthalate) textiles. Surface and Interface Analysis, 2003; 35(4): 410-412.

138. Vohrer U, Hegemann D, Oehr C. XPS, AES, and AFM as tools for study of optimized plasma functionalization. Analytical and Bioanalytical Chemistry, 2003; 375(7): 929-934.

139. Falconnet D, Csucs G, Grandin HM, Textor M. Surface engineering approaches to micropattern surfaces for cell-based assays. Biomaterials, 2006; 27(16): 3044-3063.

140. Khorasani MT, Mirzadeh H, Kermani Z. Wettability of porous polydimethylsiloxane surface: morphology study. Applied Surface Science, 2005; 242(3-4): 339-345.

141. Petermann J. Morphology in oriented semicrystalline polymers. in: Fakirov S, Editor. Oriented Polymer Materials. Hüthig & Wepf, New York. 1996.

142. Vickerman JC, ed. Surface analysis : the principal techniques Wiley: Chichester. 1997.

143. Kakudo M, Kasai N. X-ray Diffraction by Polymers. Kodansha Ltd, Elsvier Publishing Company, American Elsvier Publishing Company, Inc, Tokyo, Amsterdam, New York. 1972.

144. Warren BE. X-ray diffraction. Dover Publications, New York. 1990.

145. Ensinger Ltd. Address: Wilfried Way Tonyrefail Mid Glam CF39 8JQ. Web: www.ensinger.ltd.uk.

146. TUFNOL Limited Company. Address: Tufnol Composites Ltd, Wellhead Lane, Perry Barr, Birmingham B42 2TN. Web: http://www.tufnol.com/.

147. Tang ZG, Black RA, Curran JM, Hunt JA, Rhodes NP, Williams DF. Surface properties and biocompatibility of solvent-cast poly epsilon-caprolactone films. Biomaterials, 2004; 25(19): 4741-4748.

148. Gallo SC, Dong H. On the fundamental mechanisms of active screen plasma nitriding. Vacuum, 2009; 84(2): 321-325.

149. Griesser HJ, Chatelier RC, Gengenbach TR, Johnson G, Steele JG. Growth of human-cells on plasma polymers - putative role of amine and amide groups. Journal of Biomaterials Science-Polymer Edition, 1994; 5(6): 531-554.

150. Steele JG, Johnson G, McFarland C, Dalton BA, Gengenbach TR, Chatelier RC, Underwood PA, Griesser HJ. Roles of serum vitronectin and fibronectin in initial attachment of human vein endothelial-cells and dermal fibroblasts on oxygen-containing and nitrogen-containing surfaces made by radiofrequency plasmas. Journal of Biomaterials Science-Polymer Edition, 1994; 6(6): 511-532.

151. Priest JM, Baldwin MJ, Fewell MP. The action of hydrogen in low-pressure r.f.-plasma nitriding. Surface & Coatings Technology, 2001; 145(1-3): 152-163.

152. Korner N, Beck E, Dommann A, Onda N, Ramm J. Hydrogen plasma chemical cleaning of metallic substrates and silicon wafers. Surface & Coatings Technology, 1995; 76-77(1-3): 731-737.

153. Guzman AM, Carlson JD, Bares JE, Pronko PP. Chemical and physical changes induced in polyvinylidene fluoride by irradiation with high-energy ions. Nuclear Instruments & Methods in Physics Research Section B-Beam Interactions with Materials and Atoms, 1985; 7-8(MAR): 468-472.

154. Zhou J, Chakravartula A, Pruitt L, Komvopoulos K. Tribological and nanomechanical properties of unmodified and crosslinked ultra-high molecular weight polyethylene for total joint replacements. Journal of Tribology-Transactions of the Asme, 2004; 126(2): 386-394.

155. Owens DK, Wendt RC. Estimation of surface free energy of polymers. Journal of Applied Polymer Science, 1969; 13(8): 1741-&.

156. Gomathi N, Mishra D, Maiti TK, Neogi S. Enhanced Cell Adhesion to Helium Plasma-Treated Polypropylene. Journal of Adhesion Science and Technology, 2009; 23(13-14): 1861-1874.

157. Cottam E, Hukins DWL, Lee K, Hewitt C, Jenkins MJ. Effect of sterilisation by gamma irradiation on the ability of polycaprolactone (PCL) to act as a scaffold material. Medical Engineering & Physics, 2009; 31(2): 221-226.

158. Pena J, Corrales T, Izquierdo-Barba I, Doadrio AL, Vallet-Regi M. Long term degradation of poly(epsilon-caprolactone) films in biologically related fluids. Polymer Degradation and Stability, 2006; 91(7): 1424-1432.

159. Coombes AGA, Rizzi SC, Williamson M, Barralet JE, Downes S, Wallace WA. Precipitation casting of polycaprolactone for applications in tissue engineering and drug delivery. Biomaterials, 2004; 25(2): 315-325.

160. Reggiani M, Tinti A, Taddei P, Visentin M, Stea S, De Clerico M, Fagnano C. Phase transformation in explanted highly crystalline UHMWPE acetabular cups and debris after in vivo wear. Journal of Molecular Structure, 2006; 785(1-3): 98-105.

161. Stuart B. Infrared Spectroscopy: Fundamentals and Applications. Wiley. 2004.

162. Chanda A, Mukhopadhyay AK, Basu D, Chatterjee S. Wear and friction behaviour of UHMWPE - Alumina combination for total hip replacement. Ceramics International, 1997; 23(5): 437-447.

163. Cho HJ, Wei WJ, Kao HC, Cheng CK. Wear behavior of UHMWPE sliding on artificial hip arthroplasty materials. Materials Chemistry and Physics, 2004; 88(1): 9-16.

164. McKellop H, Shen FW, DiMaio W, Lancaster JG. Wear of gamma-crosslinked polyethylene acetabular cups against roughened femoral balls. Clinical Orthopaedics and Related Research, 1999(369): 73-82.

165. Wang A, Sun DC, Stark C, Dumbleton JH. Wear mechanisms of UHMWPE in total joint replacements. Wear, 1995; 181: 241-249.

166. Zhou J, Komvopoulos K. Wear mechanisms of untreated and gamma irradiated ultra-high molecular weight polyethylene for total joint replacements. Journal of Tribology-Transactions of the Asme, 2005; 127(2): 273-279.

167. Kim BK, Lee SY, Xu M. Polyurethanes having shape memory effects. Polymer, 1996; 37(26): 5781-5793.

168. Beamson G, Briggs D. High Resolution XPS of Organic Polymers. The Scienta ESCA300 Database. Wiley, Chichester. 1992.

169. David RL. Handbook of Chemistry and Physics, 89th ed. CRC Press. 2008.

170. Bertoti I. Characterization of nitride coatings by XPS. Surface & Coatings Technology, 2002; 151: 194-203.

171. Narkis M, Sibony-Chaouat S, Siegmann A, Shkolnik S, Bell JP. Irradiation effects on polycaprolactone. Polymer, 1985; 26: 50-54.

172. Darwis D, Mitomo H, Enjoji T, Yoshii F, Makuuchi K. Heat resistance of radiation crosslinked poly(epsilon-caprolactone). Journal of Applied Polymer Science, 1998; 68(4): 581-588.

173. Chernenko T, Matthaeus C, Milane L, Quintero L, Amiji M, Diem M. Label-free Raman spectral imaging of intracellular delivery and degradation of polymeric nanoparticle systems. Acs Nano, 2009; 3(11): 3552-3559.

174. Diem M, Matthaus C, Chernenko T, Romeo M, Miljkovic M, Bird B, Schubert J, Papamarkakis K, Bedrossian K, Laver N. Infrared and Raman Spectroscopy and Spectral Imaging of Individual Cells. in: Salzer R, Siesler HW, Editors. Infrared and Raman Spectroscopic Imaging. Wiley-VCH, Weinheim, Germany. 2009. 3-202.

175. Johnson WC, Lyons BJ. Radiolytic formation and decay of trans-vinylene unsaturation in polyethylene - fourier-transform infrared measurements. Radiation Physics and Chemistry, 1995; 46(4-6): 829-832.

176. Lyons BJ, Johnson WC. Radiolytic formation and decay of trans-vinylene unsaturation in polyethylene. Irradiation of Polymeric Materials, 1993; 527: 62-73.

177. Muratoglu OK, Harris WH. Identification and quantification of irradiation in UHMWPE through trans-vinylene yield. Journal of Biomedical Materials Research, 2001; 56(4): 584-592.

178. Muratoglu OK, O'Connor DO, Bragdon CR, Delaney J, Jasty M, Harris WH, Merrill E, Venugopalan P. Gradient crosslinking of UHMWPE using irradiation in molten state for total joint arthroplasty. Biomaterials, 2002; 23(3): 717-724.

179. Toth A, Bertoti I, Mohai M, Ujvari T. Surface modification of polyethylene by nitrogen PIII: Surface chemical and nanomechanical properties. in: Gyulai J, Szabo PJ, Editors. Materials Science, Testing and Informatics III. 2007. 255-261.

180. Premnath V, Harris WH, Jasty M, Merrill EW. Gamma sterilization of UHMWPE articular implants: An analysis of the oxidation problem. Biomaterials, 1996; 17(18): 1741-1753.

181. Tajima S, Komvopoulos K. Effect of reactive species on surface crosslinking of plasma-treated polymers investigated by surface force microscopy. Applied Physics Letters, 2006; 89(12): 4102.

182. Peacock AJ. Handbook of Polyethylene Structure, Properties, and Applications. Marcel Dekker, Inc, New York. 2000.

183. Hannay NB, ed. Solid State Chemisrty. Crystalline and Noncrystalline Solid. Vol. 3. Plenum Press: New York-London. 1976. 507-508.

184. Simis KS, Bistolfi A, Bellare A, Pruitt LA. The combined effects of crosslinking and high crystallinity on the microstructural and mechanical properties of ultra high molecular weight polyethylene. Biomaterials, 2006; 27(9): 1688-1694.

185. Wang A, Essner A, Polineni VK, Stark C, Dumbleton JH. Lubrication and wear of ultra-high molecular weight polyethylene in total joint replacements. Tribology International, 1998; 31(1-3): 17-33.

186. Bueche F. Physical properties of polymers. Interscience Publishers, New York. 1962.

187. Bhushan B. Introduction to Tribology. Wiley, New York. 2002.

188. Ge S, Wang S, Gitis N, Vinogradov M, Xiao J. Wear behavior and wear debris distribution of UHMWPE against Si3N4 ball in bi-directional sliding. Wear, 2008; 264(7-8): 571-578.

189. Muratoglu OK, Bragdon CR, Jasty M, Harris WH. The effect of radiation damage on the wear rate of UHMWPE components, in ASTM Symposium on Characterization and Properties of UHMWPE. 1996: New Orleans, LA.

190. Wang A, Sun DC, Stark C, Dumbleton JH. Effects of sterilization methods on the wear of UHMWPE acetabular cups. in Proceedings of 5th World Biomaterials Congress. 1996. Toronto, Canada: University of Toronto Press.

191. Clark P, Connolly P, Curtis ASG, Dow JAT, Wilkinson CDW. Topographical control of cell behavior .2. multiple grooved substrata. Development, 1990; 108(4): 635-644.

192. Kieswetter K, Schwartz Z, Hummert TW, Cochran DL, Simpson J, Dean DD, Boyan BD. Surface roughness modulates the local production of growth factors and cytokines by osteoblast-like MG-63 cells. Journal of Biomedical Materials Research, 1996; 32(1): 55-63.

193. Anselme K, Bigerelle M, Noel B, Dufresne E, Judas D, Iost A, Hardouin P. Qualitative and quantitative study of human osteoblast adhesion on materials with various surface roughnesses. Journal of Biomedical Materials Research, 2000; 49(2): 155-166.

194. Dalton BA, McFarland CD, Gengenbach TR, Griesser HJ, Steele JG. Polymer surface chemistry and bone cell migration. Journal of Biomaterials Science-Polymer Edition, 1998; 9(8): 781-799.

195. Hunter A, Archer CW, Walker PS, Blunn GW. Attachment and proliferation of osteoblasts and fibroblasts on biomaterials for orthopedic use. Biomaterials, 1995; 16(4): 287-295.

196. Anselme K. Osteoblast adhesion on biomaterials. Biomaterials, 2000; 21(7): 667-681.

197. Altankov G, Groth T. Reorganization of substratum-bound fibronectin on hydrophilic and hydrophobic materials is related to biocompatibility. Journal of Materials Science-Materials in Medicine, 1994; 5(9-10): 732-737.

198. Boyan BD, Hummert TW, Dean DD, Schwartz Z. Role of material surfaces in regulating bone and cartilage cell response. Biomaterials, 1996; 17(2): 137-146.

199. Margel S, Vogler EA, Firment L, Watt T, Haynie S, Sogah DY. Peptide, protein, and cellular interactions with self-assembled monolayer model surfaces. Journal of Biomedical Materials Research, 1993; 27(12): 1463-1476.

200. Vitte J, Benoliel AM, Pierres A, Bongrand P. Is there a predictable relationship between surface physical-chemical properties and cell behaviour at the interface? European cells & materials, 2004; 7: 52-63.

201. Shin H, Jo S, Mikos AG. Biomimetic materials for tissue engineering. Biomaterials, 2003; 24(24): 4353-4364.

Table 2.1 Typical properties of HDPE and UHMWPE

Property	HDPE	UHMWPE
Molecular weight (10^6 g mol^{-1})	0.05-0.25	2-6
Melting point (°C)	130-137	125-138
Poisson's ratio	0.40	0.46
specific gravity (g cm^{-3})	0.952-0.965	0.932-0.945
Tensile modulus of elasticity (GPa)	0.4-4.0	0.8-1.6
Tensile yield strength (MPa)	26-33	21-28
Tensile ultimate strength (MPa)	22-31	39-48
Tensile ultimate elongation (%)	10-1200	350-525
Impact strength, Izod (J/m of notch; 3.175 mm thick specimen)	21-214	>1070 (No break)
Degree of crystallinity (%)	60-80	39-75

Table 2.2 Comparison of low pressure plasma and active screen plasma

Method	current	Voltage (kV)	Pressure (Pa)	Power (W)
low pressure plasma	high freqency AC	5-40	0.01-100	5-600
active screen plasma	DC	＜0.5	100-500	100-600

Table 2.3 Three primary modes of AFM [142]

Comparison	Contact Mode	Non-contact Mode	Tapping Mode
Operator Zone	I zone	II zone	I/II zone
Force sensed by tip	Short range repulsive forces	Long range attractive forces	Repulsive/ attractive forces
Tip or cantilever position	Tip actually touches the sample	The tip does not contact the sample surface. The cantilever is oscillated at a frequency slightly above the cantilever's resonance frequency with an amplitude of a few nanometers (<10nm).	The cantilever is oscillated at or near its resonance frequency with an amplitude from 20nm to 100nm.
Feedback loop	Maintains constant cantilever deflection	maintains a constant oscillation amplitude or frequency	Maintains a constant oscillation amplitude by maintaining a constant RMS of the oscillation signal
Advantages	High scan speeds Atomic resolution Rough samples can be scanned easily	No force exerted on the sample surface	Higher lateral resolution (1~5nm) Lower forces and less damage
Disadvantages	Shear force and normal force can distort images Damage the soft samples	Lower lateral resolution Slow scan speed Usually only work on extremely hydrophobic samples	Slightly slower scan speed than contact mode

Table 2.4 Typical C_{1s} binding energy (E_B) for organic samples*

Functional Group	Binding energy (eV)
Hydrocarbon <u>C</u>-H, <u>C</u>-C	285.0
Alcohol, ether <u>C</u>-O-H, <u>C</u>-O-C	286.5
Carbonyl <u>C</u>=O	288.0
Acid, ester O-<u>C</u>=O	289.0

*The observed binding energy will depend on the specific environment where the functional groups are located. Most ranges are ±0.2 eV.

Table 2.5 Typical O_{1s} binding energy (E_B) for organic samples*

Functional Group	Binding energy (eV)
Carbonyl C=<u>O</u>, O-C=<u>O</u>	532.2
Alcohol, ether C-<u>O</u>-H, C-<u>O</u>-C	532.8
Ester C-<u>O</u>-C=O	533.7

*The observed binding energy will depend on the specific environment where the functional groups are located. Most ranges are ±0.2 eV.

Table 3.1 Typical physical properties of TECAFINE PE10

Property	ASTM Test Method	Typical Result	Unites
Molecular weight		6×10^6	g mol^{-1}
Density	527 / D 792	0.93	g cm^{-3}
Tensile strength at yield	527 / D 638	17	Pa
Tensile strength at break	527 / D 638	40	Pa
Elongation at break	527 / D 638	> 50	%
Modulus of elasticity in tension	527 / D 638	650	Pa
Modulus of elasticity in flexure	178 / D 790	800	Pa
Water Absorptionat saturation at 23 °C	62	0.02	%
Melting point	DIN 53 736	135	°C
Coefficient of friction against hardened and ground steel p = 0.05 N mm^{-2}, v = 0.6 m s^{-1}		0.29	
Specific heat		1.84	J(g.K)$^{-1}$
Coefficient of thermal expansion	DIN 53 483 /D 696	20	10^{-5}K^{-1}

Table 3.2 Typical physical properties of TUFSET rigid polyurethane

Property	ASTM Test Method	Typical Result	Unites
Flexural Strength	D 790	15,000	lbf/in^2
Flexural Modulus	D 790	350,000	lbf/in^2
Compressive Strength	D 695	10,000	lbf/in^2
Impact Strength Izod	D 256	1.3	ft-lbf/inch
Specific Gravity	D 792	1.2	$g\,cm^{-3}$
Hardness, durometer	D 2240	D83	
Water Absorption	D 570	0.1	%
Permittivity at 1 MHz	D 150	4.0	
Dissipation factor at 1 MHz	D 150	0.02	
Dielectric strength, 3mm	D 149	300	Vols/mile

Table 3.3 Typical physical and chemical properties of polycaprolactone

Property	ASTM Test Method	Typical Result	Unites
Synonyms		6-Caprolactone polymer	
Formula		$(C_6H_{10}O_2)_n$	
Molecular Weight	GPC	M_n 80,000	g/mol
Density at 25 °C		1.145	g/ml
Purity		>99	%
Melting point		60	°C

Table 3.4 Active screen plasma nitriding treatment conditions of UHMWPE

sample	treatment conditions		sample	treatment conditions	
	T (°C)	t (h)		T (°C)	t (h)
PE60-05h	60	0.5	PE80-05h	80	0.5
PE60-1h		1.0	PE80-1h		1.0
PE60-2h		2.0	PE80-2h		2.0
PE60-5h		5.0	PE80-5h		5.0
PE100-05h	100	0.5	PE130-05h	130	0.5
PE100-1h		1.0	PE130-1h		1.0
PE100-2h		2.0	PE130-2h		2.0
PE100-5h		5.0	PE130-5h		5.0

Table 3.5 Active screen plasma nitriding treatment conditions of PU

sample	treatment conditions		sample	treatment conditions	
	T (°C)	t (h)		T (°C)	t (h)
PU60-05h	60	0.5	PU80-05h	80	0.5
PU60-1h		1.0	PU80-1h		1.0
PU60-2h		2.0	PU80-2h		2.0
PU60-5h		5.0	PU80-5h		5.0
PU100-05h	100	0.5	PU130-05h	130	0.5
PU100-1h		1.0	PU130-1h		1.0
PU100-2h		2.0	PU130-2h		2.0
PU100-5h		5.0	PU130-5h		5.0

Table 3.6 Active screen plasma nitriding treatment conditions of PCL

sample	treatment conditions	
	T (°C)	t (min)
PCL50-10m	50	10

Table 4.1 Calculated results of 2θ and d values from XRD patterns of UHMWPE

Sample	2θ (°)		d (Å)	
peaks	110	200	110	200
PE0	21.66	23.98	4.10	3.71
PE60-05h	21.77	24.16	4.08	3.68
PE60-1h	21.59	23.95	4.11	3.71
PE60-2h	21.64	24.07	4.10	3.69
PE60-5h	21.72	24.01	4.09	3.70
PE80-05h	21.60	24.06	4.11	3.70
PE80-1h	21.65	24.08	4.10	3.69
PE80-2h	21.61	23.98	4.11	3.71
PE80-5h	21.69	24.04	4.09	3.70
PE100-05h	21.69	24.04	4.09	3.70
PE100-1h	21.77	24.08	4.08	3.69
PE100-2h	21.47	23.89	4.14	3.72
PE100-5h	21.53	23.83	4.13	3.73
PE130-05h	21.68	24.04	4.10	3.70
PE130-1h	21.62	24.00	4.11	3.70
PE130-2h	21.51	23.93	4.13	3.72
PE130-5h	21.57	23.97	4.12	3.71

Table 4.2 The crystallinity of UHMWPE before and after plasma treatment

samples	T (°C)	P (mbar)	t (h)	Crystallinity (%)
PE0				54.19±0.46
PE60-05h	60	2	0.5	54.10±0.40
PE60-1h	60	2	1	54.48±0.47
PE60-2h	60	2	2	55.20±0.57
PE60-5h	60	2	5	54.61±0.43
PE80-05h	80	2	0.5	54.64±0.83
PE80-1h	80	2	1	54.47±0.55
PE80-2h	80	2	2	54.93±0.57
PE80-5h	80	2	5	55.26±1.02
PE100-05h	100	2	0.5	54.18±0.62
PE100-1h	100	2	1	54.26±0.49
PE100-2h	100	2	2	56.13±1.66
PE100-5h	100	2	5	55.87±0.50
PE130-05h	130	2	0.5	57.58±0.62
PE130-1h	130	2	1	57.00±0.78
PE130-2h	130	2	2	59.02±1.75
PE130-5h	130	2	5	59.55±0.75

Table 4.3 Surface roughness results of UHMWPE before and after plasma treatment

Treatment conditions	Ra-before(μm)	Ra-after(μm)	ΔRa/ Ra-before
60°C, 0.5h	0.0893	0.1110	24.3%
60°C, 1h	0.0696	0.0924	32.7%
60°C, 2h	0.1540	0.1560	1.3%
60°C, 5h	0.1770	0.1860	5.1%
80°C, 0.5h	0.0916	0.1144	24.9%
80°C, 1h	0.0906	0.1067	17.7%
80°C, 2h	0.1140	0.1390	21.9%
80°C, 5h	0.0990	0.1510	52.5%
100°C, 0.5h	0.0817	0.1144	40.0%
100°C, 1h	0.0906	0.1094	20.8%
100°C, 2h	0.0880	0.1482	68.2%
100°C, 5h	0.0905	0.2252	148.8%
130°C, 0.5h	0.1080	0.3999	270.3%
130°C, 1h	0.1031	0.4130	300.6%
130°C, 2h	0.1020	0.4687	359.5%
130°C, 5h	0.1042	0.5952	471.2%

Table 4.4 Nano-indentation results of UHMWPE

Samples	H (GPa)	E (GPa)	H/E
PE	0.057819	0.796212	0.072618
PE60-0.5h	0.074847	0.867463	0.086283
PE60-1h	0.068636	0.836400	0.082061
PE60-2h	0.071923	0.955467	0.075275
PE60-5h	0.073999	0.978975	0.075589
PE80-0.5h	0.096692	1.234175	0.078345
PE80-1h	0.073703	0.948661	0.077692
PE80-2h	0.081959	1.049644	0.078083
PE80-5h	0.077964	1.101570	0.070775
PE100-0.5h	0.091068	1.259796	0.072288
PE100-1h	0.093161	1.310920	0.071065
PE100-2h	0.067699	1.030722	0.065681
PE100-5h	0.083442	1.144361	0.072916
PE130-0.5h	0.120918	1.629824	0.074191
PE130-1h	0.120918	1.629824	0.074191
PE130-2h	0.108087	1.650023	0.065506
PE130-5h	0.101727	1.709265	0.059515

Table 4.5 Wear factors of the untreated and ASPN treated UHMWPE samples

(pin-on-disc, 5.89N)

samples	Wear area ($\times10^{-3}$ mm^2)	Wear factor ($\times10^{-6}$ mm^3 m^{-1} N^{-1})	Improvement of wear resistance(%)
PE0	0.933979	11.793	untreated
PE60-0.5h	1.231172	15.545	-31.8
PE60-1h	0.683484	8.631	26.8
PE60-2h	0.650320	8.211	30.4
PE60-5h	0.702300	8.868	24.8
PE80-0.5h	1.734750	21.904	-85.7
PE80-1h	0.806137	10.179	13.7
PE80-2h	0.564521	7.128	39.6
PE80-5h	0.727040	9.180	22.2
PE100-0.5h	0.972254	12.276	-4.1
PE100-1h	0.763516	9.641	18.2
PE100-2h	0.599086	7.564	35.9
PE100-5h	1.118500	14.123	-19.8

Table 4.6 Reciprocating wear test profile area and friction coefficient of UHMWPE before and after plasma treatment (1000cycles, 3.92N)

Sample	PE	PE80-05h	PE100-05h	PE130-05h
Wear Area (nm^2)	7.75×10^8	9.23×10^8	7.10×10^8	6.03×10^8
friction coefficient	0.05	0.14	0.16	0.19

Table 4.7 Wear area (nm^2) of UHMWPE at different cycles and loads

Sample	2000cycles,3.92N	2000cycles,9.81N
PE	9.06×10^8	2.56×10^9
PE80-0.5h	9.97×10^8	2.94×10^9
PE100-0.5h	8.83×10^8	2.97×10^9

Table 4.8 Contact angle results of UHMWPE

samples	θ_{Water} (°)	samples	θ_{Water} (°)
PE0	79.9		
PE60-0.5h	72.4	PE100-0.5h	75.9
PE60-1h	72.8	PE100-1h	72.6
PE60-2h	73.7	PE100-2h	75.9
PE60-5h	74.5	PE100-5h	67.9
PE80-0.5h	68.3	PE130-0.5h	77.7
PE80-1h	69.0	PE130-1h	77.4
PE80-2h	68.3	PE130-2h	78.8
PE80-5h	72.5	PE130-5h	80.3

Table 4.9 Contact angle results with two liquids and surface energy of UHMWPE

samples	θ_{Water}(°)	$\theta_{Ethylene\ glycol}$ (°)	Surface Energy(mN/m)	Disperse Part (mN/m)	Polar Part (mN/m)
UHMWPE	79.9±2.27	60.0±1.45	26.96	14.11	12.85
PE80-05h	68.3±2.72	52.0±2.25	34.06	10.82	23.23
PE100-05h	75.9±2.34	51.3±2.67	31.40	18.38	13.02
PE130-05h	77.7±2.26	58.4±2.48	28.10	13.53	14.57

Table 5.1 Main description of FTIR data of PU and ratio of absorbance value before and after plasma treatment

Wavenumber(cm^{-1})	assignment	$A_{PU80-0.5h}/A_{PUuntreated}$(%)	$A_{PU130-0.5h}/A_{PUuntreated}$(%)
3300	N-H stretching	99.5	99.6
1700	C=O stretching	87.0	75.8
1596	N-H bending	88.9	81.7
1521	N-H bending, C-N stretching	90.1	78.3
1309	C-O stretching	89.5	81.5
1220	C-N stretching	89.5	79.0

A is absorbance value.

Table 5.2 Composition of untreated and ASPN treated PU samples

Peak	Untreated PU			ASPN treated PU		
	Position E_B* (eV)	Atomic conc. %	Atomic ratio	Position E_B* (eV)	Atomic conc. %	Atomic ratio
O 1s	532.9	18.5	O/C=0.25	532.0	19.0	O/C=0.30
N 1s	400.4	6.7	N/C=0.09	400.0	13.8	N/C=0.22
C 1s	284.9	73.7	N/O=0.36	285.0	62.4	N/O=0.72
Si 2p	102.5	1.2		102.5	1.8	
Fe 2p				710.8	3.1	

* E_B is binding energy

Table 5.3 Surface roughness results of PU before and after plasma treatment

Treatment Conditions	Ra-Before(μm)	Ra-After(μm)	ΔRa/ Ra-Before
60°C, 0.5h, 2mbar	0.055	0.056	2%
60°C, 1h, 2mbar	0.047	0.054	15%
60°C, 2h, 2mbar	0.054	0.056	4%
60°C, 5h, 2mbar	0.058	0.065	12%
80°C, 0.5h, 2mbar	0.052	0.057	10%
80°C, 1h, 2mbar	0.058	0.066	14%
80°C, 2h, 2mbar	0.062	0.064	3%
80°C, 5h, 2mbar	0.044	0.046	5%
100°C, 0.5h, 2mbar	0.049	0.058	18%
100°C, 1h, 2mbar	0.053	0.053	0%
100°C, 2h, 2mbar	0.064	0.083	30%
100°C, 5h, 2mbar	0.062	0.116	87%
130°C, 0.5h, 2mbar	0.064	0.071	11%
130°C, 1h, 2mbar	0.051	0.065	27%
130°C, 2h, 2mbar	0.066	0.517	683%
130°C, 5h, 2mbar	0.060	0.212	253%

Table 5.4 Nano-indentation results of PU

Samples	H (GPa)	E (GPa)	H/E
PU0	0.1051±0.01359	2.5245±0.1986	0.04164
PU80-0.5h	0.1107±0.01237	2.4537±0.1740	0.04513
PU80-5h	0.1160±0.01662	2.4925±0.1916	0.04653
PU100-0.5h	0.1191±0.01932	2.4904±0.2161	0.04782
PU130-0.5h	0.1219±0.01761	2.5268±0.1983	0.04823

Table 5.5 Improvement of wear resistance of PU samples before and after plasma treatment

(Pin-on-disc, 9.81N)

samples	Wear factor $(\times 10^{-3} \text{ mm}^3 \text{ m}^{-1} \text{ N}^{-1})$	Improvement of wear resistance(%)
PU0	0.54	
PU80-0.5h	0.13	76.3
PU80-1h	0.28	48.2
PU80-2h	0.40	26
PU80-5h	0.73	-35
PU100-0.5h	0.30	45.2
PU100-1h	0.24	54.6
PU100-2h	0.45	16.5
PU100-5h	0.63	-16.8
PU130-0.5h	0.52	4.0
PU130-1h	0.89	-64.8
PU130-2h	0.68	-26.4
PU130-5h	0.67	-23.8

Table 5.6 Wear area of PU before and after plasma treatment

(Reciprocating, 10000 cycles)

Loads (N)	Wear area (nm^2)		
	PU	PU80-0.5h	PU130-0.5h
9.81	8.17×10^7	5.63×10^7	8.73×10^7
19.62	2.09×10^8	2.88×10^8	2.93×10^8

Table 5.7 Contact angle results with two liquids and surface energy of PU

Samples	θ_{water} (°)	$\theta_{glycerol}$ (°)	Surface Energy (mN/m)	Disperse Part (mN/m)	Polar Part (mN/m)	Increase of surface energy(%)
PU	70.9±1.58	66.3±1.93	32.22	11.59	20.64	
PU60-0.5h	65.9	68.2	39.4	2.03	37.37	22%
PU60-1h	67.1	69.9	39.1	1.52	37.58	21%
PU60-2h	81	77.5	24.36	8.23	16.12	-24%
PU60-5h	80.4	75.8	25.29	10.46	14.83	-22%
PU80-0.5h	76.1	83.5	41.67	0.28	41.6	29%
PU80-1h	69.1	76	45.85	0.01	45.83	42%
PU80-2h	79	82.4	30.42	0.48	29.95	-6%
PU80-5h	86.3	85.8	20.87	3.12	17.75	-35%
PU100-0.5h	74.8	83	45.05	0.55	44.5	40%
PU100-1h	74.6	90.3	76.38	10.2	66.18	137%
PU100-2h	80	82.8	28.71	0.73	27.98	-11%
PU100-5h	82.4	85.9	27.98	0.31	27.67	-13%
PU130-0.5h	86.6	95.7	38.58	1.94	36.64	20%
PU130-1h	83.8	87.5	27.27	0.21	27.06	-15%
PU130-2h	81.7	85.6	29.21	0.2	29	-9%
PU130-5h	90.4	93.9	22.2	0.12	22.08	-31%

Table 6.1 Main XRD peak data of untreated and treated PCL

Sample	2θ(°)	d-spacing(Å)	Height(cts)	FWHM(°)	Area(cts 2θ°)
Untreated PCL	20.56	4.3161	270.00	3.5827	912.5646
	21.36	4.1558	3892.45	0.3725	1396.0950
	22.01	4.0343	598.97	0.3300	214.2015
	23.67	3.7556	686.78	0.6537	493.7651
Treated PCL	20.59	4.3087	315.01	3.9572	860.3523
	21.41	4.1462	4704.92	0.3977	1525.4810
	22.06	4.0247	1036.62	0.3039	199.0591
	23.73	3.7471	1093.91	0.5423	469.4535

Table 6.2 Composition of untreated and ASPN treated PCL samples

Peak	Untreated PCL			ASPN treated PCL		
	Position E_B* (eV)	Assignment	Atomic conc. %	Position E_B* (eV)	Assignment	Atomic conc. %
C 1s	285.0	$-CH_2-$		285.0		
	286.5	$-C-O-$	75.7			77.5
	288.9	$-(C=O)-O-$				
O 1s	533.5	C—O—C		533.5	C—O—C	
	532.0	C=O	24.3	532.0	C=O	21.4
				532.6	C—OH	
N 1s						1.1

* E_B is binding energy

Table 6.3 Surface roughness results of PCL before and after plasma treatment

Sample	Ra (um)
Untreated PCL	3.348 ±0.5360
PCL50-10min	3.385 ±0.3737

Table 6.4 Contact angle results with two liquids and surface energy of PCL

Sample	θ_{Water} (°)	$\theta_{Ethylene\ Glycol}$ (°)	Surface Energy (mN/m)	Disperse Part (mN/m)	Polar Part (mN/m)
PCL-untreated	75.1±0.36	60.5±0.38	28.76	9.60	19.16
PCL-treated	71.0±0.34	56.0±0.30	31.87	9.91	21.96

Table 7.1 The main FTIR data of PU before and after ASPN treatment

Wavenumber(cm^{-1})	assignment	A_1*	A_2**	A_2/A_1 (%)	1-A_2/A_1 (%)
3300	N-H stretching	0.0139	0.0126	90.7	9.3
1705	C=O stretching	0.1202	0.0866	72.0	28
1596	N-H bending	0.0568	0.0446	82.2	17.8
1521	N-H bending, C-N stretching	0.1735	0.1399	80.6	19.4
1309	C-O stretching	0.0929	0.0772	83.1	16.9
1220	C-N stretching	0.2270	0.1805	79.5	20.5

*A_1 is the absorbance value of untreated PU. **A_2 is the absorbance value of ASPN PU.

Table 7.2 Changes in the infrared spectra of PU samples are associated with hydrogen bonding before and after ASPN treatment

Wavenumber(cm^{-1})	assignment	A_1*	A_2**	A_2/A_1 (%)
1705	C=O stretching	0.1202	0.0866	72.0
	(hydrogen bonded urethane)			
1730	C=O stretching	0.1011	0.0765	75.6
	(non-hydrogen bonded urethane)			

*A_1 is the absorbance value of untreated PU. **A_2 is the absorbance value of ASPN PU at 100°C for 2h.

Table 7.3 Changes in the FTIR spectra of PU samples with increasing treatment temperature and time are associated with the C=O stretching modes at 1730 cm^{-1} and 1705 cm^{-1}.

sample	A_{1730}*	A_{1705}**	A_{1730}/A_{1705}(%)	Increase of A_{1730}/A_{1705}(%)
PU-untreated	0.1011	0.1202	84.2	
PU80-05h	0.0806	0.0937	86.0	1.8
PU100-2h	0.0765	0.0866	88.4	4.2
PU100-5h	0.0327	0.0368	89.0	4.8
PU130-05h	0.0607	0.697	87.1	2.9
PU130-2h	0.0245	0.0257	95.2	11.0
PU130-5h	0.0245	0.0248	98.8	14.6

* A_{1730} is the absorbance value at 1730 cm^{-1}. **A_{1705} is the absorbance at 1705 cm^{-1}

Table 7.4 The main FTIR data of PCL before and after ASPN treatment

Wavenumber(cm^{-1})	assignment	A$_1$*	A$_2$**	A$_2$/A$_1$ (%)
2944	symmetric C–H stretching	0.083933	0.076943	91.6717
2860	asymmetric C–H stretching	0.038674	0.034997	90.4939
1721	C=O stretching	0.833977	0.759234	91.0377
1365	CH$_2$ bending	0.156106	0.143527	91.9416
1238	C–C–O stretching	0.339748	0.310944	91.5220
1164	C–O–C bending	0.524532	0.478000	91.1289
960	C-CH$_3$ bending	0.159429	0.146321	91.7780

*A$_1$ is the absorbance value of untreated PCL. **A$_2$ is the absorbance value of ASPN PCL.

Table 7.5 The main Raman data of PCL before and after ASPN treatment

Wavenumber(cm^{-1})	assignment	A$_1$*	A$_2$**	A$_2$/A$_1$ (%)
2921	C-H	4507.96	1304.19	0.289308
1721	C=O	9633.99	2872.89	0.298204
1440	CH$_2$	13273.5	4233.78	0.318965
1303	C-C	9590.22	4530.96	0.472456

*A$_1$ is the absorbance value of untreated PCL. **A$_2$ is the absorbance value of ASPN PCL.

Table 7.6 Changes observed in the FTIR spectra of UHMWPE with increasing treatment temperature

Sample	A_{965}*	A_{1460}**	A_{965}/A_{1460} (%)	Increase of A_{965}/A_{1460} (%)
PE-untreated	0.004475	0.163705	2.73	
PE-80-05h	0.016759	0.071896	23.31	20.58
PE-130-05h	0.017439	0.071123	24.52	21.79

*A_{965} is the absorbance value at 965 cm^{-1}. **A_{1460} is the absorbance at 1460 cm^{-1}

$$H_2C=CH_2 \quad \left[H_2C-CH_2 \right]_n$$

Figure 2.1 Schematic of the chemical structure of ethylene and polyethylene

$$O=C=N-R^1-N=C=O \ + \ HO-R^2-OH \ + \ O=C=N-R^1-N=C=O \ + \ HO-R^2-OH \ + \ \cdots \longrightarrow$$

$$\cdots \ -\overset{\overset{\displaystyle O}{\|}}{C}-\underset{\underset{\displaystyle H}{|}}{N}-R^1-\underset{\underset{\displaystyle H}{|}}{N}-\overset{\overset{\displaystyle O}{\|}}{C}-O-R^2-O-\overset{\overset{\displaystyle O}{\|}}{C}-\underset{\underset{\displaystyle H}{|}}{N}-R^1-\underset{\underset{\displaystyle H}{|}}{N}-\overset{\overset{\displaystyle O}{\|}}{C}-O-R^2-O- \ \cdots$$

Figure 2.2 Generalized polyurethane reaction

$$\left[(CH_2)_5 - \overset{\overset{\displaystyle }{|}}{\underset{\underset{\displaystyle O}{\|}}{C}} - O \right]_n$$

Figure 2.3 Schematic of the chemical structure of polycaprolactone

Figure 2.4 Equilibrium contact angle θ

(a)   (b)

Figure 2.5 Active screen plasma system for surface modification of polymer

a)Schematic diagram; b) Photo of plasma furnace

Figure 2.6 Schematic of structure of a vinyl polymer

Figure 2.7 A schematic representation of indentation load - displacement curves

Figure 2.8 A schematic representation of a section through an indentation

$$Ra = \frac{1}{\ell} \int_0^\ell |f(x)| \, dx$$

Figure 2.9 The arithmetic average roughness profile

Figure 2.10 Schematic illustration of the operation of AFM

Figure 2.11 Atomic force curves for interaction of two atoms

Figure 2.12 A schematic illustration of ATR-FTIR

Figure 3.1 Schematic of nano-indentation machine

Figure 3.2 Schematic of pin-on-disc machine and test configuration

Figure 4.1 DSC curves of UHMWPE

Figure 4.2 XRD pattern of untreated UHMWPE

Figure 4.3 XRD patterns of UHMWPE after ASPN treated at different temperatures

Figure 4.4 XRD patterns of UHMWPE after ASPN treated at different time

Figure 4.5 FTIR spectra of UHMWPE

Figure 4.6 FTIR spectra of UHMWPE from 1000 to 900 cm^{-1} wavenumbers

Figure 4.7 Crystal field splitting results in doublets at 730 and 720 cm^{-1}

FTIR spectra of UHMWPE before and after plasma treatment
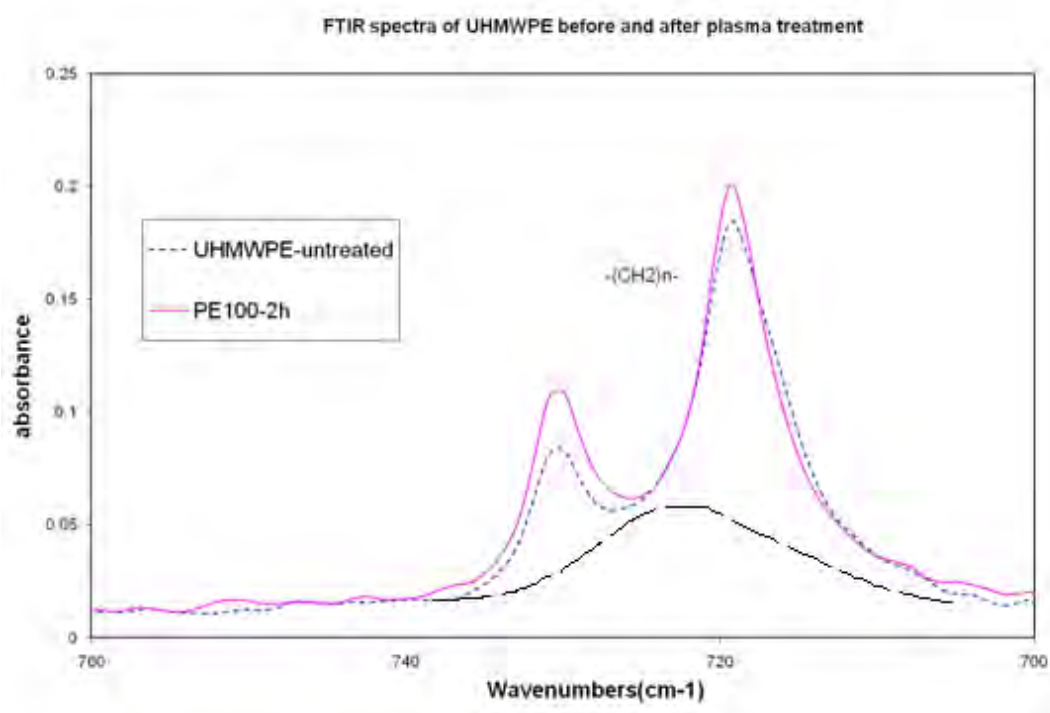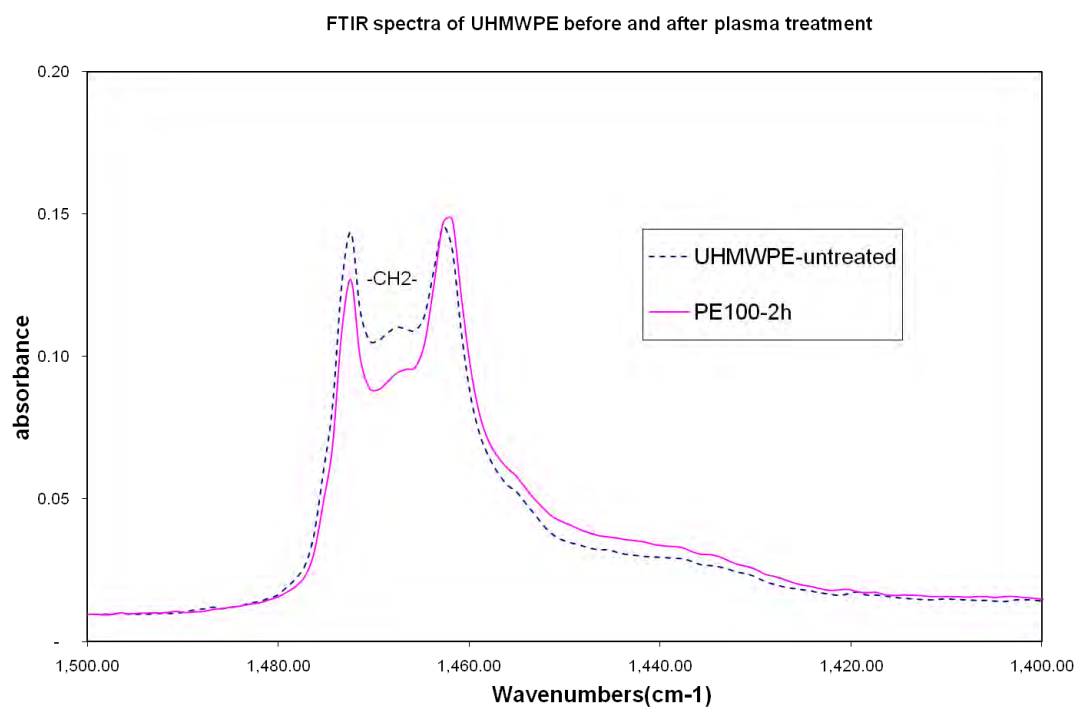
Figure 4.8 Crystal field splitting results in doublets at 1473 and 1460 cm^{-1}
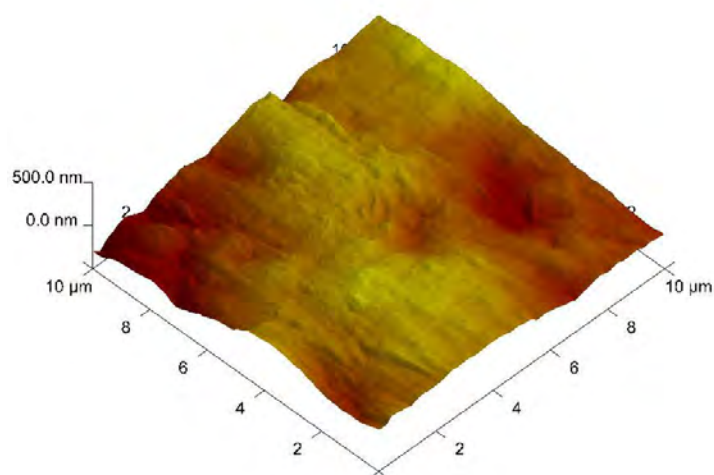
Figure 4.9 The AFM image of untreated UHMWPE
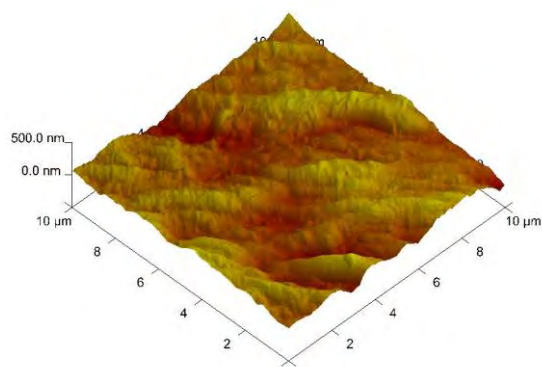
a) PE130-0.5h   b) PE130-1h
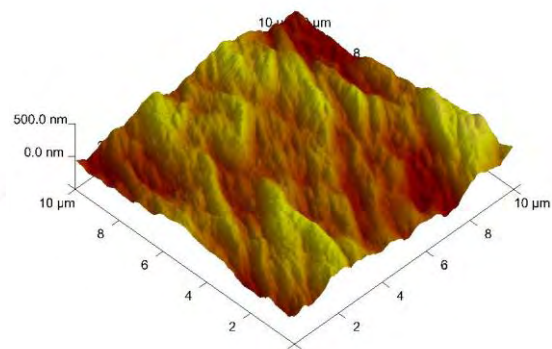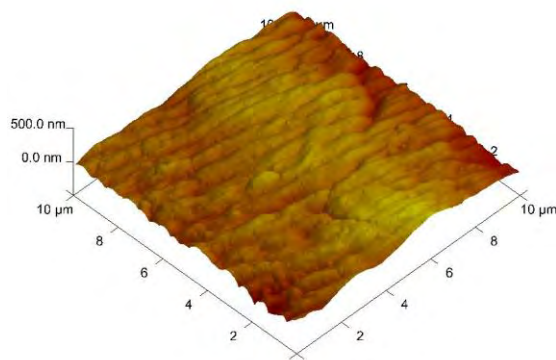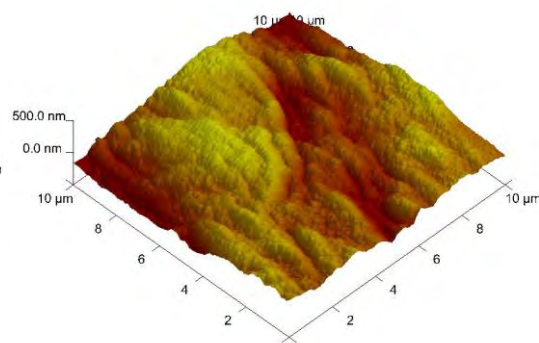
c) PE130-2h   d) PE130-5h

Figure 4.10 The AFM images of plasma treated UHMWPE at 130ºC a) PE130-0.5h; b) PE130-1h; c) PE130-2h; d) PE130-5h
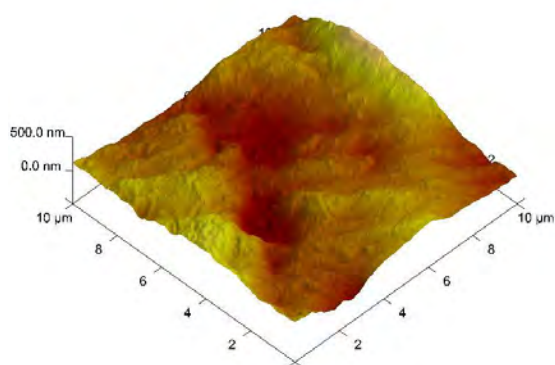
a) PE100-0.5h   b) PE100-1h
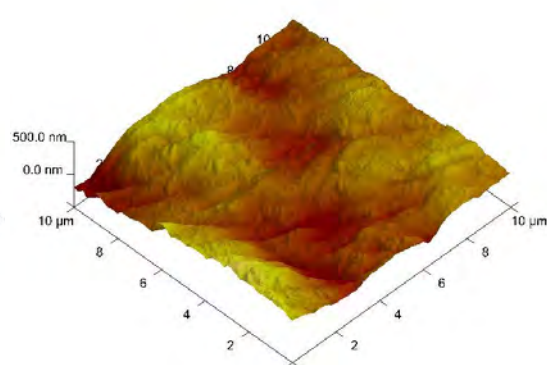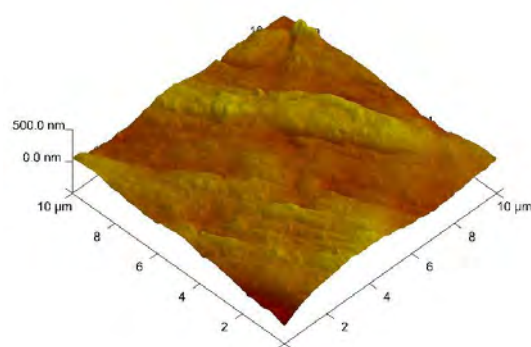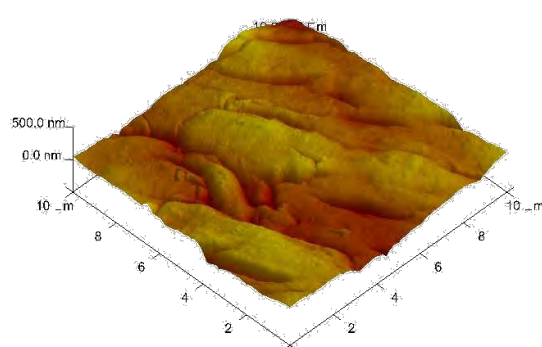
c) PE100-2h   d) PE100-5h

Figure 4.11 The AFM images of plasma treated UHMWPE at 100℃ a) PE100-0.5h; b)

PE100-1h; c) PE100-2h; d) PE100-5h
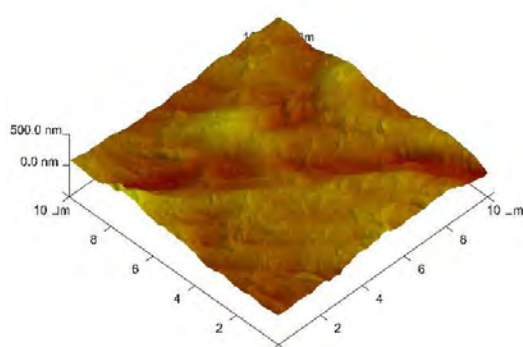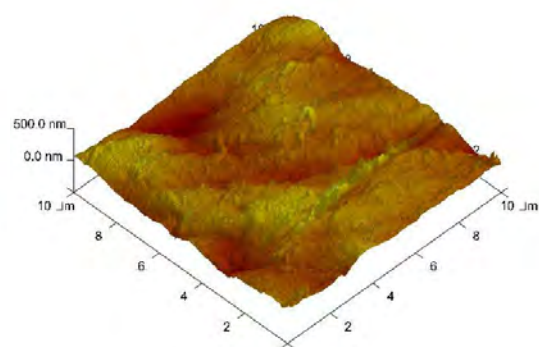
a) PE80-0.5h   b) PE80-1h
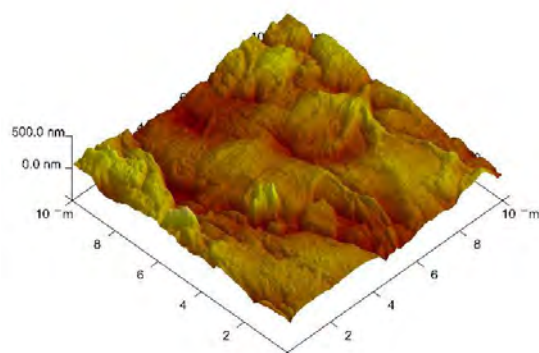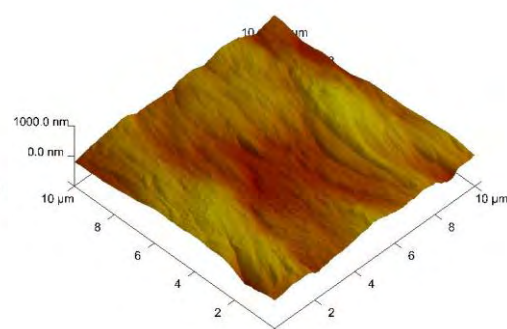
c) PE80-2h   d) PE80-5h

Figure 4.12 The AFM images of plasma treated UHMWPE at 80℃ a) PE80-0.5h; b) PE80-
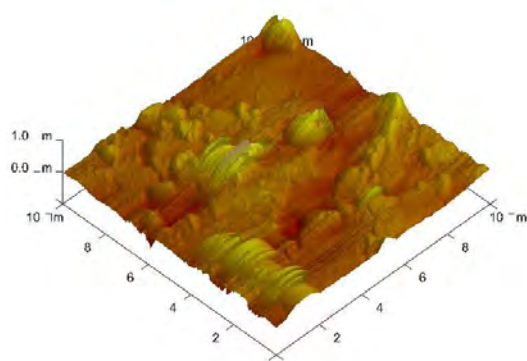
1h; c) PE80-2h; d) PE80-5h

a) PE60-0.5h   b) PE60-1h
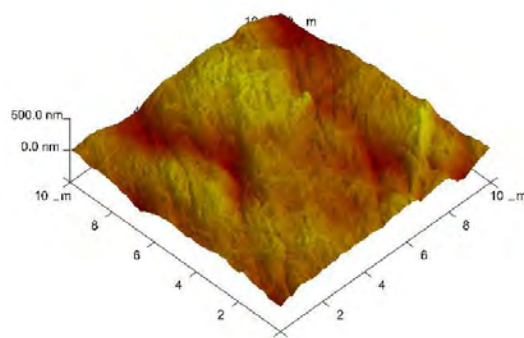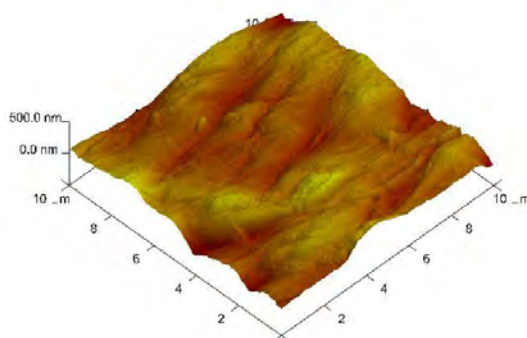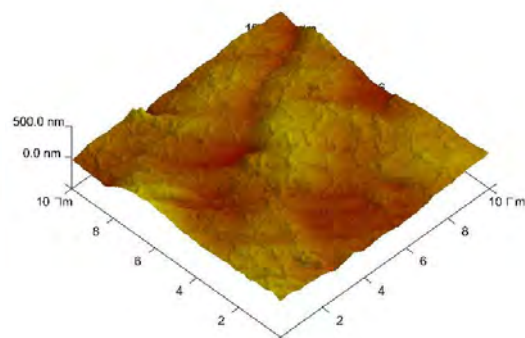
c) PE60-2h   d) PE60-5h

Figure 4.13 The AFM images of plasma treated UHMWPE at 60℃ a) PE60-0.5h; b) PE60-1h; c) PE60-2h; d) PE60-5h
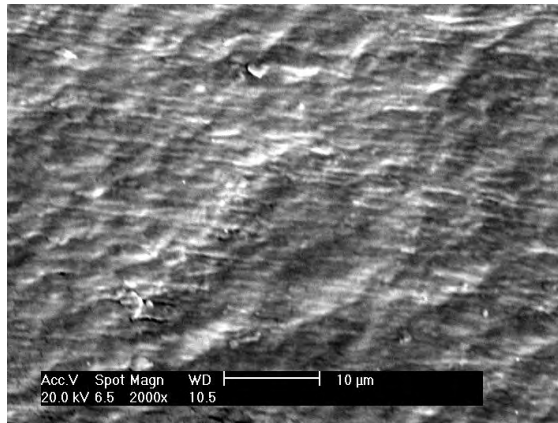
Figure 4.14 SEM image of untreated UHMWPE
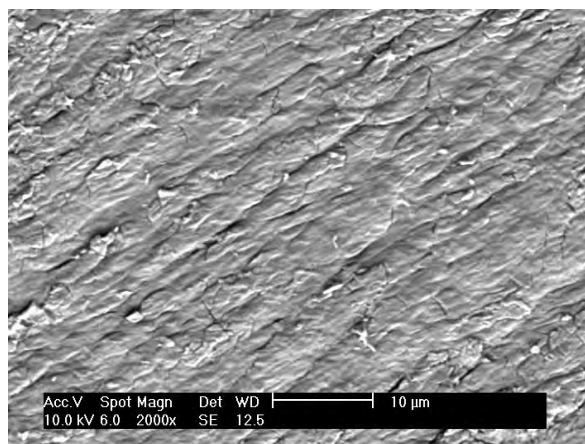
PE60-2h

Figure 4.15 SEM images of plasma treated UHMWPE at 60 ºC
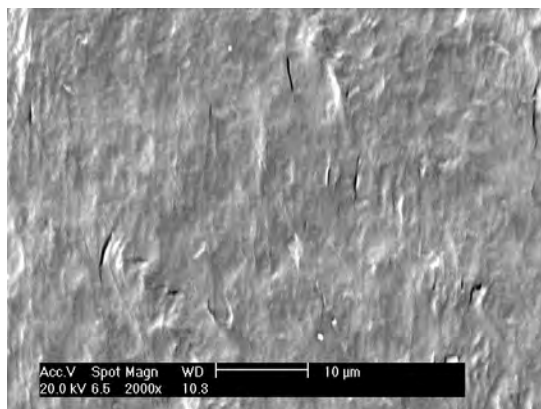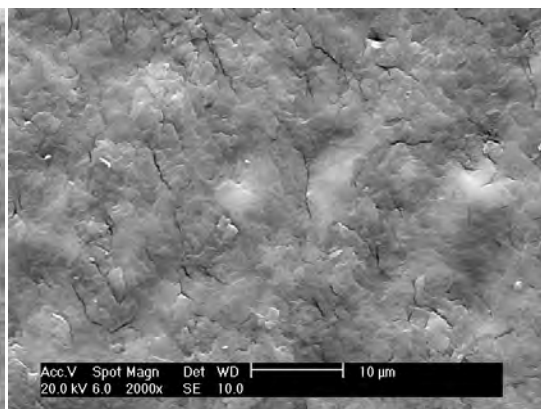
PE80-05h   PE80-2h

Figure 4.16 SEM images of plasma treated UHMWPE at 80 ºC
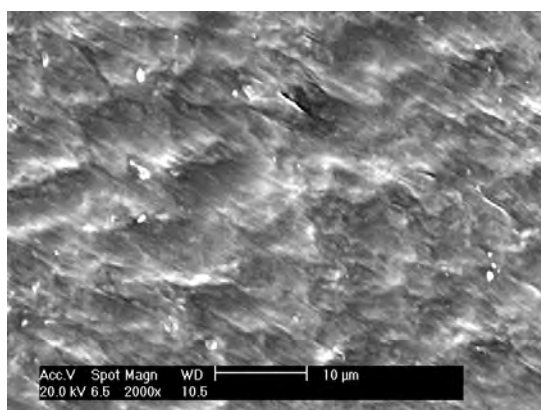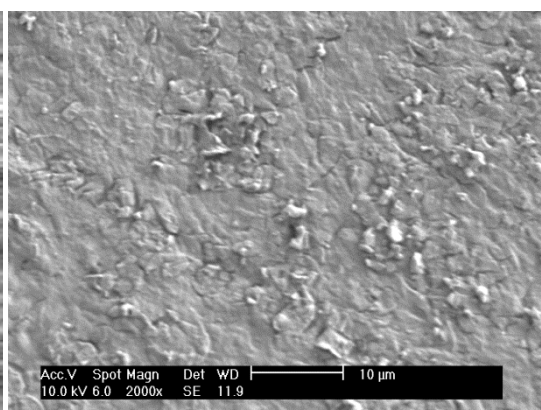
PE100-05h   PE100-1h
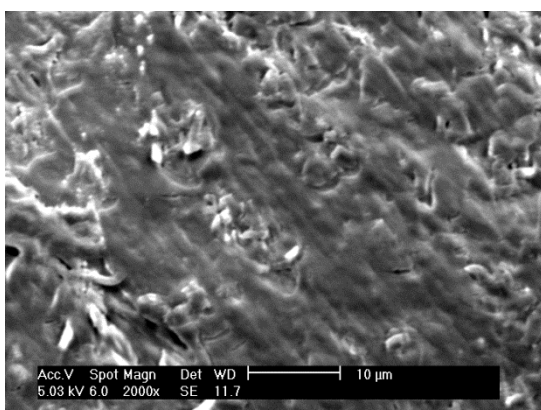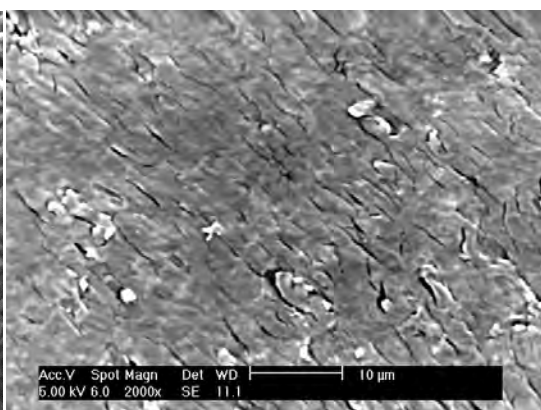
PE100-2h   PE100-5h

Figure 4.17 SEM images of plasma treated UHMWPE at 100 ºC
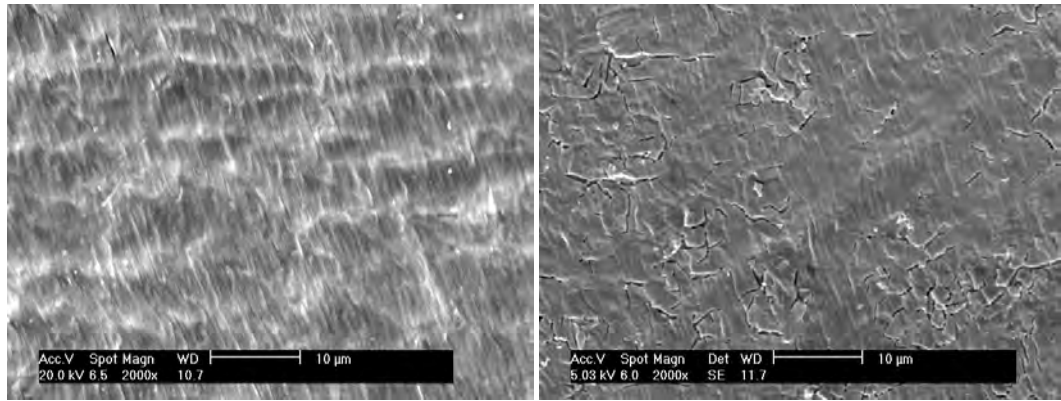
PE130-05h	PE130-2h

Figure 4.18 SEM images of plasma treated UHMWPE at 130 ºC
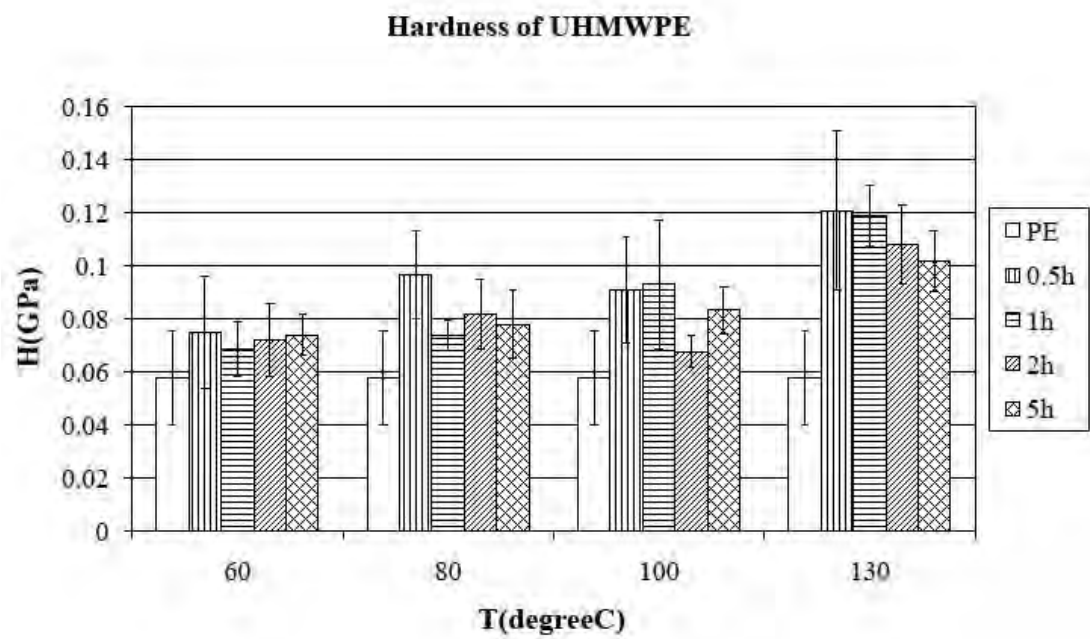
Figure 4.19 Hardness of UHMWPE before and after plasma treatment

Elastic Modulus of UHMWPE
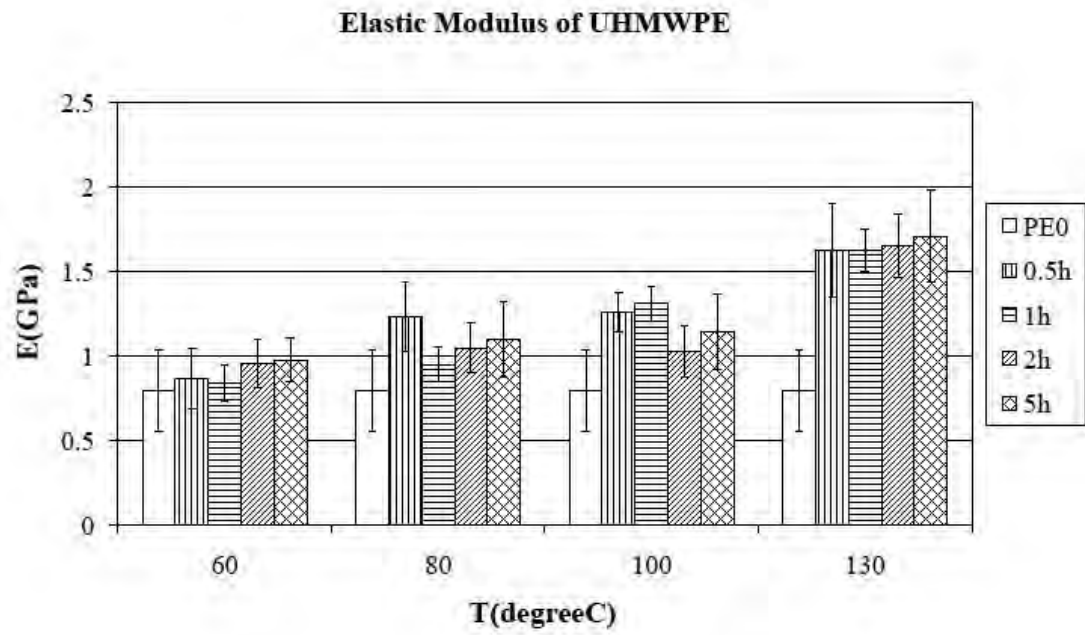
Figure 4.20 Elastic modulus of UHMWPE before and after plasma treatment
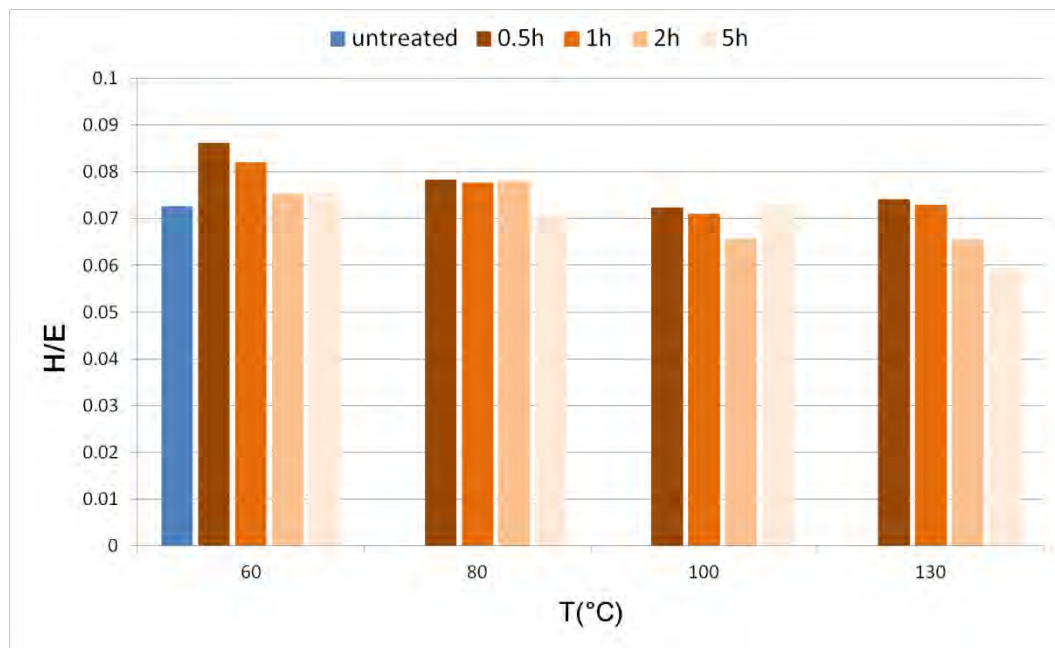
Figure 4.21 H/E values of UHMWPE before and after plasma treatment

173
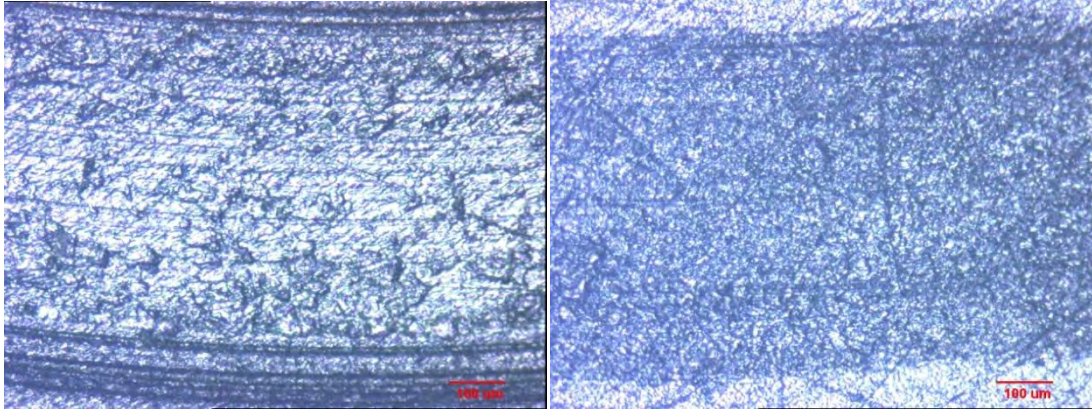
<center>(a)   (b)</center>

Figure 4.22 Morphology of wear (a) Untreated, (b) ASPN treatment
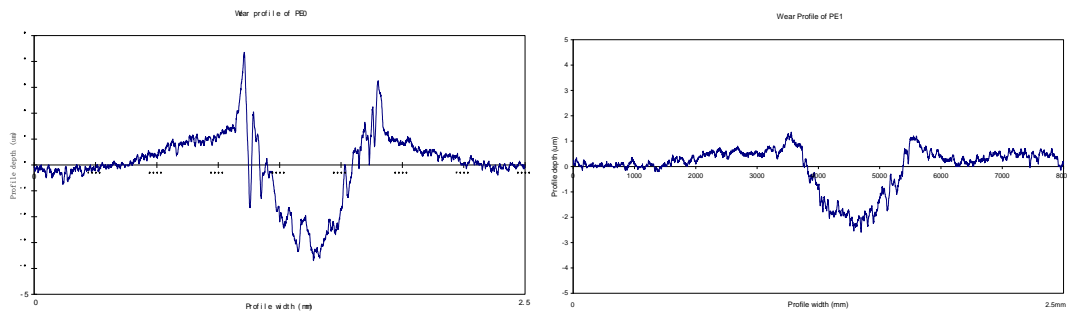
<center>(a)   (b)</center>

Figure 4.23 Wear profile of UHMWPE (a) untreated, (b) ASPN treated
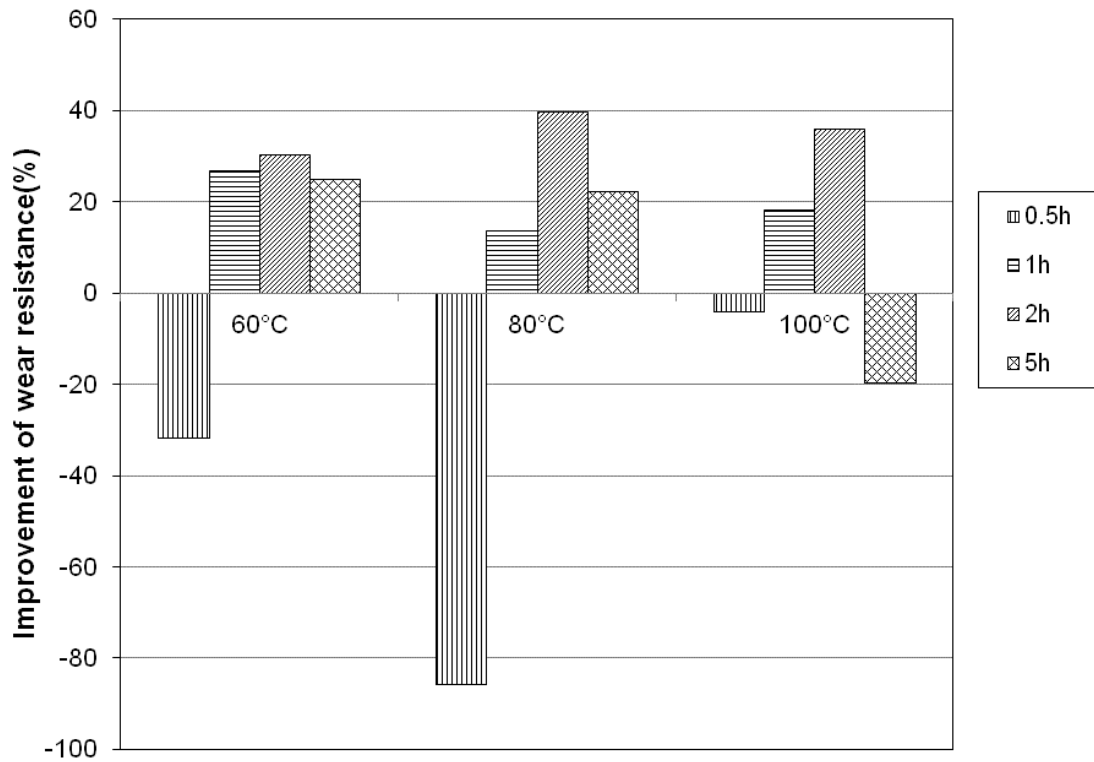
Figure 4.24 Improvement of UHMWPE wear resistance (pin on disc) after plasma treatment
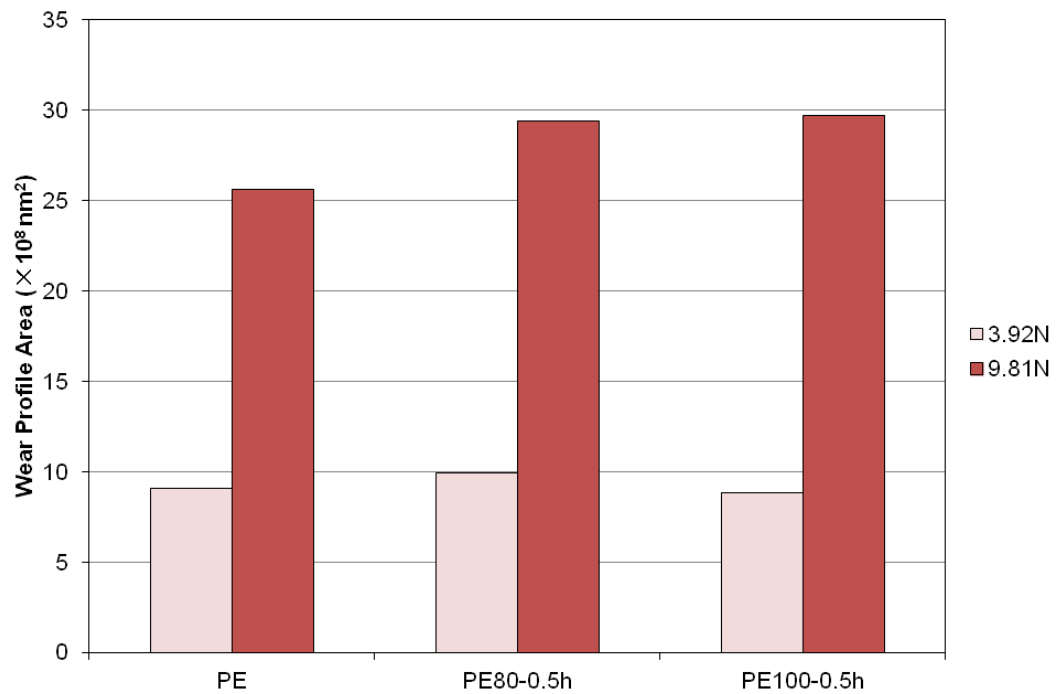
Figure 4.25 Wear area of UHMWPE at different loads before and after plasma treatment

(Reciprocating, 2000cycles)

175
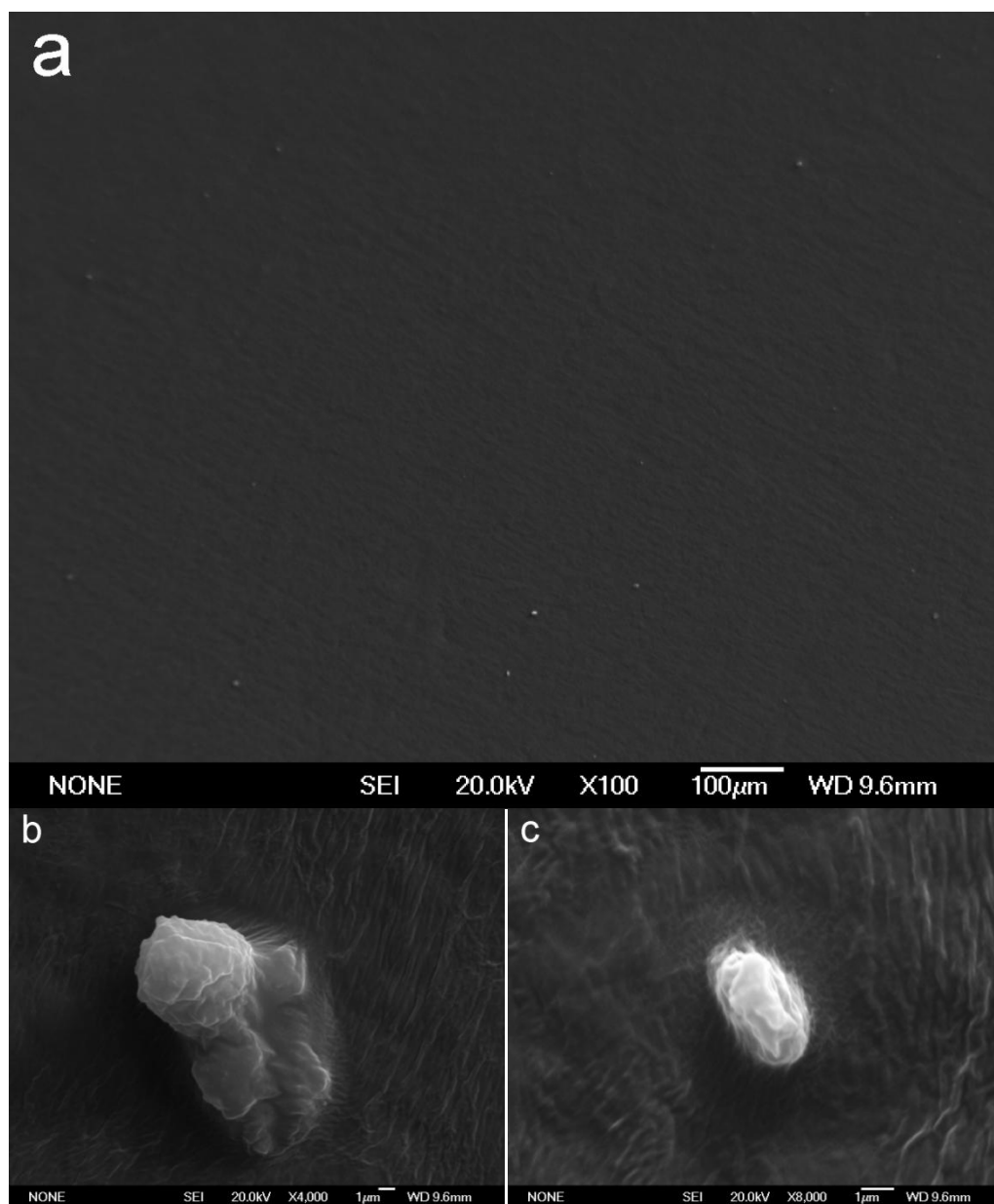
Figure 4.26 Scanning electron micrographs of cells attachment onto untreated UHMWPE

（a. ×100; b.×4000; c.×8000）
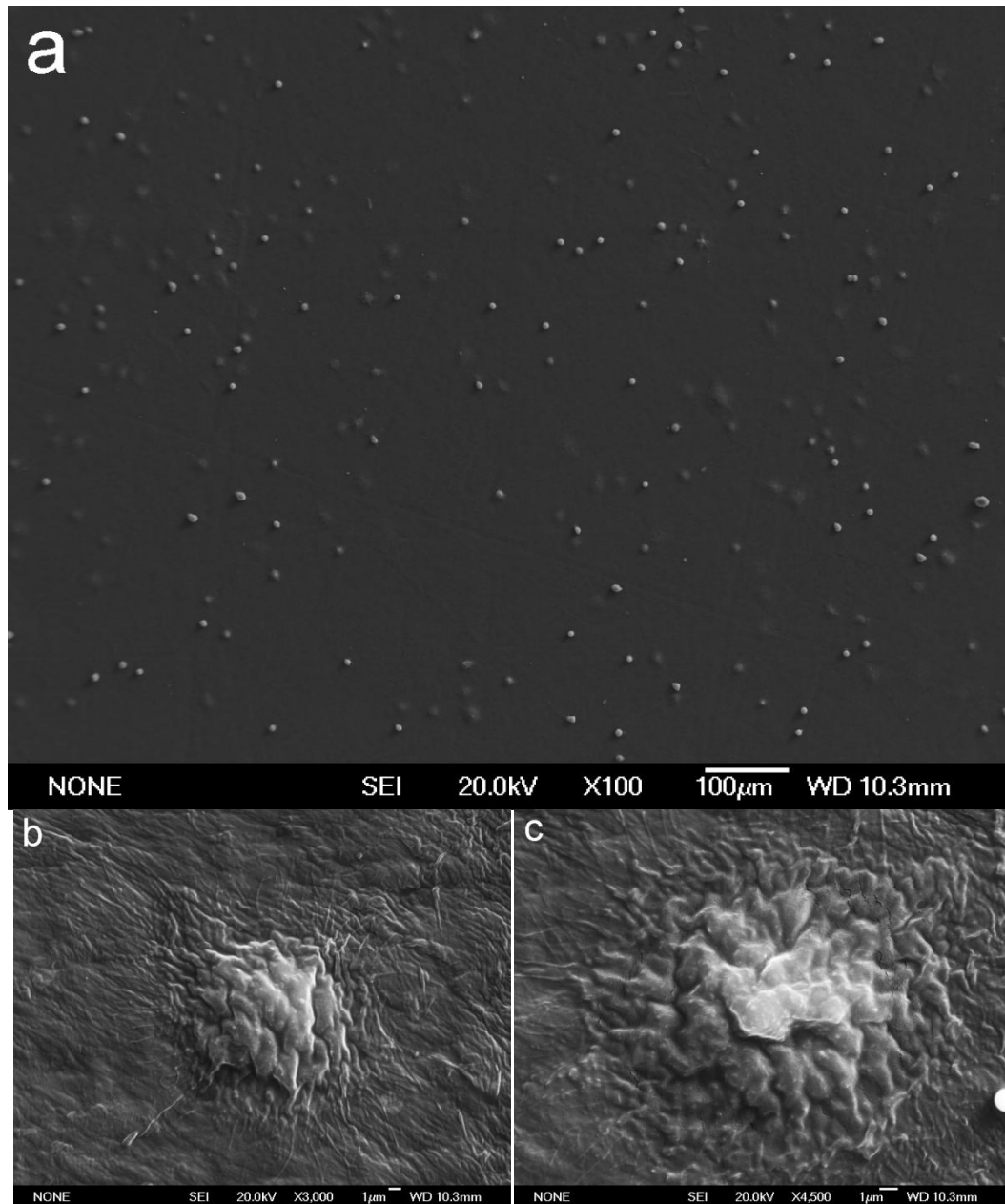
Figure 4.27 Scanning electron micrographs of cells attachment onto ASPN treated UHMWPE

at 80 ºC for 0.5 h (a. ×100; b.×3000; c.×4500)
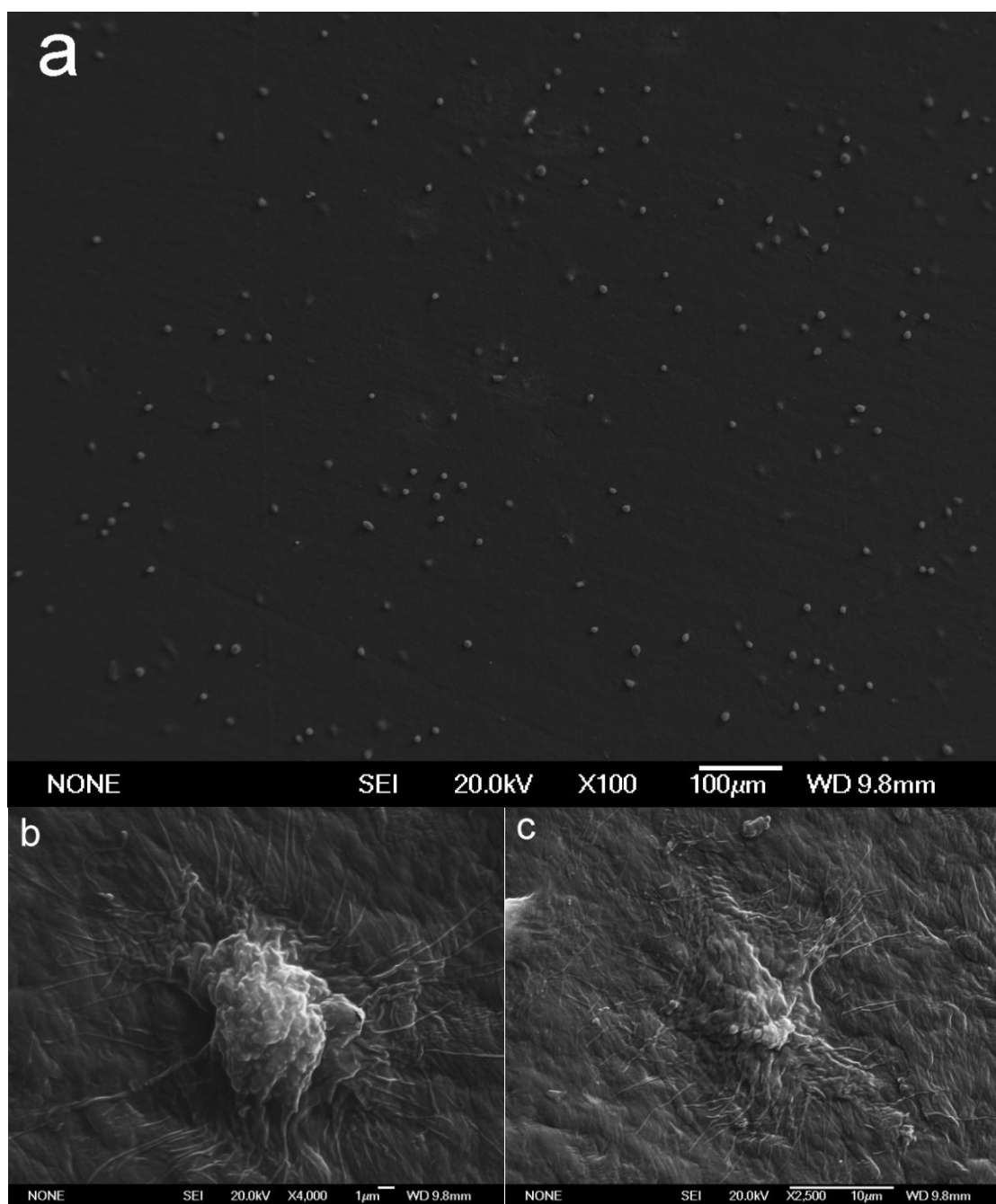
Figure 4.28 Scanning electron micrographs of cells attachment onto ASPN treated UHMWPE

at 100 ºC for 0.5 h (a. ×100; b.×4000; c.×2500)
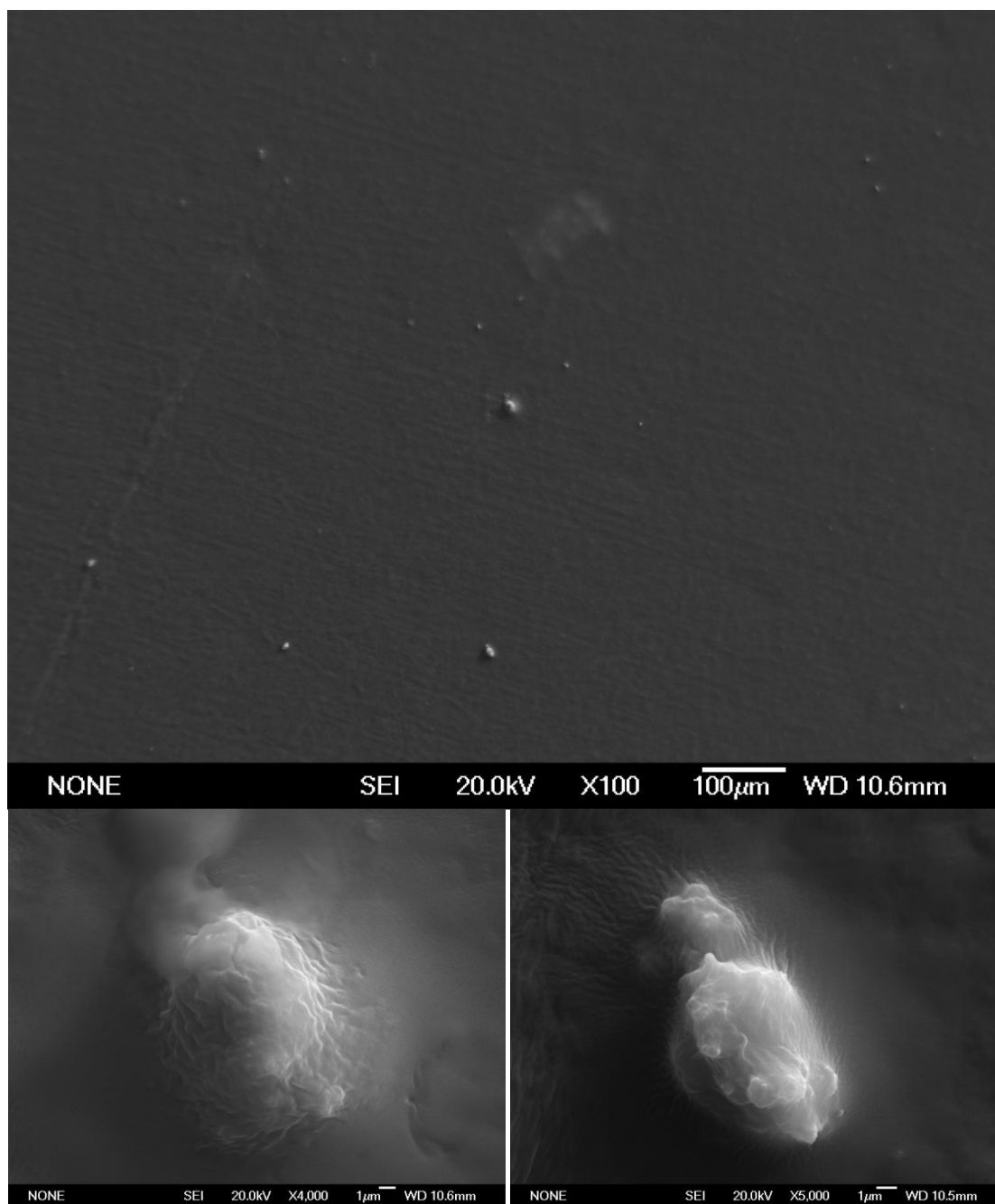
Figure 4.29 Scanning electron micrographs of cells attachment onto ASPN treated UHMWPE

at 130 ºC for 0.5 h (a. ×100; b.×4000; c.×5000)
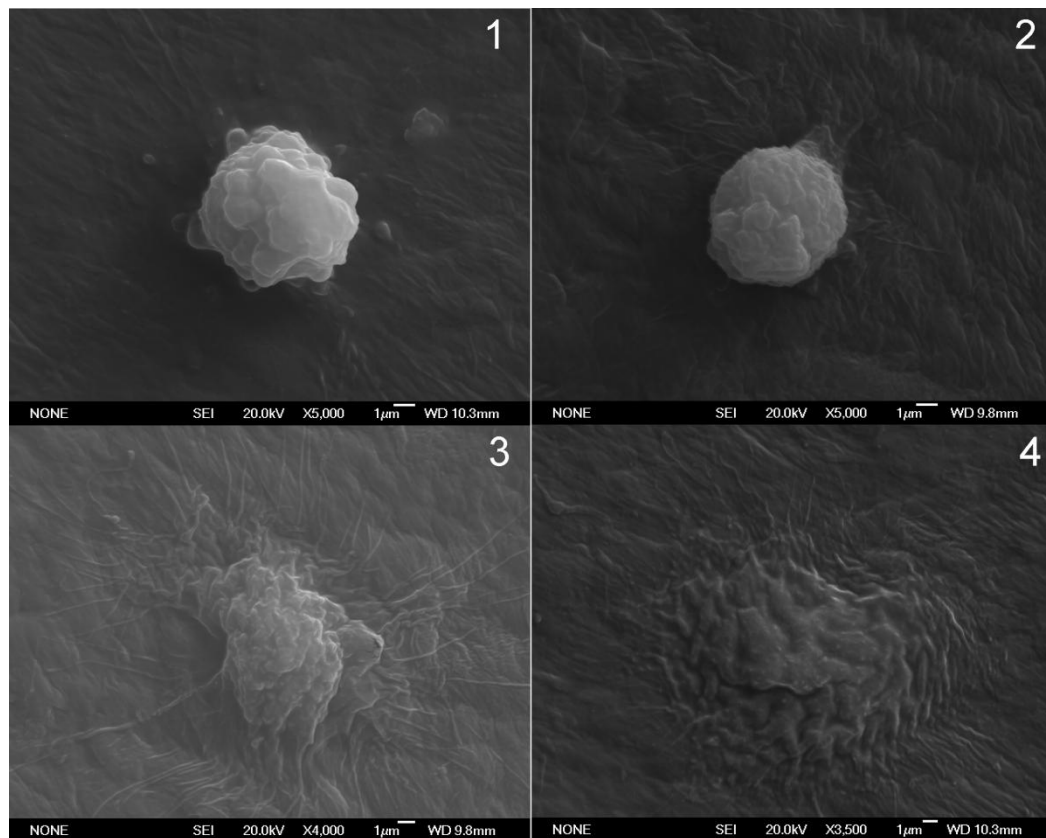
Figure 4.30 Four stages of osteoblast cells on surface of UHMWPE ASPN treated at 80 and

100 °C. 1. Adhesion; 2. Filopodial growth; 3. Cytoplasmic webbing; 4. Flat cell.
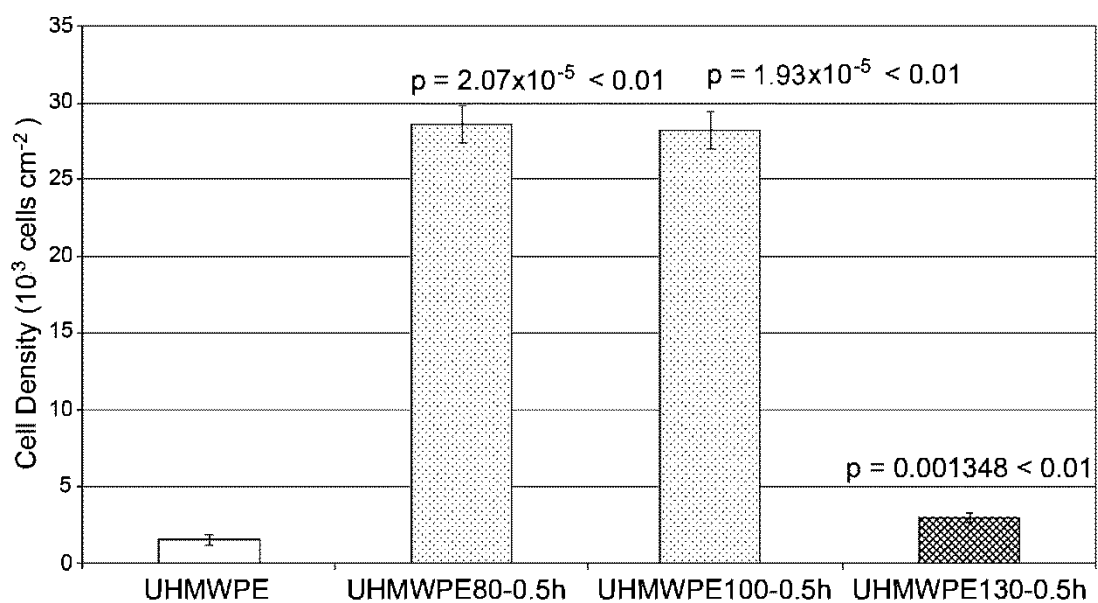
Figure 4.31 Cell density on UHMWPE surface after attachment for 1h
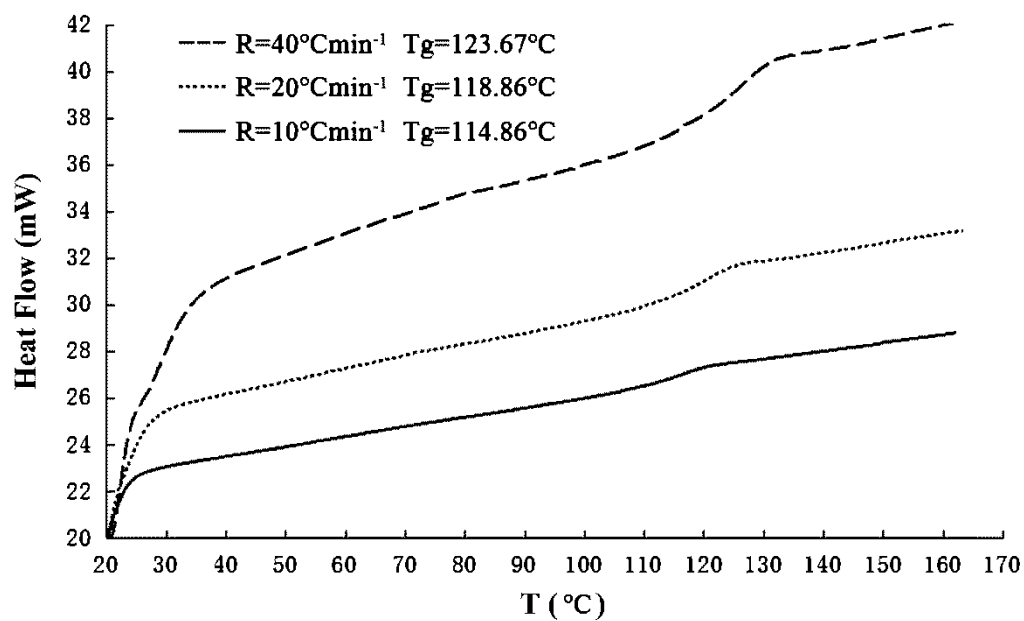
Figure 5.1 DSC curves of polyurethane at different heating rate
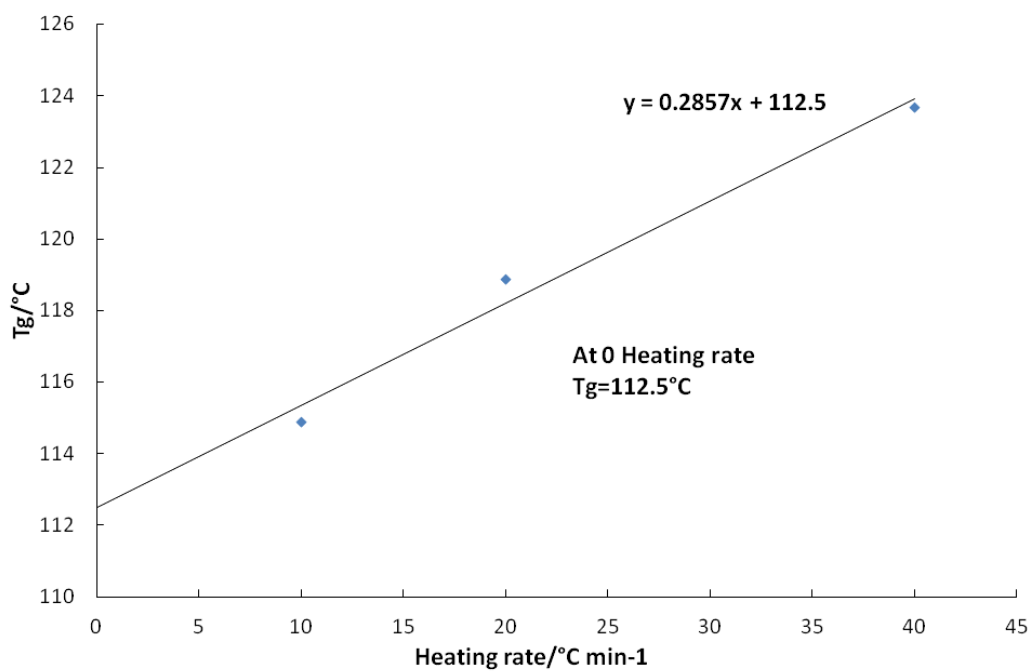
Figure 5.2 Relation between glass transition temperature T_g and heating rate
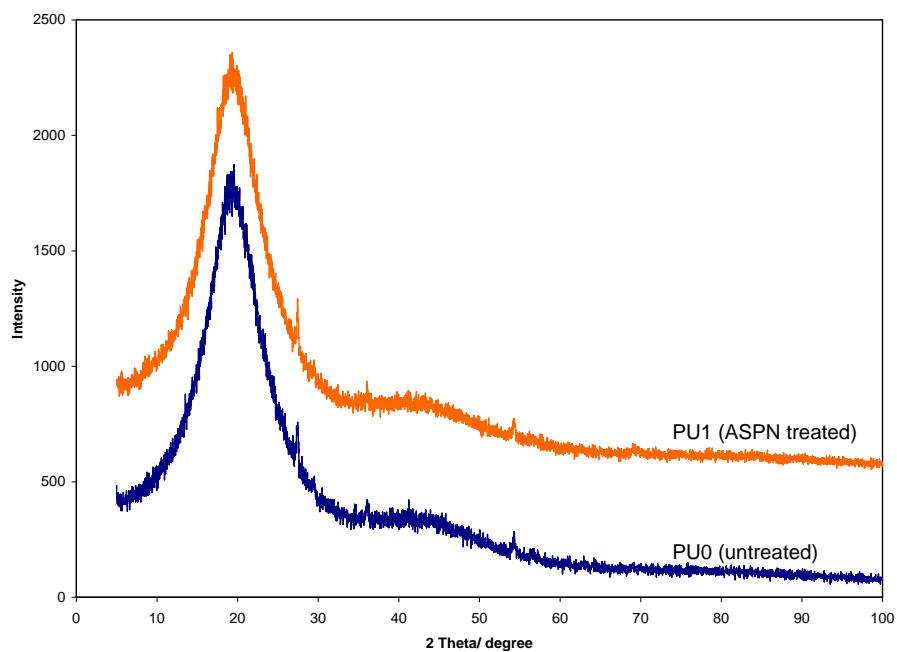
Figure 5.3 XRD patterns of PU samples
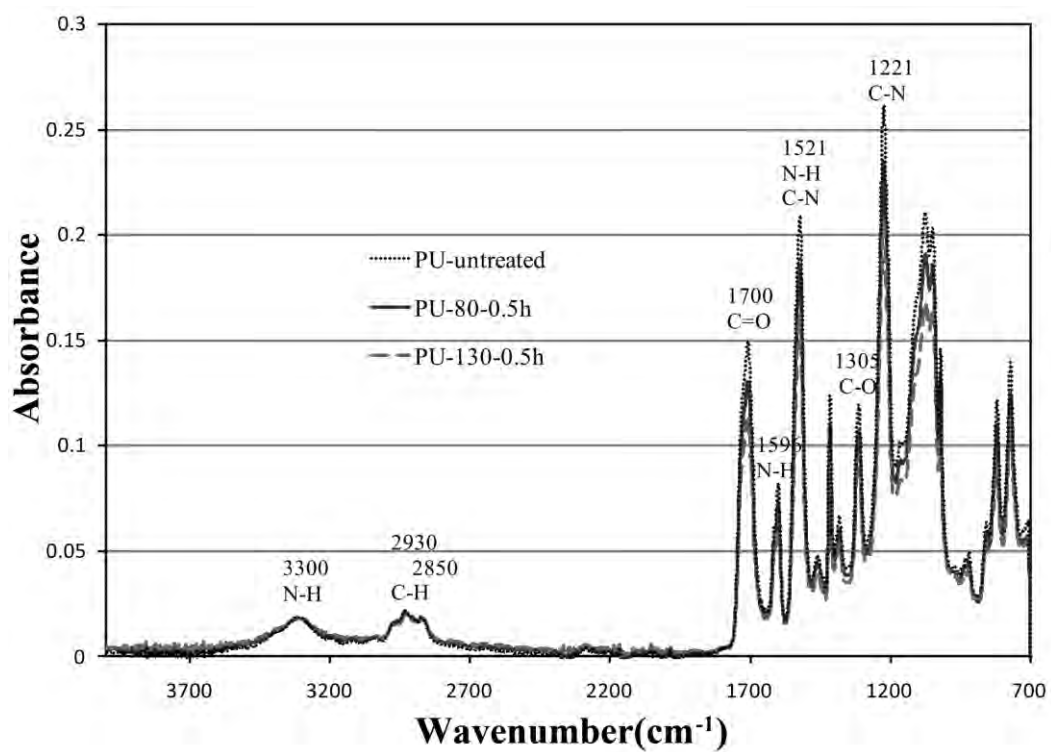
Figure 5.4 FTIR spectra of PU
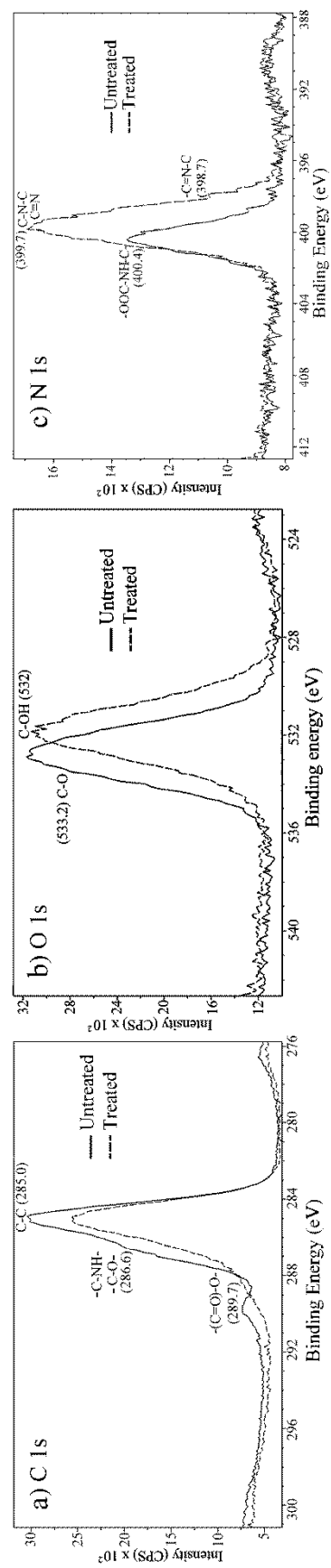
Figure 5.5 XPS spectra of polyurethane before and after plasma treatment a) C1s lines; b) O1s lines; c) N1s lines

183
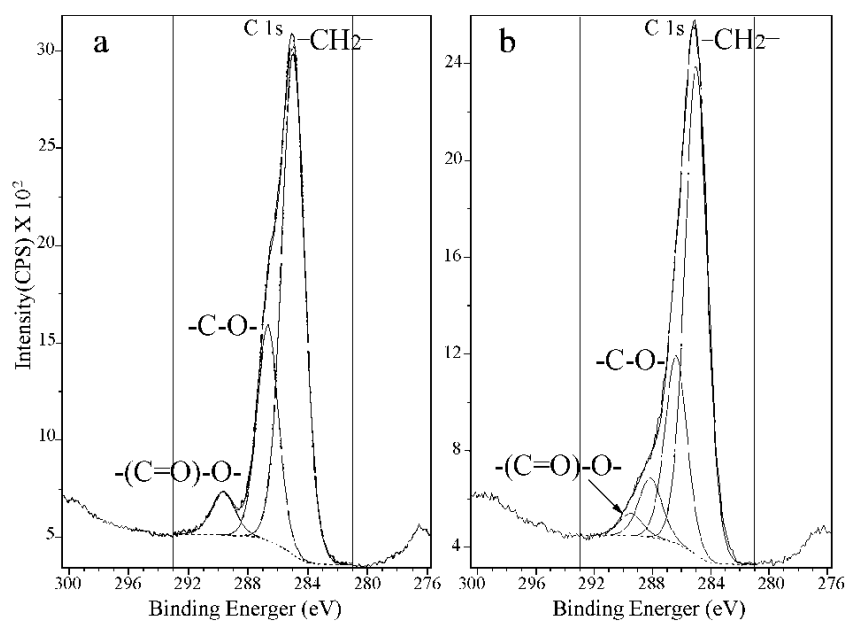
Figure 5.6 C1s peaks fit of polyurethane a) untreated; b) treated.
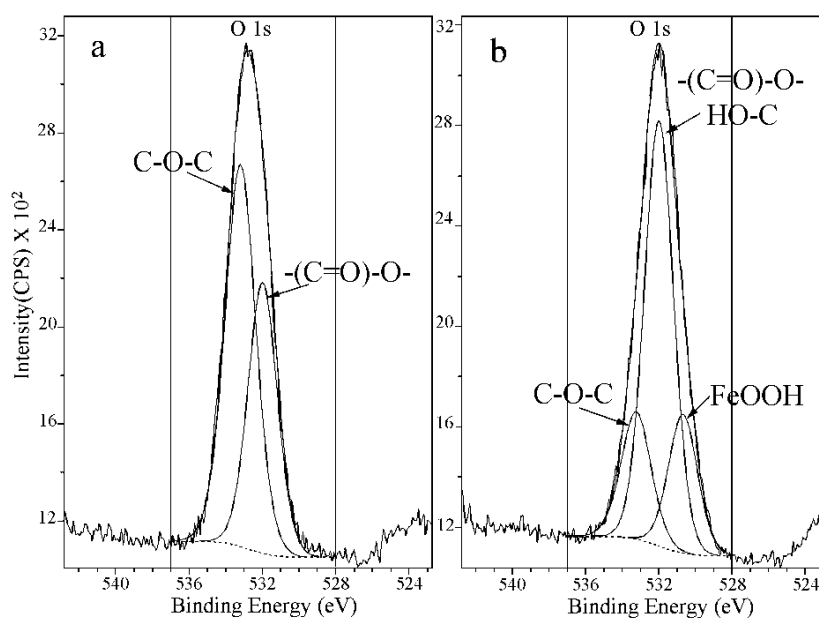
Figure 5.7 O1s peaks fit of polyurethane a) untreated; b) treated.
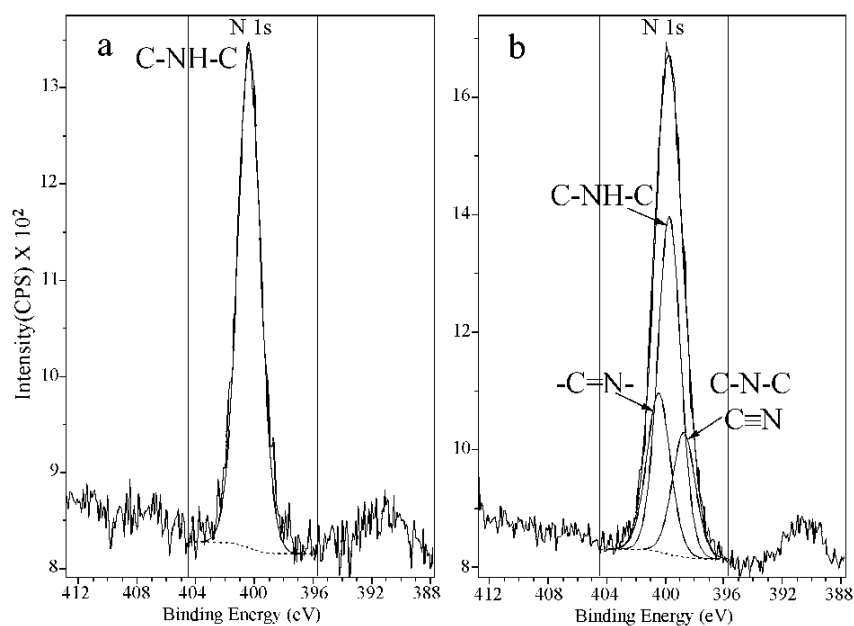
Figure 5.8 N1s peaks fit of polyurethane a) untreated; b) treated.
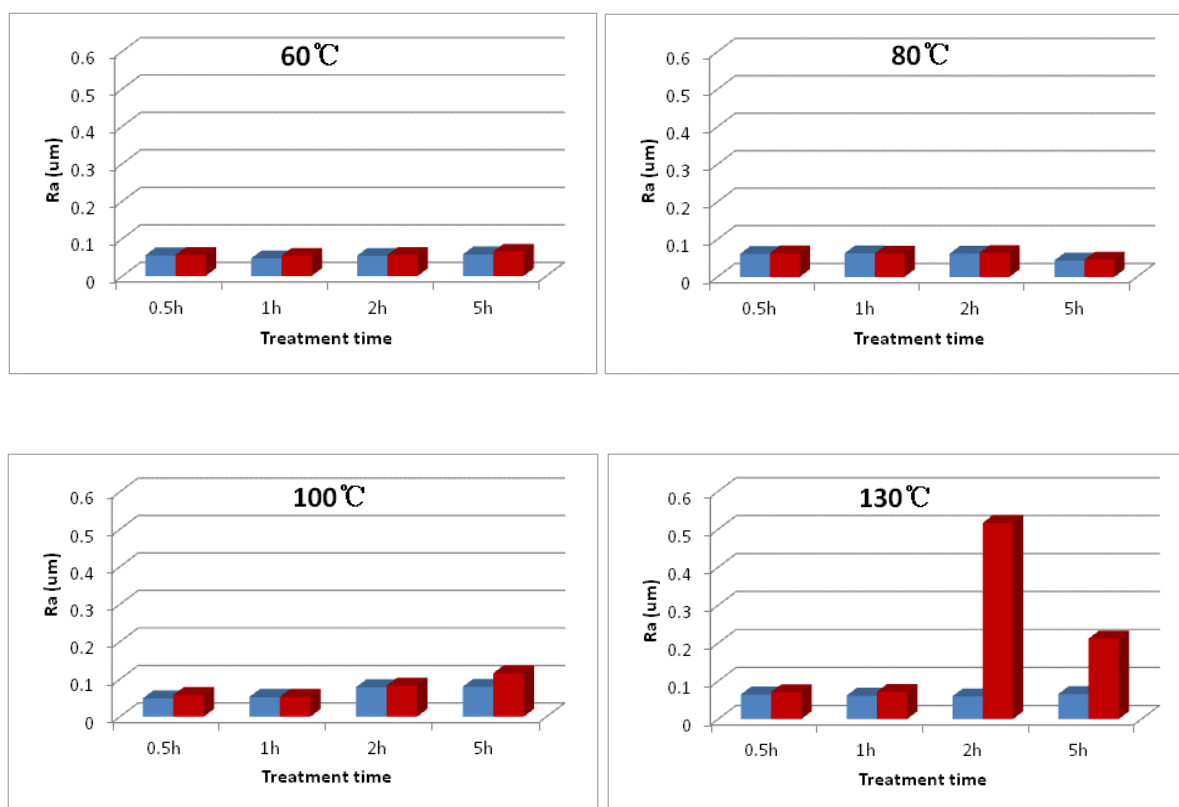
Figure 5.9 Ra before and after plasma treatment (a) Plasma treated at 60 °C; (b) Plasma

treated at 80 °C; (c) Plasma treated at 100 °C; (d) Plasma treated at 130 °C(Blue for untreated

samples, red for treated samples)
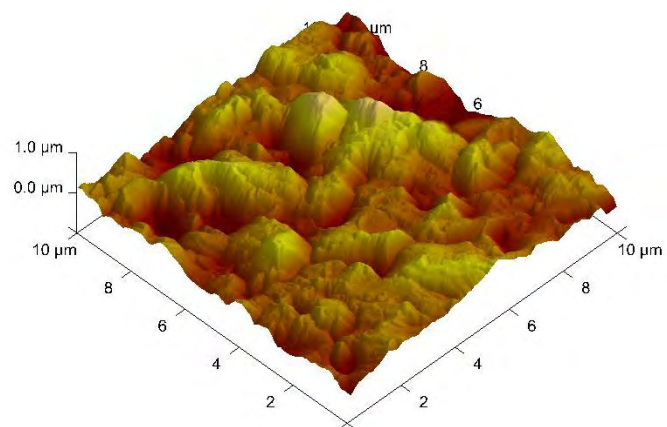
Figure 5.10 The AFM image of untreated PU
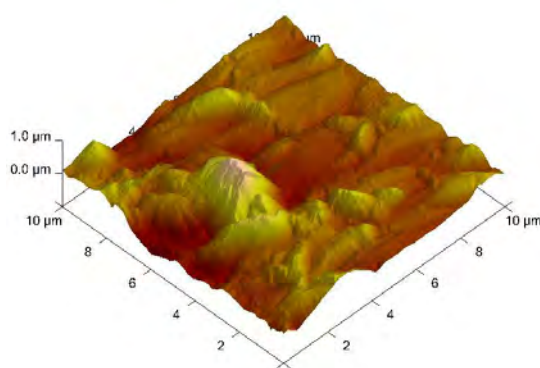
a) PU60-05h   b) PU60-1h
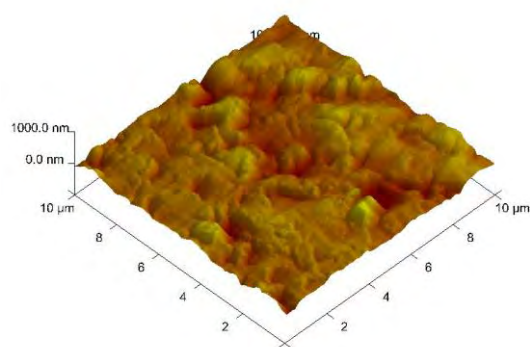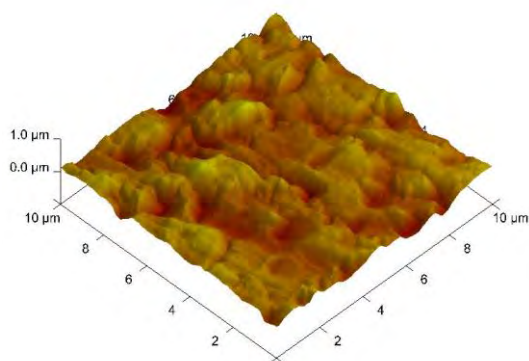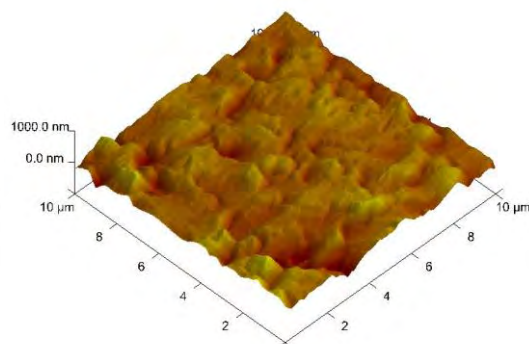
c) PU60-2h   d) PU60-5h

Figure 5.11 The AFM images of plasma treated PU at 60 °C a) PU60-05h; b) PU60-1h; c) PU60-2h; d) PU60-5h
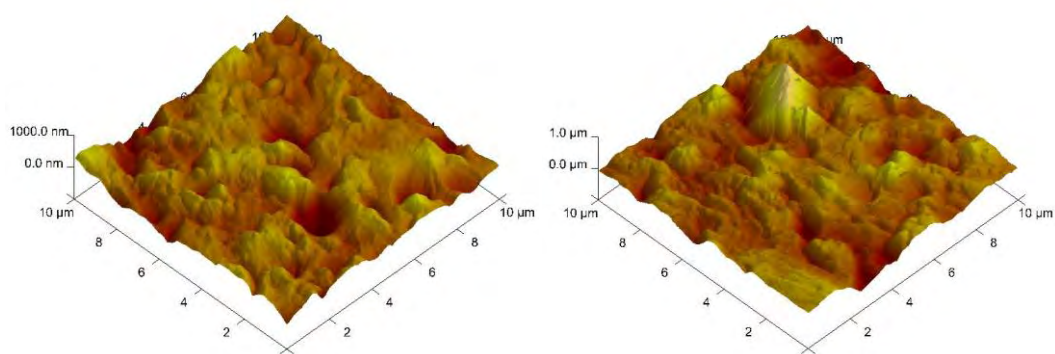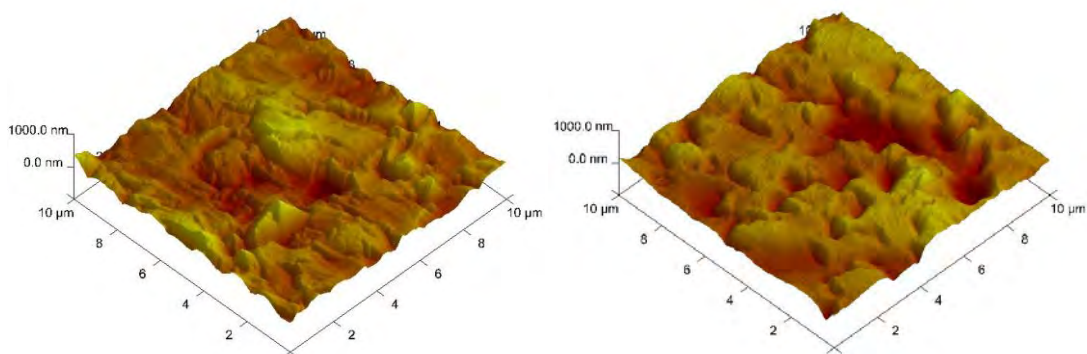
a) PU80-05h   b) PU80-1h

b) PU80-2h   d) PU80-5h

Figure 5.12 The AFM images of plasma treated PU at 80 °C a) PU80-05h; b) PU80-1h; c) PU80-2h; d) PU80-5h
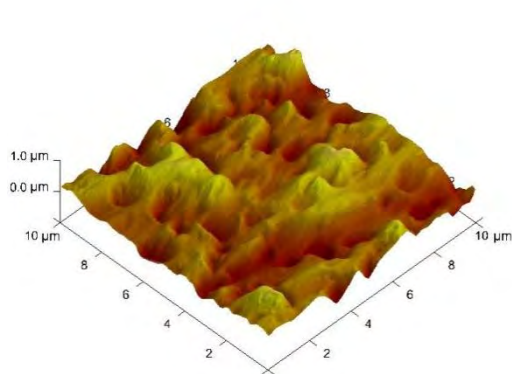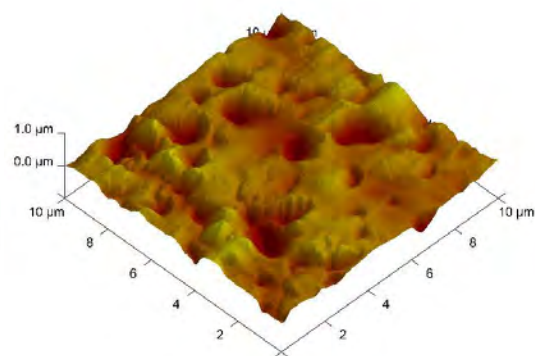
a) PU100-05h   b) PU100-1h
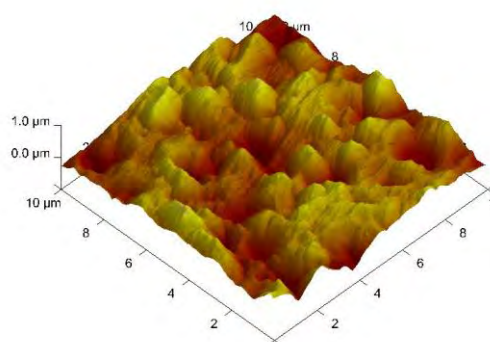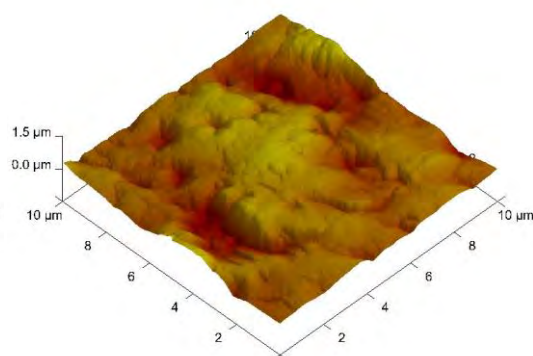
c) PU100-2h   d) PU100-5h

Figure 5.13 The AFM images of plasma treated PU at 100 °C a) PU100-05h; b) PU100-1h; c) PU100-2h; d) PU100-5h
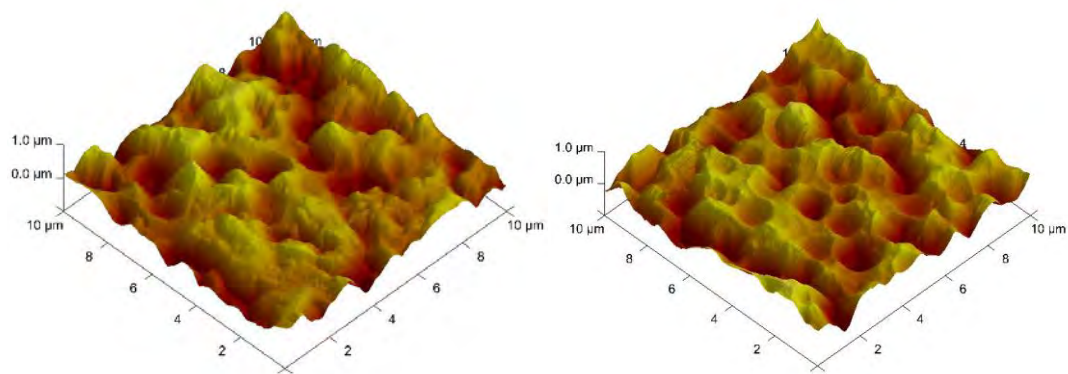
a) PU130-05h   b) PU130-1h
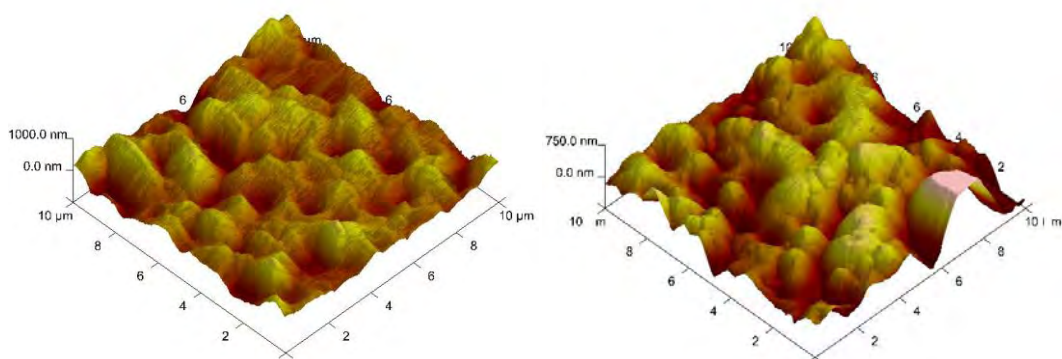
c) PU130-2h   d) PU130-5h

Figure 5.14 The AFM images of plasma treated PU at 130°C130 °C a) PU130-05h; b) PU130-1h; c) PU130-2h; d) PU130-5h
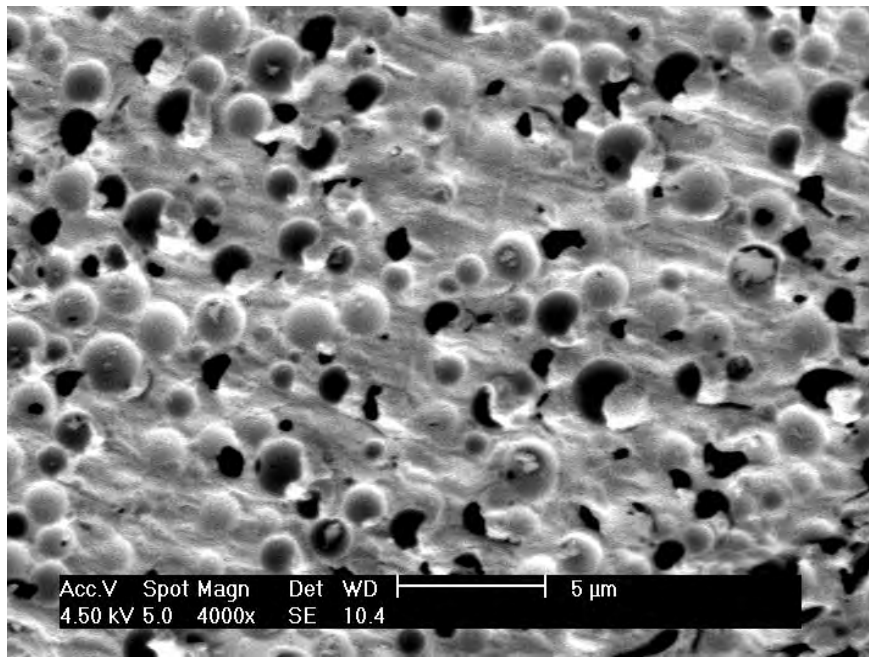
Figure 5.15 SEM image of untreated polyurethane
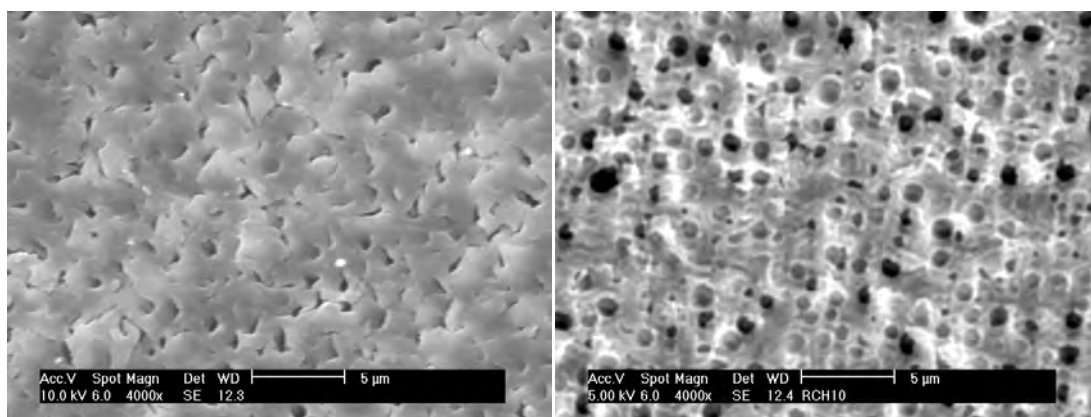
a) PU60-05h   b) PU60-1h
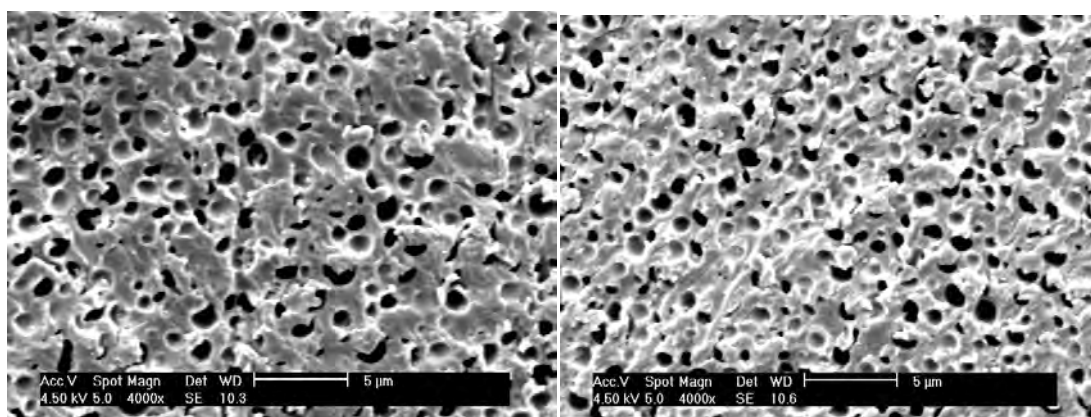
c) PU60-2h   d) PU60-5h

Figure 5.16 SEM images of plasma treated PU at 60 °C a) PU60-05h; b) PU60-1h; c) PU60-2h; d) PU60-5h
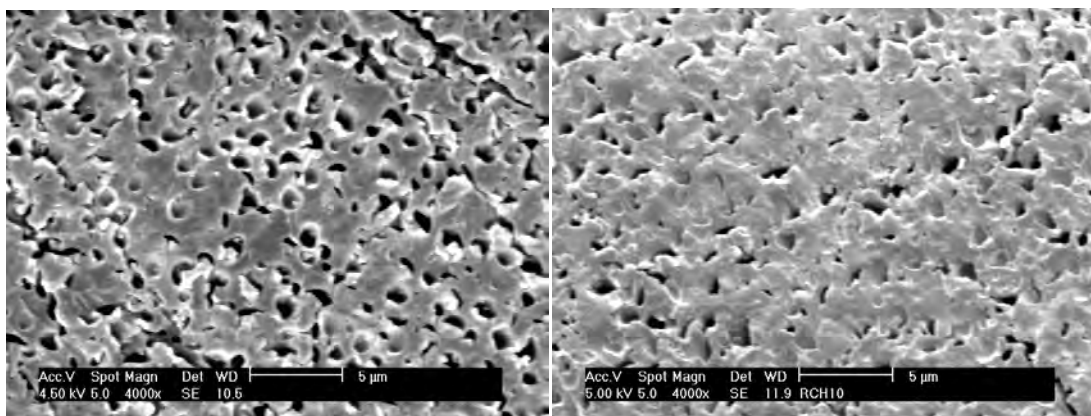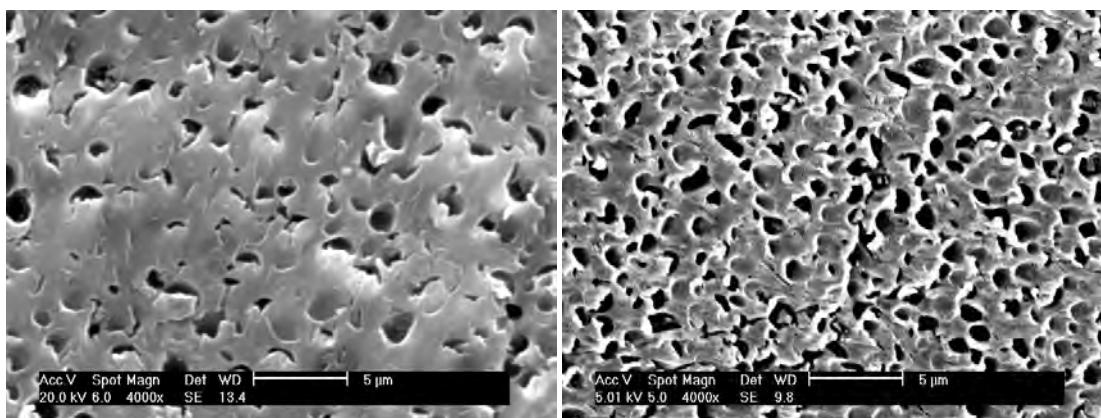
a)   PU80-05h   b)   PU80-1h

c)   PU80-2h   d)   PU80-5h

Figure 5.17 SEM images of plasma treated PU at 80 °C a) PU80-05h; b) PU80-1h; c) PU80-2h; d) PU80-5h
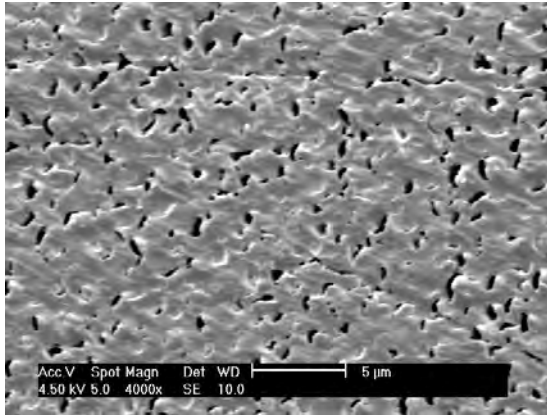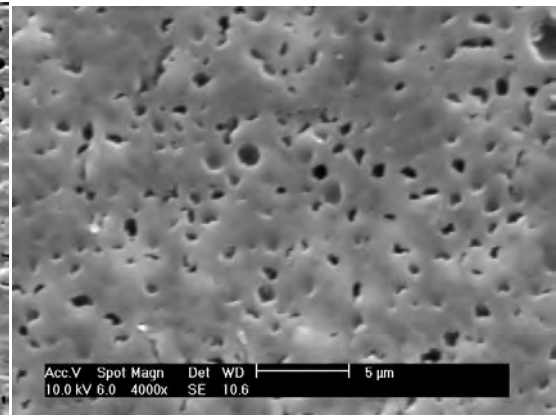
a) PU100-05h	b) PU100-1h
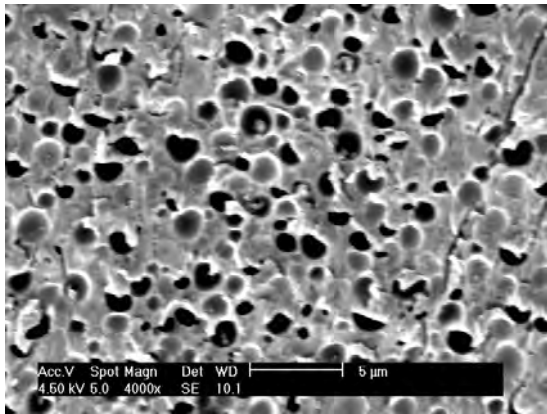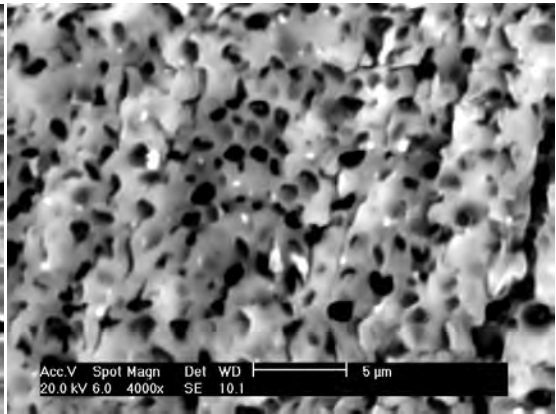
c) PU100-2h	d) PU100-5h

Figure 5.18 SEM images of plasma treated PU at 100 °C a) PU100-05h; b) PU100-1h; c) PU100-2h; d) PU100-5h
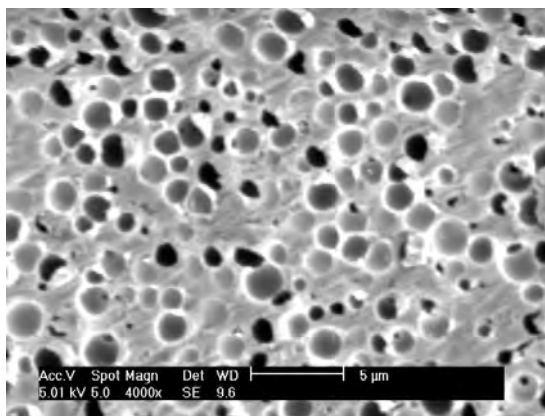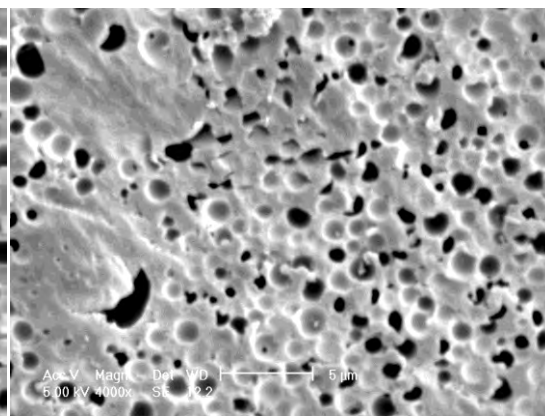
a) PU130-05h   b) PU130-1h
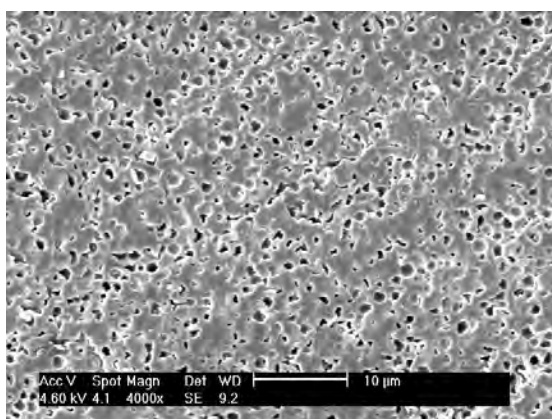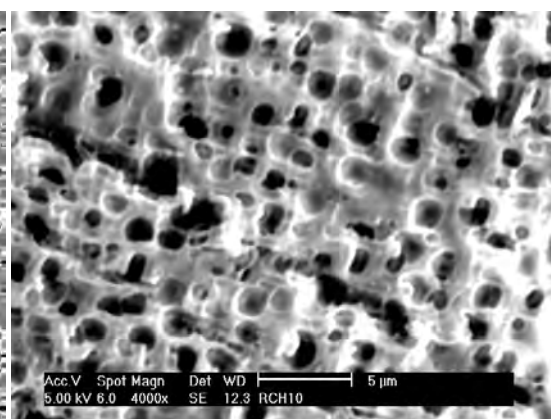
c) PU130-2h   d) PU130-5h

Figure 5.19 SEM images of plasma treated PU at 130 °C a) PU130-05h; b) PU130-1h; c)
PU130-2h; d) PU130-5h
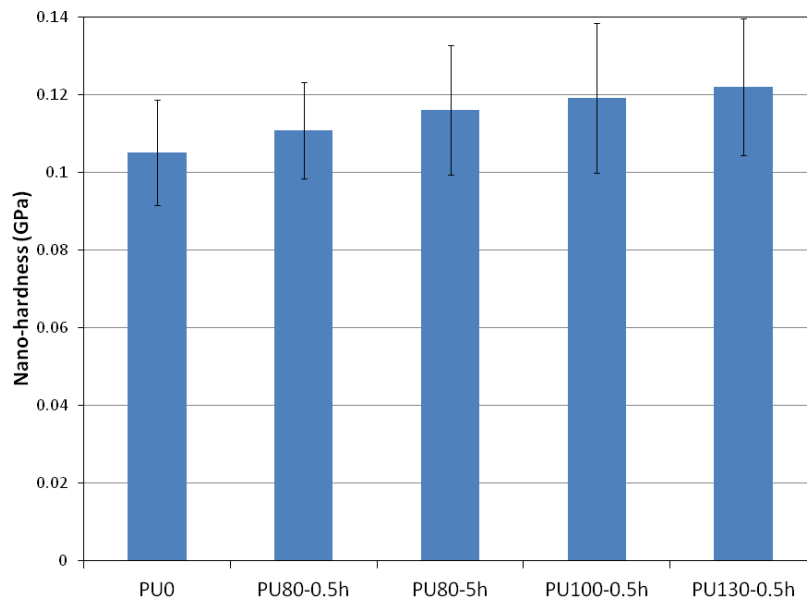
Figure 5.20 Hardness of PU before and after plasma treatment
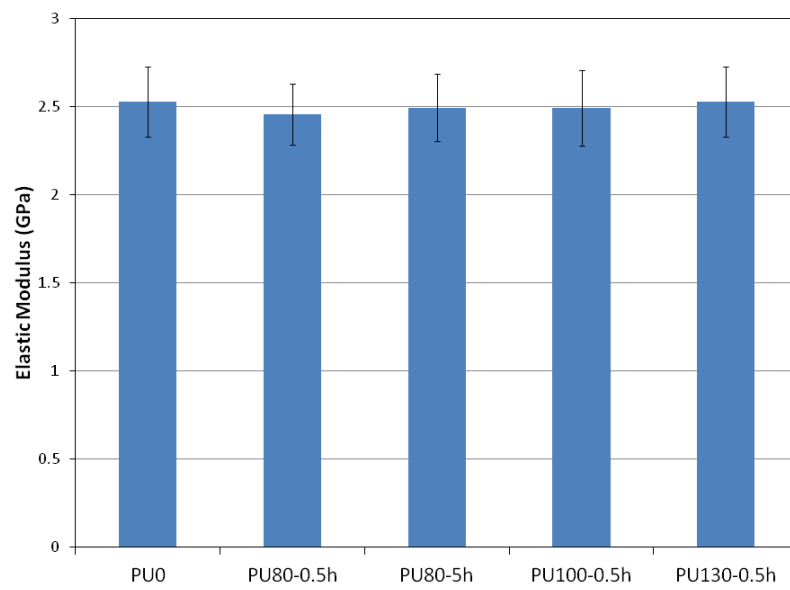
Figure 5.21 Elastic modulus of PU before and after plasma treatment
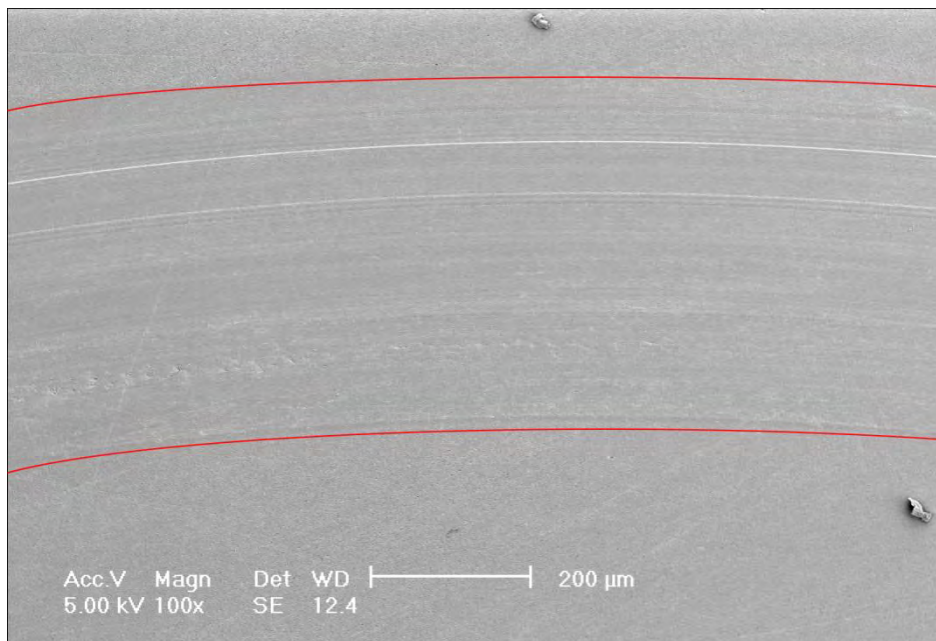
(a) Untreated
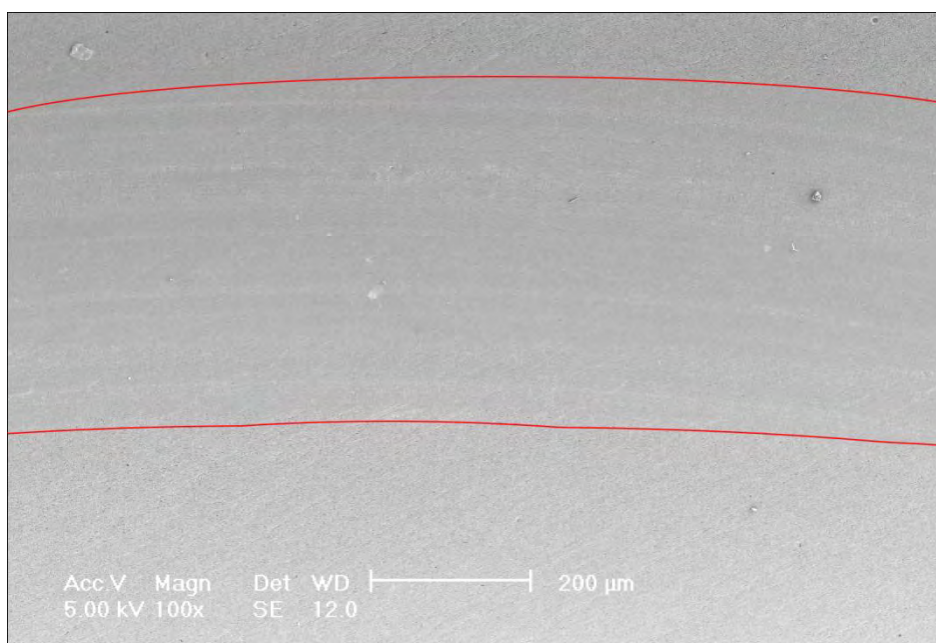
(b) Treated at 80 °C,1 h
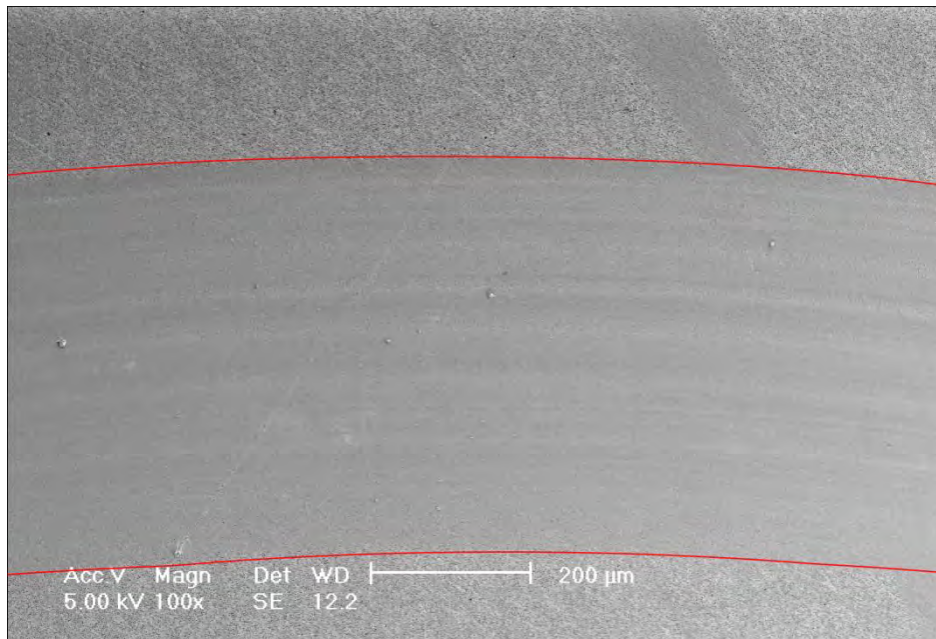
(c) Treated at 130 °C,1 h

Figure 5.22 Pin-on-disc wear track morphologies of polyurethane samples (a)Untreated; (b) Treated at 80 °C,1 h; (c) Treated at 130 °C,1 h
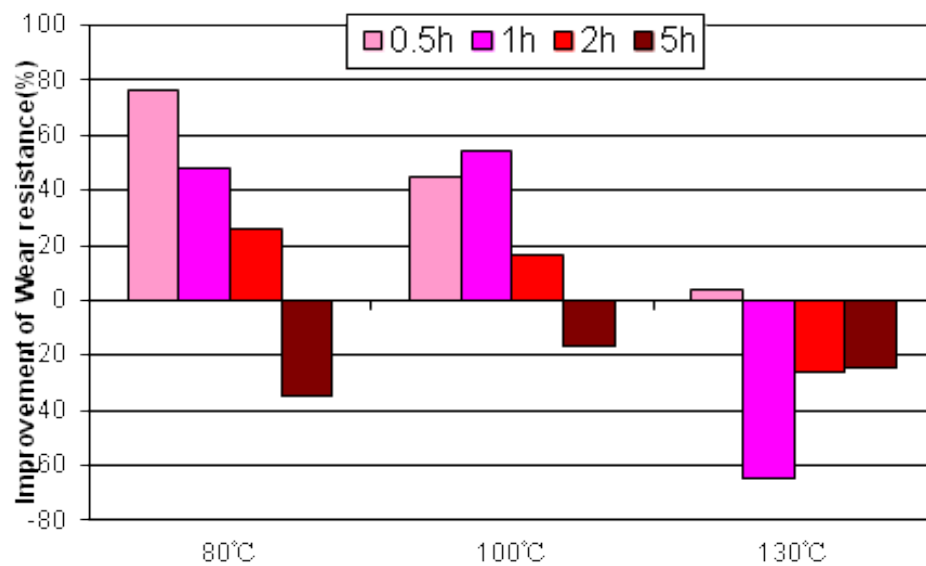
Figure 5.23 Improvement of wear resistance of PU samples before and after plasma treatment

(Pin-on-disc, 9.81 N)
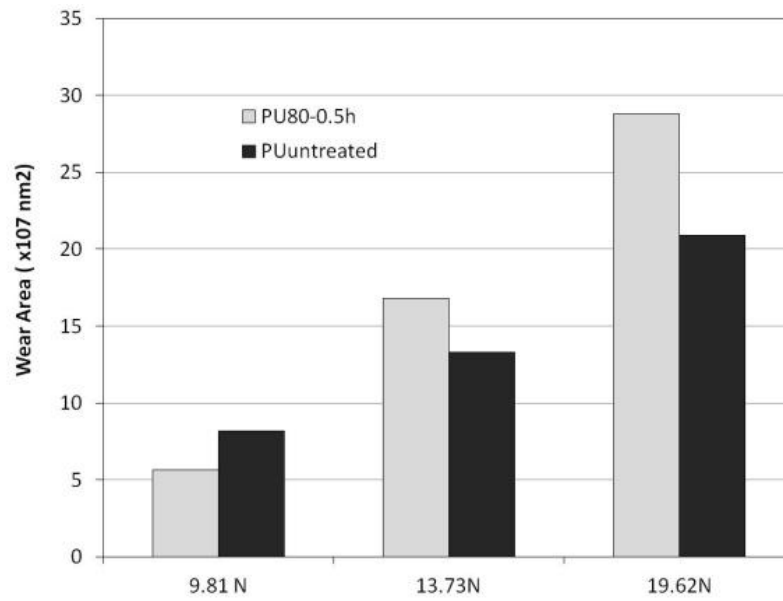
Figure 5.24 Reciprocating wear area of PU samples at different loads (10000cycles)

a   b
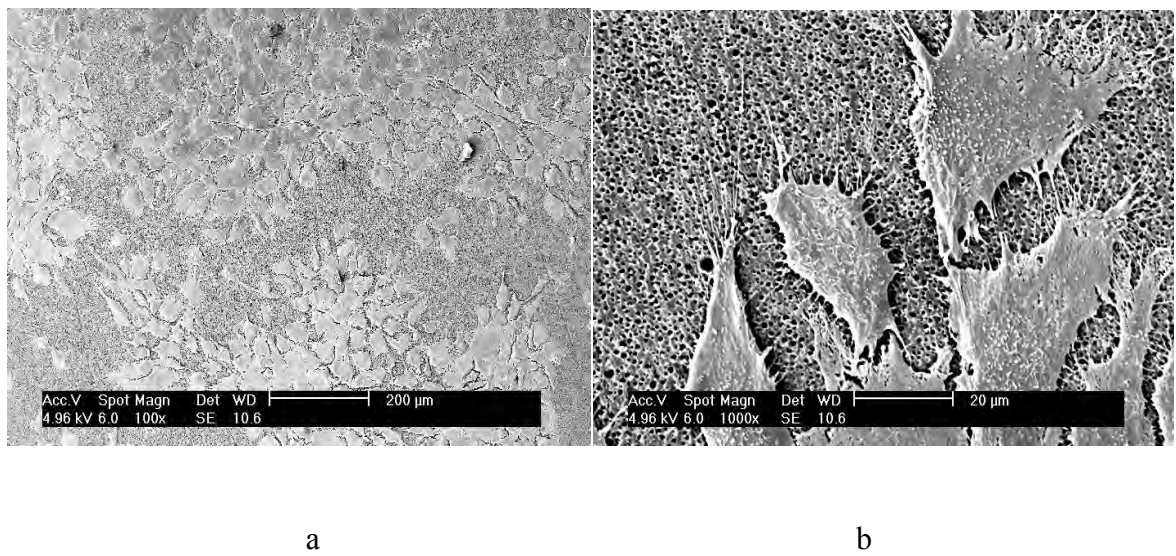
Figure 5.25 SEM micrographs of cells culture for 3days to untreated PU (a 100x, b 1000x)
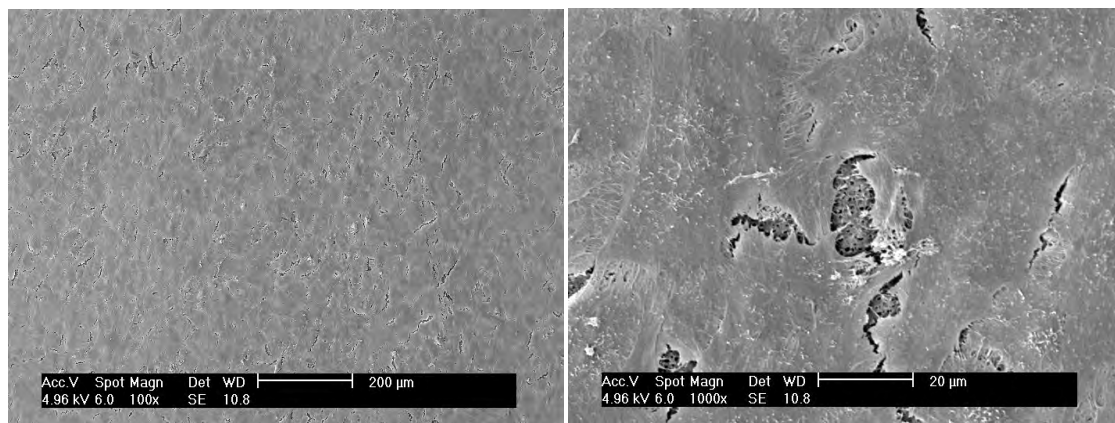
a   b

Figure 5.26 SEM micrographs of cells culture for 3days to plasma treated PU at 80 ºC for 0.5
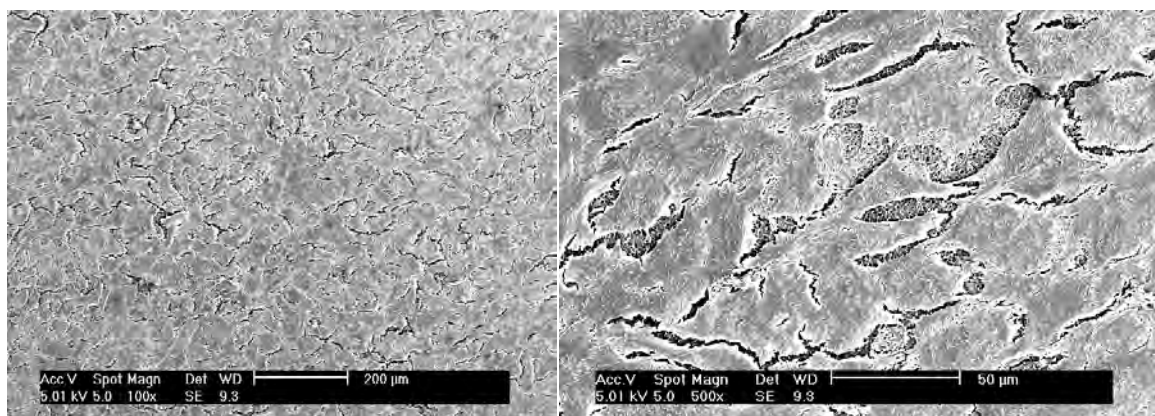
h (a 100x, b 1000x)

a   b

Figure 5.27 SEM micrographs of cells culture for 3days to plasma treated PU at 80ºC for 5h

(a 100x, b 1000x)
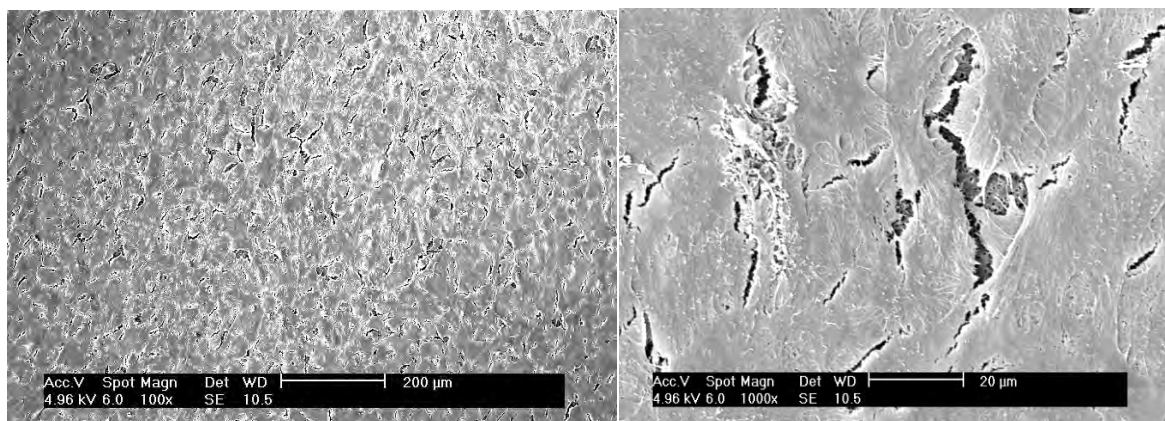
a   b

Figure 5.28 SEM micrographs of cells culture for 3days to plasma treated PU at 100ºC for
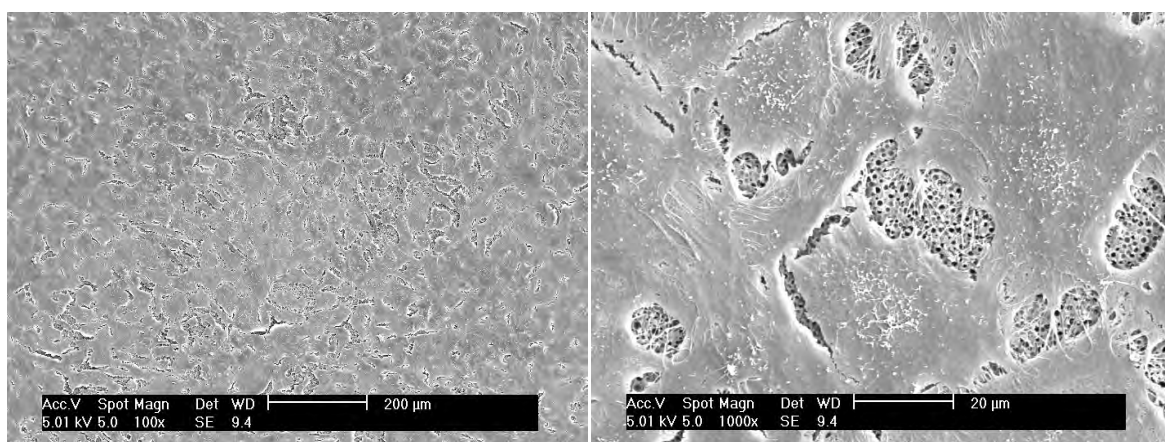
0.5h (a 100x, b 1000x)

a   b

Figure 5.29 SEM micrographs of cells culture for 3days to plasma treated PU at 130ºC for

0.5h (a 100x, b 1000x)
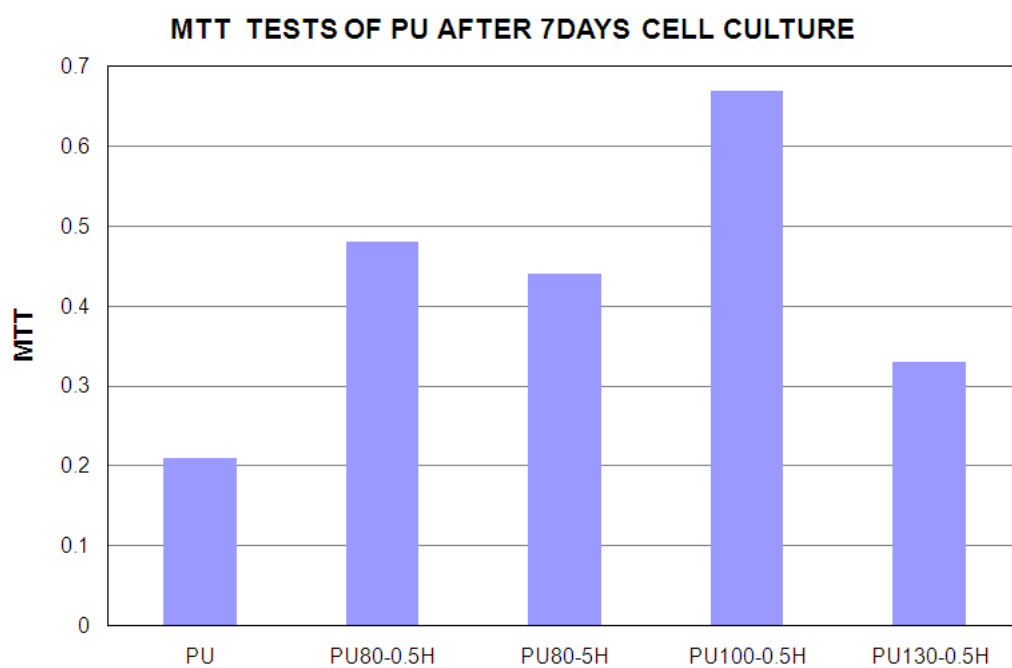
Figure 5.30 MTT results of PU after 7days cell culture
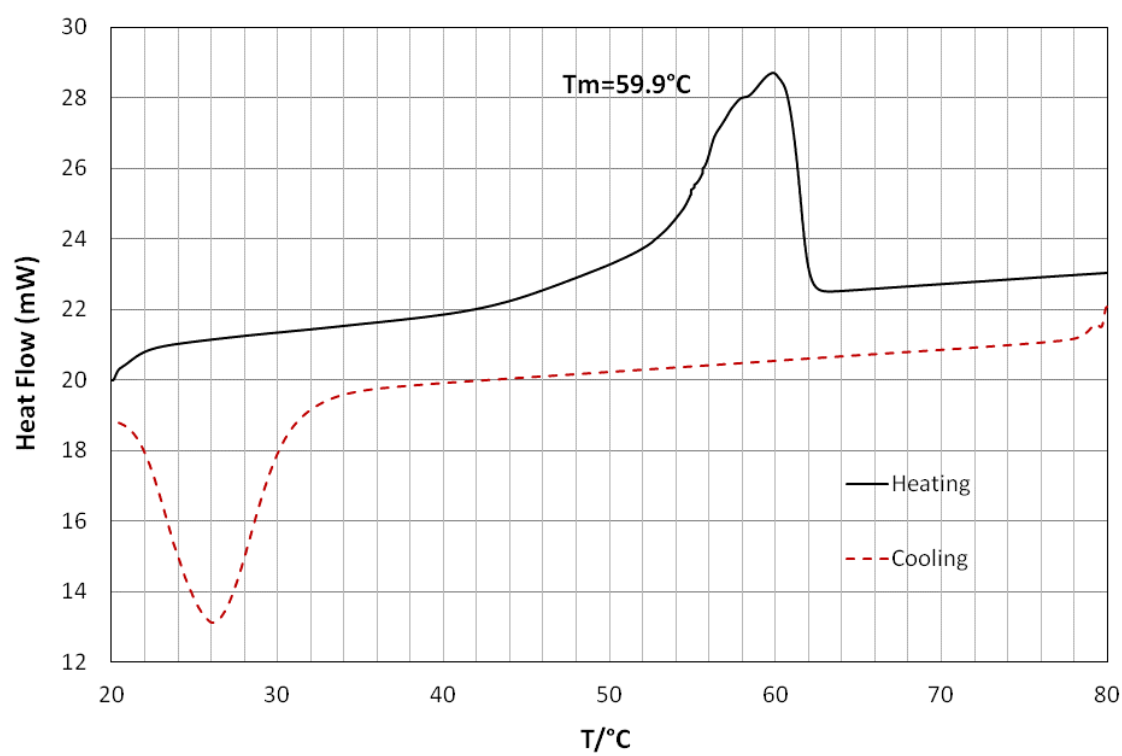
Figure 6.1 DSC curve of polycaprolactone
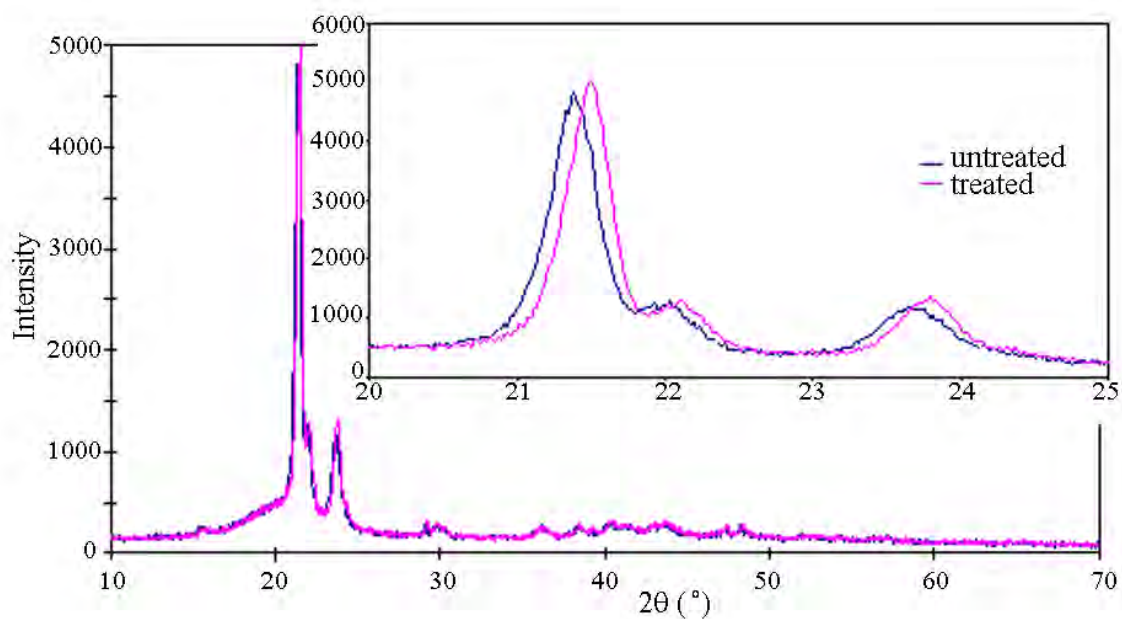
Figure 6.2 The XRD results of PCL before and after plasma treatment
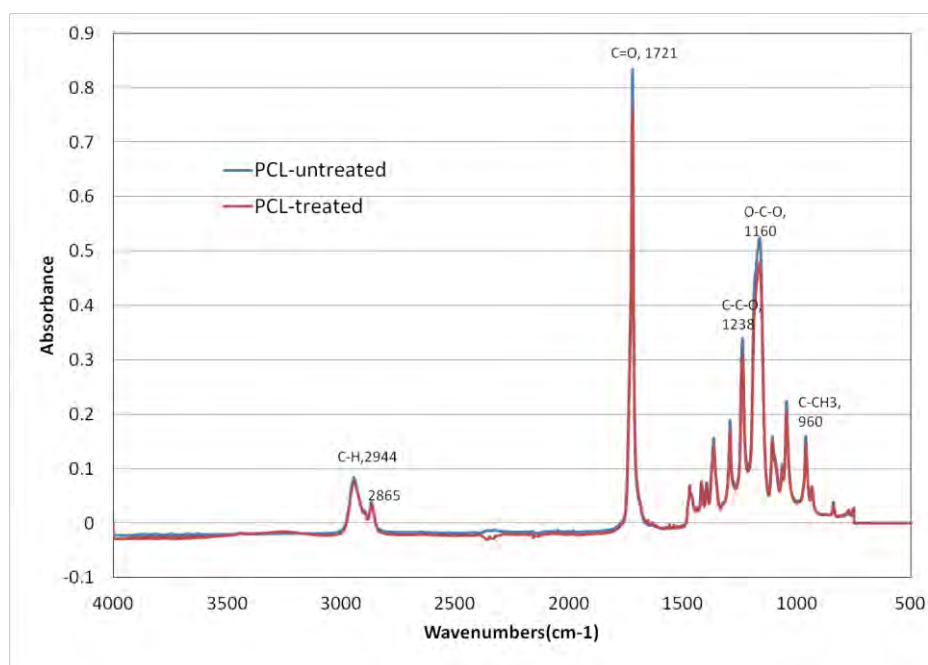
Figure 6.3 FTIR spectra of PCL 4000-500 cm^{-1} region

203
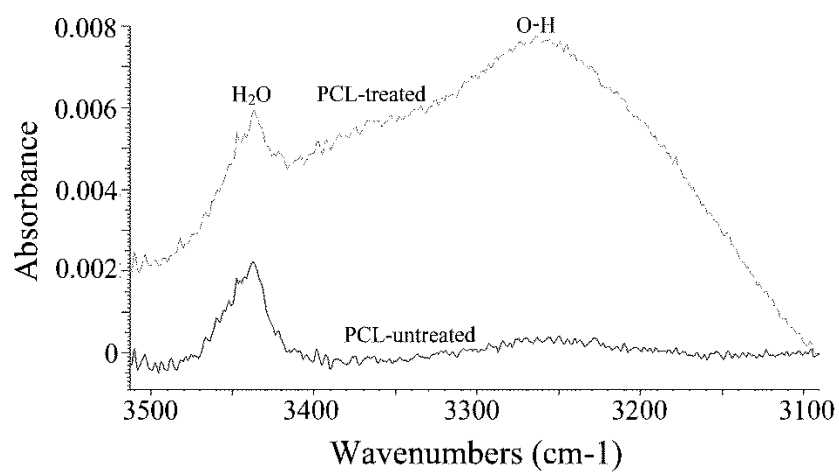
Figure 6.4 FTIR spectra of PCL 3500-3100 cm^{-1} region
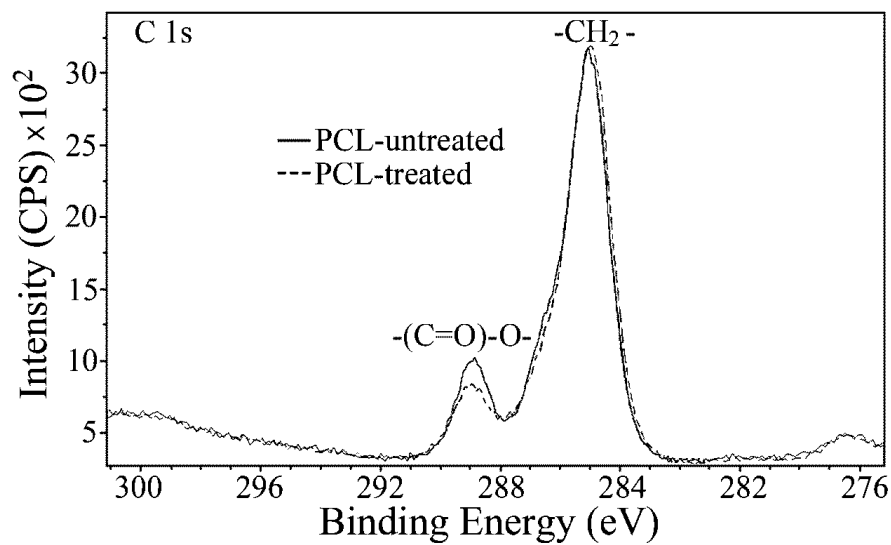
Figure 6.5 C1s spectra of PCL before and after plasma treatment
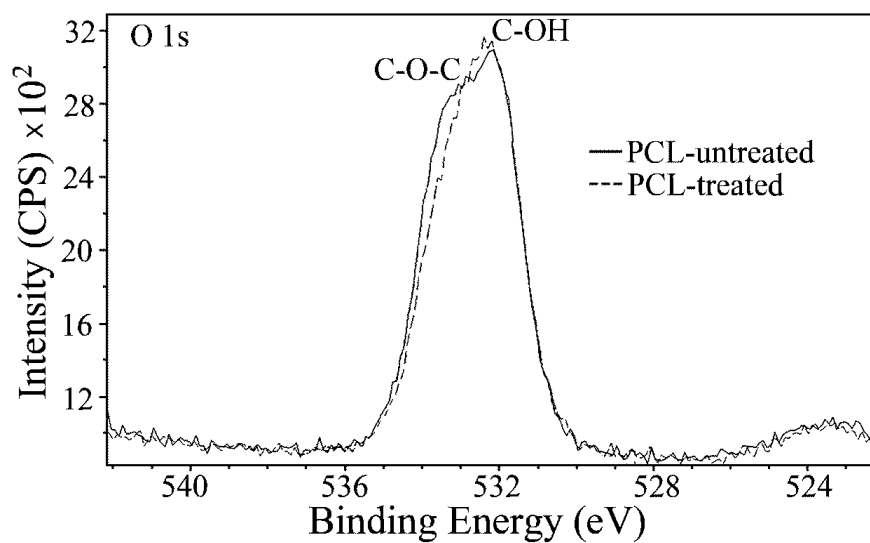
Figure 6.6 O1s spectra of PCL before and after plasma treatment
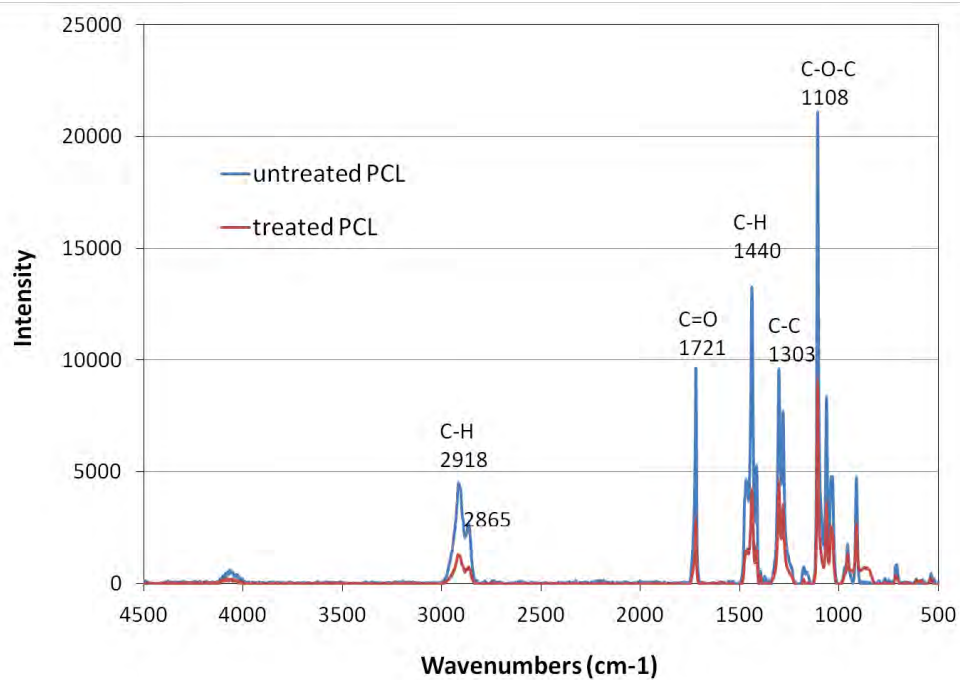
Figure 6.7 Raman spectra of PCL
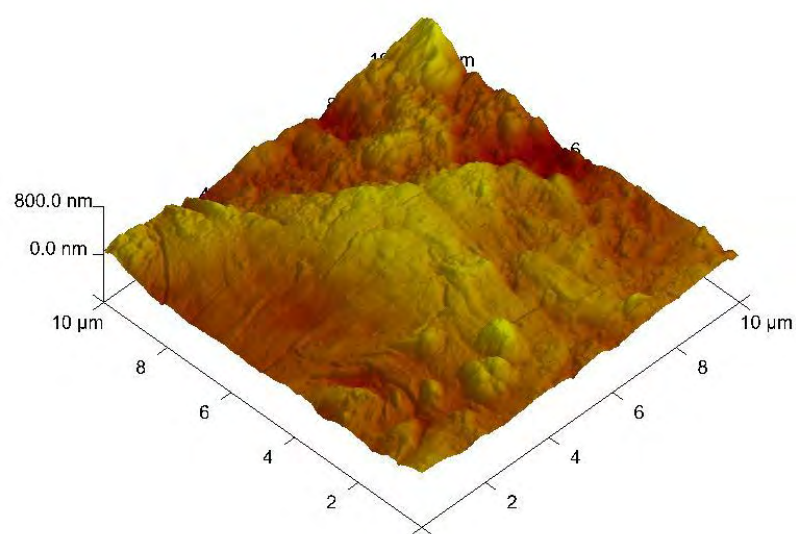
Figure 6.8 The AFM image of untreated PCL
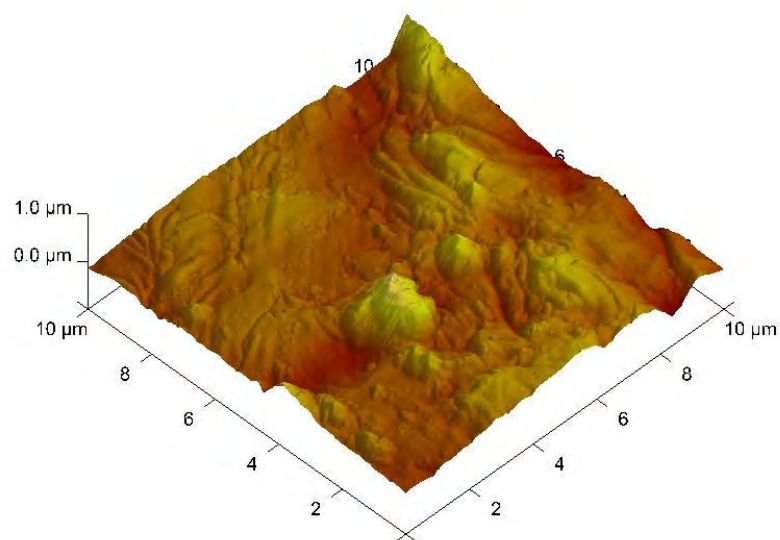
Figure 6.9 The AFM image of plasma treated PCL
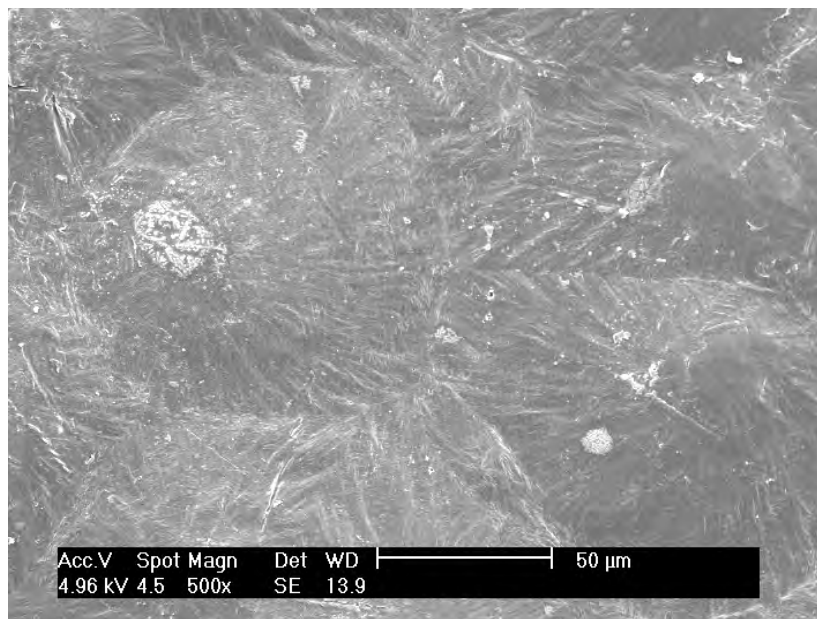
Figure 6.10 SEM image of untreated PCL
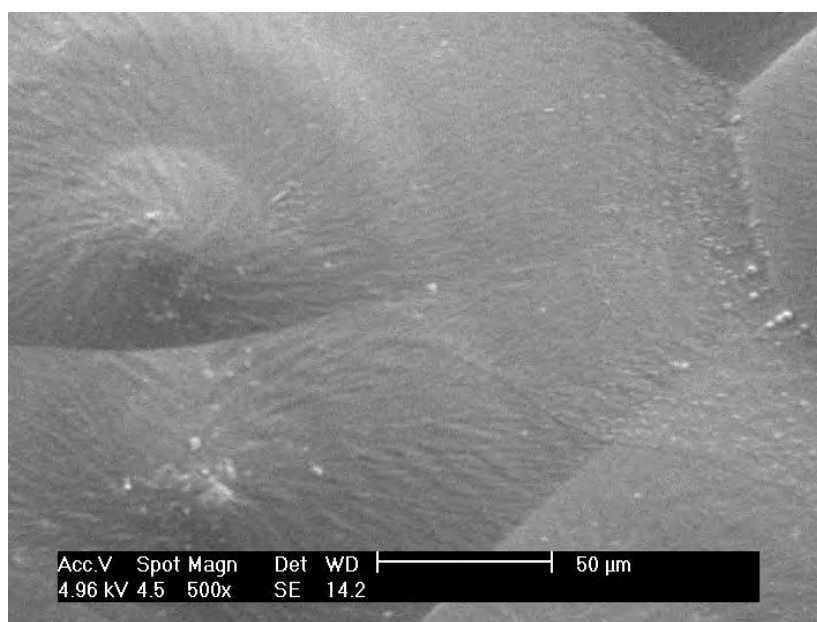
Figure 6.11 SEM image of plasma treated PCL
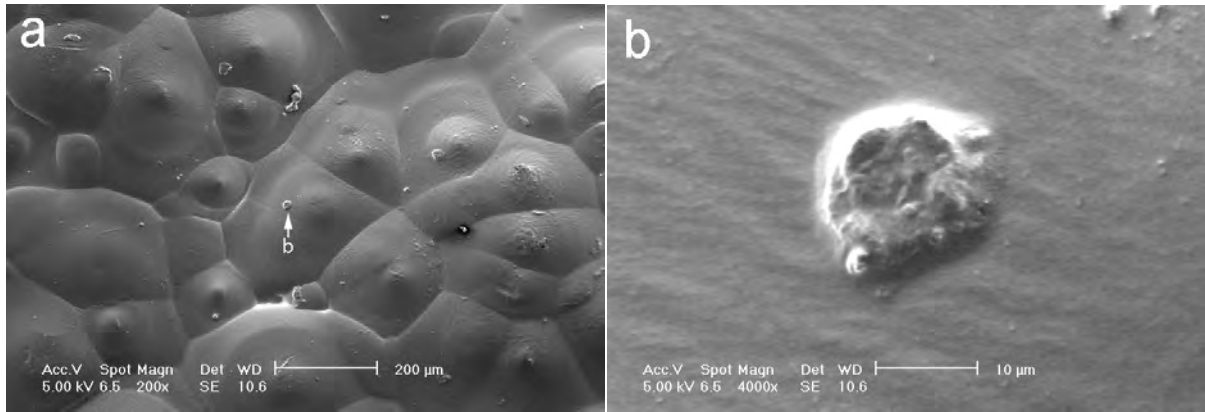
Figure 6.12 Scanning electron micrographs of cells attachment onto untreated PCL (a. low

magnification; b. high magnification)
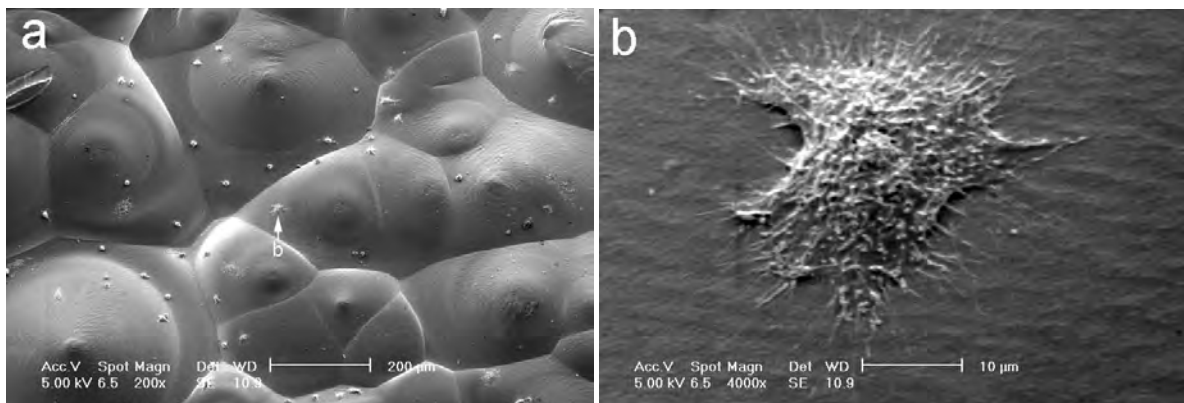
Figure 6.13 Scanning electron micrographs of cells attachment onto ASPN treated PCL (a.

low magnification; b. high magnification)
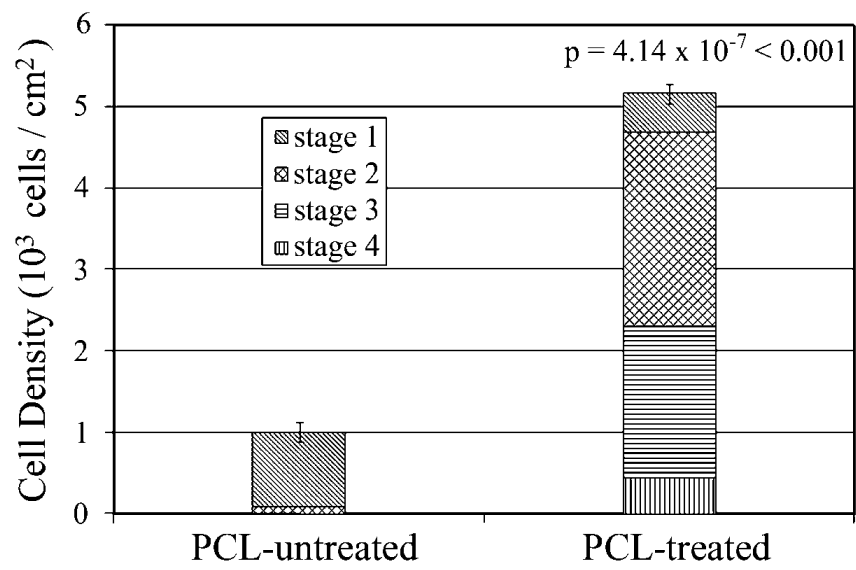
Figure 6.14 Cell density on surface after attachment for 1h
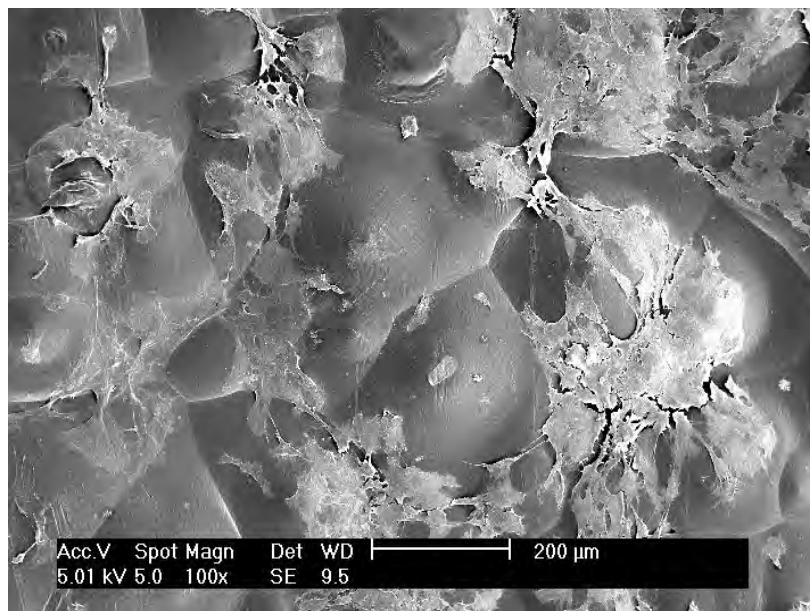
Figure 6.15 Scanning electron micrographs of cell culture for 3days onto untreated PCL
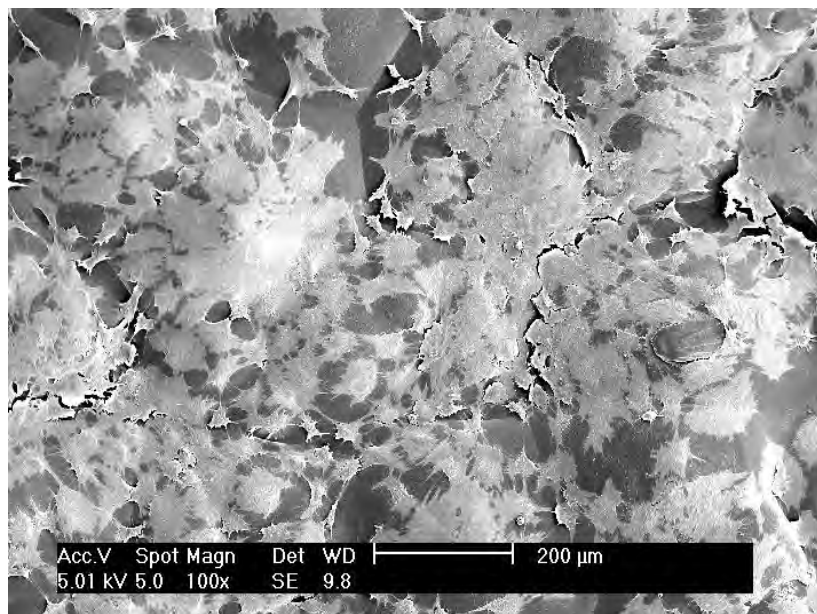
Figure 6.16 Scanning electron micrographs of cell culture for 3days onto treated PCL
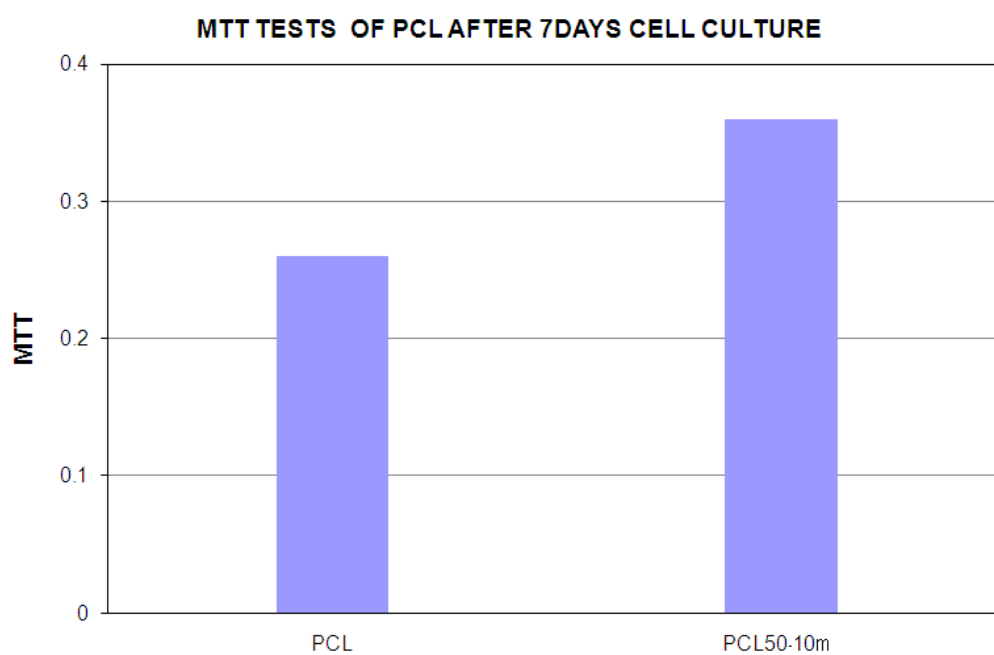
Figure 6.17 MTT results of PCL after 7days cell culture
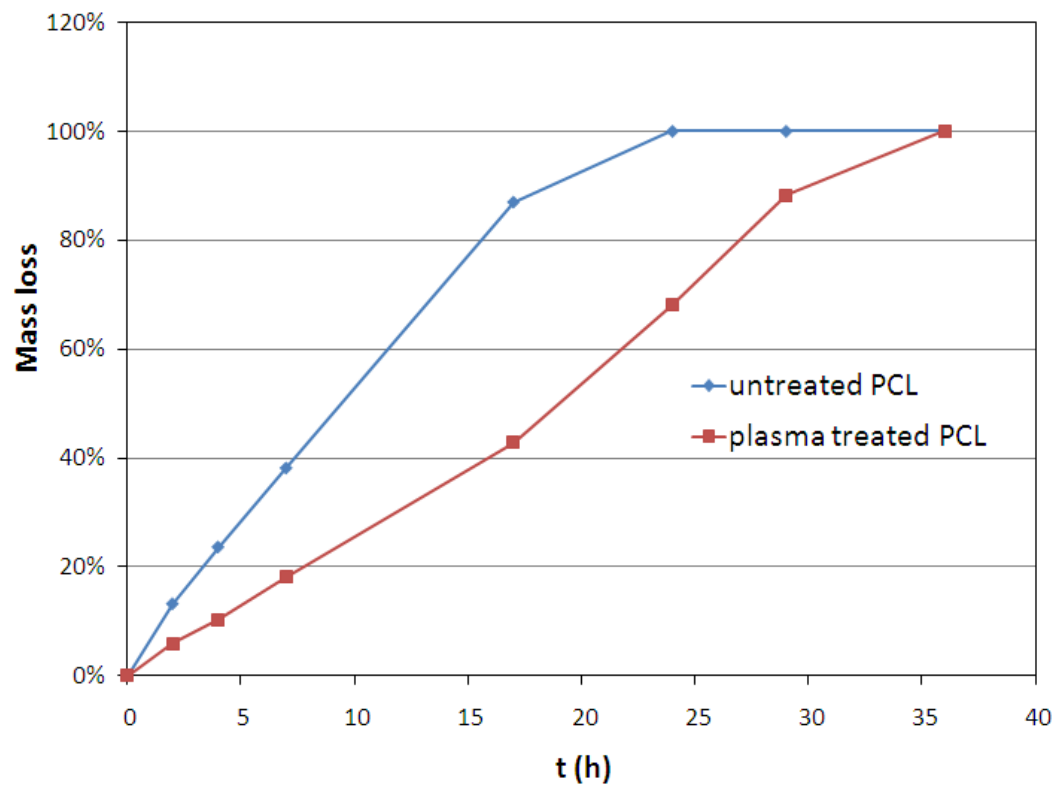
Figure 6.18 Degradation results of PCL films before and after plasma treatment
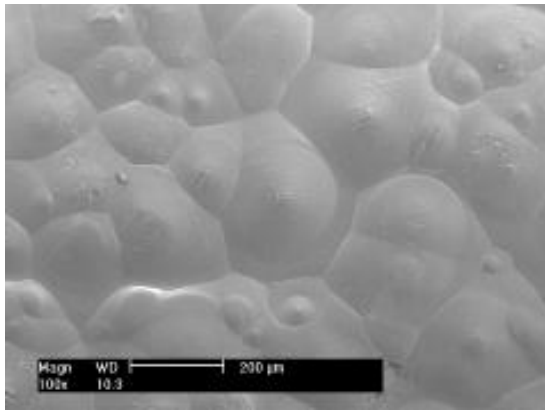
0h
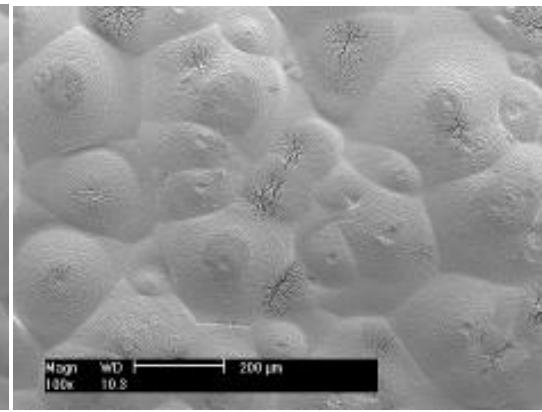
2h
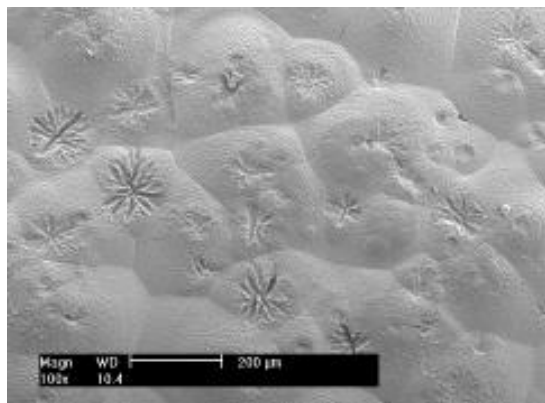
4h
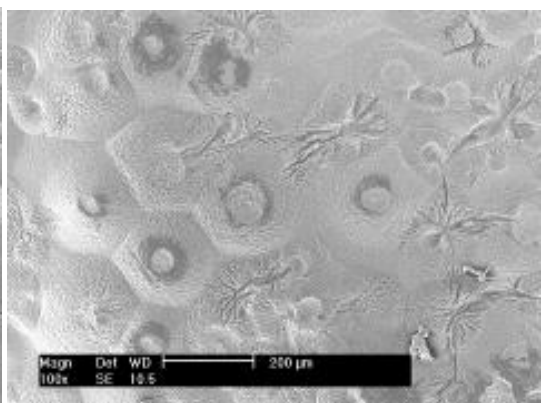
7h
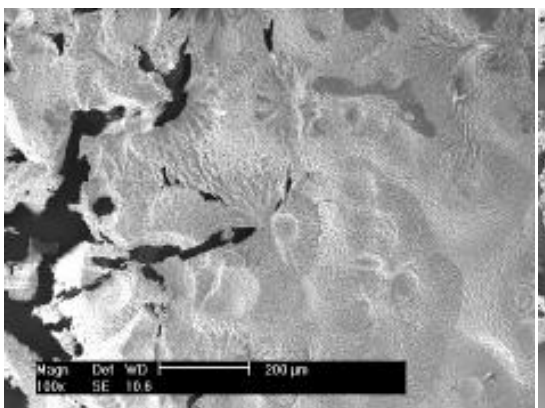
17h
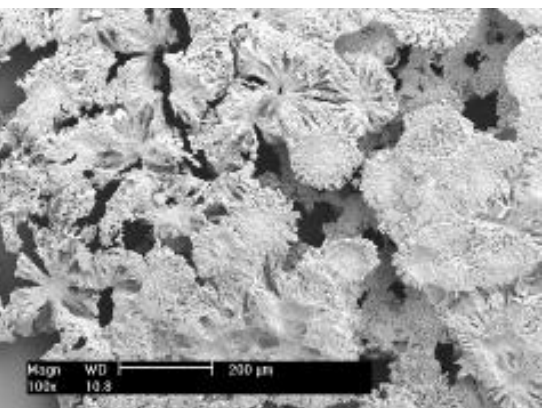
19h

Figure 6.19 SEM images of degradation of untreated samples for different times

(0h, 2h, 4h, 7h, 17h, 19h)
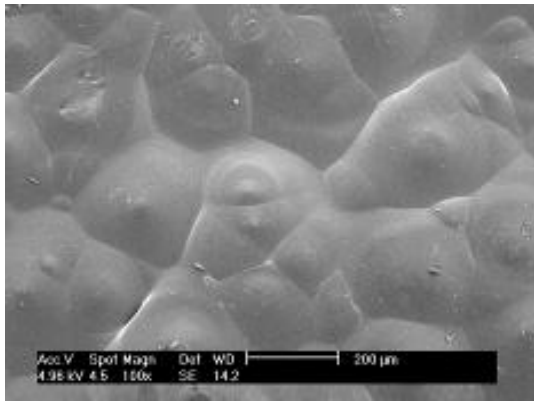
0h
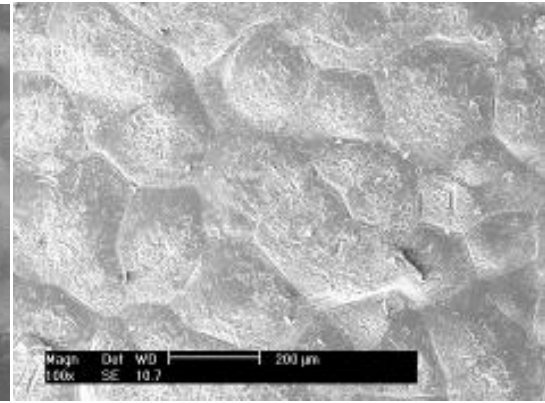
2h
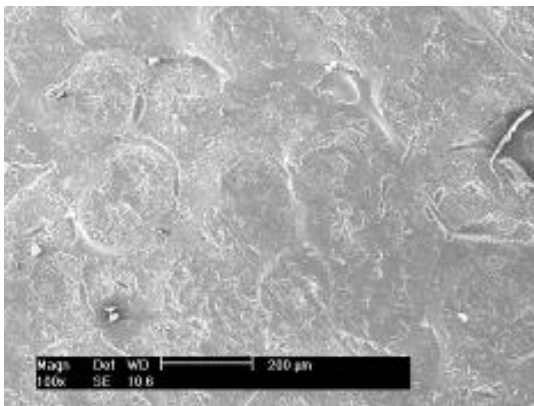
4h
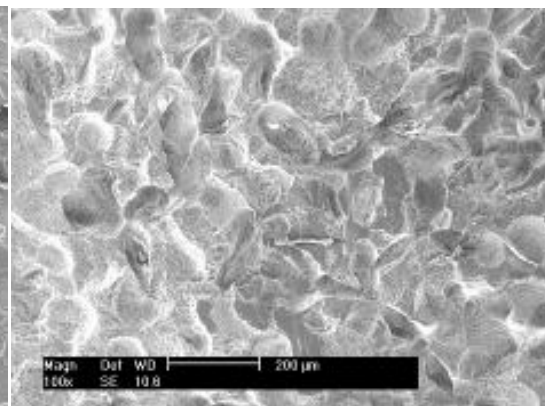
17h
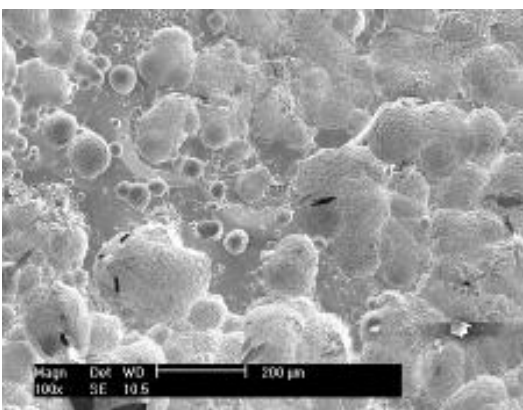
24h
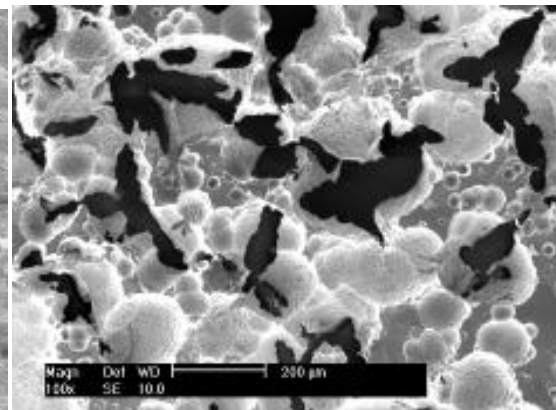
29h

Figure 6.20 SEM images of degradation of plasma treated samples for different time

(0h, 2h, 4h, 17h, 24h, 29h)

FTIR spectra of UHMWPE before and after plasma treatment
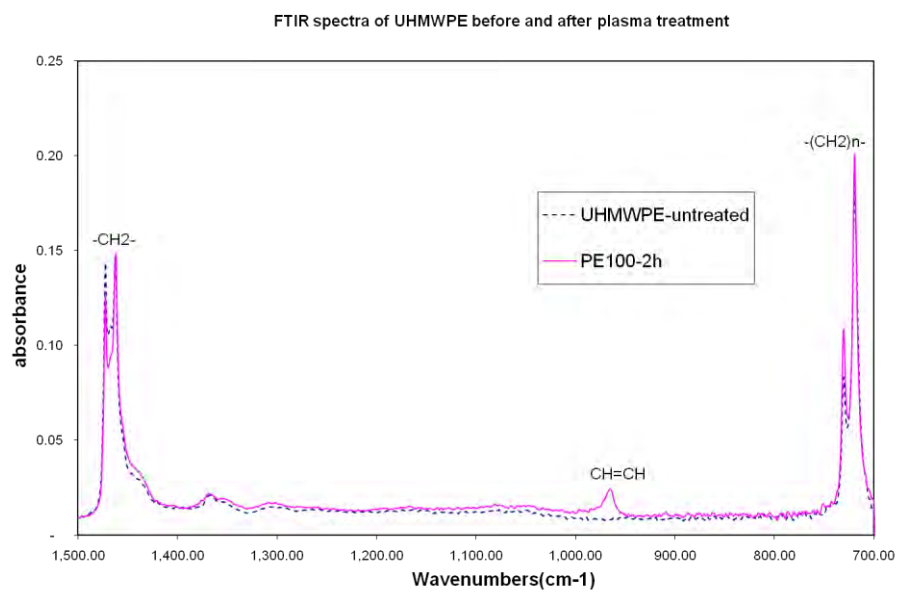
Figure 7.1 FTIR spectra of UHMWPE before and after plasma treatment at 1500-700 cm^{-1} region
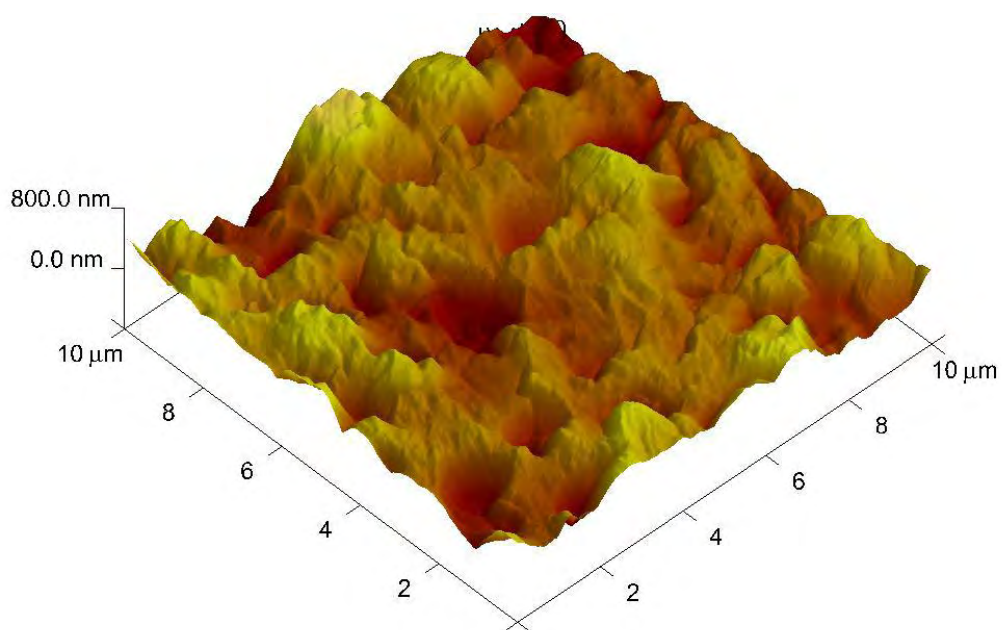
Figure 7.2 AFM image of thermal treated PU sample at 130 °C for 2h

214
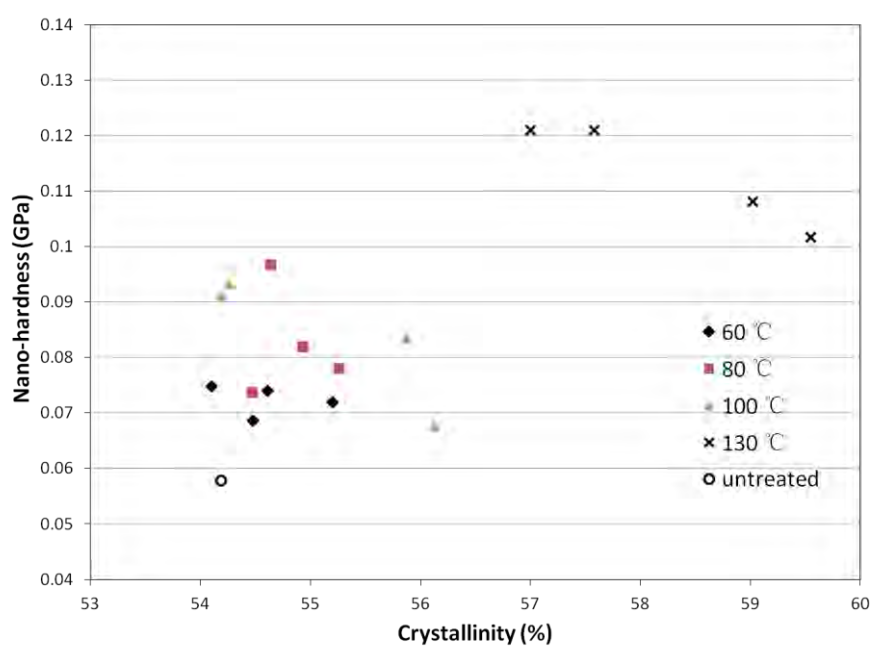
Figure 7.3 The relationship between nano-hardness and crystallinity before and after plasma
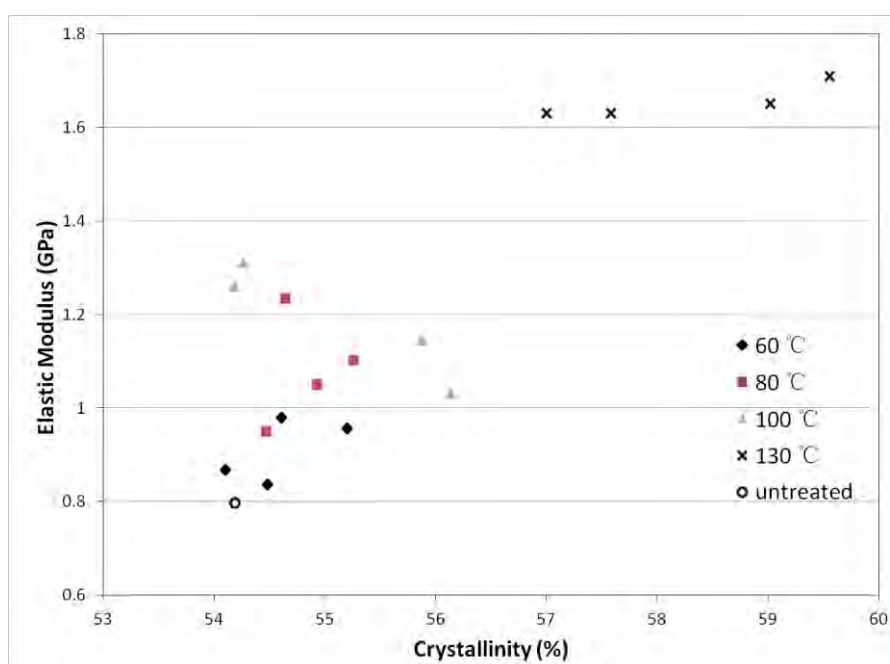
treatment

Figure 7.4 the relationship between elastic modulus and crystallinity before and after plasma
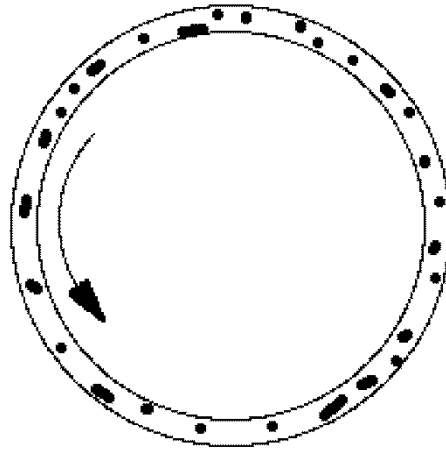
treatment

215

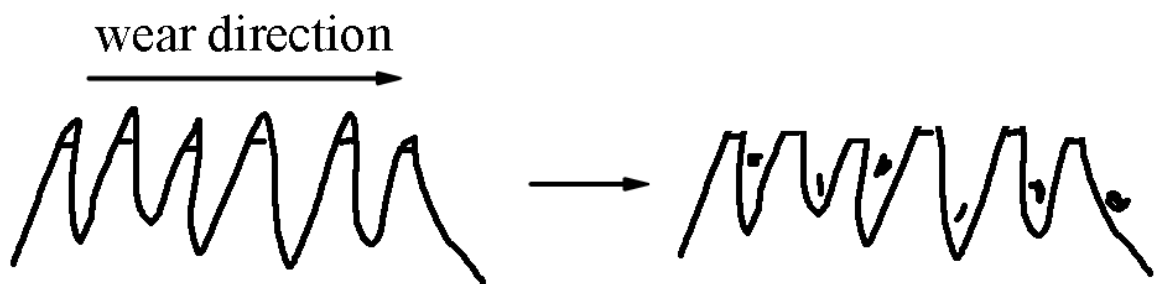Figure 7.5 Schematic of pin-on-disc wear characteristics on UHMWPE surface treated for

0.5h

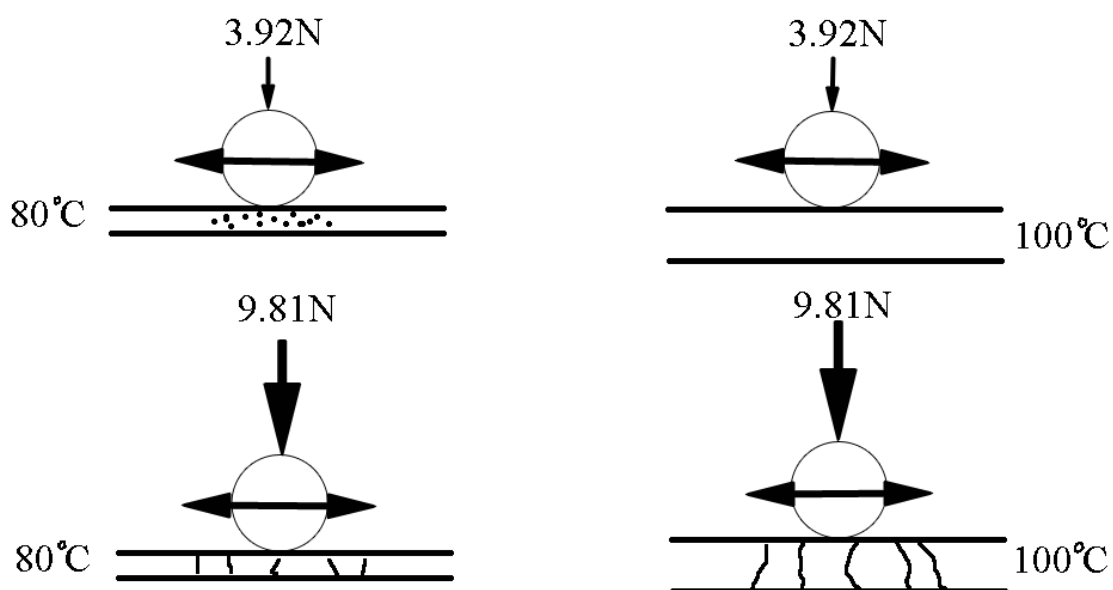Figure 7.6 Schematic of pin-on-disc wear characteristics on UHMWPE surface treated for 5h

Figure 7.7 Schematic of reciprocating wear characteristics on UHMWPE treated surfaces
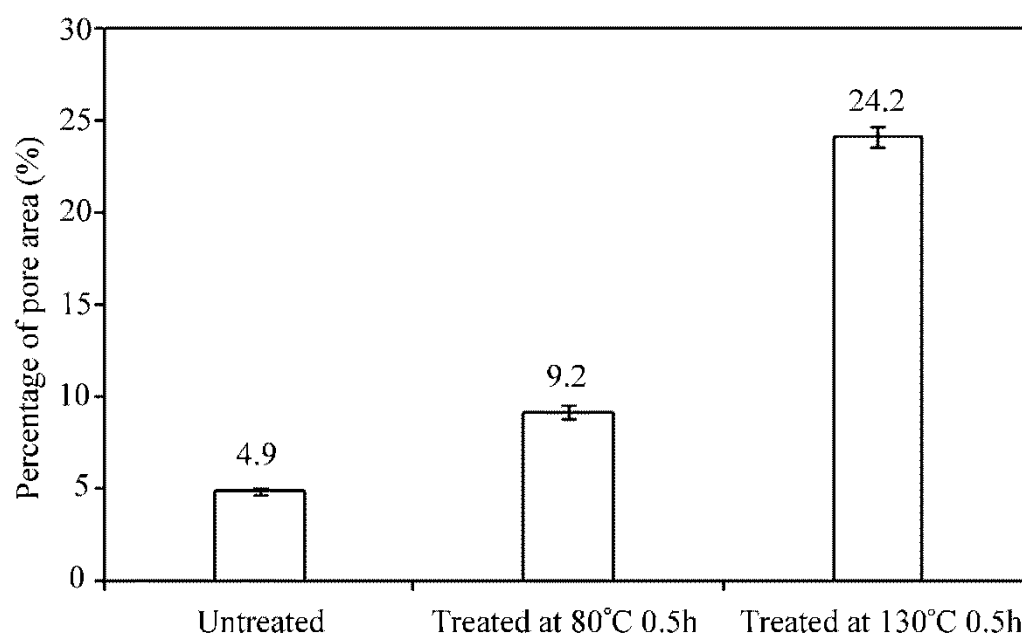

Figure 7.8 The percentage of the pore area on the surface of each sample of polyurethane after

plasma treatment